

NASA TECHNICAL MEMORANDUM

NASA TM-77408

NUMERICAL SOLUTION FOR THE INTERACTION OF SHOCK WAVE
WITH LAMINAR BOUNDARY LAYER IN TWO-DIMENSIONAL FLOW
ON A FLAT PLATE

Uriel Landau

Translation of Pitron numeri shel ha'interakziyah
beyn shikhat g'vool laminarit le'beyn gal-hailem
be's'reemah doo-meymadit al loo'akh shatoo'akh,
Ph.D. Research Thesis, Technion, Israel Institute
of Technology, Haifa, June 1976, 191 pp.



STANDARD TITLE PAGE

1. Report No. NASA TM-77408		2. Government Accession No.		3. Recipient's Catalog No.	
4. Title and Subtitle NUMERICAL SOLUTION FOR THE INTERACTION OF SHOCK WAVE WITH LAMINAR BOUNDARY LAYER IN TWO-DIMENSIONAL FLOW ON A FLAT PLATE				5. Report Date April 1984	
				6. Performing Organization Code	
7. Author(s) Uriel Landau				8. Performing Organization Report No.	
				10. Work Unit No.	
9. Performing Organization Name and Address Leo Kanner Associates Redwood City CA 94063				11. Contract or Grant No. NASW-3541	
				13. Type of Report and Period Covered Translation	
12. Sponsoring Agency Name and Address National Aeronautics and Space Administration, Washington DC 20546				14. Sponsoring Agency Code	
15. Supplementary Notes Translation of Pitron numeri shel ha'interakziyah beyn shikvat g'vo'ol laminarit le'beyn gal-hailem be's'reemah doo-meymadit al loo'akh shatoo'akh, Ph.D. Research Thesis, Technion, Israel Institute of Technology, Haifa, June 1976, 191 pp.					
16. Abstract The finite difference computation method was investigated for solving problems of interaction between a shock wave and a laminar boundary layer, through solution of the complete Navier-Stokes equations. It provided excellent solutions, was simple to perform, and needed a relatively short solution time. This allowed carrying out a large number of runs for various flow conditions, from which it was possible to study the interaction characteristics and principal factors that influence interaction.					
17. Key Words (Selected by Author(s))			18. Distribution Statement Unclassified - Unlimited		
19. Security Classif. (of this report) Unclassified		20. Security Classif. (of this page) Unclassified		21. No. of Pages	22.

N84-29160#
N-154, 621

Research Thesis submitted in partial fulfillment of the requirements for the degree of Doctor of Science in Technology.

Submitted to the senate of the Technicon -- Israel Institute of Technology, Sivan 5736, Haifa, June 1976.

This research was carried out under the supervision of Prof. M. Hanin and Assistant Prof. M. Wolfstein of the Faculty of Aeronautical Engineering.

The author wishes to express his sincere gratitude to Prof. M. Hanin and Assistant Prof. M. Wolfstein for their devoted guidance.

Dedicated to my dear wife and daughters.

TABLE OF CONTENTS

	Page
Synopsis	viii
List of Symbols	x
List of Tables for Computer Runs	xi
List of Figures	xii
1. Introduction	1
1.1. General	1
1.2. Qualitative Description of the Phenomena	2
1.3. General Background of the Research	4
2. Background and Reference Survey	6
2.1. Interaction Between Shock Wave and Laminar Boundary Layer	6
2.1.1. Background References	6
2.1.2. Experimental Studies	7
2.1.3. Analytical Studies	8
2.1.3.1. General Approach	8
2.1.3.2. Solution of the Flow Field Using Boundary Layer Equations	9
2.1.3.2.1. The Integral Moment Method	9
2.1.3.2.2. The Finite Differences Method (Boundary Layer Equations)	11
2.1.3.2.3. Other Methods of Solution	11
2.1.3.2.3.1. Division of the Boundary Layer into Subregions	11
2.1.3.2.3.2. Various Semi-empirical Methods	12
2.1.3.3. Solution of the Whole Flow Field Using Complete Navier-Stokes Equations	12
2.1.3.4. Summary and Comparison of Experimental and Theoretical Results	14
2.1.3.5. Methods Analyzing the Separation Phenomena	15
2.1.3.5.1. Theoretical Analysis of Separation	15
2.1.3.5.2. Practical Prevention Methods	16
2.2. Finite Differences Methods of Solution of Navier-Stokes Equations	16

	Page
2.2.1. Background References	16
2.2.2. Finite Difference Methods	17
2.2.3. Computation Techniques for Flows Including Shock Waves	19
2.2.4. Finite Differences for Special Cases	20
2.2.4.1. Boundary Layer Solutions	20
2.2.4.2. Approximate Solutions of Navier-Stokes Equations	20
2.3. Summary of the Main Changes and Improvements in the Present Study	20
2.3.1. Computational Scheme	21
2.3.2. Boundary Conditions	22
2.3.3. Parametrical Analysis of the Interaction Characteristics	23
3. Computation System	24
3.1. Basic Equations	24
3.1.1. Dimensional Flow Equations	24
3.1.2. Definition of Non-dimensional Variables	27
3.2. System of Non-dimensional Equations	28
3.3. Initial and Boundary Conditions	30
3.3.1. Boundary Conditions	30
3.3.1.1. Entry Cross Section Conditions	31
3.3.1.2. Boundary Conditions Along the Plate	32
3.3.1.3. Exit Cross Section Boundary Conditions	33
3.3.1.4. External Flow Boundary Conditions	34
3.3.1.5. Shock Boundary Conditions for the Shock Fitting Method	36
3.3.2. Initial Conditions	37
3.4. Finite Difference Solution Method	38
3.4.1. General	38
3.4.2. Definition of the Computational Region	39
3.4.3. Computation Grid Dimensions	39
3.4.3.1. General	39
3.4.3.2. Uniform Computation Grid	40
3.4.3.3. Non-uniform Grid	40

	Page
3.4.4. Finite Difference Scheme	40
3.4.5. Boundary Conditions in Finite Differences	43
3.4.6. Additional Computations in Finite Differences	43
3.4.7. Computer Program Procedure	43
3.5. Consistency, Stability and Convergence of the Computation Method	43
3.5.1. Consistency	43
3.5.2. Stability Criterion	44
3.5.3. Test of Stability and Convergence	46
3.5.3.1. Variation Coefficients	46
3.5.3.2. Estimate of the Order of Computational Error	47
3.5.3.3. Comparison of Accuracies of Various Methods	48
4. Results	50
4.1. Computation Method	50
4.1.1. Comparison of Brailovskaya and MacCormack Schemes	50
4.1.2. Comparison of Improvement Options	51
4.1.2.1. Grid Form	52
4.1.2.2. Finite Differences Order	52
4.1.2.3. Artificial Viscosity	53
4.1.2.4. Shock Wave Computation	54
4.1.2.5. Initial Conditions	55
4.1.2.6. Grid Mesh Dimensions	55
4.1.2.7. Roundoff Error	56
4.1.2.8. Summary of Comparison	56
4.2. Parametrical Analysis of the Results	57
4.2.1. Influence of Flow Conditions on the Interaction	58
4.2.1.1. Comparison with Previous Experimental and Computational Results	58
4.2.1.2. Shock Wave Influence	60
4.2.1.3. Mach Number Influence	61
4.2.1.4. Reynolds Number Influence	61
4.2.1.5. Shock Wave Engrance Location Influence	62
4.2.1.6. Prandtl Number Influence	62
4.2.1.7. Summary of Flow Condition Effects	63
4.2.2. Influence of Boundary Conditions Next to the Plate (Heat and Mass Transfer)	63

	Page
4.2.2.1. Heat Transfer Next to the Plate	63
4.2.2.2. Mass Transfer Close to the Plate	64
4.2.3. Suction Effect on the Separated Flow Region	65
4.2.3.1. Suction Location Influence	65
4.2.3.2. Suction Influence for Various Flow Conditions	66
4.2.3.3. Suction Required to Eliminate Separated Region	67
4.2.3.4. Approximate Formulation of the Suction Needed to Prevent Separation	67
5. Discussion and Conclusions	68
5.1. Computation Method	68
5.2. Parametrical Analysis of the Interaction	70
5.3. Suction Influence on Separation and Its Applications	71
5.4. Proposals for Continuation of the Research	71
Appendix A: Non-dimensional Definitions of Flow Parameters	72
Appendix B: Entry Flow Profile Computation (by Polhausen Method)	75
Appendix C: Evaluation of Shock Wave Force for Required Pressure Ratio	79
Appendix D: Optimal Evaluation of the Grid Dimensions	82
Appendix E: Computation of Grid Mesh Size	88
Appendix F: Computation of Flow Characteristics in the Shock Wave Direction at the External Boundary	91
Appendix G: Finite Difference Formulas	92
Appendix H: Detailed Finite Difference Equations	96
Appendix I: Boundary Conditions and Other Computations in Finite Differences	104
Appendix J: Comparison of Stability Criteria for Viscous Flow	110
Appendix K: Coefficients of the Differential Equation Remainders	111
Appendix L: General Evaluation of Computation Error	112
Appendix M: Evaluating the Computational Error by Comparing Results from Grids of Different Density	114

	Page
Appendix N: Comparison of Computation Time and Errors in Various Studies	116
Appendix O: A Formula for Suction Preventing Separation	117
Appendix P: Description of the Computer Program	119
References	135
Tables of Computer Runs	143
Figures	151

SYNOPSIS

This study analyzes the interaction between shock wave and laminar boundary layer on a flat plate numerically, mainly emphasizing the influence of suction on the separated region.

The complete compressible Navier-Stokes equations are applied to the problem in two parallel finite difference formulations, by Brailovskaya and MacCormack.

In the present scheme the outer edge of the computational region is placed just outside the viscous layer; assuming a simple wave type of the flow there, the outer boundary condition is computed by extension of the flow field characteristics. This allows the reduction of the computational region, saving computer time and storage.

To shorten computation time even more, an approximate shape of the boundary layer form along the wall, having a small separation bubble below the shock, is included in the initial conditions.

The computational field is $150 \delta_0$ long and $3 \delta_0$ wide (δ_0 - boundary layer thickness at the entry) consisting of 76×25 mesh nodes. The computer time required for obtaining a converged accurate solution (reached within about 200 time steps) is of the order of 4 CPU minutes on the IBM 370/168 computer. Good agreement with known results is achieved.

This relatively rapid solution, differing only slightly from the original MacCormack results that converge more slowly, as in other previous studies, allows the practical application of this scheme to many cases of different flow conditions within reasonable computation time.

In developing the computational scheme, several auxiliary methods were tested (though not included in the final scheme), as follows: artificial viscosity, non-uniform grid meshes, fourth order differences, exclusion of the shock wave from the computational field, and variation of initial and boundary conditions.

The present Brailovskaya scheme has been used for parametrical study of the interaction flow field for the following range of parameters: entry Mach number $2 \leq M_0 \leq 4.5$; downstream to upstream pressure ratio $1.2 \leq P_e/P_0 \leq 3.2$; and impingement Reynolds number $10^4 \leq Re_{x_s} \leq 10^6$. The influence of thermal conductivity (cooling and warming) and mass transfer (suction and injection) along the wall has been tested as well.

The results analyzed primarily were the size of the separated region, wall pressure distribution and boundary layer profiles.

The applicable interpretation of the separated region is very important since it greatly affects the performance efficiency of aircraft components, such as engine inlets and control surfaces, where such an interaction takes place.

Wall suction has been found to be a useful means for reducing separation until it disappears completely. A comprehensive analysis was made for evaluation of the amount of suction needed to prevent boundary layer separation. Given the flow conditions previously mentioned, the required suction lies in the range between $0 > V_W > -0.04$ (i.e. up to 4% of the free stream velocity).

LIST OF SYMBOLS

Letters of the Latin Alphabet

f	random function
h_x	length of computation grid mesh
h_y	width of computation grid mesh
k	thermal conductivity coefficient
l	length of computational field
m, n	indices of location in the field
p	pressure
q	ratio of lengths of adjacent meshes in the computation grid
t	time
u	velocity component in the x direction
v	velocity component in the y direction
x	horizontal coordinate of a table
y	vertical coordinate of a table
A	viscosity differentials in the y direction;
B	viscosity differentials in the x direction) per Eq. (3-11)
C	constant of Sutherland's formula
C	general expression for artificial viscosity; per Eq. (3-38)
C	random constant
C_x	x-component of the artificial viscosity
C_y	y-component of the artificial viscosity
CC_x	numerical coefficient of C_x)
CC_y	numerical coefficient of C_y) per Eq. (3-41)
C_F	friction coefficient
C_Q	thermal conductivity coefficient) definition in Appendix A

LIST OF TABLES FOR COMPUTER RUNS

- Table 1A: Check of Computation Method
- Table 1B: Check of Influence of Artificial Viscosity
- Table 2: Check of Dependence of Results on Perimeters
- Table 3: Influence of Boundary Conditions (Thermal Conductivity and Mass Transfer by the Plate) on the Field of Flow
- Table 4: Influence of Length and Location of Suction Zone on the Separation
- Table 5A: Influence of Suction on the Separation Under Various Flow Conditions; Parametric Check for Various x_s
- Table 5B: Check of Various Combinations of Flow Conditions during Suction

LIST OF FIGURES*

- Fig. 1. Field of Flow of the Interaction
- Fig. 2. Chart of Boundary Conditions
- Fig. 3. Description of Computation Grid
- Fig. 4. Flow Chart of Computation Program
- Fig. 5. Comparison Between Existing Results from Computations
- Fig. 6A. Comparison of Various Computational Options
- Fig. 6B. Comparison of Various Computational Options
- Fig. 7. Sensitivity of Results to Coefficients of Artificial Viscosity
- Fig. 7A. Influence of Non-optimal Artificial Viscosity Coefficient
- Fig. 8. Comparison of Computation in Different Grid Densities
- Fig. 9. Comparison of Computation in Various Difference Schemes
- Fig. 10. Coefficients of Stability
- Fig. 11. Distribution of Stability Coefficients R_4 and E_p in the Field of Flow
- Fig. 12A. Comparison of Stability Coefficients Between Various Grids
- Fig. 12B. Comparison of Stability Coefficients Between Various Grids
- Fig. 13. Comparison of Stability Coefficients Between Various Difference Schemes
- Fig. 14. Comparison of Stability Coefficients for Various Computer Accuracies
- Fig. 15. Comparison of Run 101 to Results from Computations and from Experiments
- Fig. 16. Diagram of Field of Flow for Run 101
- Fig. 17. Comparison of Run 102 to Results from Computation and Experiments
- Fig. 18. Diagram of Field of Flow for Run 102

*[Translator's note: The following is a complete translation of the Hebrew figure captions. The author's English version appearing on the figures is not always complete.]

- Fig. 19. Comparison of Run 103 to Results from Computation and Experiments
- Fig. 20. Diagram of Field of Flow for Run 103
- Fig. 21. Influence of Force of Shock Wave p_e/p_o on the Interaction
- Fig. 22. Diagram of Field of Flow for Run 104
- Fig. 23. Influence of Mach Number M_o on the Interaction
- Fig. 24. Diagram of Field of Flow for Run 112
- Fig. 25. Influence of Reynolds Number Re_{x_s} on the Interaction
- Fig. 26. Diagram of Field of Flow for Run 121
- Fig. 27. Influence of the Location x_s of Shock Impingement on the Interaction
- Fig. 28. Influence of Prandtl Number Pr on the Interaction
- Fig. 29. Influence of Changes in Flow Conditions p_e/p_o ; M_o ; Re_{x_s} on the Shape of the Boundary Layer
- Fig. 30. Influence of Wall Temperature T_w on the Interaction
- Fig. 31. Influence of Suction or Injection Velocity V_w Along the Wall on Interaction
- Fig. 32. Diagram of Field of Flow for Run 212
- Fig. 33. Influence of the Change of Boundary Conditions V_w ; T_w on the Shape of the Boundary Layer
- Fig. 34. Influence of the Suction Zone Length and Its Location on the Separation Zone
- Fig. 34A. Influence of Location, Start and End of the Suction Zone on the Size of the Separation Zone
- Fig. 35. Dependence of the Separation Zone on the Suction Velocity V_w for Various Pressure Ratios
- Fig. 36. Dependence of the Length of the Separation Zone on the Suction Velocity V_w for Various Mach Numbers
- Fig. 37. Dependence of the Length of the Separation Zone on the Suction Velocity V_w for Various Reynolds Numbers
- Fig. 38. Suction Velocity Required to Prevent Separation in the Plane p_e/p_o vs. M_o

Fig. 39. Suction Velocity Required to Prevent Separation in the Plane p_e/p_o vs. Re_{x_s}

Fig. 40. Suction Velocity Required to Prevent Separation in the Plane M_o vs. Re_{x_s}

Fig. 41. Tabulation of the Dependence of Suction Velocity Required to Prevent Separation for the Variable Flow Parameters Re_{x_s} ; p_e/p_o ; M_o

General Remarks

A. Unless otherwise indicated, each run was according to the Brailovskaya method.

B. The values u/u_o ; v/u_o ; $C_p T/u_o^2$ appearing on drawings are not to scale and have been designated accordingly as u ; v ; T .

NUMERICAL SOLUTION FOR THE INTERACTION OF SHOCK WAVE
WITH LAMINAR BOUNDARY LAYER IN TWO-DIMENSIONAL FLOW
ON A FLAT PLATE

Uriel Landau

1. Introduction

/10*

1.1. General

This research attempts to analyze the phenomenon of interaction between a shock wave entering the laminar boundary layer of a flat plate, as well as some of the accompanying practical projections, through the employment of the advanced methods of computation available today in the field of numerical calculation of flows.

From a practical point of view this interaction phenomenon (in which shock waves, expansion and compression fans, the boundary layer and the flow separation zone are involved) occurs at the inputs of jet engines and at the control surfaces of supersonic aircraft (when there is turbulent flow, as is true in some cases). This interaction has considerable influence on the flight performance and therefore must be considered in the design of components that are directly or indirectly involved with it so as to improve that performance during all flight conditions as much as possible. Investigations of the influence of interaction have, until recently, been carried out only experimentally (in a flight tunnel or in actual flight) because of the absence of any reliable and accurate analytical methods, which were, moreover, considered too expensive and too drawn out.

Recently, with the rapid development of computers, it has become possible gradually to provide numerical solutions to more and more problems involving voluminous computation. The time has thus arrived to develop a method of efficient and relatively inexpensive solutions for problems of this nature. The numerical solutions that have appeared in recent years on this subject constitute an important step forward and while much remains to be done to improve and expand their practical application, they represent a good basis from which to continue the task.

This study recommends a method of computation that is based on the expansion and utilization of several presently known methods and which is basically a numerical solution of the complete (Navier-Stokes equations) equations for the field of flow close to the wall, including all its zones, as a single unit. By accepting an accuracy that falls only a little short of what is presently available, a convergence can be achieved after a relatively short period of computation

*Numbers in the margin indicate pagination in the foreign text.

(a few minutes on the CPU) and a practical method is realized through which the computation method can be applied to a large scope of different flow conditions (which have never before been examined through any similar type of computation) with two primary aims:

(A) Examination of the influence of various parameters on the nature of interaction;

(B) Investigation of practical ways (especially suction) to prevent separation of the boundary layer during the interaction. The results of the calculations show that there is room for the continuation of the development of methods of this kind and for their expansion to additional cases (such as flows around corners and steps and the entry of a turbulence model into the calculations).

1.2. Qualitative Description of the Phenomenon

/11

The phenomenon of interaction, which is shown schematically in Fig. 1, occurs as the outcome of a shock wave impinging at a slant angle on the laminar boundary layer* of a flat plate.** The shock wave intersects the boundary layer while going through a process of thickening and bending and reaches the line where the flow is sonic. The pressure increase that follows the shock wave is transferred backward, upstream (upstream influence) through the subsonic portion of the boundary layer. This increase in pressure causes a gradual increase in the thickness of the layer just before the point of entrance of the shock wave. Where the shock wave is strong enough this may lead to separation of the boundary layer at the point where the internal friction at the plate becomes zero. At the point of separation the separation zone starts, which is detached from the boundary layer by the flow line and in which a recirculating flow is maintained.

Circulation of the flow in the area before the entrance of the shock wave creates a spread of the compression waves (because of the change in boundary layer thickness) which unite into a shock wave of separation at considerable distance from the plate.

The separation zone causes the return of the wave spreading since this area cannot sustain a sudden pressure increase. Most of the pressure rise generated by the impinging shock wave

*A similar phenomenon is accepted in the turbulent boundary layer but the changes in this field of flow are smaller.

**The above-mentioned interaction occurs at sufficient distance from the leading edge of the plate to permit the disregard of the influence of interaction between the boundary layer and the shock wave that emanates from the leading edge.

is attenuated by the fanning out of the expansion waves. The incident wave and the spreading of the expansion waves return the direction of the external flow toward the plate. The turn of the flow from this condition until it again becomes parallel to the plate, at the downward slope of the flow, causes the fanning out of the compression waves, which unite far from the flat plate into the reattachment shock wave. Two shock waves generated by the compression fans unite further still into one wave, the reflected shock wave.

The turn of the flow toward the plate reduces the thickness of the separation zone gradually up to the point where the boundary layer is again attached to the plate, while its thickness continues to decrease to its minimum in the zone where the external flow is parallel to the flat plate. During the downward slope of the flow from this zone the boundary layer increases again. /12

All the above-mentioned phenomena depend primarily on the strength of the incident shock wave with regard to the Mach and Reynolds numbers of the flow in the interaction zone and to the laminar or turbulent nature of the boundary layer.

The order of magnitude of the interaction zone in which the majority of the above-mentioned changes take place is a length of $100 \delta_0$ and a width of $3 \delta_0$ (δ_0 being the width of the boundary layer at the input cross section). Outside this area the influence of the interaction on the external field of flow and on the boundary layer is negligible.

From the point of view of the mathematical nature of the flow equations, there are three regions in the interaction zone:

- the parabolic region: the boundary layer (without separation zone and shock wave vicinity);
- the hyperbolic region: the external flow outside the boundary layer;
- the elliptical region: the separation zone and the vicinity of the shock wave (along its incidence to the boundary layer).

The last two regions do not conform to the boundary layer, mainly because they contain strong gradients of the same order of magnitude both in the direction of the flow and at right angles to it.

To avoid the use of three sets of separate equations for each region and the stitching together of their solutions for the lines of contact between them, the complete Navier-Stokes

equations are employed which are applicable to all regions. This set of equations in its non-continuous form is parabolic and becomes elliptical in its continuous form (the asymptotic solution is found from the continuous form). This arrangement requires initial conditions for each field and boundary conditions for all boundaries of the field of flow (since the problem being solved is an Initial Value - Boundary Value problem). Each field of interaction constitutes thus a single unit with all its regions, at least for the purpose of computation.

1.3. General Background of the Research*

/13

The subject of interaction between the shock wave and the laminar boundary layer at a flat plate for two-dimensional flow was first investigated experimentally (starting at the end of the 1940's) and afterwards through various analytical methods which gradually improved.

The first analytical solutions, which used the method of integrating the momentum along the width of the boundary layer, produced results (applicable only to special cases where experimental results already existed) that depended largely on the choice of empirical coefficients and on various mathematical assumptions.

Much progress was made by means of a solution of the boundary layer equation through finite differences, which represented a more general solution, included fewer assumptions, and provided results that were better but that still depended on the close formulation of the interaction mechanism; there also still remained the requirement to adapt the solutions to the various zones of flow.

A new direction for the improvement of the computation was taken in recent years with the expanding use of computers, which led to the founding of the new field of Computational Fluid Dynamics. Within the realm of this field many flow problems are being solved by means of numerical solution of sets of equations and boundary conditions that represent the physical phenomena far more accurately. Thus the approach developed, which is based on the solution of the entire field of flow (i.e. boundary layer, external flow, the vicinity of the incident shock wave and the separation zone) through finite differences integration of the complete equations (continuity equations, the momentum in the x and y directions and the energy) with suitable boundary conditions. This system is solved through an iterative process (by integration of the equations vs. time to obtain an asymptotic solution).

A few of those studies that used this method achieved results that were better than previous ones, the computation

*The subject is treated at length and with references in Part 2.

became more general and easier to perform. Even though there is room for improvement and perfection of the computation method, there is no doubt that this approach provides far more trustworthy solutions for physical phenomena like the above-mentioned interaction.

The main subjects still open for additional improvement (some of which was partly accomplished as one of the goals of this research) are:

a) Perfection of the method of computation to increase the accuracy of results and reduce the field of computation to the immediate vicinity of the interaction zone, as well as to speed up the rate of convergences (reduction of computing time). /14

b) Expansion of the range of computation to stronger interactions than had been computed in the past and setting up of parametric research on the influence of various factors on the interaction.

c) More accurate representation of the shock wave (in the present methods its width is several times that of its physical width, which leads to some distortion of results).

d) Examination of actual projections of the phenomenon, the chief one of which is to find a way for reducing the separation zone (especially through suction), which is responsible for the inefficient performance of the parts of an aircraft on which this interaction takes place.

These subjects, whose investigation represents the aims of this and other research studies presently carried on in this field, have been dealt with in three principal stages:

a) A definition of the differences integration, of the computation method for the equations and of the boundary conditions, that provides a resounding solution to the problem; various approaches and techniques, from which optimum combinations are formed for the computation method. Among the approaches that have been examined were: "continuous" and "non-continuous" treatment of the shock wave (in the "non-continuous" treatment the shock wave is removed from the field of computation), employment of artificial viscosity, computation of differences of the second order and of the fourth order, a uniform computation grid and a non-uniform one, varying boundary conditions and initial conditions. By means of these approaches two final schemes of computation were prepared, which are based on the methods of Brailovskaya and MacCormack.

b) Application of the method of computation to a series of variable flow conditions, for the investigation of the

characteristics of interaction and the factors that influence it, when the principal results in question are the magnitude of the separated flow zone, the shape of division of pressures and the friction along the length of the plate, as well as the boundary layer profiles.

c) Detailed examination of the influences of suction on the separation zone under various flow conditions, with the aim of finding the required condition for diminution or total elimination of the separation zone.

A detailed summary of the changes and innovations made during this study, with reference to existing studies, is presented in Section 2.3 (after a survey of the references).

2. Background and Reference Survey

/15

The subject of interaction between shock waves and boundary layers and the methods for its solution is a voluminous one and branches off into many directions. From the wealth of references on the various aspects of the subject only a few of the principal ones were chosen, which are connected with the computation methods used and the results achieved in this research study.

Later on two central subjects will be dealt with separately (each of them is subdivided into many secondary subjects):

a) The subject of interaction between the shock wave and the laminar boundary layer of the flat plate, as investigated up to the present both experimentally and analytically.

b) Various numerical methods for the solution of Navier-Stokes equations in compressive and viscous flow, which serve as the principal tool for numerical solution of problems of fluid dynamics.

2.1. Interaction Between Shock Wave and Laminar Boundary Layer

2.1.1. Background References

The references described below are mostly survey papers that deal with the subject from various points of view and in its various stages of research development.

The phenomenon of interaction, against the broad background of various flow phenomena, has been treated in a number of basic texts; Shapiro [93] deals with the subject in a broad analytical discussion of compressive flow with shock waves. Schlichting [92] (1968), [text illegible] and Stewartson [95]

(1964) treat the interaction phenomenon in a discussion of the characteristics of the boundary layer during compressive flow.

Dorrance [23] (1972) deals with viscous hypersonic flow and ascribes the various projections of the phenomenon to chemical reactions of the fluid and/or the surface area. In all of these references a general and qualitative description of the phenomenon is given.

A broad survey, accompanied by quantitative results from practical problems that involve interactions between shock waves and the boundary layer on aircraft, is presented in the collection of papers edited by Lachman [55] (1961) and in the study by Korkegi [53] (1971), in which the decreased efficiency of control surfaces and engine inlets on jet engines is described as due to the flow separation caused by interaction and which suggests ways for improvement of their performance.

2.1.2. Experimental Studies

/16

The early work dealing with interaction was experimental. This was so primarily because the physical mechanism of the phenomenon was not well enough understood at first and the analytical and computational tools were lacking for accurate treatment of the subject.

One of the earliest studies was conducted by Liepman et al. [61] (1949) and offers a qualitative analysis of the phenomenon (based on Schlieren photographs) as well as a model of the flow in the interaction zone, by means of which the magnitude of the zone that is subject to back pressure influence was set (about $50 \delta_0$). Two additional investigations were by Barry et al. [4] (1950) and Gadd et al. [28] (1954), which also describe qualitative results and analyze the interaction mechanism for the first time.

The following investigations already describe quantitative results for the pressure divisions, internal friction and thermal conductivity along the plate, for various Mach and Reynolds numbers and shock wave forces. Care is taken to maintain the two-dimensional and laminar characteristics of the flow under experimental conditions.

Chapman et al. [14] (1958) and Hakkinen et al [41] (1959) provide results for average Mach numbers and shock wave forces ($1.2 < M_0 < 2.5$; $1.2 < p_e/p_0 < 2.4$) for interactions that occur when a shock wave is incident on the boundary layer of a flat plate. Needham, Stolery [75] (1966) and Lewis et al. [60] (1968) expanded the range of flow conditions (to $M_0 = 10$ and $p_e/p_0 = 4$) when the interaction occurs around a compression

corner and part of the flow (only for the strongest interactions) is turbulent. Those results are also of significance for this research since such an interaction is similar in its appearance and in its qualitative (as well as to some extent in its quantitative) results to the one caused by a shock wave impinging on the boundary layer of a flat plate.

2.1.3. Analytical Studies

2.1.3.1. General Approach

The first attempts at solution of the interaction were based on various approximations of the boundary layer in the vicinity of the zone where a weak shock wave is incident. In those first investigations by Lighthill [62] (1950), Lighthill [63] (1953) and Stewartson [95] (1955), the first analysis of the interaction mechanism and of the back pressure influence is made, through experiments with the building of an analytical model to explain the phenomenon and by using omissions and approximations. The results obtained were not accurate and depended too much on the approximations, while the method of computation could not be extended to more general cases. /17

At a later date the approach (which remained up to date until the end of the 1960's) to the solution of interactions through boundary layer equations, with the addition of an expression that tied the external flow to the boundary layer, was developed. Those solutions were mostly obtained through the integral moment method, though some employed the method of finite differences of the boundary layer equations.

Solutions obtained through the integral moment method improved with time thanks to the perfection of computation techniques (such as different solutions for different zones and their integration, the use of semi-empirical coefficients, etc.), but their accuracy remained limited to low Mach numbers and weak shock waves; the solutions were also too dependent on the assumptions of the method of computation and on the chosen coefficients.

The method of finite differences for the solution of boundary layer equations perfected the computation and made it more general. Results improved and the range of solutions was broadened. But here, too, the disadvantage of using basic assumptions about the boundary layer in zones where they did not apply (the separation zone and the vicinity of the shock wave inside the boundary layer) was conspicuous.

Lately, with the great development in computers and the investigation of numerical methods, a new approach has taken shape (which is also typical for other solutions in compressible flow) in which complete Navier-Stokes equations are solved by

finite differences, for the entire field of flow and its various zones. The solution becomes a more general one and is only influenced by the choice of flow parameters and by the boundary conditions of the problem. This approach, which was started under the auspices of a new field called Computational Fluid Dynamics, has already yielded excellent solutions for the interaction in a number of special cases.

2.1.3.2. Solution of the Field of Flow Using Boundary Layer Equations

The different methods available for this approach will be described briefly further on. A thorough survey of the main methods applicable for the solution of interaction through use of the boundary layer equations provides the following references: Holden [45] (1965); Morduchov [73] (1955); Holder, Gadd [46] (1955); Murphy [74] (1969); Georgeff [32] (1972); Charwat [15] (1970); Panov, Schvets [79] (1967). The references apply mainly to the integral moment method, and only Murphy [74] contains finite difference methods as well. The four last-named papers describe (through analysis of the results and their comparison with experimental results) the inaccuracy of the approach, which is due mainly to omission of the gradients in the y direction (according to the boundary layer equations) in flow zones where it is not applicable (such as in the separation zone and the zone where the shock wave is incident on the boundary layer).

/18

What the studies that share this approach have in common is their reliance on the concept of free interaction by Chapman. According to it, the increase in pressure via the separation zone up to the plateau of steady pressure does not depend on a mechanism that generates the interruption (like an entering shock wave, a forward step, a compression corner, etc.). Now we will take up the methods mentioned above, each one separately:

2.1.3.2.1. The Integral Moment Method

This approach is based on an assumption of the existence of boundary layer equations in which functions or tables for the dependence of unknowns in the y direction are posited, by means of a dependent parameter x; all of this based on experimental results or theoretical assumptions. (It becomes clear then that the accuracy of those functions or tables determines the accuracy of the computation results.) The resulting equations are multiplied by weighting functions of one of the variables (velocity for the Moment Equation and temperature for the Energy Equation) and are integrated in the y direction (along the width of the boundary layer). The

result of this integration is a set of differential equations of the first order for the variables in the boundary layer that are functions of x . To this set is added an equation of the form

$$\frac{dP}{dx} = f\left(\frac{d\delta}{dx}\right) \quad \text{or} \quad \frac{dP}{dx} = f\left(\frac{V_e}{u_e}\right) \quad (2-1)$$

which expresses the interaction between the pressure change due to the impingement of the shock wave and the change in the shape of the boundary layer.

The resulting equations are integrated in the x direction as far as the decline of the flow where the adaptive equations become valid

$$\frac{dP}{dx} = \frac{d^2P}{dx^2} = 0 \quad (2-2)$$

The investigations by Glick [35] (1960) and Bray et al. [10] (1961) are based on the Integral Moment Scheme of Crocco, Lees [19] (1952), which deals with the interaction between dissipative flow and nearly isentropic flow. In those studies the continuous equations for the momentum and of the moment of the momentum, for the flow at an adiabatic wall, were considered and separate velocity profiles were used in them, both for an attached and a separated boundary layer. The start of interaction was generated by disturbance through pressure. The influences of various parameters (like suction and cooling of the wall) on the solution, which is expressed by the pressure division, the friction and the form of the boundary layer's development, were discussed.

This line of thought was extended to the non-adiabatic flow (by inserting the enthalpy profile into the energy equation) by Klineberg, Lees [52] (1969); Holden [45] (1965); Lees, Reeves [59] (1964); Georgeff [32] (1974) and also by Horton [47] (1971) who discussed the aximetric problem. /19

The investigations by Nielsen et al. [76] (1965); Goodwin et al. [38] (1967); Makofski [70] (1963) also deal with non-adiabatic flow, but they offer separate solutions for the separated zone and the boundary layer on both sides of the line of flow that separates them. In the third study the

velocity profile is defined as a function of the friction and of the pressure gradient along the plate. In Blankenship's [6] (1967) paper the solution is obtained with the aid of small disturbances to generate interaction in tubes.

The solutions demonstrated in the above studies are partly dedicated to problems of the external shock wave, which impinges on the boundary layer, and partly to problems of the pressure corner, two problems that are similar in their nature and in the results from their solutions.

2.1.3.2.2. The Finite Differences Method (Boundary Layer Equations)

This approach was developed later, thanks to developments in the use of computers. In the computation the boundary layer equations, together with the equation of interaction (2-1), constitute a series of parabolic equations that are solved numerically by an implicit method of finite differences. Similarly, the appropriate boundary conditions are formulated for upstream flow (the profile of initial flow) and for the length of the plate and the external flow as well. A solution through this method was offered by Reyhner, Flüge-Lotz [84] (1968). For the sake of including the separated (aliphatic) region in the range of computation of the (parabolic) equations, several omissions were made that do not influence the result much but which prevent unsteadiness in the process of numerical computation. Except for that, no further empirical assumptions are made and the results are much better than those from the Integral Moment Method (when compared to experimental results).

A solution through finite differences, by Baum [5] (1968), must be mentioned, which relates to interaction by means of a rounded corner and in which the boundary layer equations contain a parameter for the surface curvature.

2.1.3.2.3. Other Methods of Solution

In addition to the methods referred to in the two previous paragraphs, various partial solutions were obtained (by means of approximations of equations), using other methods than those already mentioned:

2.1.3.2.3.1. Division of the Boundary Layer into Subregions

/20

Based on Lighthill's [63] (1950) approach, the method of solution through division of the boundary layer into two sublayers and an approximation for the solution between them

was developed. Goodman [36] (1954) suggested such a solution path in which interaction is expressed by the insertion of a semi-empirical function for the pressure division around the region where the shock wave impinges. Ray [83] (1962) developed semi-empirical formulas for the description of various results like pressure division, boundary layer thickness, etc., in this way.

Rose [88] (1969) and Miller [72] (1973) perfected the method and solved the inner (viscous) part of the boundary layer through boundary layer equations and the outer (inviscid and rotational) part through a method of characteristics, with the two solutions matched to each other at the line of contact (which is the sonic line on which the shock wave impinges). For Rose's [88] solution an empirical value is needed for the length of the region that is influenced by back pressure.

Brilliant, Adamson [11] (1974) solved interaction in transonic flow through division of the field into several regions: the inner boundary layer through boundary layer equations, the outer boundary layer and also the external flow through equations of the small separate disturbances. The three regions were matched up at their lines of contact.

2.1.3.2.3.2. Various Semi-Empirical Methods

In those methods various semi-empirical functions are employed and coefficients are computed by approximation methods to get specific results that characterize the interaction.

That is how Erdos, Pallone [25] (1962); Popinski [82] (1965) and Gai [29] (1970), as well as Byrkin [12], did their work. Byrkin [12] obtained analytical approximate solutions for a number of special cases. Gai [29], who relied on computation of the sublayer of the subsonic boundary, was mostly concerned with computing the distance over which the influence of interaction was felt upstream of it, for various Reynolds numbers.

Still to be noted is Ackroyd's [1] (1969) work, which discussed analysis of the influence of various parameters on the mechanism of interaction.

2.1.3.3. Solution of the Whole Flow Field Using Complete Navier Stokes Equations

/21

Thanks to the development of fast computers in recent years, it has become possible to solve the complete Navier-Stokes equations numerically. Many investigations of a wide range of subjects have recently been provided with solutions in this way.

Solutions of the interaction between a shock wave impinging on the boundary layer have been obtained by Skoglund, Gay [94] (1969) and MacCormack [67] (1971). Since those are the most advanced studies in this field and very close to the subject of this research, their discussion will be more detailed than that of preceding work.

The two studies are based on developments in the explicit, two-stage difference schemes by Lax-Wendroff*, which helped improve convergence and increase accuracy especially near the wall. Skoglund, Gay [94] did a logarithmic transformation of the coordinates, which reduces the size of grid meshes in the vicinity of the incident shock wave on the boundary layer and increases their size gradually toward external flow in the y direction and toward upstream flow in the x direction. MacCormack [67] divided the grid into two regions; in the region near the plate the grid was divided into small spaces in the y direction and the distant region was divided into larger spaces (the meshes being uniform in each respective grid). A saving in computer time for the region close to the plate was achieved through subdivision of the computation by difference equations into x and y directions separately by a special technique. Similarly, the differences in changing directions (alternately forward and backward) were computed.

Skoglund, Gay [94] added terms for artificial viscosity for the sake of stabilizing the solution in separated flow, while MacCormack [67] did not require it since in his difference schemes there is already enough (numerical) artificial viscosity for stabilization of the solution.

In both investigations the boundary conditions were formulated in a similar manner. Skoglund and Gay [94] assumed an initial boundary layer profile per Chapman-Rubenstein at the entrance cross section, a linear extrapolation of the variables at the exit cross section, and along the plate no components of velocity, adiabatic wall temperature, as well as density from one of the equations of motion. MacCormack [67] assumed uniform flow conditions along the entire width of the entrance cross section (which, for him, was in front of the leading edge of the plate), zero gradients at the exit cross section and along the length of the plate no velocity components and zero gradients for pressure, temperature and density in the y direction.

In both studies the external flow boundary was assumed to be far enough from the plate so that the reflected flow lines of the incident shock wave will exit via the exit cross section

/22

*See Paragraph 2.2.2.

and not via the plate. Conditions at the outer boundary were therefore determined as fixed according to the formulas for shock wave transition (from both sides of the incident shock wave). The shock wave itself was determined as having a width of 1-2 grid meshes in its initial form.

In both investigations the numerical results were calculated for $M_0 = 2$; $Re_{x_s} = 3 \cdot 10^5$ and $1.2 \leq p_e/p_0 \leq 1.4$. Comparison with experimental data by Hakkinen et al [41] makes it clear that, as far as the division of pressure, the friction along the length of the plate and the length of the separated region are concerned, better results were obtained than from the methods applied previously. Both investigations achieved approximately the same accuracies, with some advantage on MacCormack's [67] side. Because of the lack of computed results for higher Mach numbers and more intense shock waves, no estimate of accuracy can be made for those ranges.

The MacCormack method has been recently perfected by MacCormack, Baldwin [69] (1975) and was adapted for use in turbulent flows. The grid form was also changed in that study so that Δy is changed through an exponential parameter which permits its outward expansion (similar to the Skoglund, Gay [94] method).

In addition to these studies, two more are worth mentioning, which deal with the numerical solution of complete Navier-Stokes equations for near (wake) problems. Allen, Cheng [2] (1979) solved for the field of flow in the wake of the rear step and Carter [13] (1972) solved the field of flow around the compression corner. Those two studies are based on the difference scheme of Brailovskaya [8] (1965) (which is also an explicit two-stage method). Allen, Cheng [2] made some changes in this scheme, which removed the Reynolds number from the conditions of CFL stability and caused acceleration of convergence particularly at low Reynolds numbers. In both of these studies the outer boundary is defined as very close to the end of the boundary layer, which is made possible by formulation of the boundary conditions for the external flow with uniform flow characteristics along the characteristic directions that extend from the field of flow to the outer boundary. Thus the influence of expansion and compression stream lines, that travel from the boundary layer to the outer boundary, can be considered.

2.1.3.4. Summary and Comparison of Experimental and Theoretical Results

Figure 5 presents a comparison of results from the principal systems demonstrated with experimental results (the equation was taken from Murphy [74] and MacCormack's [67] results were also plotted on it).

Summing up the results:

/23

a) The methods that employ the complete Navier-Stokes equations provide better solutions than those obtained from the boundary layer methods (at least within the range of flow condition under which they were obtained, i.e. $M_0 = 2$; $Re_{x_s} = 3 \cdot 10^5$ and $1.2 \leq p_e/p_0 < 1.4$).

b) For high Mach numbers and intense shock waves only results from boundary layer methods are available and those diverge the more from experimental results the larger the Mach numbers and the more intense the shock waves are. It appears that some more improvement is desirable for the solutions obtained with Navier-Stokes equation methods, as well as the extension of their use for a broader range of parameters Pr ; Re_{x_s} ; p_e/p_0 ; M_0 . The influence of heat transfer (heating and cooling) and mass transfer (suction and injection) along the plate should also be investigated.

2.1.3.5. Methods for Analysis of the Separation Phenomenon

Since the phenomenon of boundary layer separation is tied directly to interaction and is a measure of its intensity, it is important for practical considerations. We will (in addition to solutions of interaction that were demonstrated in previous paragraphs) here discuss several studies that deal with the analysis of separation against the background of various problems.

2.1.3.5.1. Theoretical Analysis of the Separation

Tani [98] (1953) and Page [77] (1960) discussed the prediction of separation with formulations of approximation (based on boundary layer equations). Stewartson, Williams [97] (1969) thoroughly analyzed the separation of flow during interaction between an incident shock wave and the boundary layer by means of equations (constructed from asymptotic developments) approximated for three different regions: the inner boundary layer, the outer boundary layer and the separated region, through adaptations of interregional connections. An estimate of the type of interference needed to create the separation and of the size of the separated region, as a function of the flow conditions, is gained from the results of the analysis.

Additional development of methods for prediction of separation from the intensity of the pressure gradient was carried out by Gerhart [33] (1973) and Messiter et al. [71] (1971).

2.1.3.5.2. Practical Prevention Methods

/24

A detailed description of flow separation phenomena and their negative consequences on aircraft performance is given by Cooke, Brebner [17] (1959). Pearcey [81] (1961) and Wuest [105] (1959) describe separation phenomena caused by various types of interaction (particularly for an incident shock wave and in a compression corner) and discuss different ways for the control of the boundary layer to prevent separation.

The principal ways suggested are: suction at the surface of the plate, special geometric design of the surface of the plane and artificial transition to obtain turbulence of the boundary layer where the capability of resistance to the pressure gradient is still stronger than in the laminar condition.

Gai [29] (1969) discussed the experimental results of the influence of suction on interaction between the shock wave and the turbulent boundary layer in the compression corner.

Anderson et al. [3] (1969) describe a combined method of suction in the separated region and injection in the stagnation region, for improvement of laminar characteristics and reduction of friction on a rough surface with a high Reynolds number.

Inger, Swean [48] (1975) analyze the influence of suction or injection in the deflection corners from the plate to the flow on a laminar boundary layer with a separated region (the analysis is performed through an approximated solution based on the Levy-Lees transformation).

2.2. Finite Difference Methods of Solution of Navier-Stokes Equations

/25

This part discusses finite difference methods that were developed in recent years to solve Navier-Stokes equations for many and varied flow problems.

2.2.1. Background References

The principles for the solution of differential equations by means of finite differences were first discussed at length by Courant, Friedrichs, Levy [18] (1928) who classified the types of problems and the various methods of computation and prepared tests for the stability of the solution. Lax [57] (1967) surveyed their approach with reference to recent developments on the subject of computation with finite differences.

Mathematical background, general numerical methods and discussion of the stability of the solution through application to practical problems are to be found in books by Forsythe, Wasov [27] (1960) and Richtmayer, Morton [85] (1967).

A detailed survey of numerical methods for all areas of fluid dynamics is given in Roache's [86] (1972) book.

A general new formulation of various difference methods and the connections between them in the solution of all types of differential equations is given by Isenberg, Davis [49] (1974) where the principles of consistency, stability and convergence are also discussed.

2.2.2. Finite Difference Methods

The approach to the solution of Navier-Stokes equations through finite differences was thoroughly outlined in the investigations by Crocco [20] (1965) and Cheng [16] (1970), who suggested a way for an asymptotic solution of the Navier-Stokes equations that are functions of time, which aspires to a solution in the constant condition. The process of integration over time is analogous to the iterative process for the solution of equations that are not functions of time. That way is justifiable since it is a more correct model of the physical process. Cheng [16] discussed in great detail the stability of the solution and the need for introduction of simulated viscosity by means of a cutoff error in the difference equations for the sake of a stable final solution.

The equations are formulated in the form of a group (by means of variables ρ , ρu , ρv , E) since that way the gradients of the variables are smaller and there is less chance for interferences with the numerical computation that might develop because of them.

Of the existing methods we will discuss below principally those that deal with the solution of equations that are time dependent. In the studies by Lax, Wendroff [58] (1964), Brailovskaya [8] (1965), as well as Palumbo, Rubin [78] (1972), basic procedures that are very much alike are discussed for the solution of a series of equations in their [term unknown] form through an explicit two-stage method. These methods differ from each other only in their choices of technique to compute the finite differences at the grid points. The technique chosen has significant influence on the cutoff error that serves as artificial viscosity and plays an important role in stabilizing the solution for the series of equations.

/26

Based on the Lax, Wendroff [58] method, many variations were developed for various cases. Rubin, Burstein [90] (1967) used this method in solving for inviscid fluids with shock waves. Thommen [100] (1966) investigated the stability of viscous flow on a plate and around a step with it.

MacCormack [67] (1969) developed perfections and improvements to the basic scheme and used them to solve the interaction problem in MacCormack [71] (discussed in this research). Skoglund, Gay [94] (1969) also solved this problem by introducing some changes into the scheme. (The last mentioned papers were discussed at length in Section 2.1.3.3.)

Even the Brailovskaya method [8] was adopted for the solution of various problems, the most important of which are those of Allen, Cheng [2] (1970) who solved the flow behind a step, and of Carter [13] (1972) who solved the flow around a compression corner. (These papers were also described in detail in Section 2.1.3.3.)

The Brailovskaya [8] and MacCormack [67] schemes were adapted for use in this research and are formulated in detail in Part 4.

The Palumbo, Rubin [78] method is similar in principle to those of Lax-Wendroff and Brailovskaya. Its distinction lies in the better arranged computation of differences, according to which the calculation of each point depends on a larger region of points (12 in number) around it. This method solved the problem of compressive flow before and after a step.

The Harlow, Amsden [43] (1971) method is basically different from the previous ones. It describes an implicit scheme for two-dimensional or three-dimensional flow in which the pressure is calculated from Poisson's equation (which is obtained from the momentum and continuity equations). In this method the variables are solved as non-identical points in the grid meshes (p , ρ , T and u , v are calculated in two combined grids alternately by the Staggered Grid Method).

The Scala, Gordon [91] (1967) method is built on an implicit-explicit scheme, using the exponential transformation of the coordinates. There are two schemes to this method: one is implicit and solves the unknowns in each field through a system of linear equations that are solved iteratively; in the second, explicit scheme, the unknowns are computed separately for each point by means of repeated substitution. The two schemes are used alternately. /27

The last three methods noted are relatively new and have, in the meantime, been tried out for very simple problems and only for occasional special cases.

It seems proper to take note of some additional studies when comparing results of various numerical methods as to their accuracy and stability of solution. Brailovskaya et al. [9] (1970) and also Dorodnitsyn et al. [22] (1972) review developments of various methods, particularly for incompressible flow. Emery [24] (1968) and Tyler et al. [99] (1972) compare a number of methods for the solution of viscous flow problems and of a one-dimensional shock wave transition in inviscid flow.

2.2.3. Computation Techniques for Flows Including Shock Waves

Due to the physical (and mathematical) discontinuity of the shock wave strong inhibitions to a numerical solution arise, which necessitate the employment of various numerical techniques for their prevention. The most accepted one is the use of artificial viscosity through the cutoff error of the scheme or by addition of more terms to the scheme. The artificial viscosity "spreads" the discontinuity of the flow over a wider region than the actual physical width (this method is known as shock capturing). In all of these methods the artificial viscosity is so constituted as to be proportional to the gradients in the field of flow.

The following studies are concerned with quantitative and qualitative evaluations of artificial viscosity and with recommendations for its use in different cases. Hirt [44] (1968) investigated the stability of nonlinear equations based on testing the cutoff error, Davis, Mallinson [21] (1972) tested the influence of the cutoff error from preceding differences in various flow problems, in computation grids of a different size. Roache [87] (1972) found a connection between the various influences of artificial viscosity on the solution of the implicit scheme in the transient and steady states.

Goodrich et al. [37] (1972) developed a perfected method for adding artificial viscosity terms to the difference scheme, which is based on consideration of the gradients in both dimensions of each field of flow. (This method was used in the present research and is described in detail in Part 4.)

Another way to overcome discontinuity was modelled by MacCormack, Warming [68] (1973). The shock wave is removed from the region of the finite difference computation by assigning double values (which are connected to each other through shock wave transition formulas) to grid points passed by the shock wave and by calculation of preceding or following differences in their vicinity so as to avoid calculation of derivatives for the shock wave path itself. This method is called shock splitting and it was also tried (with partial success only) in this research.

/28

2.2.4. Finite Differences for Special Cases Related to Research Subjects

2.2.4.1. Boundary Layer Solutions

Since the methods for the solution of boundary layer equations with finite differences are important for understanding the solution of Navier-Stokes equations, we will describe their sources briefly. A detailed survey of existing difference methods is given by Paskonov, Chudov [80] (1968) and Blottner [7] (1970). Blottner [7] and also Waiter, Leblanc [102] (1971) and Jaffe, Smith [50] (1972) developed methods for the computation of boundary layers that also contain equations of the system's chemical composition. Jaffe, Smith and Lubard, Shetz [65] (1968) also discuss the influence of changes in the boundary conditions (line injections, suction, heating and cooling) on the results. The difference method by Flügge-Lotz, Er-Young [26] (1960) is particularly suitable for help in the solution of pressure interaction problems. Werle, Bertke [104] (1972) occupy themselves with computation of the separated boundary layer by assumption of a velocity profile and its introduction into the computational model.

2.2.4.2. Approximate Solutions of Navier-Stokes Equations

These solutions, even though they are not applicable for the most general problem, are of significance for cases where the entire field of flow, or part of it, is to be described approximately and in simple fashion.

Some solutions of Navier-Stokes equations through finite differences for viscous and noncompressive flow are given by Loer [64] (1971); Lascaux, Raviart [56] (1970); Welch et al. [103] (1965) and also by Ghia, Davis [34] (1974). The non-compressibility permits transformation of the variables u , v , ρ to ψ , ω through release of pressure, which enhances the final solution considerably. Gosman et al.'s [39] (1969) book describes the method of general solution for noncompressive flow with a change in heat, mass and chemical composition. Jamet [51] (1970) discusses the difference method for compression equations that are inviscid and time dependent. The study by Gottlieb, Gustaffson [40] (1974) assumes an approximate algebraic expression for the energy equation by assumption of a fixed overall temperature and solves the hyperbolic flow through finite differences with artificial viscosity.

2.3. Summary of the Main Changes and Improvements in the Present Study

/29

Below we will summarize the main changes and improvements to be found in this study, with reference to the most advanced

existing studies; we will also describe the principles of the experimental changes that were made, but not included, in the final computation methods for various reasons. The studies to which this part refers are those by MacCormack [67] and Skoglund, Gay [94] (which solve an interaction problem similar to the subject of this study), as well as by Carter [13] (solution of interaction around a compression corner through characteristics in the outer boundary).

2.3.1. The Computational Scheme

The basic difference scheme was prepared according to two methods in parallel: the Brailovskaya [8] method (according to the Carter [13] formulation) and the MacCormack [67] method. A number of changes and options were tried out with the basic scheme, to be used in accordance with specific purposes:

a) Change of grid structure in the x direction (not included in the final scheme):

In addition to the regular, uniform grid (where $\Delta x/\Delta y = 16$) there is a possibility to use a nonuniform grid, dense in the middle and spread out toward the corners (where $1.6 < \Delta x/\Delta y < 50$ and the ratio between the lengths of two adjacent meshes is 1.1), similar to the Skoglund, Gay [94] method, which is detailed in Paragraph 3.4.3.2 and in Appendices H and I). This option was not included in the final scheme since it caused large truncation errors and strong oscillations in the solution for the vicinity of the shock wave region (as detailed in Paragraph 4.1.1).

b) Differences of the fourth order in the x direction underneath the shock wave (not included in the final scheme):

This possibility helped at first to increase accuracy of computation in the regions with sharp gradients in the x direction (in a grid where $\Delta x \gg \Delta y$), when the differences in the x direction are computed to an accuracy of $O(\Delta x^4)$, as against the regular computation with an accuracy of $O(\Delta x^2)$. Details of this method are given in Paragraph 3.4.3.1 and in Appendix H. This option was also not included in the final scheme since strong oscillations, whose origin is in the contact area between the regions of second order computation and fourth order computation, were noted in the computation. (Additional details are found in Paragraph 4.1.2.)

c) Addition of artificial viscosity (included as option in the final scheme):

The addition of terms for the artificial viscosity aids in stabilizing the solution, particularly for intense interactions.

Its employment helps, particularly during the first stages of computation when the results are still far from the final solution and subject to great changes. Expressions for artificial viscosity are based on those by Skoglund, Gay [94] with slight changes, as detailed in Paragraph 3.4.4. The use of this option aids in the solution but requires preliminary computation for optimization of several numerical coefficients (details in Paragraph 4.1.3).

/30

d) Testing stability and convergence (included as option in the final scheme):

The possibility is offered to calculate the relative change of the variables u , p , T and the remainders of the four differential equations for each point of the computational grid, at each step of the iteration. The average maximum values of these changes are a measure of the stability of the computation and the convergence of the solution (as defined in detail in Paragraph 3.5.3.1). These tests are not performed automatically during the computation; they are rather offered as optional choice (because they increase the memory stored and the computation time by nearly a factor of two).

2.3.2. Boundary Conditions

a) Removal of the shock wave from the computational field (not included in the final scheme):

In addition to the usual difference computation over the whole field of flow with the shock wave, the possibility was provided to remove the shock wave from the field so that the flow conditions in front of it and behind it would serve as boundary conditions, as described in Paragraph 3.3.1.5. This method (which, in the past, has not been tried for this type of problem) is called shock splitting, or the method of "discontinuous" computation of the shock wave path. The use of this method does not appear suitable at this stage since significant oscillations were generated along the graded border of the shock wave (as explained in detail in Paragraph 4.1.4).

b) Boundary condition of the external flow characteristics (exists in the final computation scheme):

This boundary condition is defined similar to Carter's [13] formulation and its main purpose is consideration of the influence of streamlines from the reflected shock wave on the outer boundary. This permits the cutting down of the computational field to the region close to the termination of the boundary layer (in contrast to previous studies in which the outer border was extended so that the reflected streamlines would not exit through it but rather in the downstream direction, a procedure

requiring a computational grid that is much too big). The method is explained in detail in Paragraph 3.3.1.4.

c) Boundary condition for density along the plate (exists in the final computation scheme):

This condition is computed (due to considerations for the stability of the numerical computation) on the assumption that at close range in front of the plate, all along it (in the separated region as well) there prevails the condition

$\frac{\partial T}{\partial y}|_w = 0$ as well as the adiabatic condition $\frac{\partial P}{\partial y}|_w = 0$ (as ex-

plained in Paragraph 3.3.1.2.). In some of the previous studies this boundary condition was computed from the solution to one of the equations for flow next to the plate, or through extrapolation of the density from the field to the plate. Such procedures are essentially more accurate but are sometimes cause for instability in the numerical calculation; the above-mentioned method is therefore preferable. /31

d) Polhausen profile at the entrance cross section (exists in the final scheme):

Boundary conditions at the entrance cross section are computed according to the Polhausen method for profiles of flow in supersonic boundary layers (Paragraph 3.3.1.1).

2.3.3. Parametrical Analysis of Interaction Characteristics

The computations described in this paragraph were carried out according to the final scheme in which the grid is uniform in the x and y directions; second order differences are applied for the entire computation; the shock wave is inside the field ("continuous" computation); artificial viscosity has been introduced and the boundary conditions b), c) and d) from Paragraph 2.3.2 apply.

a) Speed of convergence

In the above-mentioned computation method the solution converges, after only a few hundred iterations, to results with a relatively large truncation error; yet their accuracy is only slightly inferior when compared to previous methods of computation (which required considerably longer computation time). This way the computation is serviceable and practical and, indeed, 100 different computer runs were completed for testing the parameters of the results, each run taking up only 3-5 minutes of CPU time.

b) Parametric analysis of the results

While in previous studies analyses of results were carried out only in a few cases (because computation time was relatively long) a detailed analysis of the interaction was performed in this study, according to the principal parameters that influence it. The influence of the Mach number in the range $2 < M_0 < 4.5$, the Reynolds number $10^4 < Re_{x_s} < 10^6$, the shock wave intensity $1.2 < p_e/p_0 < 3.2$, the shock wave distance from the leading edge $3 \text{ cm} < x_s < 9 \text{ cm}$ and of the Prandtl number $0.72 < Pr < 1.0$, was tested. Also tested was the influence of heat transfer (a non-adiabatic wall) and mass transfer (suction and injection) along the plate.

c) Detailed analysis of the influence of suction on the separated region

A detailed analysis of suction influence, in combination with various flow conditions, on the interaction in general and on the separated region in particular was carried out. The required amount of suction, for each combination with Re_{x_s} ; p_e/p_0 ; M_0 to avoid boundary layer separation, was determined. These results have much practical application since the prevention of separation improves the performance of aircraft components -- particularly of control surfaces and jet engine inlets -- around which this interaction takes place.

3. Computation System

/32

3.1. Basic Equations

3.1.1. Dimensional Flow Equations

The basic flow equations are the Navier-Stokes momentum equations, the continuity equations, as well as the fluid state equation and the formula for the temperature dependence of viscosity. The equations meet the following assumptions:

- a) The coefficient of bulk viscosity is neglected.
- b) The coefficient of viscosity is a function of temperature, according to the Sutherland formula.
- c) The state equations are for an ideal gas.

Accordingly, the noninstantaneous equations are written for a viscous, compressible, heat-conducting fluid in a two-dimensional Cartesian system (per Schlichting [92])

Continuity equation

$$\frac{\partial \rho^*}{\partial t^*} + \frac{\partial}{\partial x^*}(\rho^* u^*) + \frac{\partial}{\partial y^*}(\rho^* v^*) = 0 \quad (3-1a)$$

Momentum equation
in the x direction

$$\rho^* \frac{\partial u^*}{\partial t^*} + \rho^* u^* \frac{\partial u^*}{\partial x^*} + \rho^* v^* \frac{\partial u^*}{\partial y^*} = \frac{\partial}{\partial x^*}(\bar{\sigma}_{xx}^*) + \frac{\partial}{\partial y^*}(\bar{\tau}_{xy}^*) \quad (3-1b)$$

Momentum equation
in the y direction

$$\rho^* \frac{\partial v^*}{\partial t^*} + \rho^* u^* \frac{\partial v^*}{\partial x^*} + \rho^* v^* \frac{\partial v^*}{\partial y^*} = \frac{\partial}{\partial x^*}(\bar{\tau}_{xy}^*) + \frac{\partial}{\partial y^*}(\bar{\sigma}_{yy}^*) \quad (3-1c)$$

Energy equation

$$\begin{aligned} \rho^* c_p \frac{\partial T^*}{\partial t^*} + \rho^* u^* c_p \frac{\partial T^*}{\partial x^*} + \rho^* v^* c_p \frac{\partial T^*}{\partial y^*} = \\ = u^* \frac{\partial p^*}{\partial x^*} + v^* \frac{\partial p^*}{\partial y^*} + \frac{\partial}{\partial x^*}(\bar{q}_x^*) + \frac{\partial}{\partial y^*}(\bar{q}_y^*) + \Phi \end{aligned} \quad (3-1d)$$

Equation of state

$$p^* = R \rho^* T^* \quad (3-2)$$

Sutherland's formula for viscosity

$$\mu^* = C \frac{T^{*3/2}}{S^* + T^*} \quad (3-3)$$

*This assumption is correct for a monatomic gas in which there is no internal degree of freedom for the molecule. This does not hold true for a multiatomic gas and the coefficient can reach the order of magnitude of the regular viscosity coefficient, particularly within a shock wave. Since there is no good resolution within the wave in the present computation the volumetric viscosity can be neglected. Additional details on this subject are offered by Vincenti, Kruger [101] (1965).

when

$$R_{air} = 287.04 \frac{m^2}{sec^2 \cdot ^\circ K}$$

$$S^* = 110.^\circ K$$

Stresses in the momentum equation are defined by

$$\left\{ \begin{array}{l} \sigma_x^* = \bar{\sigma}_{xx}^* + P^* = \mu^* \left[2 \frac{\partial u^*}{\partial x^*} - \frac{2}{3} \text{div}(u^*) \right] = \frac{2}{3} \mu^* \left(2 \frac{\partial u^*}{\partial x^*} - \frac{\partial v^*}{\partial y^*} \right) \\ \sigma_y^* = \bar{\sigma}_{yy}^* + P^* = \mu^* \left[2 \frac{\partial v^*}{\partial y^*} - \frac{2}{3} \text{div}(u^*) \right] = \frac{2}{3} \mu^* \left(2 \frac{\partial v^*}{\partial y^*} - \frac{\partial u^*}{\partial x^*} \right) \\ \tau_{xy}^* = \bar{\tau}_{xy}^* = \mu^* \left(\frac{\partial u^*}{\partial y^*} + \frac{\partial v^*}{\partial x^*} \right) \end{array} \right. \quad (3-4)$$

See note at the end of the paragraph.

The dissipation function in the energy equation is defined by

$$\bar{\Phi} = \mu^* \left[2 \left(\frac{\partial u^*}{\partial x^*} \right)^2 + \left(\frac{\partial v^*}{\partial x^*} + \frac{\partial u^*}{\partial y^*} \right)^2 + 2 \left(\frac{\partial v^*}{\partial y^*} \right)^2 - \frac{2}{3} \left(\frac{\partial u^*}{\partial x^*} - \frac{\partial v^*}{\partial y^*} \right)^2 \right] \quad (3-5)$$

The terms for heat conductivity are given by

$$\left. \begin{array}{l} Q_x^* = k^* \frac{\partial T^*}{\partial x^*} \\ Q_y^* = k^* \frac{\partial T^*}{\partial y^*} \end{array} \right\} \quad (3-6)$$

We define the function of total energy for the energy equation as

$$E^* = \rho^* \left[c_v T^* + \frac{1}{2} (u^{*2} + v^{*2}) \right] \quad (3-7)$$

Note: The stresses in the momentum equation are based on Hooke's Law for fluids, whose general formula is

34

$$\bar{\sigma}_{ij}^* = (-p^* + \lambda^* u_{i,j}^*) \delta_{ij} + \mu^* (u_{i,j}^* + u_{j,i}^*)$$

Stokes' assumption $\lambda^* + \frac{2}{3} \mu^* = 0$ is set against this formula (its significance being the neglect of volumetric viscosity). That is how we obtain Eqs. (3-4).

3.1.2. Definition of Non-dimensional Variables

We will define the system of non-dimensional variables as follows:

$$\left. \begin{aligned} x &= \frac{x^*}{x_s^*} & y &= \frac{y^*}{x_s^*} & \dot{t} &= \frac{\dot{t}^*}{t_{REF}^*} = \frac{t^*}{x_s^*/u_0^*} \\ u &= \frac{u^*}{u_0^*} & v &= \frac{v^*}{u_0^*} & & \\ \rho &= \frac{\rho^*}{\rho_0^*} & P &= \frac{p^*}{\rho_0^* u_0^{*2}} & T &= \frac{T^*}{u_0^{*2}/C_p} \\ \mu &= \frac{\mu^*}{\mu_0^*} & \gamma &= \frac{C_p}{C_v} & S &= \frac{S^*}{u_0^{*2}/C_p} \\ E &= \frac{E^*}{\rho_0^* u_0^{*2}} = \rho \left[T/\gamma + (u^2 + v^2)/2 \right] \end{aligned} \right\} \quad (3-8)$$

We will also define the coefficients:

$$\left. \begin{aligned} \text{Reynolds number} & R_{E_{x_s}} = \frac{\rho_0^* u_0^* x_s^*}{\mu_0^*} \\ \text{Mach number} & M = \left[\frac{u^{*2} + v^{*2}}{\gamma R T^*} \right]^{1/2} \\ \text{Prandtl number} & Pr = \frac{\mu^* C_p}{k^*} \end{aligned} \right\} \quad (3-9)$$

When x^*_s -- reference length (distance from the leading edge to the shock wave continuation impinges on the plate);
 (\cdot)₀ -- condition of external flow at the entrance cross-section.

We thus obtain the non-dimensional values for external flow at the entrance cross-section (reference values):

/35

$$u_0 = 1 \quad T_0 = \frac{1}{(\gamma-1) M_0^2} \quad p_0 = \frac{1}{\gamma M_0^2} \quad (3-10)$$

$$\rho_0 = 1 \quad \mu_0 = 1$$

Since $(V^*)_0 = 0$ (see Paragraph 3.3.1.1), we obtain $V_0 = 0$ when

$$M_0 = (M)_0 = \left[\frac{u_0^{*2}}{\gamma R T_0^*} \right]^{1/2}$$

3.2. System of Non-dimensional Equations

A system of non-dimensional equations is obtained from these last expressions. The four differential equations will be written in group form for the group variables ρ , ρu , ρv , E . This form is handier for use in numerical computation (the gradients of these are smaller and prevent the tendency to diverge).

The general form of the differential equation is

$$\frac{\partial W}{\partial t} + \frac{\partial F}{\partial x} + \frac{\partial G}{\partial y} = S = \frac{\partial A}{\partial x} + \frac{\partial B}{\partial y} \quad (3-11)$$

when

$$W = \begin{bmatrix} \rho \\ \rho u \\ \rho v \\ E \end{bmatrix} \quad F = \begin{bmatrix} \rho u \\ \rho + \rho u^2 \\ \rho u v \\ u(E + p) \end{bmatrix} \quad G = \begin{bmatrix} \rho v \\ \rho u v \\ \rho + \rho v^2 \\ v(E + p) \end{bmatrix}$$

$$S = \frac{1}{Re} \frac{\partial}{\partial x} \begin{bmatrix} 0 \\ \sigma_x \\ \tau_{xy} \\ \frac{\mu}{Pr} \frac{\partial T}{\partial x} + u \sigma_x + v \tau_{xy} \end{bmatrix} + \frac{1}{Re} \frac{\partial}{\partial y} \begin{bmatrix} 0 \\ \tau_{xy} \\ \sigma_y \\ \frac{\mu}{Pr} \frac{\partial T}{\partial y} + u \tau_{xy} + v \sigma_y \end{bmatrix} \quad (3-11a)$$

when (in non-dimensional formulation)

/36

$$\left. \begin{aligned} \sigma_x &= \frac{2}{3} \mu \left(2 \frac{\partial u}{\partial x} - \frac{\partial v}{\partial y} \right) \\ \sigma_y &= \frac{2}{3} \mu \left(2 \frac{\partial v}{\partial y} - \frac{\partial u}{\partial x} \right) \\ \tau_{xy} &= \mu \left(\frac{\partial u}{\partial y} + \frac{\partial v}{\partial x} \right) \\ E &= p \left[\frac{T}{\gamma} + \frac{1}{2} (u^2 + v^2) \right] \end{aligned} \right\} \quad (3-11b)$$

the equation of the non-dimensional state is

$$\rho = \frac{\gamma-1}{\gamma} p T \quad (3-12)$$

The formula for non-dimensional viscosity is

$$\mu = \frac{S + \frac{1}{(\gamma-1) M_0^2}}{S + T} \left[(\gamma-1) M_0^2 T \right]^{3/2} = \sqrt{(\gamma-1) M_0^2 T} \frac{1 + S(\gamma-1) M_0^2}{1 + S/T} \quad (3-13)$$

for $S = 110^\circ K$

$$S = \frac{S^*}{u_0^{*2} / c_p} = \frac{S^*}{(\gamma-1) M_0^2 T_0^*}$$

since the formula for non-dimensional viscosity also depends on the temperature (dimensional) T_0^* of the external flow.

Four differential equations (3-11) and two algebraic equations (3-12) and (3-13) represent the system of six equations in six unknown quantities, when the procedure for solution is in fact carried out through the differential equations (into which pressure p and viscosity μ are inserted from the algebraic equations) from which solutions for the unknowns ρ , u , v , T are obtained.

In addition to the solution for those unknowns, the Mach number and the flow function in the field of flow are also computed by means of the following non-dimensional connections:

$$\text{Mach number} \quad M = \left[\frac{u^2 + v^2}{(\gamma-1) T} \right]^{1/2} \quad (3-14)$$

Flow function $\psi(b) = \psi(a) + \int_a^b (u dy - v dx)$ (3-15)

when a, b are random points in the field of flow (the flow function is computed according to the definition

$$\left(\rho u = \frac{\partial \psi}{\partial y} ; \rho v = -\frac{\partial \psi}{\partial x} \right)$$

The coefficients of friction and heat transfer along the length of the plate are also computed by means of dimensionless values, as follows:

/37

Friction coefficient $C_f = \frac{2}{Re_{x_s}} \mu \left. \frac{\partial u}{\partial y} \right|_w$ (3-16)

Heat transfer coefficient $C_q = \frac{(\gamma-1) M_0^2}{Pr \cdot Re_{x_s}} \mu \left. \frac{\partial T}{\partial y} \right|_w$ (3-17)

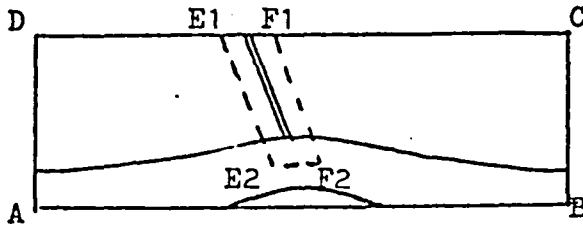
(Computation of heat transfer is carried out only for non-adiabatic boundary conditions.) Details about development of the last four non-dimensional equations are given in Appendix A.

3.3. Initial and Boundary Conditions

The above-defined equations constitute a system of partial differential, nonlinear equations of parabolic characteristics vs. time, which, in its permanent form, becomes a system with aliphatic characteristic. The problem is defined as an initial value-boundary value problem and requires definition of the boundary condition along the length of all boundaries of the field of computation and the initial condition inside each field of computation. For the four differential equations we require boundary conditions and initial conditions for the components of velocity v; u and for density ρ and temperature T. (The pressure p and viscosity μ are computed, according to the boundary and initial conditions, by means of the algebraic equations of state and viscosity.)

3.3.1. Boundary Conditions

The boundaries of the computational field include four sections, as defined in the following diagram.



AD Entrance cross section
 AB Plate
 BC Exit cross section
 CD External flow

E_2F_2 (as shown in Fig. 2).

According to the computational method where the shock wave is removed from the region considered by the computation (the "non-continuous" method), the external flow included two sections F_1C and DE_1 plus the boundary section upstream from the shock wave, E_1E_2 and the boundary section downstream of it, E_2F_2 (as shown in Fig. 2).

3.3.1.1. Entry Cross Section Conditions

/38

With the assumption of $\frac{\partial p}{\partial x} = 0$ and $\frac{\partial T}{\partial y} \Big|_{y=0} = 0$ in the vicinity of the entry cross section, a velocity profile is obtained through Polhausen's method (which assumes the velocity profile as the progression range of the coordinate normal to the plate, which fulfils the conditions on the plate and at the edge of the boundary layer) in the following manner (all expressions non-dimensional):

$$\left. \begin{aligned} \frac{u}{u_0} &= 2\eta - 2\eta^3 + \eta^4 \\ u_0 &= 1 \end{aligned} \right\} \quad (3-18)$$

$$\left. \begin{aligned} \frac{T}{T_0} &= 1 + \sqrt{Pr} \frac{\gamma-1}{2} M_0^2 \left[1 - \left(\frac{u}{u_0} \right)^2 \right] \\ T_0 &= \frac{1}{(\gamma-1)M_0^2} \end{aligned} \right\} \quad (3-19)$$

Under assumption of fixed pressure (since $\partial p / \partial y = 0$ at the entry cross section)

$$\left. \begin{aligned} \frac{p}{p_0} &= \frac{1}{T/T_0} \\ p_0 &= 1 \end{aligned} \right\} \quad (3-20)$$

The profiles of T ; u ; p are here given as a function of η , the connection between η and y is given as

$$y = 5.836 \sqrt{\left(\frac{\mu_w}{\mu_0} \right) \left(\frac{T_0}{T_w} \right) \left(\frac{x_0^+ / x_s^+}{Re} \right)} \left[\eta + \sqrt{Pr} \frac{\gamma-1}{2} M_0^2 \left(\eta + \frac{4}{3} \eta^3 + \frac{8}{3} \eta^5 - \frac{2}{3} \eta^6 - \frac{4}{7} \eta^7 + \frac{1}{2} \eta^8 - \frac{1}{9} \eta^9 \right) \right] \quad (3-21)$$

Component v of the velocity at the entry cross section may be neglected

$$V = 0 \quad (3-22)$$

Detailed development of the boundary conditions at the entry cross-section are given in Appendix B.

3.3.1.2. Boundary Conditions Along the Plate

From the nonslip conditions along the plate, we obtain for velocity components

$$u = 0 \quad (3-23)$$

$$v = 0 \quad (3-24)$$

When mass transfer via the plate is made possible, then the v condition changes to: 39

$$\text{For injection} \quad v > 0 \quad (3-24a)$$

$$\text{For suction} \quad v < 0$$

(In these cases the value of v is on the order of a few percent of u .)

The adiabatic condition along the plate dictates the boundary condition for temperature T

$$\frac{\partial T}{\partial y} = 0 \quad (3-25)$$

When the plate is kept at a fixed temperature, the T condition changes to

$$T = \text{const.} \quad (3-25a)$$

The boundary condition for density can be computed in several ways:

(a) from one of the motion equations (continuity or momentum), which assumes a simpler form next to the plate;

(b) through extrapolation from the third or fourth order of density in the field of flow, towards the plate;

(c) from knowledge of pressure and temperature at the plate (through the state equation) when the temperature is given

per (3-25) or (3-25a) and pressure at the plate is computed on the assumption that next to the plate the relation

$$\frac{\partial p}{\partial y} = 0 \quad (3-26)$$

is valid. This condition (which prevails in the regular boundary layer over its entire width) is particularly well fulfilled in this interaction in the lower part of the boundary layer (which is close to the plate) and in the separated region, in spite of the interaction influences. The assumption is therefore justified (see the note).

Of the three ways available, the last one was chosen due to consideration of stability for the numerical computation (even though it is less accurate, basically, than the other two). The main reason was the tendency of solutions available through the other two methods (particularly the first one) to oscillations, since the local computation of the derivatives close to the plate is not accurate and distorts the numerical values.

Note: During previous tests in this investigation (before formula (3-26) was introduced for computation of the boundary conditions) and also in other computational studies, it was found that the assumption of $\partial p / \partial y = 0$ is valid as a very good approximation for the entire length of the plate; its use is thus entirely justified.

/40

3.3.1.3. Exit Cross Section Boundary Conditions

The location of the exit cross section is so determined that no further significant changes in flow characteristics can occur in the x direction. It can therefore be assumed with good approximation that

$$\frac{\partial u}{\partial x} = \frac{\partial v}{\partial x} = \frac{\partial p}{\partial x} = \frac{\partial \Gamma}{\partial x} = 0 \quad (3-27)$$

That is a bit misleading, because there are very small gradients in the x direction (because of the renewed development of the boundary layer downstream of the interaction), but due to the hyperbolic characteristics of the boundary layer these distortions in the flow field (which are relatively small) do not have any influence on the interaction region; so the distortion, if it exists at all, is only a local one.

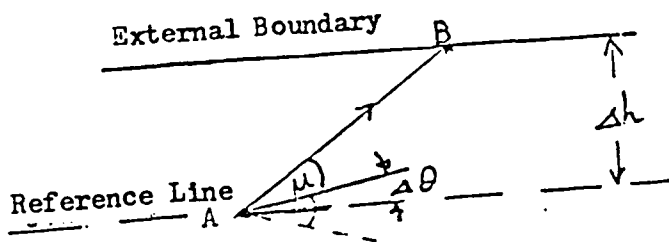
3.3.1.4. External Flow Boundary Conditions

The location of this boundary is so determined as to be in the inviscid region, as close as possible to the plate but sufficiently far from the region where changes in the interaction are taking place. The order of magnitude of this distance is $(2-3)\delta_0$ (a computational assessment of this magnitude is given in Appendix D).

In contrast to previous studies (like Skoglund, Gay [94] and MacCormack [67]) where this boundary was chosen to be sufficiently distant so that its boundary conditions were uniform and fixed (and reflected waves went out through the exit cross section), in this investigation the boundary conditions are influenced, because of the proximity of the external boundary to the region of interaction, by the form the development of the boundary layer assumes and by the compression and expansion streamlines that emanate from it. These conditions are thus not of uniform nature and they must be computed point by point from the actual conditions in the flow field.

Uniform flow characteristics are therefore used for flow outside the boundary layer along the directions of the characteristics, so that the external boundary condition is updated during the computation process in accordance with changes of the flow characteristics in the field.

Basically, this is done in 41 the following stages:



(a) A reference line is fixed from which characteristics* fan out to the external boundary; this line is close to the external boundary and outside the boundary layer;

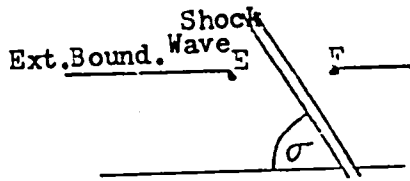
(b) For each point A on the reference line the direction of the local flow $\Delta\theta$ and of the local Mach angle μ is computed; their sum β gives the direction of this characteristic;

$$\beta = \mu + \Delta\theta = \tan^{-1} \left(\frac{1}{\sqrt{M_A^2 - 1}} \right) + \tan^{-1} \left(\frac{V_A}{U_A} \right) \quad (3-28)$$

(c) Point B is fixed at the external boundary (where the flow characteristics are identical to those of A) by extending

*Two characteristics emerge from each point, as shown in the diagram, but for the purpose of showing the influence of the streamlines on the external boundary, the upper characteristic is necessary (which reaches that boundary).

a straight line from A to the external boundary at angle β . An approximately straight characteristic* is assumed, which is justified since Δh is very small. This computation is done along the length of the external boundary, except for the point where the shock wave enters the field.



(d) Computation for both sides of the shock wave at the external boundary is carried out by means of Rankine's and Hugoniot's shock wave formulas. The shock wave is defined as pressure jump

$$S_h = \frac{P_F}{P_E}$$

which is compelled at the external boundary between the two reference points E and F. The flow characteristics at point F are computed from those of E (where the values are fixed by the characteristics scheme explained in the foregoing paragraphs).

Shock wave transition formulas for stage (d):

/42

$$U_F = (U_E \sin \sigma + V_E \cos \sigma) \frac{(\gamma - 1) M_E^2 \sin^2 \sigma + 2}{(\gamma - 1) M_E^2 \sin^2 \sigma} \sin \sigma + (U_E \cos \sigma - V_E \sin \sigma) \cos \sigma \quad (3-29)$$

$$V_F = (U_E \sin \sigma + V_E \cos \sigma) \frac{(\gamma - 1) M_E^2 \sin^2 \sigma + 2}{(\gamma - 1) M_E^2 \sin^2 \sigma} \cos \sigma + (U_E \cos \sigma - V_E \sin \sigma) \sin \sigma \quad (3-30)$$

$$T_F = T_E \frac{\left(1 + \frac{\gamma - 1}{2} M_E^2 \sin^2 \sigma\right) \left(\frac{2\gamma}{\gamma - 1} M_E^2 \sin^2 \sigma - 1\right)}{\frac{(\gamma + 1)^2}{2(\gamma - 1)} M_E^2 \sin^2 \sigma} \quad (3-31)$$

The pressure given is provided by the compulsory pressure jump

$$P_F = P_E \cdot S_h \quad (3-32)$$

Density is provided by the state equation

*The characteristics should actually be curved because straight characteristics are present in non-rotational flow only; this non-rotationality is not preserved in this instance because of the intersection between the shock wave and the streamlines, which causes curvature of the wave. This phenomenon is neglected when the computational grid is very fine and so it is permitted to assume the characteristics of this region to be straight lines.

$$P_F = \frac{\gamma}{\gamma-1} \frac{P_F}{T_F} \quad (3-33)$$

The angle of the shock wave σ is given by the relation

$$\sigma = \sin^{-1} \left[\frac{\sqrt{(Sh + \frac{\gamma-1}{\gamma+1}) \frac{T+1}{2\gamma}}}{ME} \right] \quad (3-34)$$

Details of the development of these equations are given in Appendix F.

It must be pointed out that since the flow characteristics upstream of the shock wave at E change as functions of flow characteristics in the field, the characteristics of F will also be dependent on these changes so that here is an expression of the influence of interaction on the incident shock wave itself (while previous studies assumed fixed values for both sides of the shock wave for the entire process of computation).

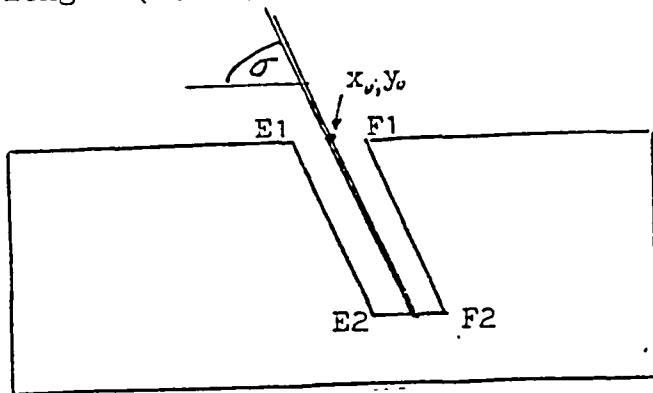
Note: In general the pressure ratio p_e/p_o serves as characteristic parameter for the interaction, and a ratio p_F/p_E must be found that will match it. This procedure is iterative and explained fundamentally in Appendix C.

3.3.1.5. Shock Boundary Conditions for the Shock Fitting ("Noncontinuous") Method

/43

This method is intended to take the shock wave out of the field of computation, with the purpose of attenuating the disturbances of stability that arise because of the strong gradients along the shock path.

In this method the boundary of the field of computation is assumed to be on both sides of the shock wave along its entire length (for the external flow boundary to the sonic line).



The process of computation is carried out as follows:

- (a) From the shock wave angle (Eq. 3-34), we find the initial location of the shock wave in the field, and from it we get the boundaries $e = E_1E_2$,

upstream of the shock wave and $f = F_1 F_2$, downstream of it (assuming a straight shock wave);

(b) Variable values along e are determined from the upstream conditions while values along f are determined from the values in e, by means of formulas for the shock wave transition given in Paragraph 3.3.1.4;

(c) After updating the variable values in the entire flow field (through a difference scheme) the local gradient of the shock wave is brought up to date through

$$\sigma(y) = \sin^{-1} \left[\frac{\sqrt{\left(\frac{p_+(y)}{p_-(y)} + \frac{\gamma-1}{\gamma+1} \right) \frac{\gamma+1}{2\gamma}}}{Me(y)} \right] \quad (3-35)$$

and according to it the location of the shock wave is updated

$$x_s(y) = x_0 + \int_{y_0}^y \tau_g [\sigma(y)] dy \quad (3-36)$$

The computation is continued per paragraphs (b) and (c).

3.3.2. Initial Conditions

/44

From the purely mathematical point of view no importance attaches to the way initial conditions are chosen because, if there is a single value solution (which is assumed) it must be an expression that is not a function of the initial condition. However, when we talk of a numerical solution for an iterative process, which represents integration over time, it must be taken into account that the closer initial conditions come to the final solution, the faster convergence will occur and reduce computation time.

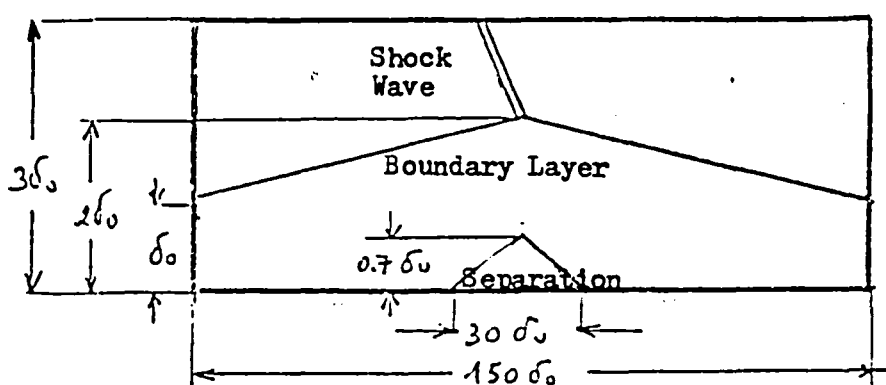
Initial conditions are chosen so as not to conflict with two main limitations:

(a) It is undesirable for initial conditions to be too far from the solution since oscillations in the values of the variables can develop during the computation procedure (particularly during the early stages), which can not always be restrained (see also Roache [86]).

(b) Initial conditions that are too close to the solution impair the general nature of the computational scheme and its

ability to solve various problems where the solution is not always known beforehand.

Initial conditions for computation have therefore been assumed as combination of the following data (as in Skoglund, Gay [94]):



(a) The profile of the boundary layer was assumed to be of slightly larger shape up to the shock wave and smaller again afterwards in the downstream direction, with a small separated region existing at the end of the incident shock wave;

(b) The shock wave itself spread to the width of two meshes outside the boundary layer and to the width of 4-10 meshes in the subsonic part of the boundary layer. The flow characteristics downstream of the shock wave (in the supersonic region) were assumed to be uniform and were computed from formulas for shock wave transition. Definition of these conditions is simple and general and can be applied in identical manner for the entire combination of flow conditions. That way we get an initial guess at the solution, which allows speeding up of the convergence.

3.4. Method of Finite Difference Solutions

/45

3.4.1. General

As mentioned before, two difference schemes were prepared simultaneously; that of Brailovskaya and that of MacCormack (though most of the computations were later carried out with the Brailovskaya scheme, since it offered savings in computer time and simplicity of operation, as will be explained in Paragraph 4.1.1).

The two methods share a similar truncation error:

$$\left. \begin{aligned}
 E_T(\text{MAC.}) &= o(\Delta t^2, \Delta x^2, \Delta y^2) \\
 E_T(\text{BRA.}) &= o(\Delta t, \Delta x^2, \Delta y^2)
 \end{aligned} \right\} \quad (3-37)$$

The difference in dependence on Δt has almost no influence since the gradients vs. time are very small in the asymptotic solution (as was also shown by Carter [13] in his comparison of accuracies in various schemes).

Those two methods have already been employed successfully in the solution for flows with mixed regions (parabolic, hyperbolic and aliphatic ones), as explained in paragraph 2.1.3.3).

3.4.2 Definition of the Region of Computation

Based on consideration for achieving the maximum possible accuracy and the minimum size of computational field required that would permit inclusion of all interaction phenomena (as is done in the sources listed in paragraph 2.1.3) the dimensions of the field of computation were determined as shown below:

$$\left. \begin{aligned}
 \text{Length of field} & \quad l_x = 150 \delta_0 \\
 \text{Width of field} & \quad l_y = 3 \delta_0
 \end{aligned} \right\} \quad (3-38)$$

The considerations for this choice of dimensions are detailed in appendix D'.

Location of the shock wave was always fixed so that the intersection between its continuation and the plate would be in the center of the region of computation.

3.4.3 Computation Grid Dimensions

3.4.3.1 General

Difference computations were prepared simultaneously for two grids: one of them had a uniform mesh size while in the other the longitudinal dimensions of the meshes increased directly with their distance from the center.

The grid mesh dimensions were also set (similar to the field dimensions) as fixed multiples of δ_0 and not as invariable longitudinal dimensions since the ratio between them and the boundary layer thickness is an important parameter which determines the accuracy of results.

Computation of the number of points in the grid through these two methods is presented in appendix E'. Considerations for deciding the mesh dimensions are explained in appendix D'. The various difference schemes in all methods, as well as an analysis of result accuracies, are detailed in appendices G' and H'.

3.4.3.2 Uniform Computation Grid

Dimensions for the grid meshes were fixed at

$$\left. \begin{aligned} \Delta x &= 2 \delta_0 \\ \Delta y &= 0.125 \delta_0 \end{aligned} \right\} \quad (3-39)$$

resulting in a ratio of $\Delta x / \Delta y = 16$.

A number of difference schemes were prepared for this grid; two of them offer the accustomed accuracy (of the second order) with the Brailovskaya and MacCormack methods, one of them offers improved accuracy (of the fourth order in the x-dimension) with the Brailovskaya method, which is designated to increase the accuracy of computation in the regions with strong gradients in the x-direction. All of the schemes are explained at length in appendices G' and H'.

3.4.3.3 Non-Uniform Grid

Grid dimensions were fixed as

$$\left. \begin{aligned} \Delta x_{\min} &= 0.2 \delta_0 & \Delta x_{\max} &\approx 6 \delta_0 \\ \frac{\Delta x_{\max}}{\Delta y} &\approx 50 & \frac{\Delta x_{\min}}{\Delta y} &= 1.6 & \Delta y &= 0.125 \delta_0 \end{aligned} \right\} \quad (3-40)$$

Δx increased gradually towards the boundaries of the field according to the formula for geometrical progression, with a growth ratio of $q = 1.1$.

3.4.4 Finite Difference Scheme

Based on the general formulation of the differential equations (3-11), two difference schemes were written for the general case:

47

Brailovskaya scheme

$$\begin{aligned} \bar{W}_{m,n}^{t+1} &= W_{m,n}^t - \Delta t \left[\left(\frac{\Delta F}{\Delta x} \right)_{m,n}^t + \left(\frac{\Delta G}{\Delta y} \right)_{m,n}^t - S_{m,n}^t \right] \\ W_{m,n}^{t+1} &= W_{m,n}^t - \Delta t \left[\left(\frac{\Delta F}{\Delta x} \right)_{m,n}^{t+1} + \left(\frac{\Delta G}{\Delta y} \right)_{m,n}^{t+1} - S_{m,n}^t \right] \end{aligned} \quad (3-41)$$

with the truncation error $E_T(W) = o(\Delta t, \Delta x^2, \Delta y^2)$

MacCormack Scheme

$$\bar{W}_{m,n}^{t+1} = W_{m,n}^t - \Delta t \left[\left(\frac{\Delta F}{\Delta x} \right)_{m,n}^t + \left(\frac{\Delta G}{\Delta y} \right)_{m,n}^t - S_{m,n}^t \right] \quad (3-42)$$

$$W_{m,n}^{t+1} = \frac{1}{2} \left\{ W_{m,n}^t + \bar{W}_{m,n}^{t+1} - \Delta t \left[\left(\frac{\Delta F}{\Delta x} \right)_{m,n}^{t+1} + \left(\frac{\Delta G}{\Delta y} \right)_{m,n}^{t+1} - S_{m,n}^{t+1} \right] \right\}$$

with the truncation error $E_T(W) = o(\Delta t^2, \Delta x^2, \Delta y^2)$

For this scheme a division of the difference computation exists for the x and y directions. Detailed formulation of the two schemes and of the various stages of computation in them is given in appendix H'.

The general procedure of computation is as follows:

a) From the last $W_{m,n}^t$ values $F_{m,n}^t$; $G_{m,n}^t$; and $S_{m,n}^t$ are computed by means of definitions in formulas (3-11).

b) $\bar{W}_{m,n}^{t+1}$ is computed from the first stage of the difference scheme and from it the expressions $\bar{F}_{m,n}^{t+1}$; $\bar{G}_{m,n}^{t+1}$ and $\bar{S}_{m,n}^{t+1}$ are calculated (but only for the MacCormack scheme).

c) $W_{m,n}^{t+1}$ is computed from the second stage of the difference scheme and through it the final computation of the variables is carried out.

The explicit definition of the solved variables in the equation system is as follows:

The variables determined by the differential equations

$$\begin{bmatrix} \rho \\ u \\ v \\ T \end{bmatrix} = \begin{bmatrix} w(1) \\ \frac{w(2)}{w(1)} \\ \frac{w(3)}{w(1)} \\ \gamma \left[\frac{w(4)}{w(1)} - \frac{w(2)^2 + w(1)^2}{2 w(1)^2} \right] \end{bmatrix} \quad (3-43)$$

The variables determined by the algebraic equations

$$\begin{bmatrix} \rho \\ \mu \end{bmatrix} = \begin{bmatrix} \frac{\gamma-1}{\gamma} \rho T \\ \sqrt{(\gamma-1) M_0^2 T} \frac{1 + S(\gamma-1) M_0^2}{1 + S/T} \end{bmatrix}$$

Artificial viscosity must be added to the difference schemes (3-41) and (3-42) by adding the expression $C_{m,n}$ to $S_{m,n}$. (In fact this is only done for scheme (3-41)). This expression is introduced into the difference scheme as an option, for the sake of stabilizing the solution during the early stages of iteration when the results are still far from convergence to the end solution. Sometimes this allows better control of the strong gradients, which makes the danger of divergence more remote. The definition of $C_{m,n}$ is similar to that formulated by Skoglund, Gay [94] and Goodrich et al. [37], but it is somewhat simpler.

$$\left. \begin{aligned} C_{m,n} &= \frac{C_{x_{m,n}}}{\Delta x^2} + \frac{C_{y_{m,n}}}{\Delta y^2} \\ C_{x_{m,n}} &= CC_x \left[\left| u_{m+1,n} - u_{m,n} \right| (v_{m,n+1} - v_{m,n}) - \left| u_{m,n} - u_{m-1,n} \right| (w_{m,n} - w_{m-1,n}) \right] \\ C_{y_{m,n}} &= CC_y \left[\left| v_{m,n+1} - v_{m,n} \right| (w_{m,n+1} - w_{m,n}) - \left| v_{m,n} - v_{m,n-1} \right| (w_{m,n} - w_{m,n-1}) \right] \end{aligned} \right\} \quad (3-44)$$

when CC_x and CC_y are uniform numerical coefficients at all grid points (as against other methods, where the coefficients

change as function of the local Courant number). At any rate, these coefficients are chosen for providing optimum influence on the stability of the numerical solution.

3.4.5 Boundary Conditions in Finite Differences

The formulation of boundary conditions for finite differences in accordance with the definitions in section 3.3. is detailed at length in appendix J.

3.4.6 Additional Computations in Finite Differences

Computations of flow functions and Mach numbers in each field of flow, as well as of coefficients of friction and of heat transfer along the plate, are carried out with finite differences according to the definitions of section 3.3. Details of the computation are given in appendix J.

3.4.7 Computer Program Procedure

Fig. 4 shows a general flow diagram of the computer program as prepared for an IBM 168 computer. The region surrounded by the dash line includes the computation of differential equations and boundary conditions with finite differences. In the corners of the rectangles the names of the subroutines have been indicated.

The diagram explains the basic computation for the Brailovskaya scheme, as explained in section 4.1.2.8.

All subroutines of the computer program, as well as the manner of employing the program in all its options, are explained in appendix Q. Also, a list of variables in the program with FORTRAN notations and details about their location in the various subroutines, is provided.

3.5 Consistency, Stability and Convergence of the Computation Method

450

3.5.1 Consistency

The difference schemes defined in the previous paragraph contain truncation errors (which were computed in the reference sources in which the schemes were developed) of the following form

$$\left. \begin{aligned} E_r (\text{Brailovskaya}) &= o(\Delta t, \Delta x^2, \Delta y^2) \\ E_T (\text{MacCormack}) &= o(\Delta t^2, \Delta x^2, \Delta y^2) \end{aligned} \right\} (3-45)$$

The truncation errors fulfill the consistency condition in principle

$$\lim_{\substack{\Delta t \rightarrow 0 \\ \Delta x \rightarrow 0 \\ \Delta y \rightarrow 0}} (E_T) \rightarrow 0 \quad (3-46)$$

The existence of this condition is given by the fact that the grid is fine enough so that all changes in the flow field can be identified in it. An extremely fine grid is, in fact, required for it, which is not practical. For that reason an optimum grid size is chosen, between desired accuracy of computation and acceptable time for the computation and memory size. This interferes somewhat with maintenance of the consistency condition (as will be seen further on in paragraph 4.1.6). Divergence from consistency is expressed by the final size of the grid meshes, causing truncation errors that are not negligible, particularly in regions with strong gradients (where Δy , Δx , Δt of the truncation are multiplied by high values for derivatives of the variables). This is expressed, among other things, by significant differences between the solutions for different schemes (for instance MacCormack [67] and Skoglund, Gay [94]), which appear to be consistency schemes on the fact of it, because of their truncation error. This phenomenon also stands out in differences between results received from the same scheme, when the grid is made finer (as in MacCormack [67]).

3.5.2 Stability Criterion

There is no possibility for demonstrating a criterion of stability that is both compulsory and sufficient for the difference scheme of the system of complete differential equations, because of their complexity and non-linearity. It is therefore customary to develop approximate differential equations and to employ them for the well known analysis by von Neumann, with its significance in testing whether the difference scheme of these equations restrains oscillations in the solution or increases them. The criterion received from this analysis gives the stability condition for small disturbances only; this is only a compulsory condition (and not sufficient) in the general case since the non-linear expressions generally try to increase disturbances in the solutions and not to diminish them. The analysis relates only to testing reaction to periodic disturbances and also does not include a test of the boundary condition influences. The stability criterion is therefore only an approximate expression and in practical computations one needs to be more rigorous.

/51

Carter [13] prepared such a stability analysis for the Brailovskaya scheme along the following stages:

- a) Linearization of complete equations in their non-vectorial form for two cases - nonviscid flow (for which mixed derivatives of viscosity and the dissipation term were neglected) and viscous flow (for which the convection terms were neglected).
- b) Writing the difference scheme for the approximate equations.
- c) Placing of a single component of the Fourier series into the solution.
- d) Confirmation of the amplification matrix, which expresses the relation between values for variables in two adjacent iterations.
- e) Computation of the Eigenvalue of the amplification matrix and establishment of the criterion that would validate the von Neumann condition (which demands that this value be equal to or less than 1). Such a criterion is in effect a maximum value for Δt , because the Eigenvalue of the amplification matrix is a direct function of Δt .

For nonviscid flow the condition

$$\Delta t \leq \left[\frac{|u|}{\Delta x} + \frac{|v|}{\Delta y} + c \sqrt{\frac{1}{\Delta x^2} + \frac{1}{\Delta y^2}} \right]^{-1} = \Delta t_1 \quad (3-47)$$

is received (also known as the CFL condition after Courant, Friedrichs and Levy) while for viscous flow*

$$\Delta t \leq \frac{\text{Pr} \cdot \text{Re}}{2\gamma \frac{\mu}{\rho} \left(\frac{1}{\Delta x^2} + \frac{1}{\Delta y^2} \right)} = \Delta t_2 \quad (3-48)$$

is presented. In an analysis by MacCormack [67] of the scheme he developed, condition (3-47) is also found. MacCormack [67] and also Skoglund, Gay [94], who solved the system of complete Navier-Stokes equations did not at all refer to the condition Δt_2 of the viscous flow in spite of the fact that the following relation must be fulfilled

$$\Delta t = \min \left[\Delta t_1 ; \Delta t_2 \right] \quad (3-49)$$

The justification for it is found in Carter's [13] analysis, who found that in such problems almost always $\Delta t_1 < \Delta t_2$ so that in practice only the existence of Δt_1 is required, in other words the CFL condition (3-47).

Allen, Cheng [2] (who also solved the Navier-Stokes equations for flow in the wake of the final step) arrived at the conclusion that only the CFL condition must be validated by solving the system of equations for fixed viscosity, which prevented the existence of the condition for Δt_2 .

* In other references expressions are found that are slightly different from (3-48) and they are given in detail in appendix K'.

Consequently, in this investigation the stability condition will from now on refer only to the CFL condition. Since computation of the stability criterion is only carried out as approximation this investigation will have to establish a more stringent condition, which is

$$\Delta t = \alpha \cdot \Delta t_1 \quad (3-50)$$

where $\alpha = 0.5$. This value is in practice an optimum one since higher values brought the difference scheme to the threshold of instability, while lower values slowed the pace of convergence considerably.

3.5.3 Test of Stability and Convergence of Results

3.5.3.1 Variation Coefficients of the Results

As measure of the convergence and stability of the numerical solution we have, in this study, employed several coefficients that are computed from the chronological results of the computation (in each area of iteration).

a) Variation coefficients of the variables

$$\left. \begin{aligned} E_{u_{m,n}}^t &= \frac{U_{m,n}^t - U_{m,n}^{t-1}}{U_0} \\ E_{p_{m,n}}^t &= \frac{P_{m,n}^t - P_{m,n}^{t-1}}{P_0} \\ E_{T_{m,n}}^t &= \frac{T_{m,n}^t - T_{m,n}^{t-1}}{T_0} \end{aligned} \right\} \quad (3-51)$$

b) Coefficients of the differential equation remainders (truncation errors)

453

$$R_{m,n}^t = \frac{2W_{m,n}^{t-1} - W_{m,n}^t - W_{m,n}^{t-2}}{\Delta t} \quad (3-52)$$

when there are four systems for R for

$$W = \rho; \rho u; \rho v; \rho \left[\frac{T}{\gamma} + \frac{u^2 + v^2}{2} \right]$$

(detailed development of the remainder coefficients is given in appendix L').

A maximum value and a mean value (r.m.s.) are computed for these coefficients in each field of flow. From the results it is possible to examine the degree of convergence by investigating

the development of the coefficients (their most frequent values or their averages) in the course of the iterations during computation. Likewise, the division of coefficient values in the field may be checked and from it may be learned where the areas most sensitive to oscillations in the solution are.

It is clear that to reach convergence these coefficients must decrease steadily down to the order of the truncation error for the difference scheme (or to the order of the computer's rounding error, if that is larger than that of the truncation error).

Stability of the computation must be expressed in the monotonous decrease of the coefficients' values as the iteration progresses, as well as those of their moderate and continuous gradients in the field of computation.

3.5.3.2 Estimate of the Order of Magnitude of the Computational Error

In the constant state* the Brailovskaya and MacCormack schemes have a truncation error of $O(\Delta x^2; \Delta y^2)$ but it is very different to evaluate its exact numerical value since it is multiplied by various derivatives and those depend a lot on the nature of the field of flow and of the boundary conditions.

According to the computation in appendix M' we get $\Delta t = O(10^{-3})$; $\Delta y = O(10^{-3})$; $\Delta x = O(10^{-2})$; and from them we learn that the fixed error of the variables (like for instance u , p , T) must be $O(10^{-6})$ (without consideration of the values for the derivatives with which Δx , Δy and Δt are multiplied and ignoring the boundary areas where the truncation error itself is considerably larger).

According to appendix N' a computational estimate was carried /54 out for the magnitude of the truncation error in a regular grid of 76×25 points, in comparison to computation for a grid twice as fine in each direction and containing 147×48 points. According to this evaluation it was found that the error for the variables was on the order of $O(10^{-3})$.

A check of the actual results of the computation reveals that most of the errors in the variables were in the order of $O(10^{-3})$ (per Fig. 10) and even the averages were around $O(10^{-4})$ (per Fig. 11).

*When the complete solution has oscillatory components there is an additional contribution to the truncation error, multiplied by Δt in the Brailovskaya scheme and by Δt^2 for MacCormack's scheme.

In the light of all this a final evaluation can be made for the computational accuracy of variables, which is in the range $0(10^{-3}) - 0(10^{-4})$.

Note: The rounding error of the computer is in the seventh digit, which means the addition of an error of $0(10^{-6})$ to the other errors of computation (because the definitive value of the non-dimensional variables is on the order of $0(1)$). It is clear that this error has no influence at all, as has even been proven in one computation for comparison with double the rounding error (of 13 digits), as explained in Fig. 14.

3.5.3.3 Comparison of Orders of Accuracies for Results with Different Methods

In appendix 0' a table is shown comparing various methods for obtaining results to problems of interaction between shock waves and boundary layers. The table shows that the computation accuracy in the present study falls short by 1 -2 orders of magnitude of the published accuracies for other methods. This difference also exists between the original MacCormack method (in MacCormack [67]) and the same method employed in this study for special boundary conditions. This fact hints at the close possibility that the boundary conditions caused a larger computation error (apparently because in the region of the incident shock wave, where the boundary conditions of the characteristics are close to those of the shock wave transition path, a significant local distortion is generated in the fulfillment of the flow equations, which also influences a part of the computational field that is not negligible). In spite of it this computation error does not affect the final accuracy of the solution very much, when compared to experimental results and previous computational results (as will be made clear further on in part 4).

On balance, the differences between results from all computation methods (MacCormack [67] Skoglund, Gay [94], and the present research) and experimental results (Hakkinen et al [41]) are on the order of several magnitudes greater than the advertised accuracy of the methods of computation (particularly when close to the shock wave and in the separated region, which are two of the most important areas). There is therefore no great practical significance to the "lower" relative accuracy of computation in this investigation.

155

Since a larger computation error requires less computation time for convergence, solutions were obtained relatively more quickly for this study than for previous ones (an additional factor that speeded the convergence was the choice of suitable initial conditions) and their accuracy, when related to experimental results, fell only slightly short of MacCormack's [67] work. (See section 4.2.1.1).

This outcome shows, among other things, that it is worthwhile to accept larger computational errors as a tradeoff against shortened computer time, for the solution of problems of this nature.

4. Results

156

4.1. Computation Method

Prior to analyzing the results of computation with the difference scheme there is need to determine the structure of the final computation within which it will be executed (among the various suggested methods and options for computation). Considerations of accuracy of the results and simplicity of execution will be the determining factor.

The equations that will be presented in the following paragraph all deal with the case in which

$$R_{e_{x_s}} = 3 \times 10^5; p_e/p_o = 1.4; M_o = 2 \text{ (below the reference condition)}$$

This case was chosen because a separated flow already exists in it and there are various experimental results available for it, as well as theoretical ones, for comparison. The computer runs for this part are illustrated in Table 1.

At first the basic schemes for the Brailovskaya and MacCormack methods will be compared, then the options and various changes made in the basic scheme will be investigated.

4.1.1. Comparison of the Brailovskaya and MacCormack Schemes

The computation schemes were prepared according to the two methods by Brailovskaya [8] and MacCormack, as indicated in section 3.2 (except for the difference methods themselves, all other characteristic components were introduced into the computation scheme, such as identical initial conditions and boundary conditions for both schemes). These schemes were applied in runs 001 and 051 equally and their results are compared in Figs. 9 and 13.

It turns out that in the results from both schemes are very much alike, with a slight advantage to MacCormack's scheme (where the separated region is slightly larger than the upstream direction). The convergence process is very similar for the two methods, continuing for about 200 iterations* and even the error coefficients are similar. The computation time per iteration is almost identical for both methods but the memory required for MacCormack's method is 1.5 times larger than that for the Brailovskaya method.

*It should be mentioned that in the MacCormack scheme (in the initial conditions tested) there is one iteration in the x-direction for each 8 iterations in the y-direction and the basic Δt in the y-direction is about 10% larger than the Δt of the Brailovskaya method, so that the number of iterations is only approximately the same.

The fact that the errors in the two schemes are of the same order of magnitude (about $O(10^{-4})$) while those in MacCormack's [67] (in which the other components of the computation, like boundary conditions, initial conditions and also the size of the computation field, are different but where the mesh size of the grid is similar) method were of the order of magnitude $\sim O(10^{-6})$, strengthens the assumption that the main cause for computation errors is inherent in the boundary conditions of the external flow (this is also the main difference between MacCormack's [67] original work and the MacCormack scheme applied in this study). We will see that the distortion in the fulfillment of the flow equations, in the region of contact between transition conditions of the incident shock wave and conditions of the characteristics, is relatively large and the truncation error that it creates (which extends inward into the flow field) is the main cause for this difference. But, as already mentioned, accuracy of the actual results does not fall short of that in the original study by MacCormack [67].

It thus remains to choose between the use of the Brailovskaya method or the MacCormack method for this research. From the point of view of accurate results it was preferable to choose MacCormack's method because of its slight advantage, but because the computer program was designated for a large scale exercise (of about 100 runs) to carry out parametric investigation of the results, it was important to use the program with the smallest memory that would permit quick and efficient operation from the technical point of view. For that reason the Brailovskaya method was chosen for the continuous work in this study.

4.1.2 Comparison of Various Improvement Options

In this paragraph various options and changes in the basic computation method by Brailovskaya, which was chosen for use in this study, will be compared.

The comparison will be made with reference to the experimental results by Hakkinen et al. [41] and with reference to the analytical results by MacCormack [67] and Skoglund, Gay [94].

The results of those comparisons are shown in Figs. 6 - 14 and relate to the pressure division and friction along the plate, to velocity profiles at various cross-sections and also to the development of stability coefficients.

A comparison is made for each option or suggestion of change separately, with the reference method applied being the basic one (which is defined by a uniform grid, second order differences over the entire field, continuous computation of the shock wave path, without artificial viscosity and with initial conditions that already include a schematic form of the field of interaction and, finally, with a regular roundoff accuracy to 6-7 decimals). The run employing the basic reference method is indicated in Table 1 as run No. 001.

4.1.2.1 Influence of the Computation Grid Form

/58

Two main disadvantages of the non-uniform grid are made clear in the comparison between a uniform and a non-uniform grid in the x-direction (dense in the middle around the shock wave and sparse towards the extremities), which is illustrated in Figs. 6a and 12a by the runs 001 and 006. They are: a tendency to develop oscillations in the solution close to the region of the incident shock wave and also computation errors that are on the average much higher and stem, among other things, from a truncation error that is greater in a significant part of the computation field (as shown in appendix G').

In the non-uniform grid there is a strong pressure gradient in the x-direction next to the shock wave (which also accompanies the oscillations around it), the significance of it being that the shock wave is not sufficiently "spread out" by this method. The separated region has a length that is similar to that in the uniform grid but it is a little further back in the upstream direction of the flow, which provides a better exhibition of how far back the influence interaction reaches. The velocity profiles for both methods are very similar.

Summing up, it may be said that at this stage the employment of a non-uniform grid is not indicated because, in addition to the added confusion that its use causes, it does not offer the expected results (unless additional perfections were accomplished).

4.1.2.2 Influence of the Order of Accuracy of Finite Differences

Computation of the fourth order differences (only in the x-direction) in that part of the field that is underneath the point of entry of the shock wave (between the sonic line and the wall) is carried out in run 003 and its results are demonstrated for comparison in Fig. 6a. The use of this method was originally designated to improve accuracy in the local derivatives for the regions with strong gradients, however, because of the distortion in results generated at the line of contact between two computation schemes (of the second and fourth order) disturbances develop that express themselves, among other things, by oscillations of the separation $p_w(x)$ underneath the point of entry of the shock wave. On the other hand, a slightly larger separated region in the upstream direction of the flow is obtained than in the computation using the basic method (with second order differences in each field). Once again there are almost no differences in the velocity profiles.

We can then sum up in saying that the incomplete "marriage" of the two difference systems in the computation field degrades the accuracy of the solution; it is therefore inadvisable to use the fourth order differences method for this stage (what's more since it requires a memory size and computation time that are 1.5 times greater than those in the basic method).

Note: In the first attempt the fourth order differences were not used for the whole field since it is not advisable to compute with them in the vicinity of the shock wave (for fear that a local derivative will be dependent on values from both sides of the shock wave, which can be of much greater influence in the fourth order differences scheme where each point is a function of four neighboring points in the x-direction as against two points in the second order differences scheme). An additional reason is that away from the shock wave such a computation is superfluous, because there are no strong gradients in the x-direction, which must be suppressed by the use of this method. On top of it all, a fourth order differences computation for the entire field will cause a significant increase in memory size and required computer time (about 5 times). From all that has been said above the conclusion is reached that the use of this method is worthwhile only for the subsonic part of the boundary layer (which is also the more interesting one with regards to computation results).

4.1.2.3 Influence of Artificial Viscosity

Preliminary computation of about 150 iterations of artificial viscosity, which was followed by 200 additional iterations in the regular computation (without artificial viscosity) is carried out in run 005, with the results compared to the basic method in Fig. 6a. It appears that artificial viscosity improves the results somewhat and, in particular, has a beneficial influence for better "spreading" of the gradients around the shock wave and on the enlargement of the region affected back of the pressure division. The size of the separated region and the velocity profiles do not change, however.

The only drawback in this method is that the coefficients of artificial viscosity, CC_y and CC_x , change with the flow conditions and in a manner that cannot be computed in advance, so that the optimum values have to be determined in each case separately. Figure 7 shows the results of computations for three different combinations of artificial viscosity coefficients (one of which is the optimum one that is used for comparison in Fig. 6a). Since this optimization involves many tryouts for each case, it is not practical when a large number of runs has to be carried out under different flow conditions* (in which the Mach and Reynolds numbers, the intensity of the shock wave, etc., change); for which reason artificial viscosity has not been introduced in the rest of the runs for this study from here on. Just the same, were there a way to develop a simple method for forecasting the value of artificial viscosity coefficients as function of the flow conditions, it would be worthwhile to use this option to increase the accuracy of results.

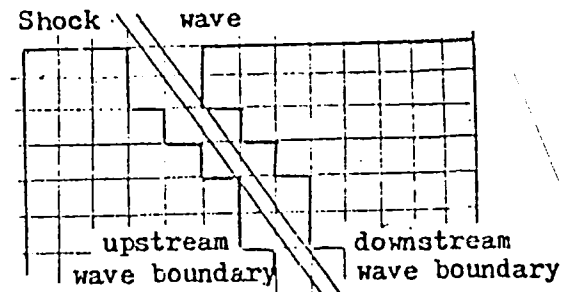
*In Fig. 7a the results of three cases for different flow conditions, with and without artificial viscosity, are compared where the optimum coefficients are those chosen from the reference case only ($p_e/p_o=1.4$; $Re_{x_s}=3 \times 10^5$; $Mo=2$). The negative influence of this artificial viscosity illustrates that the optimum coefficients of one case are far from being so in another.

4.1.2.4 Influence of Shock Wave Computation Method

In contrast to the basic computation method for which the shock wave is in the center of the computation field (and which is also known as the "continuous" method) a method was examined in which the shock wave is removed from the computation field in a way so that its two sides, up to the sonic line, serve as boundary conditions as explained in paragraph 3.3.1.5 (this method is also known as "discontinuous"). That method was employed for runs 007 and 008 (where fourth order differences were also introduced underneath the shock wave). The results are shown for comparison in Fig. 6b.

Comparison of the results brings out that the "discontinuous" method causes a very strong gradient of pressure in the x-direction underneath the shock wave, which is accompanied by some slight overshooting downstream of the shock wave. In addition, oscillations can be seen in the velocity profile below the shock wave. In addition, oscillations can be seen in the velocity profile below the shock wave. Oscillations in the solution below the shock wave increase when fourth order differences are introduced into the discontinuous method (in accordance with the explanation in paragraph 4.1.2.2). In spite of all this there is a small advantage to the "discontinuous" method, which is expressed in some effect of the pressure to the rear that enlarges the separated region.

One of the main reasons for oscillation of the solution near the shock wave in the "discontinuous" method is that during the iterative computation of the boundary conditions downstream of the shock wave there is no possibility for any careful consideration of the reflected streamlines that return in the path of the wave (the local intensity of the wave in each iteration is computed according to the local ratio of pressures from both sides, the pressures being average pressures of the vicinity). No accurate local intensity can therefore be obtained for the shock wave and for the shape of its curvature into the boundary layer (for which reason its location is also not accurate). An additional factor, contributing to oscillations, is the form of the boundary on both sides of the wave, which is built in the form of steps and for which the difference computation is not accurate (this phenomenon is also familiar from other sources like Roache [86], for instance).



This final factor is notably expressed in a non-uniform grid where the step structure in the vicinity of the shock wave is even denser and the oscillations of the result even greater, until it reaches divergence after 100 iterations (as shown in run 009).

It should be pointed out, finally, that the "discontinuous method" in its present form is not as satisfactory as the basic "continuous" method when looking at the results but the idea of the removal of the shock wave, around which the strongest gradients in the field operate, is worth additional research since it points a way for conquering the most difficult obstacle in this computation - the path of the shock wave.

4.1.2.5 Influence of Initial Conditions

As has already been mentioned in paragraph 3.3.2, it is desirable that the initial conditions not be too far distant from the solution, to avoid a potential danger of divergence, while on the other hand there is no point in being too meticulous about it so that the general nature of the method is not lost. According to the initial conditions formulated in paragraph 3.3.2, convergence was obtained to an accuracy of $O(10^{-3}) - O(10^{-4})$ after 200 iterations (as is indicated in Fig. 10). For initial conditions that are more removed from the solution (like a boundary layer that is undeveloped and uniform along its entire length, without appropriate "spreading" of the shock wave, etc.) a much slower convergence was obtained, on the order of 500 - 1000 iterations, in accordance with the distance of the initial conditions from the form of the final solution.

4.1.2.6 Influence of the Size of Grid Mesh Dimensions

To verify considerations for the choice of grid mesh dimensions (which was made in paragraph 3.4.3 and in appendix D') an additional computation, with a grid that is approximately two times finer, is carried out (where the number of points is 147×48 as against 76×25 for the regular grid) by means of the basic method. This fine grid is used in run 041 and the results are explained in Figs. 8 and 12b.

The results obtained show a "spread" for the pressure gradient that is just a little bit better but, generally, the differences in results from the regular grid and from the fine grid are of no significance (and they are even smaller than the differences obtained by MacCormack [67] in a similar comparison). If there are any big differences at all they are indicative of a lack of refinement for getting an accurate solution, but the order of magnitude of the differences in this case is quite significant, considering the range of accuracy expected from this program.

In the fine grid (which requires 4 times the size of memory and 4 times the computer time for iteration) convergence was obtained after about 400 iterations so that the computation with it takes about 8 times longer than computation with the regular size grid, without getting the reward of significant improvement in results.

From results of the computations using the regular grid and the fine grid, a forecast was made for a number of points in the grid for an accurate solution of the difference method and from it we obtain an evaluation of the order of magnitude for the computation error*. Based on that computation, which is found in appendix N, the error in the regular grid is on the order of $O(10^{-3})$ and in the fine grid it is 4 times smaller.

4.1.2.7 Influence of the Computer Roundoff Error on Accuracy

As explained in paragraph 3.5.3.2, an accuracy of results is obtained that is $O(10^{-3} - 10^{-4})$ so that there is not much point in increasing the regular roundoff accuracy of the computer (which is between 6 -7 decimals) to double its value (to 13 decimals). To demonstrate that conclusively run 031 was carried out with double the roundoff accuracy. Results of this run are almost completely identical (to the fourth or fifth decimal) to those of run 001 (with the regular roundoff accuracy). Equally, the error coefficients are nearly alike as shown in Fig. 14.

It should be pointed out that computation with double the roundoff accuracy requires double the memory size and 1.5 times the computer time used for the regular computation.

Based on the above, all following computations in the program will be carried out with regular roundoff accuracy only.

4.1.2.8 Summary of Comparison of Computation Methods

Comparison of the various types of computation suggested in this chapter with the form of the basic computation discloses that actually the basic form, without any attempts for "perfections" of any kind, is the most efficient and practical to operate for a large series of runs under different flow conditions.

In spite of the fact that the other methods will give slightly better results in certain regions, they offer disadvantages that could not be overcome at this stage. In addition, these methods complicate the computation scheme and, generally, increase the computer time and the required memory size. This decision is not a final one, of course, and it is quite possible that additional basic research will solve part of the problems mentioned to make it possible to combine these methods in a new and improved computation scheme.

*See bottom of page 54 [of original.]

We will now sum up briefly the basic computation method, which will be employed in this study from now on:

/63

a) a uniform computation grid in x and y directions, over a computation region of $3 \times \delta_0 \times 150 \delta_0$ containing 76×25 grid plate.

b) roundoff error of 6-7 decimals.

c) difference method of the second order, using the Brailovskaya method for each region computed.

d) no expression of artificial viscosity added to the difference equation.

e) "continuous" computation of the shock wave path, i.e., the shock wave in the center of the computation field and defined as external compulsion only for the boundary conditions.

f) initial conditions include an approximate and very general description of the interaction field.

A convergent* solution is obtained with this method (characterized by asymptotic values for the stability coefficients) after about 200 iterations.

Computer IBM 370/168, on which the runs required for this investigation were performed, needs 4 minutes of CPU per run and a memory size of 256K (for continuous computation of the stability coefficients about double the time and memory size will be required).

4.2 Parametrical Analysis of the Results

/64

Analysis of the results of computation for various flow conditions, as obtained through the basic computation method, will be carried out below.

*The description of development of the stability coefficients in Fig. 10 shows that after about 200 iterations they approach an approximate asymptotic value, the average order of magnitude for errors of the most frequent variables is about $O(10^{-3})$ and the order of magnitude for the average derivatives is $O(10^{-2})$. Those values are in accord with evaluation of errors as explained in appendix L, which is $O(10^{-3} - 10^{-4})$ of the actual values of the variables.

A description of the division of errors in the field, in Fig. 11, acknowledges that the main errors of computation are concentrated around the shock wave in the center of the field.

4.2.1 Influence of Flow Conditions on the Interaction

For most of the flow conditions for which computations were made neither experimental nor theoretical data exist for comparison; therefore the analysis will be made with the assumption that the results are correct, which is based on a comparison with the few results available until now.

The runs described in this part are concentrated in Table 2.

4.2.1.1. Comparison with Previous Experimental and Computational Results

Runs 101, 102 and 103 were made for comparison with existing results for the following conditions:

$$\begin{aligned} Mo &= 2, \text{Re}_{x_s} = 3 \times 10^5, x_s = 5 \text{ cm} \\ p_e/p_o &= 1.2, 1.4, 1.9 \end{aligned}$$

Comparison is made with experimental results of Hakkinen et al. [41]* for all three cases and also for computation results of MacCormack [67]** and Skoglund, Gay [94] for $p_e/p_o = 1.2, 1.4$ only.

In Fig. 15 a comparison is made for $p_e/p_o = 1.2$ where the flow has not yet separated. The results of run 101 are very close to those of MacCormack [67] (except for the slightly stronger pressure gradient and the slightly greater friction downstream, in the computational results).

The most important comparison was made in Fig. 17 for $p_e/p_o = 1.4$, where the flow has already separated. It turns out that for all computational methods (including the present one demonstrated by run 102) a lower pressure is obtained upstream, when compared with experimental data***, just as the boundary

165

*From a description of the experiment and attached Schlieren photographs it is certain that the experiment was performed under laminary flow conditions.

**Results of MacCormack's computations in this paragraph are from his basic study, MacCormack [67], as contrasted with results of the present investigation in 4.1.1, using MacCormack's scheme.

***The difference arises perhaps from the inaccuracy of measurement in the separated region (another possibility is a computational error common to all methods of computation; but that does not appear likely in view of the successful solutions for a variety of problems, obtained through these computation schemes).

layer is smaller below the shock wave.*

The difference between results from run 102 and the other computational data is not a big one. In consideration of these small differences it may be said that the MacCormack method is the best one, that of Skoglund, Gay [94] is the least good one and the computational method used here is somewhere in the middle.

In general we will see that the present method shows a slightly larger pressure gradient below the shock wave and less pressure increase in the upstream flow, as compared to MacCormack's[67] method, but a more accurate pressure (compared to experimental data) for the downstream flow after the shock wave. In the present method the separated region is slightly smaller and the friction coefficient for the downstream flow is greater. There are no significant differences in the velocity profiles of all three methods of computation.

Fig. 19 explains the comparison of data from run 103 for $p_e/p_o = 1.9$ to experimental results alone (computational results are lacking). The pressure division is perfectly correct but even here the upstream pressure increase is smaller and the separated region smaller, when compared with experimental data. Friction of the downstream flow is also lower. As with results for $p_e/p_o = 1.4$ the velocity profile below the shock wave, as obtained through computation, shows a thinner boundary layer and a separated region that extends less into the field.

In addition to the comparisons listed above, flow field charts with iso-Mach lines, iso-flow lines and iso-pressure lines were plotted in Figs. 16, 18 and 20, for runs 101, 102 and 103. These charts present a good picture of the flow field, which compliments the obtained results from Figs. 15, 17 and 19. The charts clearly show the separated region, the incident shock wave and the reflected streamlines, as well as the development of the pressure change in the field.

166
/66

* This phenomenon must also be laid to an erroneous measurement in that region. There is an additional possibility, namely that during the experiment the flow in this region was subject to characteristics of turbulence that changed the y gradient of the velocity profile, leading to an increase of the separated region (while all numerical computations are only for laminar flow). As a matter of fact, a transfer of the experimental velocity profile from Fig. 17, in the y-direction, up to the coalescence of the points where $u = 0$, shows a much better fit between the experimental profile and those obtained through the computation methods.

To summarize, it has been shown that a comparison of data from the present method of computation, with existing results from computations and experiments, shows them to be entirely reasonable and falling only slightly short of those from the competing MacCormack [67] method (in the range of data where such a comparison was possible). For strong interaction, for which only experimental data were available for comparison, it appears that the separated region is smaller but the form of its development, with the intensity of the shock wave and the Mach number, is in general accordance with experimental data (as we shall see during the continuation of this data analysis).

The advantage of the present method is in its relatively early convergence (apparently with a large error of computation, which does not, however, degrade the accuracy of the final result very much), which permits its practical application for large numbers of runs with different flow conditions.

Note: as already mentioned in paragraph 4.1.2.3, some slight improvement in the accuracy of results might have been achieved by the use of artificial viscosity, but, for the sake of simplicity of operation and avoidance of additional computations to find its optimum coefficients, it was not done.

In the following paragraphs the parametric analysis of the influence of the various flow conditions on the interaction field will be performed (through the runs illustrated in Table 2).

4.2.1.2. Influence of Shock Wave Intensity

Fig. 21 describes the influence of the shock wave (in the range of pressure ratios $1.2 < p_e/p_o \leq 3.15^*$) on the interaction when $Mo = 2$; $Re_{x_s} = 3 \times 10^5$ (in runs 101, 102, 103 and 104). The increase in intensity of the shock wave enlarges the region to the rear that is influenced by the pressure and, along with it, the size of the separated region also increases towards the upstream direction to the flow. At the same time the separated region enters deeper into the field and because of it the edge of the boundary layer moves further away from the wall. Fig. 22 describes the flow field picture in run 104 where a very intense shock wave of $p_e/p_o = 3.15$ exists. We can see the change in flow field characteristics more clearly by comparing it to weaker interactions (as in Figs. 16, 18 and 20.)

/67

*In this comparison no shock intensities higher than for $Mo=2$ were included and for $p_e/p_o = 3.7$ a subsonic region starts after the shock wave (run 105) and the boundary conditions of the characteristics cannot be applied.

It must be stated that in reality a transition of the boundary layer may develop so that it will be turbulent for intense shock waves (particularly downstream of the shock wave) so that the (laminar) computation results won't be so accurate; but the main interaction phenomena take place upstream of the flow and are not much influenced by that.

4.2.1.3. Mach Number Influence

Fig. 23 describes the influence of the Mach number on interaction in the range* $2 < Mo < 4.5$, when $p_e/p_o = 3.15$ and $Re_{x_s} = 3 \times 10^5$ (runs 104, 111, 112 and 113). The comparison was made for a relatively intense shock so as to obtain the Mach number influence at strong interactions.

It appears that the higher the Mach number the more acute the angle at which the shock wave enters the field, which weakens the interaction. That is visible from the results, inasmuch as the higher Mo the more the region to the rear, subject to influence of pressure and of size of the separated region, will decrease.

Fig. 24 describes the flow field of run 112, with a high Mach number of $Mo = 4$. The weakening of the force of interaction, when compared to lower Mach numbers (as in Fig. 22 for instance), is clearly visible in this picture.

4.2.1.4 Reynolds Number Influence

Fig. 25 describes the Reynolds number influence on interaction in the range $1 \times 10^4 \leq Re_{x_s} \leq 1 \times 10^6$, when $Mo = 2$, $p_e/p_o = 1.4$ (runs 121, 122, 102 and 123).

The results show that a decrease in the Reynolds number pushes the pressure increase downstream because of the shock wave. This is in agreement with a similar investigation carried out by Reyhner, Flügge-Lotz [84] for $Mo = 3$. The separated region increased with the change in Re_{x_s} from 1×10^4 to 3×10^5 but decreased gradually when the Reynolds number was further increased. One possible explanation for that is that the computation method tends to show (though in a very coarse manner) the solution for turbulent flow for this range of the Reynolds number, while in reality a transition towards turbulent flow in the boundary layer exists for this range (around $Re_{x_s} \approx 1 \times 10^6$), in which changes are much smaller because of the much stronger flow resistance to pressure gradients (which also decreases the influence of interaction and, with it, the size of the separated region). /68

*For higher Mach numbers (for the same pressure ratio $p_e/p_o = 3.15$) instabilities start to develop in the solution. This is expressed in run 114, for $p_e/p_o = 3.15$, $Mo = 5$, where the solution diverges after 150 iterations.

Together with the above, the difficulties of exactly determining the size of the separated region from computed results must be pointed out. This is due to a somewhat unclear determination of the border between the separated region and the boundary layer (because the changes in velocity components are very small for this region).

4 Fig. 26 describes the flow field in run 121 for $Re_{x_s} = 1 \times 10^4$, showing the influence of a low Reynolds number on the interaction field as compared to the influence of higher values (as in Fig. 16, for instance).

4.2.1.5 Influence of Shock Wave Entrance Location

Fig. 27 describes the influence of a change in the location of shock wave impingement for the range $3 \text{ cm} \leq x_s \leq 7 \text{ cm}$, when $p_e/p_o = 1.4$ and $Mo = 2$ and the Reynolds number of the reference point $x_s = 5 \text{ cm}$ is 3×10^5 . The results were obtained from runs 131, 102 and 132.

It becomes clear that the larger the distance between the impingement location of the shock wave on the plate and the leading edge, the smaller the pressure gradient along the plate and the greater the influence of pressure towards the rear and on the size of the separated region. In fact, this is the result of local growth of the boundary layer thickness in the interaction region with the increase in x_s , so that the boundary layer becomes more sensitive to pressure gradients.

4.2.1.6 Prandtl Number Influence

Fig. 28 describes the comparison between results for $Pr=0.72$ (value for air) and 1.0 (an approximate value used often because it simplifies part of the equations), when $Mo = 2$, $p_e/p_o=1.4$ and $Re_{x_s} = 3 \times 10^5$ (runs 102, 141). It turns out that neither pressure division, the friction coefficient, or the separated region show any change because of it. The only difference expressed is a slight change in the temperature profile next to the plate, which causes an adiabatic wall temperature that is about 5% higher for $Pr = 1.0$. It is to be expected that this influence will grow with the Mach number and that, because of it, the form of the boundary layer and the friction coefficient will change slightly. /69

Those results were found to be in good agreement with a similar study by Reynher, Flügge-Lotz [84] for $Mo = 3$.

From this investigation it may be concluded that the approximations of $Pr = 1.0$, that are occasionally made in various studies, are generally justified and particularly when the Mach numbers are low.

4.2.1.7 Summary of Flow Condition Effects

From examination of the parameters in this section it appears that the pressure ratio (i.e. the shock wave intensity exerts the most important influence on the interaction, especially on the size of the separated region.

The Reynolds number, too, influences results considerably, particularly since the width of the boundary layer and its sensitivity to pressure gradients depend on it.

The other parameters like Mach number, location of the shock wave impingement and the Prandtl number, exert much less influence if at all.

Fig. 29 describes the influence of parameters Mo , p_e/p_o and Re_{x_s} on the development of the boundary layer along the interaction field. As expected, the Reynolds number is the primary determinant for shape and width of the boundary layer development while the influence of p_e/p_o and Mo is of a much smaller order.

4.2.2 Influence of Boundary Conditions next to the Plate (Heat and Mass Transfer)

470

The influences of heat transfer (maintenance of the plate at a fixed non-adiabatic temperature) and mass transfer (suction or self-injection into the plate) on the flow field in general and on the separated region in particular, when all other flow conditions (only in this part) remain fixed at the values $Mo=2$; $p_e/p_o = 1.4$; $Re_{x_s} = 3 \times 10^5$, will be described further on. The runs for this section are described in Table 3.

4.2.2.1. Influence of Heat Transfer Next to the Plate

The influence of maintaining the plate at various fixed temperatures in the range* $0.4 < T_w < 1.4$ (when $T_w = C_p T_w^\# / U_o^\#^2$), as obtained from runs 201 and 206, is described in Fig. 30.

Maintaining the plate at a fixed non-adiabatic temperature causes a heat transfer next to the plate that influences the temperature profile but, as it appears from the drawing, the influence is localized only and attenuates quickly until it disappears entirely at about the middle of the boundary layer. The thermal conductivity coefficient next to the plate changes according to the plate temperature; its value is negative for a plate temperature that is higher than the adiabatic one and, conversely, positive when it is lower.

*The temperature of the adiabatic wall for $Mo = 2$ is $T_w = 1.05$.

On the other hand, the pressure division, the boundary layer development and the size of the separated region as result of temperature changes along the plate, are hardly influenced at all.

Those results are in agreement with data computed by Reyhner, Flügge-Lotz[84] for interaction that ends next to a blunt corner.

It may be concluded that there is no practical way to control the size of the separated region through heat transfer along the plate.

4.2.2 Influence of Mass Transfer Close to the Plate

In contrast to heat transfer, mass transfer close to the plate (which is expressed here by introduction of suction, or injection, normal to the plate length) does have significant influence on the flow field of interaction, and particularly on the size of the separated region*.

471

Fig. 31 describes the influence of velocity, normal to the plate and next to it, in the range of $-0.03 \leq V_w \leq +0.02$ (when $V_w = \frac{V_w^\#}{U^\#}$), as obtained from runs 211 to 215.

What stands out in particular is the strong influence on the friction coefficient, the size of the separated region and the profiles of the boundary layer. The suction next to the plate causes the boundary layer to "stick" to it by reducing the separated region until it disappears completely (in this case at $V_w = -0.02$). Injection, on the other hand, causes a broadening of the boundary layer and an increase in the separated region. The friction coefficient increased with the increase in suction velocity and decreased with the increase of injection velocity into the plate.

Pressure division is almost unaffected, except for slight oscillations in the initial and final regions of that section of the plate where suction or injection are present (these oscillations, which are not visible in Fig. 31, are apparently the result of local numerical discontinuities in the boundary conditions on the plate). In addition to what was said above, suction influences the slight delay in pressure increase downstream of the shock wave while injection causes slight acceleration upstream of the shock wave.

*Parametrical analysis of the influence of suction on the various flow conditions and the conditions required to prevent separation of flow are shown in the following section 4.2.3.

Fig. 32 describes the flow field influenced by a suction of $V_w = -0.02$ (run 212). The figure shows clearly how the flow lines bend and the separated region disappears, when compared to flow without suction influence under the same conditions (as in Fig. 16).

Fig. 33 describes the influence of suction and injection on development of the boundary layer shape.

Finally, about influence of boundary conditions on the interaction it can be stated that heat transfer has almost none, while mass transfer has very significant influence on the size of the separated region and on the shape of the boundary layer.

4.2.3 Detailed Analysis of Suction Effect on the Separated Flow Region

172

This section goes into more detail to explain the influence of suction on the separated region for various flow conditions and the amount of suction required to prevent separation for those conditions. The subject receives a great deal of attention in comparison with other parametrical studies, since it is of important practical significance.

4.2.3.1. Influence of the Location of Suction Along the Plate

In runs 211 to 229 the influence of changing the location where suction on the plate starts in the region* $2.6 \text{ cm} < x < 4.4 \text{ cm}$ (when termination of suction is always $-0.03 > V_w > 0$, with flow conditions being: $Mo = 2$, $p_e/p_o = 1.4$ and $Re_{x_s} = 3 \times 10^5$). The results show that this has no actual influence on the solution and they are nearly identical for all cases.

Since in this comparison the suction region always includes the entire separated region, the assumption was made that only suction in the separated region proper had any influence on the results (mainly because of the size of the separated region), while no change at all was to be expected in the results due to suction from any section outside it.

To verify this assumption, an additional series of computer runs was arranged (runs 251 to 267 described in Table 4) for $Mo = 2$, $p_e/p_o = 1.4$, $Re_{x_s} = 3 \times 10^5$ and $V_w = -0.02$. For those runs the start and finish locations of suction changed over a

*The suction region always starts before the start of flow separation along the plate, in this case.

very broad range, so that many cases could be included where only part of the separated region was influenced by suction while a part was not. The data shown in Figs. 34 and 34a confirm that suction is effective (as far as its influence on the separated region is concerned) only when it operates within the region but not outside it. To benefit most from suction it must therefore be maintained over the entire separated region.

Since it is not known in every case just where the separated region will appear, the following parametrical tests were run for suction. The region of suction is thus very broad and covers most of the plate length so as to obtain maximum benefit from its influence for each case.

4.2.3.2 Influence of Suction for Various Flow Conditions

73

In the series of runs described in Table 5 (runs 301 to 452) the influence of the following parameters was examined: $5 \times 10^4 \leq Re_{x_s} \leq 1 \times 10^6$; $2 \leq Mo \leq 4$; $1.2 \leq p_e/p_o \leq 3.2$ and $3 \text{ cm} > x_s \geq 7 \text{ cm}$, with suction changing over the range $-0.3 > V_w > 0$. Results of the runs are shown in Figs. 35, 36 and 37, with the size of the separated region as a function of suction velocity for various flow conditions and in non-dimensional form.

The figures disclose that the pressure ratio p_e/p_o influences the increase of the separated region and so contributes to the increase in suction velocity required to eliminate it. It should be noted here once more, as has already been said in paragraph 4.2.1.1 that the separated region obtained through computation is smaller than the one in reality, particular for high pressure ratios; however, the general purpose of the influence exerted by the pressure ratios on the separated region, for various suction velocities, appears to be superficial and reasonable.

The influence of the Mach number tends toward decrease of the separated region, so the suction velocity required to eliminate it decreases as the Mach number increases.

The influence of the Reynolds number is more complex. As already described in paragraph 4.2.1.4, the separated region starts to decrease when Re_{x_s} exceeds the value of 3×10^5 (while in the lower range the separated region increased together with Re_{x_s}). On the other hand, when the suction intensity increases ($V_w < .18$) the opposite situation is created, with the separated region continuing to increase with the Reynolds number, at least to $Re_{x_s} = 10^6$. If we base ourselves on the estimate offered in paragraph 4.2.1.4 we can claim that an increase in suction causes rejection of the tendency for

transition and with it for turbulent flow, so that suction is responsible for the return to laminar flow, which is apparently also expressed in the numerical solution. To sum it up, the more the Reynolds number goes up the stronger is the suction required to eliminate the separated region.

The impingement point of the shock wave exerts next to no influence. In the figures the non-dimensional results for x_s vary as they combine, with good approximation, to one line. (That result is forced by circumstances since the length of the non-dimensional separated region is also referenced to x_s).

4.2.3.3 Suction Required to Eliminate the Separated Region

/74

Figs. 38, 39 and 40 (which were constructed from the previous Figs. 35, 36 and 37), describe the dependence of suction velocity, needed for elimination of the separated region, on each of the main parameters (pressure ratio, Mach number and Reynolds number).

With the aid of appropriate extrapolation from those figures a summary table was drawn up in Fig. 41 where the needed suction velocity for prevention of separation is given as the function of those three parameters.

It is also appropriate to recall that Carter [13], in his investigation of the influence of suction on the flow around a rounded corner at an angle of 10° (for which he got a pressure ratio of $p_e/p_0 = 2.2$) with $Mo = 3$ and $Re_{x_s} = 1.68 \times 10^4$, found a requirement for suction estimated at $V_w = 0.1$ to prevent separation; despite the difference in the form of interaction in this research, it turns out that this value is very good agreement with that received from the table in Fig. 41 for such flow conditions.

4.2.3.4 Approximate Formulation of the Suction Needed To Prevent Separation

In the computation described in appendix 0, a single-valued connection was found between the characteristics of the separated region and the suction velocity needed for its elimination.

The separated region is characterized by its dimensions Δx_s ; Δy_s and by the maximum negative value of the flow function (with the focus of the bubble in its center) which is Ψ_{mx} .

The connection is, to a good approximation,

$$\frac{V_w s \sqrt{\rho}}{\Psi_{mx}} = \text{const.} \quad (4-1)$$

where the fixed value is in the range 0.3 - 0.42, the bubble area is defined as $v = \Delta x_s \cdot \Delta y_s \cdot 1$ and the flow function $\Psi = \Psi/\rho$ Formula (4-1) was tested for 10 different combinations of flow conditions ($Mo; Re_{x_s}; p_e/p_o$).

5. Discussion and Conclusions

75

The finite difference computation method, investigated in this study for solving problems of interaction between shock wave and laminar boundary layer (through solution of the complete Navier-Stokes equations), provided excellent solutions when compared with the experimental and theoretical information presently available. The simplicity of the method's operation and the relatively short time needed for the solution, permitted the execution of a large number of runs for various flow conditions, from which it was possible to learn about the interaction characteristics and the principal factors that influence it.

Special emphasis was placed on researching the influence of suction on the prevention of flow separation next to the plate, which is of great practical significance.

We will now discuss results and main conclusions reached from this study:

5.1 Computation Method

The method of computation demonstrated in this study is characterized by the following factors:

a) The method is constructed simultaneously with the second order difference schemes of Brailovskaya and MacCormack, for a uniform grid.

b) The field of computation stretches over a range of 150 δ_0 length and 3 δ_0 width around a region where the shock wave impinges on the plate. The field is divided into a grid of 76 x 25 points that forms uniform meshes with the dimensions 2 δ_0 x 0.125. Convergence for a normal computation occurs within about 200 iterations and the obtained accuracy for the variables (through truncation error) is in the range of $0(10^{-3}) - 0(10^{-4})$. Such a computation, carried out on an IBM 370/168 computer, took 4 minutes of CPU time.

c) Boundary conditions for this computation are:

1. Inlet cross-section - profile of boundary layer per Polhausen.
2. Exit cross-section - zero gradients in the flow direction.

3. Plate - no velocity components (non-slip condition) and no gradients normal to the direction of temperature (adiabatic plate) and pressure (for approximate computation of density).
4. External flow - according to the characteristics from the field (except for the two sides of the shock wave), this boundary condition distinguishes the present computation method, with reference to the other existing solutions, and it permits the reduction of the computation field up to near the boundary layer.

d) The computation results agree in the main with those known from experiments, except that a much smaller separated region is obtained for very strong interactions, but the tendency in the development of this section with changing flow conditions is in the right direction and the right proportions. 176

The results are in good agreement with those from previous computations and fall only slightly short of MacCormack's results, while showing improvement over those by Skoglund, Gay (those two studies were solved with schemes similar to the one used here, though the external boundary was assumed to be far from the plate and fixed conditions were given for its entire length, from both sides of the shock wave. The solution in those studies converged after several thousand iterations to a truncation error of less than $\sim 0(10^{-6})$).

e) A number of additional auxiliary methods were tried during this study, but were not introduced into the final method of computation because they have not yet shown themselves suitable for that. They are, however, worth additional research so that they may become helpful in improving the results.

1. Artificial viscosity - an option was prepared for addition of artificial viscosity terms to the difference scheme, which improves the results slightly but requires computation for optimization of the numerical coefficients.
2. Non-uniform grid - with changing dimensions in the x-direction so that it is dense in the center (next to the shock wave) and sparse towards the ends. The solution for such a grid has a tendency for oscillation near the shock wave.
3. Fourth order finite differences - these were used for the x-direction, below the shock wave, but caused oscillations in the zone of contact with the region of second order computation (in the vicinity of the sonic line).

4. Removal of the shock wave from computation field - this "discontinuous" computation of the shock wave by fixing its two sides as boundaries of the field, did not bring the expected results and caused oscillations around the shock wave.

5.2 Parametrical Analysis of the Interaction

477

The influence of shock wave intensity, $1.2 \leq p_e/p_o \leq 3.2$ and its location of operation $3 \text{ cm} \leq x_s \leq 7 \text{ cm}$, were investigated. The Mach numbers $2 \leq Mo \leq 4.5$, Reynolds numbers $1 \times 10^5 \leq Re_{x_s} \leq 1 \times 10^6$ the Prandtl numbers $Pr = 0.72, 1.0$ were used. Also investigated was the influence of heat transfer in the range $0.4 \leq T_w \leq 1.4$ and mass transfer in the range $-0.03 \leq V_w \leq 0.02$ along the length of the plate (non-dimensional values).

The principal results obtained were:

- a) Increase of pressure ratio in the flow field enlarges the separated region and the pressure influence to the rear (pressure increase in front of incident shock wave location).

- b) The further the location of the incident shock wave from the leading edge the more "spreads" the influence of the shock, which is expressed in the decrease of the pressure gradient and enlargement of the separated region.

- c) Increase of the Mach number weakens the force of the interaction and reduces the separated region.

- d) Increase of the Reynolds number for the point of incidence of the shock wave enlarges the separated region, but above the value of 3×10^5 it reduces it. Also, the pressure gradient is moved forward in the upstream direction of the flow. (Because of the possibility that at high Reynolds numbers the flow may no longer be laminar past the shock wave, it is not certain whether the results for this region are reliable).

- e) Influence of the Prandtl number on the result is nearly negligible, except for a small local change in the temperature profile in the lower part of the boundary layer.

- f) Mass transfer (suction or injection) next to the plate influences the size of the separated region greatly; strong suction can completely eliminate the separation and reduce the boundary layer thickness significantly while injection brings about the opposite results. Pressure division and the rest of the variables in the flow field are almost unaffected.

5.3 Suction Influence on the Separated Region and its Practical Application

478

Because there is great practical implication to the reduction of the separated region during the interaction, many suction conditions were investigated in various combinations with the flow conditions so as to gain detailed information about its influence.

First it was found that the suction influence is effective only in the separated region proper; active suction along this entire region must therefore be aspired to.

It turned out that the suction values required for prevention of separation are in the range $0 > V_w > -0.04$, for the range of various flow conditions investigated (per the previous paragraph). A detailed table and charts were prepared of the suction velocity required for prevention of separation as function of the main flow characteristics Mo , Re_{x_s} and p_e/p_o ; also an approximate empirical formula was found that connects the above suction velocity to the characteristics of the separated region (its dimensions and the value of the flow function within it).

It is to be noted that, in spite of inaccuracies in the computation of the separated region during the strong interactions, the results are methodical and consistent and so permit examination of the relative influence of the various suction conditions on the size of the separated region, for various flow conditions.

At any rate, it is clear that one cannot rely on the results (the suction values needed to prevent separation) with complete confidence, but only as a relative size and as approximate order of magnitude.

The two principal results in this paragraph - effectivity of suction within the confines of the separated region alone and the order of magnitude of the suction velocity needed to prevent separation, which is up to 4% of the expected speed - are of important practical significance for the design of aircraft components where separation of the boundary layer must be prevented during interactions of this kind (particularly at jet engine inlets and at control surfaces).

5.4 Proposals for Continuation of the Research

479

From the results of this research, as well as from similar studies carried out in the past or recently, it appears that it will be worthwhile in the future to concentrate on the following subjects:

a) Improvement of those numerical methods that have not yet been developed sufficiently (as mentioned in paragraph 5.1), so as to increase the accuracy of their results.

b) Extension of the computation method to turbulent flow by introducing the appropriate model of turbulence. This subject is particularly important because turbulent flow occurs in a significant part of practical interaction problems.

c) Formulation of the computation method into a general form so that it would be suitable to a wide spectrum of interaction problems like a compression corner, forward and rear steps, etc. The method's utility should be such as to lend itself for quick and easy use for all cases.

d) Adaptation of the computation method to any combination of geometric boundary conditions so as to permit investigation of flow over complex bodies on which a number of forms of interactions of different types occur (so the method will become a sort of "numerical wind tunnel").

This final subject will not be realized in the near future since it requires a lot of development and the use of a memory size and of computer time that are so large as to be impractical at this stage. But with future development in computers, it is to be expected that the matter will then be more practical.

Appendix A' - Non-dimensional definitions of characteristic flow parameters

/80

a. Mach Number

By definition

$$M = \sqrt{\frac{u^{*2} + v^{*2}}{\gamma R T^*}}$$

(A-1)

by setting

$$u^* = u u_0^*$$

$$v^* = v u_0^*$$

$$T^* = T u_0^{*2} / C_p$$

$$R = C_p - C_v \quad \gamma = C_p / C_v$$

we get

$$M = \sqrt{\frac{u^2 + v^2}{(\gamma - 1) T}}$$

(A-2)

b. Flow function

We will define a non-dimensional flow function through non-dimensional variables below:

$$\begin{cases} \frac{\partial \Psi}{\partial x} = -\rho v \\ \frac{\partial \Psi}{\partial y} = \rho u \end{cases} \quad (A-3)$$

and we will get the change of the flow function between two points through the linear integral

$$\Psi(b) - \Psi(a) = \int_a^b (\rho u dy - \rho v dx) \approx \rho_{\text{avg}} \int_a^b (u dy - v dx) \quad (A-4)$$

When ρ_{avg} is the average density between points a and b

c. Friction Coefficient

By definition

$$\begin{cases} C_F = \frac{\tau^*}{\frac{1}{2} \rho_0^* u_0^{*2}} \\ \tau^* = \mu^* \frac{\partial u^*}{\partial y^*} \end{cases} \quad (A-5)$$

by setting

$$Re_{x_s} = \frac{\rho_0^* u_0^* x_s^*}{\mu_0^*}$$

$$\begin{aligned} u^* &= u u_0^* \\ \mu^* &= \mu \mu_0^* \\ y^* &= y y_0^* \end{aligned}$$

we get

$$C_F = \left(\frac{2}{Re_{x_s}} \right) \mu \frac{\partial u}{\partial y} \quad (A-6)$$

d. Heat transfer coefficient

By definition

$$\begin{cases} C_Q = \frac{Q^*}{\rho_0^* u_0^* c_p T_0^*} \\ Q^* = k^* \frac{\partial T^*}{\partial y^*} \end{cases} \quad (A-7)$$

By setting $Re_{x_s} = \frac{\rho_0^* u_0^* x_s^*}{\mu_0^*}$

$$Pr^* = \frac{\mu^* c_p}{Pr}$$

$$\mu^* = \mu \mu_0^*$$

$$T^* = T u_0^{*2} / c_p$$

$$y^* = y x_s^*$$

/81

we get $C_Q = \frac{1}{Pr Re_{x_s}} \mu \frac{\partial T}{\partial y} \left(\frac{u_0^{*2}}{c_p T_0^*} \right)$

with the reference condition $V = 0$ and so $M_0^{*2} = \frac{u_0^{*2}}{\gamma R T_0^*}$

the following is valid

$$R = c_p - c_v \quad \gamma = c_p / c_v$$

(A-8)

from which we get

$$C_Q = \frac{M_0^{*2} (\gamma - 1)}{Pr Re_{x_s}} \mu \frac{\partial T}{\partial y}$$

Assumptions for the computation are:

$$a) \quad \frac{\partial p^*}{\partial x^*} = 0 \quad (B-1)$$

$$b) \quad \left(\frac{\partial T^*}{\partial y^*} \right)_{y^*=0} = 0 \quad (B-2)$$

c) The relation between the profiles of temperature and velocity in the laminar boundary layer and compression on a flat plate is (per Schlichting [92]):

$$\frac{T^*}{T_0^*} = \frac{T}{T_0} = 1 + \sqrt{Pr} \frac{\gamma-1}{2} M_0^2 \left[1 - \left(\frac{u^*}{u_0^*} \right)^2 \right] = \frac{p_0^*}{p^*} \quad (B-3)$$

We define the momentum equation as

$$\frac{d\theta^*}{dx^*} = \frac{\mu_w^*}{\rho_0^* u_0^*} \left(\frac{\partial u^*}{\partial y^*} \right)_{y^*=0} \quad (B-4)$$

when momentum thickness is given by

$$\theta^*(x^*) = \int_0^{\delta^*(x^*)} \frac{\rho^*}{\rho_0^*} \frac{u^*}{u_0^*} \left(1 - \frac{u^*}{u_0^*} \right) dy^* \quad (B-5)$$

also

$$\delta_1^*(x^*) = \int_0^{\delta^*(x^*)} \frac{\rho^*}{\rho_0^*} dy^* \quad (B-6)$$

We define a new variable

$$\eta = \frac{1}{\delta_1^*} \int_0^{y^*} \frac{\rho^*}{\rho_0^*} dy^* \quad (B-7)$$

and get

$$y^* = \delta_1^* \int_0^\eta \frac{\rho_0^*}{\rho^*} d\eta \quad \delta^* = \delta_1^* \int_0^1 \frac{\rho_0^*}{\rho^*} d\eta \quad (B-8)$$

Through exchange of variables from y^* to η

we get (B-5) again

$$\left(\begin{array}{l} y^*=0 \Rightarrow \eta=0 \\ y^*=\delta \Rightarrow \eta=1 \end{array} \right) \quad (B-9)$$

$$\theta^* = \delta_1^* \int_0^1 \frac{u^*}{u_0^*} \left(1 - \frac{u^*}{u_0^*} \right) d\eta$$

Now we assume a velocity profile of the following shape:

$$\frac{u^*}{u_0^*} = c_1 \eta + c_2 \eta^2 + c_3 \eta^3 + c_4 \eta^4 \quad (B-10)$$

Its profile fulfills the following condition:

$$\eta=1 \left\{ \begin{array}{l} u^* = u_0^* \\ \frac{\partial u^*}{\partial \eta} = 0 \\ \frac{\partial^2 u^*}{\partial \eta^2} = 0 \end{array} \right. \quad (B-11)$$

The momentum equation in the x-direction $\eta=0$ $\frac{\partial^2 u^*}{\partial y^{*2}} = 0$
 Its profile coefficients are calculated from these

$$\frac{u^*}{u_0^*} = \frac{u}{u_0} = 2\eta - 2\eta^3 + \eta^4 \quad (B-12)$$

$$\int_0^1 \frac{u^*}{u_0^*} \left[\frac{\partial}{\partial \eta} \left(\frac{u^*}{u_0^*} \right) \right] d\eta = \left(\frac{\partial u^*}{\partial y^*} \right)_{y^*=0} = 2 u_0^* \frac{\rho_{u^*}}{\rho_0^*} \quad (B-13)$$

$$\int_0^1 \frac{u^*}{u_0^*} \left(1 - \frac{u^*}{u_0^*} \right) d\eta = \frac{37}{315} \delta_1^* \quad (B-14)$$

(B-14) over x, substitute h, together
 I assume that

is approximately valid.

$$\frac{360}{17} \left(\frac{\mu_w^*}{\mu_0^*} \right) \left(\frac{\rho_w^*}{\rho_0^*} \right) \left(\frac{u_0^* x_0^*}{u_0^*} \right) \quad (B-15)$$

$$\quad (B-16)$$

$$\frac{1}{1 + \sqrt{1 - \frac{1}{2} M_0^2}} \quad (B-17)$$

$$\frac{1}{\sqrt{1 - \frac{1}{2} M_0^2}} \quad (B-18)$$

and also valid is
$$v_0^* x_0^* / u_0^* = x_0^{*2} / Re_{x_0} = x_0^* x_s^* / Re_{x_s} \quad (B-19)$$

From substitution of (B-3) and (B-12) into (B-8a) and integration over y^* we finally get the following non-dimensional expression

$$y = 5.836 \sqrt{\left(\frac{\mu_w}{\mu_0}\right) \left(\frac{T_0}{T_w}\right) \left(\frac{x_0^* x_s^*}{Re_{x_s}}\right)} \left[\eta + \sqrt{Pr} \frac{\gamma-1}{2} M_0^2 \left(\eta + \frac{4}{3} \eta^3 + \frac{8}{5} \eta^5 - \frac{2}{3} \eta^6 - \frac{4}{7} \eta^7 + \frac{1}{2} \eta^8 - \frac{1}{9} \eta^9 \right) \right] \quad (B-20)$$

Formulas (B-3), (B-12) and (B-20) define the flow profile.

As to component v of the velocity at the inlet section $v = 0$ can be assumed, based on the following evaluation: /84

$v(y)$ fulfills the order of magnitude $0 < v(y) < u \frac{\partial \delta}{\partial x}$ (B-21)

We then calculate the numerical value of this order of magnitude through the use of the following data (which demonstrate the computation condition in this study)

$$M_0 = 0 \quad Re_{x_s} = 3 \times 10^5 \quad x_0^* = 0.015 \text{ m.} \quad x_s^* = 0.05 \text{ m.} \quad (B-22)$$

we get

$$\left. \begin{aligned} \eta &= 1 \\ \frac{\mu_w}{\mu_0} &= \frac{S + \frac{1}{(\gamma-1) M_0^2}}{S + T_w} \left[(\gamma-1) M_0^2 T_w \right]^{3/2} \approx 1.96 \\ \frac{T_w}{T_0} &= \left[1 + \sqrt{Pr} \frac{(\gamma-1)}{2} M_0^2 \right] \approx 1.68 \end{aligned} \right\} \quad (B-23)$$

through substitution in (B-20) we get

$$\delta^* = 5.836 \sqrt{\left(\frac{\mu_w}{\mu_0}\right) \left(\frac{T_0}{T_w}\right) \left(\frac{x_0^* x_s^*}{Re_{x_s}}\right)} \left[1 + \frac{2.63}{630} \sqrt{Pr} \frac{\gamma-1}{2} M_0^2 \right] = \approx 5.8 \sqrt{\frac{1.96 \cdot 0.01}{1.68 \cdot 3 \times 10^5}} \sqrt{x_0^*} \left(1 + \sqrt{0.72} \frac{0.4}{2} \cdot 4 \cdot \frac{2.63}{630} \right) \approx 0.0033 \sqrt{x_0^*} \quad (B-24)$$

and from (B-15) we get $\frac{\partial \delta}{\partial x} \Big|_{x_0} = \frac{\partial \delta^*}{\partial x^*} \Big|_{x_0^* = 0.015} = 0.0135$

from the condition at the end of the boundary layer

$\frac{v}{u} \approx \frac{\partial \psi}{\partial x}$ where $\mu=1$ is valid

we get

$$0 < v(y) < o(10^{-2}) \quad (\text{B-25})$$

(Note: in the region of flow conditions $2 < Mo < 5$ and $10^4 < Re < 10^6$ there is no change in the order of magnitude of $V(y)$).

From this evaluation it becomes clear that V may be neglected at the inlet section with good approximation and we may assume that

$$V = 0 \quad (\text{B-26})$$

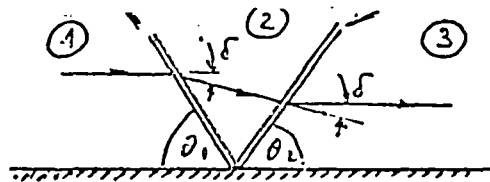
The pressure ratio parameter p_e/p_o characteristic for interaction (next to parameters x_s , Re_{x_s} , Mo) expresses the pressure ratio between exit cross-section and inlet cross-section. This pressure ratio is generated by the transition along the incident shock wave and the diffuse reflected flow lines (which combine into the reflected shock at great distance from the plate). As a practical matter, either experimentally or theoretically, the pressure ratio p_2/p_1 from both sides of the incident shock wave at the external boundary of the field is furnished and as result, the ratio p_e/p_o is obtained.

It is generally not possible to calculate p_2/p_1 directly from p_e/p_o and so an iterative computing procedure is required.

We will show a sample procedure for a simple case dealing with a shock wave that touches the plate and is reflected from it (without consideration of the boundary layer).

Given data: $p_3/p_1, M_1$ incident wave reflected wave

Required: p_2/p_1



Solution procedure:

a. an initial value is assumed for p_2/p_1 , for instance
$$\frac{p_2}{p_1} = \sqrt{\frac{p_3}{p_1}} \quad (C-1)$$

b. from the formulas for an oblique shock wave we get the angle of the incident wave
$$\theta_1 = \sin^{-1} \left[\frac{\sqrt{\left(\frac{p_2}{p_1} - 1\right) \frac{\gamma+1}{2\gamma} + 1}}{M_1} \right] \quad (C-2)$$

c. angle of flow deflection $\delta = \tan^{-1} \left[\frac{\{(M_1 \sin \theta_1)^2 - 1\} \cot \theta_1}{\frac{\gamma+1}{2} M_1^2 - \{(M_1 \sin \theta_1)^2 - 1\}} \right] \quad (C-3)$

d. angle of the reflected wave
$$\theta_2 = \theta_1 + \delta \quad (C-4)$$

e. Mach number downstream of shock wave
$$M_2 = \frac{1}{\sin(\theta_1 - \delta)} \sqrt{\frac{(M_1 \sin \theta_1)^2 + \frac{2}{\gamma-1}}{\frac{2\gamma}{\gamma-1} [(M_1 \sin \theta_1)^2 - 1]}} \quad (C-5)$$

f. Final pressure ratio
$$(C-6)$$

$$\left(\frac{p_3}{p_1}\right)' = \frac{p_2}{p_1} \cdot \frac{p_3}{p_2} = \frac{p_2}{p_1} \left[1 + \frac{2\gamma}{\gamma+1} \{(M_2 \sin \theta_2)^2 - 1\} \right]$$

g. when $|(p_3/p_1)' - (p_3/p_1)| > \epsilon$ then (p_2/p_1) is corrected through

and from here we return to stage b.
$$\frac{p_2}{p_1} = \begin{cases} \frac{p_2}{p_1} + \eta & \left(\frac{p_2}{p_1} > \frac{p_2}{p_1} + \epsilon \right) \\ \frac{p_2}{p_1} - \eta & \left(\frac{p_2}{p_1} < \frac{p_2}{p_1} - \epsilon \right) \end{cases} \quad (C-7)$$

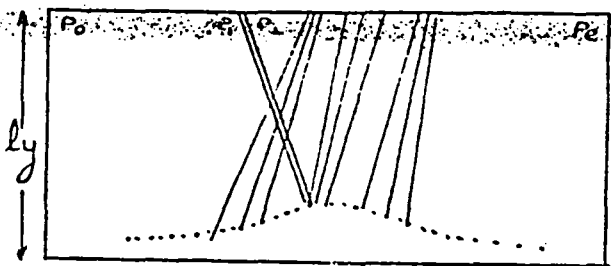
This process converges quickly and it becomes clear that the first guess in a. is very close to the final solution.

When speaking of the region close to the plate (not far from the edge of the boundary layer) there is as yet no reflected wave but only a series of diffuse compression expansion flow lines, as explained in paragraph 1.2. /86

Since the form of the flow lines and their direction are not known in advance, it is impossible to set up a computation like that described for the model.

Therefore, it is advisable to assume an initial pressure ratio p_2/p_1 (an approximation of $p_2/p_1 = \sqrt{p_3/p_1}$ is recommended) and to find the resulting (p_3/p_1) , from the flow field solution and then to correct p_2/p_1 based on the amount of divergence of (p_3/p_1) , from the given value of (p_3/p_1) .

It must be pointed out that it is more important (particularly for the purpose of comparison with other results) to obtain an accurate p_e/p_o ratio (indicated in the sample by p_3/p_1) than the right combination of waves and diffuse flow lines that generate this value.



An additional factor influencing p_2/p_1 is the nature of the intersection between the incident shock wave and the reflected diffuse flow lines, determined by the distance between the external boundary and

the plate. The closer the external boundary layer is to the plate the greater the influence of the intersection of reflected diffuse lines with the wave on its intensity at the boundary (the intersection causes bending of the wave and thus reinforces it).

Since calculation of intensity of the incident wave for p_e/p_o is anyway iterative, that phenomenon is not important during the initial stage of evaluating shock intensity and its influence is anyway expressed by the solution of the field flow during continuation of the iterative computation.

Just the same, it is not desirable that most of the reflected diffuse lines reach the external boundary upstream of the incident wave, since the influence of the wave's bending in the flow field will then not be properly accounted for; on the

other hand, it is not desirable to have the external boundary too far from the plate, so as not to increase the number of gridpoints unduly. Experience has shown that as long as no more than 25% of the reflected diffuse flow lines intersect the external boundary before they meet up with the wave itself, the solution is not much affected. Based on this criterion, the width of the field, ly , is determined in appendix D'.

In addition to the factors mentioned, the influence of Δx on the accuracy of the reflected diffuse flow lines must be noted. Δx must be at least one order of magnitude smaller than the length of the reflected diffuse lines zone so that their influence be a close approximation of the real situation (see appendix D').

During practical computation an initial evaluation is made of $p_2/p_1 = \sqrt{p_e/p_o}$, which is corrected in accordance with the results obtained until the desired value for p_e/p_o is reached.

The computation grid must include the region in which the majority of physical changes in the flow field occur. The grid density must be sufficiently high to permit observation of the main phenomena in the flow field, but it is also desirable to keep the number of grid points as small as possible so as not to place too heavy a load on the numerical computation. Also desirable is that the ratio of the dimensions $\Delta x/\Delta y$ not be too large for reasons of computation stability.

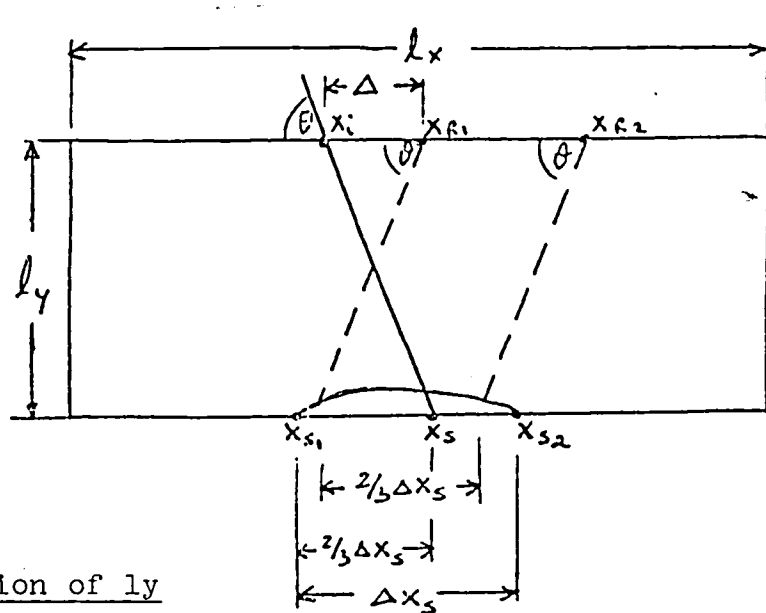
These considerations will be brought to bear in the evaluation of $\Delta x, \Delta y, l_x, l_y$.

a. Evaluation of l_x

Based on experimental results and on theoretical evaluations (see also paragraph 2.1.2), it was found that the region in which the principal changes in the flow field occur is about 150% long and is divided into two more or less equal parts on both sides of the point where the shock wave enters the boundary layer.

Therefore $l_x = 150\%$ (D-1)

During earlier computations (at the start of this study) it was found that, based on this evaluation, the location of the boundary downstream is far enough from the zone of interaction to fully justify the definition of a boundary condition of zero gradients in the x-direction. Also investigated and verified was the existence of the adjustment condition (in addition to $\frac{\partial p}{\partial x} = 0$ at that location). $\frac{\partial^2 p}{\partial x^2} = 0$



b. Evaluation of l_y

From the point of view of the region where changes occur in the flow field, ly must be of the order of magnitude of $2 - 3\delta_0$ (as obtained from previous theoretical and experimental results). We do have to consider an additional factor in this study, though, and that is the proximity of the incident wave to the diffuse reflected lines, which stems from the closeness of the external boundary to the plate; for that reason we will employ the sketch. The shock wave enters the upper boundary at point x_1 at the angle α and its continuation reaches the plate at point x_s (with approximate assumption that the wave will not bend and will arrive at the plate).

/88

The separated region stretches between points x_{s1} and x_{s2} and its length is Δx_s . From the end of the boundary layer above this section emerge the diffuse reflected flow lines (compression lines at the ends and expansion lines in the middle).

Based on previous theoretical and experimental results, it is known that the largest part of the separated region is located before point x_s (because of the influence to the rear, exerted by the pressure rise through the boundary layer); for the purpose of an approximate calculation we will then assume that $2/3$ of the Δx_s section is located before point x_s .

Since the density of the diffuse flow lines is much lower at the periphery than in the center of the reflection zone, we will only concern ourselves with the central $2/3$ of the reflection zone in this evaluation.

Let us also assume that the angle of reflection of the diffuse lines is equal to θ (actually the value is very close to θ , because of the small local flow angle which is on the order of just a few degrees).

Based on the foregoing data and evaluations we will now calculate the distance of points x_1 and x_{R1} from the front end of the field. It must be ascertained that Δ is positive or, at the least, of very small negative value so that all, or the majority, of the reflected flow lines will go to the external boundary downstream of the shock wave.

Based on the foregoing evaluations

$$x_s = 0.5 l_x$$

$$x_i = x_s - \frac{ly}{\tan \theta} = 0.5 l_x - \frac{ly}{\tan \theta}$$

(D-2)

we then define

$$\left. \begin{aligned} x_{s_2} - x_{s_1} &= \Delta x_s \\ x_{R_2} - x_{R_1} &= \frac{2}{3} \Delta x_s \end{aligned} \right\} \quad (D-3)$$

and get

$$\begin{aligned} x_{R_1} &= \left[0.5 l_x - 0.67 (0.67 \cdot \Delta x_s) \right] + \frac{l_y}{\tan \theta} = \\ &= 0.5 l_x - 0.45 \Delta x_s + \frac{l_y}{\tan \theta} \end{aligned}$$

l_x was already determined, previously as $l_x = 150 \cdot \delta_0$

we designate

$$\left. \begin{aligned} x_i / \delta_0 &= x_1 & x_{R_i} / \delta_0 &= x_2 \\ \Delta x_s / \delta_0 &= x & l_y / \delta_0 &= l \end{aligned} \right\} \quad (D-4)$$

and ultimately obtain

$$\left. \begin{aligned} x_1 &= 75 - \frac{l}{\tan \theta} \\ x_2 &= 75 - 0.45x + \frac{l}{\tan \theta} \end{aligned} \right\} \quad (D-5)$$

From computational results for $2 < Mo < 5$ and $1 < p_e/p_0 < 3$ (which agree with $10^\circ < \theta < 40^\circ$) the following orders of magnitude are known for the separated zone:

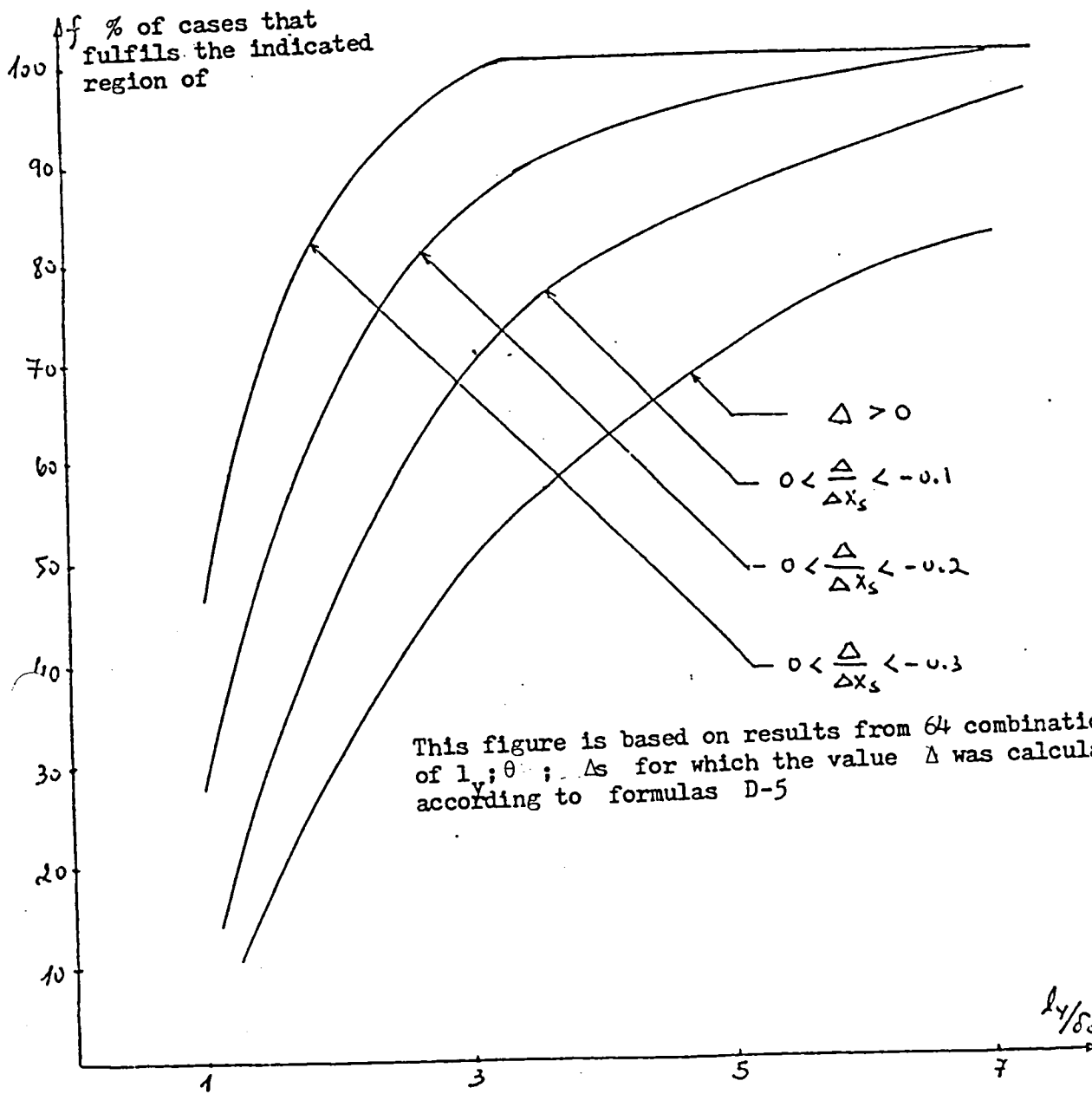
/89

$$\Delta x_s = (20 + 50) \delta_0 \quad (D-6)$$

Now we will investigate the influence of l_y on Δ in the region $(1 - 7) \delta_0$: for this purpose x_1 and x_2 are calculated for 16 different combinations of θ and

- Δx_s for which
- $\Delta x_s = 20\delta_0; 30\delta_0; 40\delta_0; 50\delta_0$
 - $\theta = 10^\circ; 20^\circ; 30^\circ; 40^\circ;$

and the results are tested for the following values of l_y/δ_0 : 1, 3, 5, 7. The results are sketched on the next page.



From the computational results it appears that in the region $1.5\delta_0 < l_y < 3\delta_0$ the value f increased greatly for a Δ that was either positive or slightly negative, while in the range $3\delta_0 < l_y < 7\delta_0$ this increase occurs much slower and more gradually until it reaches an asymptotic value. The results can be summed up in the following table:

/90

$\frac{l_y}{\delta_0}$	1	3	5	7
$\Delta > 0$	10%	50%	68%	81%
$0 < \frac{\Delta}{\Delta x_s} < .2$	30%	89%	95%	100%

It appears then that $l_y = 3\delta_0$ supplies effectively the requirement that no more than a quarter of the reflected diffuse lines reach the external boundary before the shock wave. The improvement available from $l_y = 5\delta_0$ or $l_y = 7\delta_0$ carries little weight in consideration of the needed increase in gridpoints (1.7 times and 2.4 times, respectively). The optimum choice will thus be -

$$l_y = 3\delta_0 \quad (D-7)$$

c. Evaluation of Δy

To be able to detect changes along the width of the boundary layer Δy must be an order of magnitude smaller than δ_0 ; so as not to exceed this principle the maximum value of Δy will be

$$\Delta y = 1/8\delta_0 \quad (D-8)$$

Note: Because of the increase of the boundary layer by $\Delta y < 0.1\delta_0$ in the interaction zone proper.

d. Evaluation of Δx (For Uniform Grid)

There are two requirements that limit Δx and they are:

1). For the sake of stability it is desirable to maintain a dimensional ratio of $\Delta x / \Delta y < 20$ and because it has been determined that $\Delta y = 1/8\delta_0$ it is required that $\Delta x < 2.5\delta_0$.

2). Δx must be an order of magnitude smaller than the length of the reflected flow lines zone so that the lines may be detected. That length is, according to its evaluation in paragraph b., about $2/3 \times (20 - 50) \delta_0 = (13 - 33) \delta_0$ and therefore $1 < \Delta x / \delta_0 < 3$ must be valid.

From those two requirements it was determined that

$$\Delta x = 2.\delta_0 \quad (D-9)$$

e. Evaluation of Δx (For a Non-Uniform Grid)

For a non-uniform grid it is required that in its center $\Delta x = O(\Delta y)$ be valid. In this study the value chosen is $\Delta x_{\min} = 1.6\Delta y = 0.2\delta_0$ (D-10)

According to the ratio of 1.1 for growth of grid meshes towards the periphery (see considerations in appendix G') we find that $\Delta x < 2\delta_0$ remains valid in the zone of reflected flow lines.

The field dimensions are defined as follows: (E-1)

$$\left. \begin{aligned} l_x &= a_x \delta_0 \\ l_y &= a_y \delta_0 \end{aligned} \right\}$$

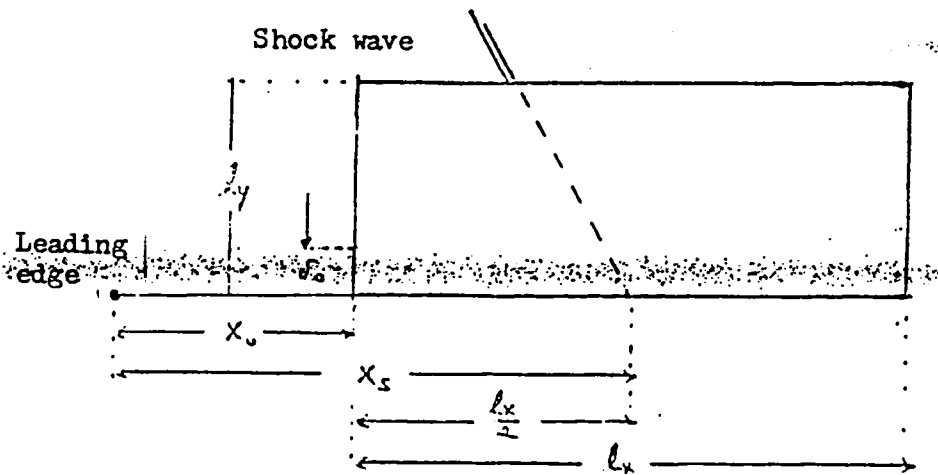
The mesh dimensions of the uniform grid (E-2)

$$\left. \begin{aligned} \Delta x &= b_{1x} \delta_0 \\ \Delta y &= b_{1y} \delta_0 \end{aligned} \right\}$$

The mesh dimensions of the non-uniform grid (E-3)

$$\left. \begin{aligned} \Delta x_{min} &= b_{2x} \delta_0 \\ \Delta y &= b_{2y} \delta_0 \end{aligned} \right\}$$

With the coefficients a_x , a_y , b_{1x} , b_{2x} , b_y the choice of subjects increases



The following relations exist (from now on all length values are dimensional):
According to appendix A'

$$\delta_0 = \sqrt{\left(\frac{1260}{37}\right) \left(\frac{\mu_0}{\rho_0}\right) \left(\frac{T_0}{T_w}\right) \left(\frac{x_0 x_s}{Re x_s}\right) \left[1 + \frac{263}{630} \sqrt{Fr} \frac{\gamma-1}{2} M_0^2\right]} = k_1 \sqrt{x_0} \quad (E-4)$$

also valid is

$$x_0 = x_s - \frac{l_x}{2} \quad (E-5)$$

$$l_x = a_x \delta_0 \quad (E-6)$$

Those are the three equations with the unknowns l_x , x_0 and δ_0 and the procedure for their solution is as follows:

After extraction of δ_0 and x_0 we get $\frac{l_x}{a_x} = K_1 \sqrt{x_s - \frac{l_x}{2}}$

We designate $K = (K_1 a_x)^2$ and get a quadratic equation for l_x

$$2 l_x^2 + K l_x - 2 K x_s \quad (E-7)$$

From the two solutions we choose the practical physical value and get

/92

$$l_x = \frac{-K \pm \sqrt{K^2 + 16 K x_s}}{4} \Rightarrow \frac{K (\sqrt{1 + 16 x_s / K} - 1)}{4} \quad (E-8)$$

while δ_0 and x_0 are determined through (E-5) and (E-6). Through (E-1), (E-2), (E-3) and δ_0 we determine l_y and also Δx and Δy (after substituting the coefficients in those formulas).

The number of gridpoints in the y-direction in both grids is

$$N = \text{int} \left(\frac{l_y}{\Delta y} \right) + 1 \quad (E-9)$$

The number of gridpoints in the x-direction of the uniform grid is

$$M_1 = \text{int} \left(\frac{l_x}{\Delta x} \right) + 1 \quad (E-10)$$

The number of gridpoints in the x-direction, in a non-uniform grid, is based on the mesh length in the center of the field being Δx_{\min} . The mesh length increases from the center of the field towards its periphery according to the formula for a geometrical series with a growth ratio g .

So we get

$$M_2 = 2n + 2 \quad (E-11)$$

when n is determined by

$$(E-12)$$

and its solution is

$$2 \Delta x_{\min} g \frac{g^n - 1}{g - 1} + \Delta x_{\min} = l_x = \frac{a_x}{b_2 x} \Delta x_{\min} \quad (E-13)$$

$$n = \text{int} \left[\frac{\log_{10} \left[1 + \frac{\left(\frac{a_x}{b_2 x} - 1 \right) (g - 1)}{2g} \right]}{\log_{10}(g)} \right]$$

According to the previously determined considerations the following coefficient values were chosen:

$$\left. \begin{array}{l} b_{1x} = 2 \\ b_{2x} = 0.2 \\ b_y = 0.125 \end{array} \right\} \begin{array}{l} a_x = 150 \\ a_y = .3 \end{array} \quad (E-14)$$

and then we get the number of gridpoints

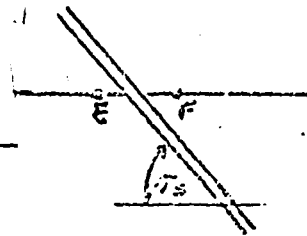
$$\left. \begin{array}{l} M = 76 \\ N = 25 \end{array} \right\} (E-15)$$

The number of points was limited to this value (76 x 25 = 1900) by considerations for an optimum between high accuracy and reasonable computer time (one computer run without calculations of coefficient stability for 1900 gridpoints takes 1.0 - 1.5 minutes and at least several hundred runs (iterations) are required until convergence is reached).

Given a shock wave with intensity $Sh = p_F/p_E$

Shock wave

External boundary



It is required to calculate the flow at F as function of the characteristics at E.

From the Rankine-Hugoniot relations we get the angle at which the wave enters

$$\frac{p_F}{p_E} = Sh = \frac{2\gamma}{\gamma+1} \left\{ M_E^2 \sin^2 \sigma_s \right\} - \frac{\gamma-1}{\gamma+1} \quad (F-1)$$

$$\sigma_s = \sin^{-1} \left[\frac{\sqrt{\left(Sh + \frac{\gamma-1}{\gamma+1} \right) \frac{p_E}{\rho_E c^2}}}{M_E} \right] \quad (F-2)$$

Velocity components at E:

$$V_{En} = U_E \sin \sigma_s + V_E \cos \sigma_s$$

across the shock wave

$$V_{Et} = U_E \cos \sigma_s - V_E \sin \sigma_s \quad (F-3)$$

parallel to the shock wave

Velocity components at F:

$$V_{Fn} = V_{En} \left[\frac{(\gamma-1)M_E^2 \sin^2 \sigma_s + \gamma}{(\gamma+1)M_E^2 \sin^2 \sigma_s} \right]$$

across the shock wave

$$V_{Ft} = V_{Et} \quad (F-4)$$

parallel to the shock wave

Velocity components at F according to the original directions (of the first axes)

in the x-direction

$$U_F = V_{Fn} \sin \sigma_s + V_{Ft} \cos \sigma_s \quad (F-5)$$

in the y-direction

$$V_F = V_{Fn} \cos \sigma_s - V_{Ft} \sin \sigma_s$$

We also get

$$T_F = T_E \left[\frac{\left(1 + \frac{\gamma-1}{2} M_E^2 \sin^2 \sigma_s \right) \left(\frac{2\gamma}{\gamma-1} M_E^2 \sin^2 \sigma_s - 1 \right)}{\frac{\gamma+1}{2(\gamma-1)} M_E^2 \sin^2 \sigma_s} \right] \quad (F-6)$$

and from the state equation we get

$$p_F = \frac{T_F}{T_E} \frac{p_E}{p_E} \quad (F-7)$$

a. Uniform grid, second order accuracy in the x and y directions

According to Taylor's development around m

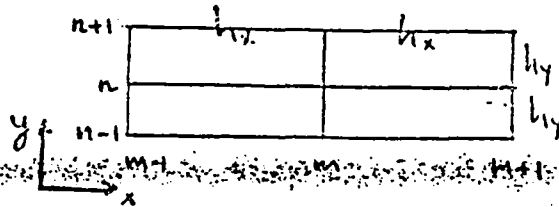
$$f_{m-1} = f_m - h f'_m + \frac{h^2}{2} f''_m - \frac{h^3}{6} f'''_m + \frac{h^4}{24} f^{(4)}_m + o(h^5) \quad (G-1a)$$

$$f_{m+1} = f_m + h f'_m + \frac{h^2}{2} f''_m + \frac{h^3}{6} f'''_m + \frac{h^4}{24} f^{(4)}_m + o(h^5) \quad (G-1b)$$

by subtraction we get $f'_m = \frac{f_{m+1} - f_{m-1}}{2h} + o(h^2)$ } (G-2)

by addition we get $f''_m = \frac{f_{m+1} - 2f_m + f_{m-1}}{h^2} + o(h^2)$ }

For a grid with uniform spacing in the x and y directions we get



$$\left. \frac{\partial f}{\partial x} \right|_{m,n} = \frac{f_{m+1,n} - f_{m-1,n}}{2h_x} + o(h_x^2) \quad (G-3)$$

$$\left. \frac{\partial f}{\partial y} \right|_{m,n} = \frac{f_{m,n+1} - f_{m,n-1}}{2h_y} + o(h_y^2)$$

$$\left. \frac{\partial^2 f}{\partial x^2} \right|_{m,n} = \frac{f_{m+1,n} - 2f_{m,n} + f_{m-1,n}}{h_x^2} + o(h_x^2)$$

$$\left. \frac{\partial^2 f}{\partial y^2} \right|_{m,n} = \frac{f_{m,n+1} - 2f_{m,n} + f_{m,n-1}}{h_y^2} + o(h_y^2)$$

$$\left. \frac{\partial^2 f}{\partial x \partial y} \right|_{m,n} = \frac{(f_{m+1,n+1} - f_{m+1,n-1}) - (f_{m-1,n+1} - f_{m-1,n-1})}{4h_x h_y} + o(h_x^2, h_y^2)$$

b. Uniform grid, fourth order accuracy in the x-direction (and second order accuracy in the y-direction)

According to Taylor's development around m

$$f_{m-2} = f_m - 2h f'_m + 2h^2 f''_m - \frac{4}{3} h^3 f'''_m + \frac{2}{3} h^4 f^{IV}_m + o(h^5) \quad (G-4a)$$

$$f_{m-1} = f_m - h f'_m + \frac{h^2}{2} f''_m - \frac{h^3}{6} f'''_m + \frac{h^4}{24} f^{IV}_m + o(h^5) \quad (G-4b)$$

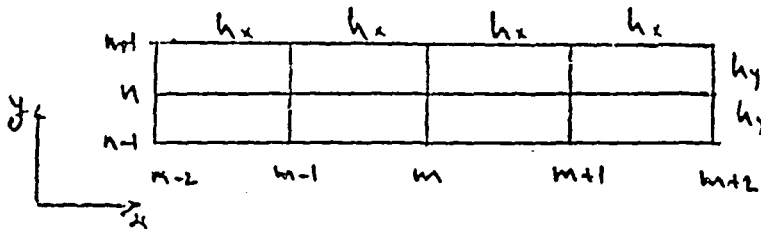
$$f_{m+1} = f_m + h f'_m + \frac{h^2}{2} f''_m + \frac{h^3}{6} f'''_m + \frac{h^4}{24} f^{IV}_m + o(h^5) \quad (G-4c)$$

$$f_{m+2} = f_m + 2h f'_m + 2h^2 f''_m + \frac{4}{3} h^3 f'''_m + \frac{2}{3} h^4 f^{IV}_m + o(h^5) \quad (G-4d)$$

$$f'_m = \frac{f_{m-2} - 8f_{m-1} + 8f_{m+1} - f_{m+2}}{12h} + o(h^4) \quad (G-5)$$

$$f''_m = \frac{-f_{m-2} + 16f_{m-1} - 30f_m + 16f_{m+1} - f_{m+2}}{12h^2} + o(h^4)$$

For a grid with uniform spacing in x and y directions, with fourth order differences in the x-direction and second order differences in the y-direction, we get



$$\left. \frac{\partial f}{\partial x} \right|_{m,n} = \frac{f_{m-2,n} - 8f_{m-1,n} + 8f_{m+1,n} - f_{m+2,n}}{12h_x} + o(h_x^4) \quad (G-6)$$

$$\left. \frac{\partial f}{\partial y} \right|_{m,n} = \frac{f_{m,n+1} - f_{m,n-1}}{2h_y} + o(h_y^2)$$

$$\left. \frac{\partial^2 f}{\partial x^2} \right|_{m,n} = \frac{-f_{m-2,n} + 16f_{m-1,n} - 30f_{m,n} + 16f_{m+1,n} - f_{m+2,n}}{12h_x^2} + o(h_x^4)$$

$$\left. \frac{\partial^2 f}{\partial y^2} \right|_{m,n} = \frac{f_{m,n+1} - 2f_{m,n} + f_{m,n-1}}{h_y^2} + o(h_y^4)$$

$$\left. \frac{\partial^2 f}{\partial x^2} \right|_{m,n} = \frac{1}{24 h_x h_y} \left[(f_{m-2,n+1} - 8f_{m-1,n+1} + 8f_{m+1,n+1} - f_{m+2,n+1}) + \right. \\ \left. - (f_{m-2,n-1} - 8f_{m-1,n-1} + 8f_{m+1,n-1} - f_{m+2,n-1}) \right] + o(h_x^4, h_y^4) \quad (G-6)$$

Note: when h_y is one order of magnitude smaller than h_x (for the uniform grid of the computation $\frac{h_x}{h_y} = 16$), a higher accuracy is obtained in (G-3) for derivatives of y , which is not expressed in the finite difference equations because of the lower accuracy for x -derivatives.

In contrast to it, the accuracy of x -direction derivatives improves in (G-6) and reaches the same order as the derivatives in the y -direction, so that in general the accuracy of the difference equations improved. This improvement in accuracy is particularly convenient near where the shock wave impinges on the boundary layer, where relatively strong gradients of the variables exist.

c. Non-Uniform grid in the x -direction, second order accuracy in the x and y directions

According to Taylor's development around m

$$f_{m-1} = f_m - h f'_m + \frac{h^2}{2} f''_m - \frac{h^3}{6} f'''_m + \frac{h^4}{24} f^{(4)}_m + o(h^5) \quad (G-7a)$$

$$f_{m+1} = f_m + qh f'_m + \frac{q^2 h^2}{2} f''_m + \frac{q^3 h^3}{6} f'''_m + \frac{q^4 h^4}{24} f^{(4)}_m + o(h^5) \quad (G-7b)$$

Through $[(a) \times q^2 - (b)]$ we get

$$f'_m = \frac{(f_{m+1} - f_m)/q + (f_m - f_{m-1}) \cdot q}{h(1+q)} + R_1 \quad (G-8)$$

Through $[q \times (a) - (b)]$ we get

$$f''_m = \frac{(f_{m+1} - f_m) - (f_m - f_{m-1})}{\frac{h^2 q}{2(1+q)}} + R_2$$

when the errors are

$$R_1 = \frac{1}{qh(1+q)} \left[-\frac{h^3}{6} q^2 (1+q) f'''_m - \frac{h^4}{24} q (q^2-1) f^{(4)}_m \right] \Rightarrow o(h^2 q) \\ R_2 = \frac{1}{\frac{h^2 q}{2(1+q)}} \left[-\frac{h^3}{6} q (q^2-1) f'''_m - \frac{h^4}{24} q (q^2+1) f^{(4)}_m \right] \Rightarrow o(h(q-1)) \quad (G-9)$$

For $q = 1$ the errors in the two derivatives are $O(h^2)$; to preserve the order of magnitude it is necessary that $1 - q \approx h$. In practice, the accuracy of the derivatives becomes impaired when $q < 1.1$ and so we will choose $q = 1.1$ for the difference computations of a non-uniform grid.

For a grid with changing spacings in the x-directions and uniform ones in the y-direction, when the differences are computed to a second order of accuracy in both directions, we get

$$\left. \frac{\partial f}{\partial x} \right|_{m,n} = \frac{(f_{m+1,n} - f_{m,n})/q + (f_{m,n} - f_{m-1,n})q}{h_x(1+q)} + o(h_x^2 q)$$

(G-10)

$$\left. \frac{\partial f}{\partial y} \right|_{m,n} = \frac{f_{m,n+1} - f_{m,n-1}}{2h_y} + o(h_y^2)$$

$$\left. \frac{\partial^2 f}{\partial x^2} \right|_{m,n} = \frac{(f_{m+2,n} - f_{m,n}) - (f_{m,n} - f_{m-2,n})q}{h_x^2(1+q)} + o(h_x^2(1+q)^2)$$

$$\left. \frac{\partial^2 f}{\partial y^2} \right|_{m,n} = \frac{f_{m,n+2} - 2f_{m,n} + f_{m,n-2}}{h_y^2} + o(h_y^4)$$

$$\left. \frac{\partial^2 f}{\partial x \partial y} \right|_{m,n} = \frac{(f_{m+1,n+1} - f_{m,n+1})/q + (f_{m,n+1} - f_{m-1,n+1})q}{2h_y h_x(1+q)} - \frac{(f_{m+1,n-1} - f_{m,n-1})/q + (f_{m,n-1} - f_{m-1,n-1})q}{2h_y h_x(1+q)} + o(h_y^2, h_x^2)$$

a. The Brailovskaya scheme (for uniform and non-uniform grids)

The complete difference equations will be formulated further on, in their general form and to a second order accuracy (without artificial viscosity terms). Let us define the symbols as follows

	Non-uniform grid	Uniform Grid
$q =$	$\Delta x_m / \Delta x_{m-1}$	1.0
$h_x =$	$\frac{1}{2} (\Delta x_m + \Delta x_{m-1})$	Δx
$h_y =$	Δy	Δy

The general form of the equations

$$\frac{\partial W}{\partial t} + \frac{\partial F}{\partial x} + \frac{\partial G}{\partial y} = S \quad (H-1)$$

First integration stage

$$W_{m,n}^{\bar{t+1}} = W_{m,n}^t - \frac{\Delta t}{2 h_x} \left[(F_{m+1,n}^t - F_{m,n}^t) \frac{1}{q} + (F_{m,n}^t - F_{m-1,n}^t) q \right] +$$

$$- \frac{\Delta t}{2 h_y} \left[G_{m,n+1}^t - G_{m,n-1}^t \right] + \Delta t \cdot S_{m,n}^t \quad (H-2)$$

Second integration stage

$$W_{m,n}^{t+1} = W_{m,n}^t - \frac{\Delta t}{2 h_x} \left[(F_{m+1,n}^{\bar{t+1}} - F_{m,n}^{\bar{t+1}}) \frac{1}{q} + (F_{m,n}^{\bar{t+1}} - F_{m-1,n}^{\bar{t+1}}) q \right] +$$

$$- \frac{\Delta t}{2 h_y} \left[G_{m,n+1}^{\bar{t+1}} - G_{m,n-1}^{\bar{t+1}} \right] + \Delta t \cdot S_{m,n}^t$$

The equations for fourth order accuracy are written in similar form according to appendix G' paragraph b.

The expressions for the equations of a uniform grid, to second order accuracy, will be detailed further on in the form in which they appear in the original Brailovskaya [8] scheme and also in the computer program. (parallel terms for a non-uniform grid and for fourth order differences, were developed for the computer program in similar fashion, by means of the definitions given in appendix G').

$$W_{m,n} = \begin{bmatrix} \rho \\ \rho u \\ \rho v \\ E \end{bmatrix}_{m,n} = \begin{bmatrix} w_1 \\ w_2 \\ w_3 \\ w_4 \end{bmatrix}_{m,n} \quad (H-3)$$

$$F_{m,n} = \begin{bmatrix} \rho u \\ \rho + \rho u^2 \\ \rho uv \\ u(E + \rho) \end{bmatrix}_{m,n} = \begin{bmatrix} w_2 \\ \rho + w_2 \cdot u \\ w_2 \cdot v \\ u(w_4 + \rho) \end{bmatrix}_{m,n} \quad (H-4)$$

$$G_{m,n} = \begin{bmatrix} \rho v \\ \rho uv \\ \rho + \rho v^2 \\ v(E + \rho) \end{bmatrix}_{m,n} = \begin{bmatrix} w_3 \\ w_3 \cdot u \\ \rho + w_3 \cdot v \\ v(w_4 + \rho) \end{bmatrix}_{m,n} \quad (H-5)$$

$$S_{m,n} = \frac{1}{Re} \frac{\partial}{\partial x} \begin{bmatrix} 0 \\ \sigma_x \\ \tau_{xy} \\ \frac{\mu}{Pr} \frac{\partial T}{\partial x} + u\sigma_x + v\tau_{xy} \end{bmatrix}_{m,n} + \frac{1}{Re} \frac{\partial}{\partial y} \begin{bmatrix} 0 \\ \tau_{xy} \\ \sigma_y \\ \frac{\mu}{Pr} \frac{\partial T}{\partial y} + u\tau_{xy} + v\sigma_y \end{bmatrix}_{m,n} = \quad (H-6)$$

$$\left[\begin{array}{c} 7h_5 + 6h_5 + 8h_5 + 6h_5 + 9h_5 + 5h_5 + 4h_5 + 3h_5 + 2h_5 + 1h_5 \\ 11h_5 + 9h_5 + 7h_5 + 5h_5 \\ 17h_5 + 15h_5 + 13h_5 + 11h_5 \\ 0 \end{array} \right] \frac{\partial^2}{\partial x^2} = (H-6)$$

When

/100

(H-7)

$$S_{21} = \frac{4}{3} \frac{\partial}{\partial x} \left(\mu \frac{\partial u}{\partial x} \right) = \frac{2}{3h_x^2} \left[(\mu_{m+1,n} + \mu_{m,n})(u_{m+1,n} - u_{m,n}) - (\mu_{m,n} + \mu_{m-1,n})(u_{m,n} - u_{m-1,n}) \right]$$

$$S_{22} = \frac{\partial}{\partial y} \left(\mu \frac{\partial u}{\partial y} \right) = \frac{1}{2h_y} \left[(\mu_{m,n+1} + \mu_{m,n})(u_{m,n+1} - u_{m,n}) - (\mu_{m,n} + \mu_{m,n-1})(u_{m,n} - u_{m,n-1}) \right]$$

$$S_{23} = \frac{\partial}{\partial y} \left(\mu \frac{\partial v}{\partial x} \right) = \frac{1}{4h_x h_y} \left[\mu_{m,n+1} (v_{m+1,n+1} - v_{m-1,n+1}) - \mu_{m,n-1} (v_{m+1,n-1} - v_{m-1,n-1}) \right]$$

$$S_{24} = -\frac{2}{3} \frac{\partial}{\partial x} \left(\mu \frac{\partial v}{\partial y} \right) = -\frac{1}{6h_x h_y} \left[\mu_{m+1,n} (v_{m+1,n+1} - v_{m+1,n-1}) - \mu_{m-1,n} (v_{m-1,n+1} - v_{m-1,n-1}) \right]$$

$$S_{31} = \frac{4}{3} \frac{\partial}{\partial y} \left(\mu \frac{\partial v}{\partial y} \right) = \frac{2}{3h_y^2} \left[(\mu_{m,n+1} + \mu_{m,n})(v_{m,n+1} - v_{m,n}) - (\mu_{m,n} + \mu_{m,n-1})(v_{m,n} - v_{m,n-1}) \right]$$

$$S_{32} = \frac{\partial}{\partial x} \left(\mu \frac{\partial v}{\partial x} \right) = \frac{1}{2h_x} \left[(\mu_{m+1,n} + \mu_{m,n})(v_{m+1,n} - v_{m,n}) - (\mu_{m,n} + \mu_{m-1,n})(v_{m,n} - v_{m-1,n}) \right]$$

$$S_{33} = \frac{\partial}{\partial x} \left(\mu \frac{\partial u}{\partial y} \right) = \frac{1}{4h_x h_y} \left[\mu_{m+1,n} (u_{m+1,n+1} - u_{m+1,n-1}) - \mu_{m-1,n} (u_{m-1,n+1} - u_{m-1,n-1}) \right]$$

$$S_{34} = -\frac{2}{3} \frac{\partial}{\partial y} \left(\mu \frac{\partial u}{\partial x} \right) = -\frac{1}{6h_x h_y} \left[\mu_{m,n+1} (u_{m+1,n+1} - u_{m-1,n+1}) - \mu_{m,n-1} (u_{m+1,n-1} - u_{m-1,n-1}) \right]$$

$$S_{41} = \frac{1}{Pr} \frac{\partial}{\partial x} \left(\mu \frac{\partial T}{\partial x} \right) = \frac{1}{2Pr h_x^2} \left[(\mu_{m+1,n} + \mu_{m,n})(T_{m+1,n} - T_{m,n}) - (\mu_{m,n} + \mu_{m-1,n})(T_{m,n} - T_{m-1,n}) \right]$$

$$S_{42} = \frac{1}{Pr} \frac{\partial}{\partial y} \left(\mu \frac{\partial T}{\partial y} \right) = \frac{1}{2Pr h_y} \left[(\mu_{m,n+1} + \mu_{m,n})(T_{m,n+1} - T_{m,n}) - (\mu_{m,n} + \mu_{m,n-1})(T_{m,n} - T_{m,n-1}) \right]$$

$$S_{43} = \frac{4}{3} \frac{\partial}{\partial x} \left(\mu u \frac{\partial u}{\partial x} \right) = \frac{1}{3h_x^2} \left[(\mu_{m+1,n} u_{m+1,n} + \mu_{m,n} u_{m,n})(u_{m+1,n} - u_{m,n}) - (\mu_{m,n} u_{m,n} + \mu_{m-1,n} u_{m-1,n})(u_{m,n} - u_{m-1,n}) \right]$$

$$S44 = \frac{\partial}{\partial x} (\mu v \frac{\partial v}{\partial x}) = \frac{1}{2h_x} \left[(\mu_{m+1,n} v_{m+1,n} + \mu_{m,n} v_{m,n}) (v_{m+1,n} - v_{m,n}) - (\mu_{m,n} v_{m,n} + \mu_{m-1,n} v_{m-1,n}) (v_{m,n} - v_{m-1,n}) \right]$$

$$S45 = \frac{4}{3} \frac{\partial}{\partial y} (\mu v \frac{\partial v}{\partial y}) = \frac{1}{2h_y} \left[(\mu_{m,n+1} v_{m,n+1} + \mu_{m,n} v_{m,n}) (v_{m,n+1} - v_{m,n}) - (\mu_{m,n} v_{m,n} + \mu_{m,n-1} v_{m,n-1}) (v_{m,n} - v_{m,n-1}) \right]$$

$$S46 = \frac{\partial}{\partial y} (\mu u \frac{\partial u}{\partial y}) = \frac{1}{2h_y} \left[(\mu_{m,n+1} u_{m,n+1} + \mu_{m,n} u_{m,n}) (u_{m,n+1} - u_{m,n}) - (\mu_{m,n} u_{m,n} + \mu_{m,n-1} u_{m,n-1}) (u_{m,n} - u_{m,n-1}) \right]$$

$$S47 = \frac{\partial}{\partial x} (\mu v \frac{\partial u}{\partial y}) = \frac{1}{4h_x h_y} \left[\mu_{m+1,n} v_{m+1,n} (u_{m+1,n+1} - u_{m+1,n-1}) - \mu_{m-1,n} v_{m-1,n} (u_{m-1,n+1} - u_{m-1,n-1}) \right]$$

$$S48 = -\frac{2}{3} \frac{\partial}{\partial x} (\mu u \frac{\partial v}{\partial y}) = -\frac{1}{12h_x h_y} \left[\mu_{m+1,n} u_{m+1,n} (v_{m+1,n+1} - v_{m+1,n-1}) - \mu_{m-1,n} u_{m-1,n} (v_{m-1,n+1} - v_{m-1,n-1}) \right]$$

$$S49 = \frac{\partial}{\partial y} (\mu u \frac{\partial v}{\partial x}) = \frac{1}{4h_x h_y} \left[\mu_{m,n+1} u_{m,n+1} (v_{m+1,n+1} - v_{m-1,n+1}) - \mu_{m,n-1} u_{m,n-1} (v_{m+1,n-1} - v_{m-1,n-1}) \right]$$

$$S4A = -\frac{2}{3} \frac{\partial}{\partial y} (\mu v \frac{\partial u}{\partial x}) = -\frac{1}{12h_x h_y} \left[\mu_{m,n+1} v_{m,n+1} (u_{m+1,n+1} - u_{m-1,n+1}) - \mu_{m,n-1} v_{m,n-1} (u_{m+1,n-1} - u_{m-1,n-1}) \right]$$

b. MacCormack scheme (only for a uniform grid)

/101

The general form of the equations

$$\frac{\partial W}{\partial t} + \frac{\partial F}{\partial x} + \frac{\partial G}{\partial y} = S = \frac{\partial S_1}{\partial x} + \frac{\partial S_2}{\partial y} \quad (H-8)$$

and in another form

$$\begin{aligned} A = F - S_1 \\ B = G - S_2 \end{aligned} \quad \frac{\partial W}{\partial t} + \frac{\partial A}{\partial x} + \frac{\partial B}{\partial y} = 0 \quad (H-9)$$

Here follows the general description of the scheme:

The first integration stage

$$W_{m,n}^{t+\Delta t} = W_{m,n}^t - \frac{\Delta t}{\Delta x} (A_{m+1,n} - A_{m-1,n}) - \frac{\Delta t}{\Delta y} (B_{m,n+1} - B_{m,n-1}) \quad (H-10)$$

when

$$\left. \begin{aligned} m_i &= m + m_d \\ n_j &= n + n_d \\ m_d &= \text{mod}(t, 2) \\ n_d &= \text{mod}(t - m_d, 4) / 2 \end{aligned} \right\} \quad (\text{H-11})$$

The second integration stage

$$W_{m,n}^{t+1} = \frac{1}{2} \left[W_{m,n}^t + W_{m,n}^{\bar{t}+1} - \frac{\Delta t}{\Delta x} (A_{m_i, n}^{\bar{t}+1} - A_{m_i-1, n}^{\bar{t}+1}) - \frac{\Delta t}{\Delta y} (B_{m, n_j}^{\bar{t}+1} - B_{m, n_j-1}^{\bar{t}+1}) \right] \quad (\text{H-12})$$

when

$$\left. \begin{aligned} m_i &= m + m_d \\ n_j &= n + n_d \\ m_d &= \text{mod}(m_d + 1, 2) \\ n_d &= \text{mod}(n_d + 1, 2) \end{aligned} \right\} \quad (\text{H-13})$$

Note: the function mod is defined by

$$\text{mod}(x, y) = x - \text{INT}\left(\frac{x}{y}\right) \cdot y \quad (\text{H-14})$$

$$W_{m,n} = \begin{bmatrix} p \\ pu \\ pv \\ E \end{bmatrix}_{m,n} = \begin{bmatrix} w_1 \\ w_2 \\ w_3 \\ w_4 \end{bmatrix}_{m,n} \quad (\text{H-15}) \quad \underline{/102}$$

$$A_{m,n} = \begin{bmatrix} pu \\ p + pu^2 \\ puv \\ u(E+p) \end{bmatrix}_{m,n} - \frac{1}{Re} \begin{bmatrix} 0 \\ \sigma_x \\ \tau_{xy} \\ \frac{\mu}{\rho_i} \frac{\partial T}{\partial x} + u\sigma_x + v\tau_{xy} \end{bmatrix}_{m,n} = \quad (\text{H-16})$$

$$= \begin{bmatrix} W_2 \\ \rho + W_2 u \\ W_2 v \\ u(W_2 + p) \end{bmatrix}_{m,n} - \frac{\mu_{m,n}}{Re} \begin{bmatrix} 0 \\ \frac{3}{2} \left[\frac{1}{\Delta x} (u_{m+1,n} - u_{m-1,n}) - \frac{1}{2\Delta y} (v_{m,n+1} - v_{m,n-1}) \right] \\ \left[\frac{1}{2\Delta y} (u_{m,n+1} - u_{m,n-1}) + \frac{1}{2\Delta x} (v_{m+1,n} - v_{m-1,n}) \right] \\ \frac{1}{2Pr\Delta x} [T_{m+1,n} - T_{m-1,n}] + \frac{2}{3} u_{m,n} \left[\frac{1}{\Delta x} (u_{m+1,n} - u_{m-1,n}) - \frac{1}{2\Delta y} (v_{m,n+1} - v_{m,n-1}) \right] \\ + v_{m,n} \left[\frac{1}{2\Delta y} (u_{m,n+1} - u_{m,n-1}) + \frac{1}{2\Delta x} (v_{m+1,n} - v_{m-1,n}) \right] \end{bmatrix}$$

$$B_{m,n} = \begin{bmatrix} \rho v \\ \rho uv \\ \rho + \rho v^2 \\ v(E+p) \end{bmatrix}_{m,n} - \frac{1}{Re} \begin{bmatrix} 0 \\ \tau_{xy} \\ \sigma_y \\ \frac{\mu}{Pr} \frac{\partial T}{\partial y} + u\tau_{xy} + v\sigma_y \end{bmatrix}_{m,n} \quad (H-17)$$

$$= \begin{bmatrix} W_3 \\ W_3 u \\ \rho + W_3 v \\ v(W_3 + p) \end{bmatrix}_{m,n} - \frac{\mu_{m,n}}{Re} \begin{bmatrix} 0 \\ \left[\frac{1}{2\Delta y} (u_{m,n+1} - u_{m,n-1}) + \frac{1}{2\Delta x} (v_{m+1,n} - v_{m-1,n}) \right] \\ \frac{3}{2} \left[\frac{1}{\Delta y} (v_{m,n+1} - v_{m,n-1}) - \frac{1}{2\Delta x} (u_{m+1,n} - u_{m-1,n}) \right] \\ \frac{1}{2Pr\Delta y} [T_{m,n+1} - T_{m,n-1}] + u_{m,n} \left[\frac{1}{2\Delta y} (u_{m,n+1} - u_{m,n-1}) + \frac{1}{2\Delta x} (v_{m+1,n} - v_{m-1,n}) \right] \\ + \frac{2}{3} v_{m,n} \left[\frac{1}{\Delta y} (v_{m,n+1} - v_{m,n-1}) - \frac{1}{2\Delta x} (u_{m+1,n} - u_{m-1,n}) \right] \end{bmatrix}$$

During the actual integration the computation is split up into x and y directions. For all KI runs in the y-direction a computation for the x-direction is made where KI = INT (DTX/DTY)

$$\boxed{DTX = 0.5 \Delta x / [\alpha_0 (1 + M_0)]} \quad \boxed{DTY = 0.5 \Delta y / [\alpha_0 (1 + 0.25 M_0)]} \quad (H-18)$$

A set of computer runs for the y-direction is I while for the x-direction it is II when

$$I1 = INT(I/KI) \quad (H-19)$$

Details of the computation procedure

1). Computation in the x-direction -

First the values A, B are calculated according to the definitions and then integration of the difference scheme is carried out per time period ΔT_x .

$$\overline{W_{m,n}} = [W_{m,n}] - \frac{\Delta T_x}{\Delta x} \{ [A_{mi,n}] - [A_{mi-1,n}] \} - \frac{\Delta T_y}{\Delta y} \{ [B_{m,nj}] - [B_{m,nj-1}] \} \quad (H-20)$$

when

$$\left. \begin{aligned} m_i &= m + I1 - INT(I1/2) * 2 \\ n_j &= n + INT \left\{ \frac{[I1 + m - m_i - INT(\frac{I1 - m_i + m}{2}) * 4]}{2} \right\} \end{aligned} \right\} \quad (H-21)$$

This arrangement generates alternately forward and rear differences in the x and y directions.

From the results of the \overline{W} values the values $\overline{\rho}$, $\overline{\mu}$, \overline{T} , \overline{p} , \overline{V} , \overline{U} , are calculated and from them the values of \overline{A} .

Finally, the average derivative in the x-direction is calculated, for use in the KI runs to come in which only integration in the y-direction is carried out.

$$\left[F_{m,n} \right] = \frac{1}{2 \Delta x} \{ [A_{mi,n}] - [A_{mi-1,n}] + [\overline{A}_{li,n}] - [\overline{A}_{li-1,n}] \} \quad (H-22)$$

when

$$\left. \begin{aligned} m_i &= m + I1 - INT(I1/2) * 2 \\ l_i &= m + m_i - m + 1 - INT(\frac{m_i - m + 1}{2}) * 2 \end{aligned} \right\} \quad (H-23)$$

Note: Experience has shown the desirability of the definition $[F_{m,n}] = 0$ for the first run (because the calculation of the derivative is not accurate) and afterwards the computation stage for the y-direction is performed.

2). Computation in the y-direction -

/104

First the values for B are calculated, according to the definitions and then the stages of integration are performed, according to the time period ΔTY .

First integration

$$[\bar{W}_{m,n}] = [W_{m,n}] - \frac{\Delta TY}{\Delta y} \left\{ [B_{m,nj}] - [B_{m,nj-1}] \right\} - \Delta TY [F_{m,n}] \quad (H-24)$$

when

$$n_j = n + I - INT(I/2) * 2 \quad (H-25)$$

This arrangement generates alternately forward and rear differences.

From the results of \bar{W} values the values $\bar{\rho}$, $\bar{\mu}$, \bar{T} , \bar{P} , \bar{V} , \bar{U} are calculated and from them those for \bar{B} .

Second integration

$$[W_{m,n}] = \frac{1}{2} \left\{ [W_{m,n}] + [\bar{W}_{m,n}] - \frac{\Delta TY}{\Delta y} \left[[B_{m,nj}] - [B_{m,nj+1}] \right] - \Delta TY [F_{m,n}] \right\} \quad (H-26)$$

when

$$\left. \begin{aligned} n_j &= n + n_j 1 - n + 1 - INT\left(\frac{n_j 1 - n + 1}{2}\right) * 2 \\ n_j 1 &= n + I - INT(I/2) * 2 \end{aligned} \right\} \quad (H-27)$$

This arrangement generates alternately forward and rear differences, which are opposite in direction to those of the first integration.

3). Final calculation of the variables U, V, p, T, μ , ρ is performed from the final values obtained for W.

a. Boundary Conditions at the Entry Section

According to formula (3-19) the relation $\eta_n = f(y_n)$ (I-1) is valid and in that way the suitable η is obtained for all gridpoints in the y-direction. From equations (3-16) to (3-18) we can obtain $\rho_{1,n}$; $T_{1,n}$; $u_{1,n}$ as function of

$$u_{1,n} = 2\eta_n - 2\eta_n^3 + \eta_n^4 \quad (I-2)$$

$$T_{1,n} = \frac{1}{(\gamma-1) M_0^2} \left[1 + \sqrt{\text{Pr}} \frac{\gamma-1}{2} M_0^2 (1 - u_{1,n}^2) \right] \quad (I-3)$$

$$\rho_{1,n} = \frac{1}{1 + \sqrt{\text{Pr}} \frac{\gamma-1}{2} M_0^2 (1 - u_{1,n}^2)} \quad (I-4)$$

$$V_{1,n} = 0 \quad (I-5)$$

and from the equations of state and of viscosity we also get

$$\mu_{1,n}; \rho_{1,n}$$

b. Boundary Conditions Along the Wall

Velocity components from the non-slip condition

$$\left. \begin{aligned} u_{m,1} &= 0 \\ v_{m,1} &= 0 \end{aligned} \right\} \quad (I-6)$$

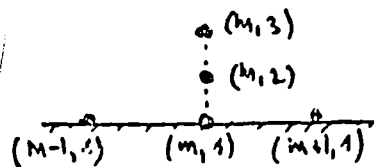
when for suction $v_{m,1} < 0$

and for injection $v_{m,1} > 0$

Temperature must fulfill the adiabatic condition $\frac{\partial T}{\partial y} \Big|_{y=0} = 0$

and we will assume the following relation (which fulfills that condition as: $T_{m,n} = a + by^2$) (I-7)

The coefficients a and b we will find by substituting the values $(m,3)$; $(m,2)$ into the equation



$$T_{m,2} = b(\Delta y)^2 + a$$

$$T_{m,3} = b(2\Delta y)^2 + a$$

From the solution of the two equations we get

/106

but $T_{m,1} = T_{m,n} \Big|_{y=0} = a$

$$b = - \frac{T_{m,2} - T_{m,3}}{3\Delta y^2} \quad a = \frac{4}{3} T_{m,2} - \frac{1}{3} T_{m,3}$$

and therefore

$$T_{m,1} = \frac{4}{3} T_{m,2} - \frac{1}{3} T_{m,3} \quad (I-8)$$

According to the considerations in paragraph 3.3.1.2, pressure will be computed for the condition

Similar to the temperature computation we then get

$$\frac{\partial p}{\partial y} \Big|_{y=0} = 0$$

$$P_{m,1} = \frac{4}{3} P_{m,2} - \frac{1}{3} P_{m,3} \quad (I-9)$$

and from the equations of state and viscosity we also get $\mu_{m,1}$; $\rho_{m,1}$

Here we will bring up a few more methods for computing which are basically more accurate (without the approximate assumption of $\frac{\delta p}{\delta y} = 0$) but result in an unsteady solution for numerical computation:

1). Linear extrapolation -

Assuming the relation

$$p_{m,n} = a + by$$

we get

$$p_{m,1} = 2p_{m,2} - p_{m,3} \quad (I-10)$$

2). Square extrapolation -

Assuming the relation $p_{m,n} = a + by + cy^2$

we get

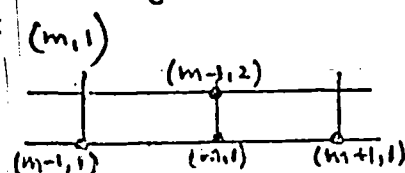
$$p_{m,1} = 3p_{m,2} - 3p_{m,3} + p_{m,4} \quad (I-11)$$

3). Development of continuity equation

$$\frac{\partial p}{\partial t} + \frac{\partial (p u)}{\partial x} + \frac{\partial (p v)}{\partial y} \Rightarrow \frac{\partial p}{\partial t} + p \frac{\partial u}{\partial x} + u \frac{\partial p}{\partial x} + p \frac{\partial v}{\partial y} + v \frac{\partial p}{\partial y} = 0 \quad (I-12)$$

We develop the expression around point:

while neglecting the second order



and finally we get

(I-13)

$$\frac{p_{m,1}^{(t)} - p_{m,1}^{(t-1)}}{\Delta t} + p_{m,1}^{(t)} \frac{u_{m+1,2}^{(t)} - u_{m-1,2}^{(t)}}{2\Delta x} + p_{m,1}^{(t)} \frac{v_{m,2}^{(t)} - 0}{2\Delta y} = 0$$

$$\rho_{m,1}^{(t)} = \frac{\rho_{m,1}^{(t-1)}}{1 + \Delta t \left[\frac{u_{m+1,2}^{(t-1)} - u_{m-1,2}^{(t-1)}}{\Delta x} + \frac{v_{m,2}^{(t-1)}}{\Delta y} \right]}$$

4). Development of the approximate equation of continuity - /107

This is the approximate formulation of the continuity equation

$$\frac{\partial \rho}{\partial t} \approx - \frac{\partial \rho v}{\partial y} \quad (\text{I-14})$$

and after development of the expression around point $(m,1)$ we get

$$\rho_{m,1}^{(t)} = \rho_{m,1}^{(t-1)} - \frac{\rho_{m,1,2}^{(t-1)} \cdot v_{m,1,2}^{(t-1)}}{\Delta y} \quad (\text{I-15})$$

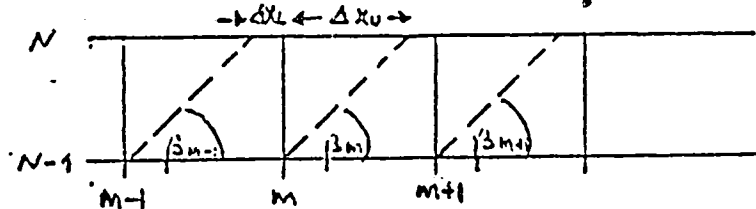
c. Boundary Conditions at the Exit Section

Based on the gradients of the variables in the x-direction being zero, we get

$$\left. \begin{aligned} u_{M,n} &= u_{M-1,n} \\ v_{M,n} &= v_{M-1,n} \\ \rho_{M,n} &= \rho_{M-1,n} \\ T_{M,n} &= T_{M-1,n} \end{aligned} \right\} \quad (\text{I-16})$$

d. Boundary Conditions for the External Flow

Computation of the characteristics for the external boundary:



The characteristics are computed from the next to the last line vs. the last line and their direction β_m is defined by

$$\beta_m = \mu_{m,N-1} + \theta_{m,N-1} = \text{tg}^{-1} \left(\frac{1}{\sqrt{M_{m,N-1}^2 - 1}} \right) + \text{tg}^{-1} \left(\frac{v_{m,N-1}}{u_{m,N-1}} \right) \quad (\text{I-17})$$

The value of a random variable $F_{m,N}$ will thus be determined as a function of its values from line N-1

$$F_{m,N} = \frac{F_{m,N-1}(\Delta x_U) + F_{m-1,N-1}(\Delta x - \Delta x_L)}{(\Delta x - \Delta x_L + \Delta x_U)} \quad (\text{I-18})$$

when the lines of the characteristics bisect the vertical grid lines, the definition of $F_{m,N}$ will change accordingly.

The values at the external boundary, at the first point downstream of the shock wave, are defined according to equations (3-26) to (3-29) in paragraph 3.3.1.4, so that the values of point (m_s, N) ahead of the shock wave define the values of point $(m_s + 1, N)$ behind it.

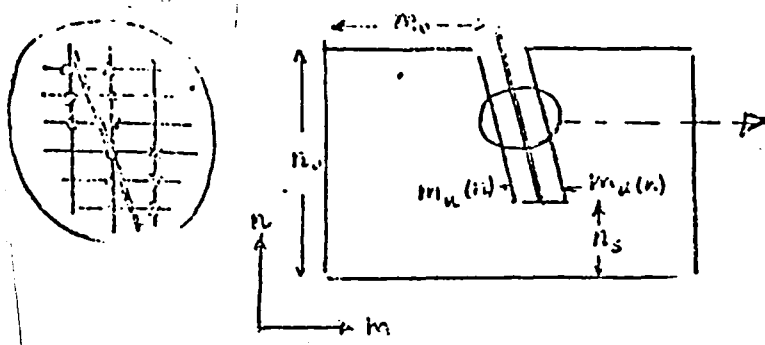
For reasons of computation stability we compared the values of point $(m_s + 2, N)$ with those of $(m_s + 1, N)$: there appears to be almost no effect on the results but it does tend to prevent fluctuations in the solution. /108

The value of $V_{m_s+1, N}$ is not computed from the transition equation of the shock wave like the rest of the variables, because the changes in this variable are of the same amount as its actual value and such a computation would cause severe oscillations in the solution. This value is therefore computed through extrapolation of V from the field by means of the characteristics method, similar to calculation of the rest of the points at the external boundary.

e. Boundary Conditions on Both Sides of the Shock Wave in the Field, for "Non-Continuous" Computation.

This boundary condition is computed according to the following stages:

- 1). The first iteration gives the point of entry into the field (M_0, N_0) and its intensity Sh_0 from which the entrance angle is calculated:



$$\alpha_{s_0} = \sin^{-1} \left[\frac{\sqrt{(Sh_0 + \frac{\gamma-1}{\gamma+1}) \frac{\gamma+1}{2\gamma}}}{M_0} \right] \quad (I-19)$$

- 2). Computation of the initial location of the shock wave in the field (assuming a straight shock wave)

$$m(n) = m_0 + (n_0 - n) \tan(\alpha_{s_0}) \quad (I-20)$$

- 3). Setting of the upper boundary of the shock wave $M_u(N)$ and of its downstream boundary

$$m_u(n) =$$

4). Location of the lower boundary at n_s so that it is close to the sonic line where $M = 1$ (through s computational test).

5). Computation of values upstream of the shock wave (for points $M_u(n)$) through extrapolation of values from the upstream flow.

6). Computation of the values downstream of the shock wave (along points $(M_d(n))$ from values calculated for $M_u(n)$ from formulas for the transition of a slanted shock wave, which are given in paragraph 3.3.1.4).

The value for the velocity component V downstream of the shock wave is not computed that way (for the same reasons as discussed in previously in section d.) but through extrapolation from nearby points at the downstream flow.

7). After correcting the computation for the entire flow field by means of the difference scheme, we find the new local gradient of the shock wave $\sigma_s(n)$ from the local pressure ratio.

on both sides of the shock wave boundaries from the formula

$$\sigma_s(n) = \sin^{-1} \left[\frac{\sqrt{\left(\frac{P_d}{P_u} \right)^{\frac{\gamma-1}{\gamma+1}} \frac{\gamma+1}{2\gamma}}}{M} \right] \quad (I-21)$$

8). From the local gradient the location of the shock wave is brought up to date

/109

$$M(n) = M_0 + \int_{n_0}^n f_j[\sigma(n)] dn \quad (I-22)$$

afterwards one continues according to paragraph (3) to (8) and so on repeatedly.

f. Additional Computations (Based on the Definitions in Appendix A')

1). Mach number -
$$M_{m,n} = \sqrt{\frac{u_{m,n}^2 + v_{m,n}^2}{(\gamma-1) T_{m,n}}} \quad (I-23)$$

2). Flow function (I-24)

$$\begin{aligned} \Psi_{m,n} = & \Psi_{m-1,n-1} + \frac{1}{2} (\rho_{m,n} + \rho_{m,n-1}) \left(\frac{u_{m,n-1} + u_{m,n}}{a} \right) \Delta y + \\ & - \frac{1}{2} (\rho_{m,n-1} + \rho_{m-1,n-1}) \left(\frac{v_{m,n-1} + v_{m-1,n-1}}{2} \right) \Delta x \end{aligned}$$

3). Friction Coefficient along the plate - (I-25)

Per definition

$$C_{F_n} = \left(\frac{2}{Re_{x_s}} \right) \mu_{m,1} \left(\frac{\partial u}{\partial y} \right)_{m,1}$$

We will calculate $\left(\frac{\partial u}{\partial y} \right)_{m,1}$ in the following manner:

we assume that the following relation exists next to the plate

by substituting the points $u_{m,n} = a_0 + a_1 y + a_2 y^2$ $\left(\frac{\partial u}{\partial y} \right)_{m,1} = a_1$ we get
 $u_{m,1} = a_0$ $(m,1), (m,2), (m,3)$

$$u_{m,2} = a_0 + a_1 \Delta y + a_2 \Delta y^2$$

$$u_{m,3} = a_0 + 2a_1 \Delta y + 4a_2 \Delta y^2$$

from the solution of the three equations $a_1 = \frac{1}{2\Delta y} (4u_{m,2} - 3u_{m,1} + u_{m,3})$

and finally we get

$$C_{F_m} = \frac{1}{Re_{x_s} \Delta y} \mu_{m,1} (4u_{m,2} - 3u_{m,1} + u_{m,3}) \quad (I-26)$$

4). Heat transfer coefficient along the plate -

Per definition

$$C_{Q_m} = \frac{Mo^2 (\gamma - 1)}{\rho_r Re_{x_s}} \mu_{m,1} \left(\frac{\partial T}{\partial y} \right)_{m,1} \quad (I-27)$$

we calculate $\left(\frac{\partial T}{\partial y} \right)_{m,1}$ like $\left(\frac{\partial u}{\partial y} \right)_{m,1}$ and get

$$\left(\frac{\partial T}{\partial y} \right)_{m,1} = \frac{1}{2\Delta y} (4T_{m,2} - 3T_{m,1} + T_{m,3}) \quad (I-28)$$

Finally, we get

$$C_{Q_m} = \frac{Mo^2 (\gamma - 1)}{2 \rho_r Re_{x_s} \Delta y} \mu_{m,1} (4T_{m,2} - 3T_{m,1} + T_{m,3})$$

Based on various approximations in the development of linear equations for compressive and viscous flow, different Δt criteria were obtained for assurance of stability in the computation. Some of the most important results (in dimensionless form) are shown below:

a. According to Brailovskaya[8] without the energy equation $\Delta t \leq \frac{Re}{8} = Fb_1$ (J-1)

b. According to Brailovskaya[8] with the energy equation $\Delta t \leq \frac{Pr Re M_0^2 (\gamma - 1)}{8} = Fb_2$ (J-2)

c. According to Skoglund, Gay [94] $\Delta t \leq \frac{3 \rho Re}{16} = F_s$ (J-3)

d. According to Carter [13] $\Delta t \leq \frac{0.5 \rho_1 Re}{\gamma \mu / \rho} = F_c$ (J-4)

If we set the non-dimensional values (the approximate values) $Pr \cong 0.7$ $\gamma = 1.4$ $\mu \cong 1$ $\rho \cong 1$ we get

$$\left. \begin{aligned} Fb_1 &= 0.125 Re \\ Fb_2 &= 0.035 M_0^2 Re \\ F_s &= 0.18 Re \\ F_c &= 0.25 Re \end{aligned} \right\} \text{(J-5)}$$

For $2 < Mo < 4$ all the expressions offer approximate values in the range $F/Re = 0.1 - 0.2$.

In this research only the criterion of F_0 was taken into account because it is based on a minimum of approximations of the basic equations.

Arrangement of the general computation with difference schemes for the t-th iteration

For the Brailovskaya scheme

$$\left. \begin{aligned} W^{\bar{t}} &= W^{t-1} - \Delta t \left[\begin{array}{c} \text{derivative} \\ \text{נגזרות} \end{array} \right]^{t-1} \\ W^t &= W^{t-1} - \Delta t \left[\begin{array}{c} \text{derivative} \\ \text{נגזרות} \end{array} \right]^{\bar{t}} \end{aligned} \right\} \quad (K-1)$$

For the MacCormack scheme

$$\left. \begin{aligned} W^{\bar{t}} &= W^{t-1} - \Delta t \left[\begin{array}{c} \text{derivative} \\ \text{נגזרות} \end{array} \right]^{t-1} \\ W^t &= \frac{1}{2} \left\{ W^{t-1} + W^{\bar{t}} - \Delta t \left[\begin{array}{c} \text{derivative} \\ \text{נגזרות} \end{array} \right]^{\bar{t}} \right\} \end{aligned} \right\} \quad (K-2)$$

when all derivatives in each scheme are calculated as described in appendix H'. The remainder of the differential equation is defined by

$$R^{t-1} = \left(\frac{\partial W}{\partial t} \right)^{t-1} + \left[\begin{array}{c} \text{derivative} \\ \text{נגזרות} \end{array} \right]^{t-1} \quad (K-3)$$

According to the rear differentials we get

$$\left(\frac{\partial W}{\partial t} \right)^{t-1} = \frac{W^{t-1} - W^{t-2}}{\Delta t} \quad (K-4)$$

From the previous definitions

$$\left[\begin{array}{c} \text{derivative} \\ \text{נגזרות} \end{array} \right]^{t-1} = \frac{W^{t-1} - W^{\bar{t}}}{\Delta t} \quad (K-5)$$

In the same way of making use of the approximation of the rear derivative of $\frac{\delta W}{\delta t}$ $W^{\bar{t}}$ can be exchanged for W^t .

Then we get

$$R^{t-1} = \frac{2W^{t-1} - W^t - W^{t-2}}{\Delta t} \quad (K-6)$$

This expression provides, of course, only an order of magnitude estimate for the remainder and not its exact value, because of the approximations in the computation procedure.

We will perform an evaluation for the following reference conditions: $p_e/p_o = 1.4$; $Re_{x_s} = 3 \times 10^5$; $Mo = 2$;

Reference dimensions are: $x_{ref} = x_s = 5 \times 10^{-2}$

$$\delta_o = 4 \times 10^{-4} \text{ m}$$

From this we get:

$$t_{ref} = \frac{x_{ref}}{U_s} = \frac{5 \times 10^{-2}}{700} = 7 \times 10^{-5}$$

$$\Delta x = \frac{150}{75} \delta_o / x_{ref} = \frac{8 \times 10^{-4}}{5 \times 10^{-2}} = 1.6 \times 10^{-2} = o(10^{-2})$$

$$\Delta y = \frac{3}{24} \delta_o / x_{ref} = \frac{5 \times 10^{-5}}{5 \times 10^{-2}} = 1 \times 10^{-3} = o(10^{-3})$$

$$\Delta t = \frac{0.5 \Delta t_{CFL}}{t_{ref}} = \frac{5 \times 10^{-8}}{7 \times 10^{-5}} = 7 \times 10^{-4} = o(10^{-3}) + o(10^{-4})$$

$$\frac{\Delta W}{\Delta i} = (\text{numerical error}) + E_T$$

The truncation error for the Brailovskaya scheme is determined through $E_T = o(\Delta t, \Delta x^2, \Delta y^2)$

If we take into consideration the influence of the oscillatory solution component as well (because there is no significance to the dependence on Δt in the steady solution), we shall see that the truncation error (which is of the same order of magnitude as the reminders of the differential equations) is $E_T = (10^{-3}) - (10^{-4})$. The order of magnitude of the variables themselves, however, is Δt times larger, in other words $(10^{-6}) - (10^{-7})$.

This analysis does not take into account the value of the double derivatives Δt , Δx , Δy in the complete formula for truncation error which, in certain regions, may increase to several times that amount.

It is also known that near the boundaries, and particularly in the region where the shock wave enters, the truncation error is greater since the local deviation between the accurate flow equations and the difference equations is larger.

As we will see from the results (see Figs. 10 -14 and also appendix M') an average order of magnitude of $\underline{O(10^{-3}) - O(10^{-4})}$ is obtained for the errors of variables which indicates that the lastmentioned factors exert significant influence.

Appendix M' - Evaluation of the Computational Error (Through Comparison of Results from Grids of Different Density)

A comparison of results was made between those from the regular grid (run 001) and those from the fine grid (run 041), for the following parameters:

$$X_s = 0.05m; p_e/p_o = 1.5; Re_{x_s} = 3 \times 10^5; M_0 = 2;$$

Regular grid parameters - $\Delta x = 7.97 \times 10^{-4}$; $\Delta y = 4.98 \times 10^{-5}$

Regular grid parameters - $\Delta x = 4.10 \times 10^{-4}$; $\Delta y = 2.51 \times 10^{-5}$

(The exact ratio for the mesh of the grids is 1:1.944 in the x-direction and 1:1.984 in the y-direction).

The results obtained for two characteristic points (for which the location comes closest to being alike for both grids)

	Type of grid	Non-dimensional values			Location in the field	
		U	P	T	M	N
Before the shock wave	Regular grid	0.1377	0.1730	1.0250	19	2
	Fine grid	0.1493 0.1481*	0.1751 0.1751*	1.0293 1.0294*	36	3
After the shock wave	Regular grid	0.2004	0.2585	1.1171	55	2
	Fine grid	0.1973 0.1957*	0.2522 0.2522*	1.1209 1.1211*	106	3

*Since the points from the regular grid and from the fine grid shown here do not match up completely, an interpolation was carried out from the fine grid results to the appropriate points in the regular grid.

Let us assume that the computational grid errors relate to each other as the square of the grid spacings (and that is based on a truncation error of the order $O(h^2)$ of the difference scheme)

$$f_C - \text{for the regular grid} \quad \frac{f_C - f}{f_F - f} = \frac{h^2}{(h/2)^2} = 4 \quad (M-1)$$

$$f_F - \text{for the fine grid}$$

From here we get the exact value of the solution

/114

$$f = \frac{4f_F - f_C}{3} \quad (M-2)$$

That way we will find the exact values for the points examined and any divergence from them in the two grids.

Type of grid	Non-dimensional values			Location in the field		
	U	P	T	M	N	
Before the shock wave	Regular grid	0.1516	0.1758	1.0310		
	Fine grid	$\Delta U_C = .0139$	$\Delta P_C = .0028$	$\Delta T_C = .0064$	19	2
		$\Delta U_F = .0035$	$\Delta P_F = .0007$	$\Delta T_F = .0016$	36	3
After the shock wave	Regular grid	0.1941	0.2501	1.1220		
	Fine grid	$\Delta U_C = .0063$	$\Delta P_C = .0084$	$\Delta T_C = .0029$	55	2
		$\Delta U_F = .0016$	$\Delta P_F = .0021$	$\Delta T_F = .0012$	106	3

It turns out that the errors in the regular grid are on the order of $O(10^{-3})$ approximately (in the fine grid they are smaller by a factor of 4).

A table of comparison was prepared, based on various studies made previously:

Parameter Compared	Lax-Wandroff Method		Brailovskaya Method		
	MacCormack [67] MC	Skoglund, Gay [94] SG	Kronzon [94] KR	Carter [13] CA	Present Study UR
$\Delta x/\delta_0$	3 - 6	.3 - 20	.07 - .17	.3 - .6	2
$\Delta y/\delta_0$.15	.2 - 7	.07	.05 - .1	.125
$\Delta x/\Delta y$	20 - 40	1 - 2	1 - 2	3 - 7	16
Gridpoints	1000 - 2000	2000 - 3500	2000 - 7000	2000 - 5000	2000
Accuracy	$\sim 10^{-6}$	$\sim 10^{-6}$	$10^{-5} - 10^{-6}$	10^{-5}	$10^{-5} - 10^{-4}$
Max. number of iterats.	5000 - 9000	2000 - 8000	500 - 1000	1500 - 3000	200

UR, SG, MC - interaction of shock wave entering the boundary layer

KR - interaction of flow due to a rear step

CA - interaction of flow due to a forward compression corner

NOTES:

- a. Δy for method MC relates to a grid that is fine and close to the boundary layer (while in the coarse, outer grid $\Delta y/\delta_0 = 1.5 - 3$).
- b. The wide range of change in Δx and Δy , in method SG, stems from a change in the grid so that its mesh size becomes a minimum close to the plate center, but increases in both x and y directions as one moves toward the periphery.
- c. The accuracy criterion for convergence is not well enough defined to apply to the same variables and in the same way for the various methods, so that the comparison must remain a qualitative one only.

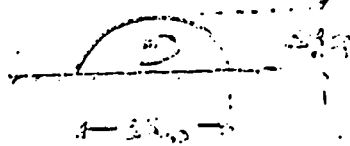
The comparisons do bring out that the method used here requires a relatively shorter time for convergence (by a whole order of magnitude) with lower accuracy than in previous studies (but, as will be shown, with no significant computation errors).

Appendix 0' - Formula for Computation of Suction Required to Prevent Separation

A test was made to find, from the results of runs for suction under various flow conditions, a connection between the suction required to prevent separation and the data for the separated zone.

For that purpose the following parameters are defined (all non-dimensional):

Area of separated zone (the bubble)



$$Q = (\Delta x_{sp}) (\Delta y_{sp}) \cdot 1$$

(for depth of unit)

(0-1)

Function of the flow at the bubble focus (the most negative value)

$$\psi_{max} = \left(\frac{v}{U} \right)_{max}$$

(0-2)

when defined as

$$\psi = \int (u \, dy - v \, dx)$$

Suction velocity (required to eliminate the separated zone)

(when suction is normal to the wall)

$$v_{ws} = v_{ws} \Big|_{\Delta y_{sp}=0}$$

(0-3)

Now we will compute the expression C, which is defined by

$$C = \frac{v_{ws} \sqrt{\psi}}{\psi_{max}}$$

(0-4)

for various flow conditions

Note even when v_{ws}, ψ, ψ_{max} have dimensions the value of C will be non-dimensional because the dimensions of its components are

$$[v_{ws}] = \text{m/s} ; [\psi] = \text{m}^2 ; [\psi_{max}] = \text{m}^2/\text{sec}$$

From the computation table (on the following page) it becomes clear that, generally, the value for C is in the region $C = 0.30 - 0.42$ (except in one instance where $C = 0.24$. In that case Re is exceptionally low and it becomes difficult to locate the boundaries of the separated region accurately, because of the small differences in the velocity component values).

Since the cases examined cover a wide range of flow conditions, it may be assumed that the value expresses a singular relation between the suction required to prevent separation and the parameters of the separated region.

To sum it up: the suction required to prevent separation can be designed by means of this formula:

$$V_{w,c} = C \frac{\Psi}{\rho} \quad C = 0.2 \rho \cdot D_b \quad (0-5)$$

COMPUTATION TABLE:

/117

Run No.	Original flow conditions without suction									Suction to prevent separation per Fig. 4.1
	Flow parameters			Bubble dimens. (accdg. to nr. of meshes)		Mesh dimens. in the grid		Parameters for the bubble focus		
	M_0	R_0/ρ_0	Re_{z_0}	ΔM_{z_0}	ΔN_{z_0}	$\Delta x \cdot 10^4$	$\Delta y \cdot 10^5$	ψ_{max}	(ρ/ρ_{max})	
102	2.0	1.4	3×10^5	11.5	3.5	8.00	5.00	-.0011	.6511	-.023
103	2.0	1.9	3×10^5	12.5	4.0	8.00	5.00	-.0015	.7221	-.029
104	2.0	3.15	3×10^5	15.0	4.5	8.00	5.00	-.0026	.9472	-.035
111	3.0	3.15	3×10^5	12.0	5.5	8.74	5.46	-.0011	.4794	-.027
112	4.0	3.15	3×10^5	10.5	3.5	9.54	5.96	-.0005	.3480	-.018
112	4.0	1.9	3×10^5	8.5	2.5	9.54	5.96	-.0003	.3516	-.012
113	4.5	3.15	3×10^5	10.0	3.5	9.92	6.20	-.0004	.3123	-.016
122	2.0	1.4	5×10^4	6.0	2.5	11.40	7.10	-.0011	.7342	-.015
123	2.0	1.4	1×10^6	12.5	3.5	5.33	3.33	-.0010	.6464	-.026
124	2.0	1.4	5×10^6	13.0	4.0	2.75	1.72	-.0007	.6421	-.029

	$U = \frac{\Delta M_{z_0} \cdot \Delta N_{z_0} \cdot \Delta x \cdot \Delta y}{(z_0)^2} \quad (z_0 = 0.05)$	$\sqrt{U} \times 10^2$	$\frac{y_w}{z_0}$	$U_{max} = (\Psi/\rho)_{max}$	$C = \frac{\lambda \sqrt{U} (\frac{y_w}{z_0})}{(\Psi/\rho)_{max}}$
		2.54			3.45 α_0^{-1}
102	6.44×10^{-4}	2.73	-.023	1.69	
103	8.00	3.29	-.029	2.08	
104	10.20	3.55	-.035	2.74	
111	12.60	3.55	-.027	2.29	
112	8.36	2.89	-.018	1.44	
112	4.83	2.20	-.012	0.85	
113	8.61	2.93	-.016	1.28	
122	4.85	2.21	-.015	1.50	
123	3.10	1.76	-.026	1.55	
124	0.98	0.99	-.029	1.09	
					3.08

a. Description of the Basic Program

Fig. 4 shows a basic block diagram in which the various subroutines and their operation in the program are described. Below we will describe the main program and the subroutines attached to it.

1) Main Program MAIN

In this program control of the computer run procedure is exercised through the calling up of various subroutines. In it there are also definitions for a number of parameters that determine the desired options for computation, the form of the output and also the possibility for loading or unloading results into/from the assembler. Details of the parameters are given in paragraph c.

2) ARVIS - Artificial Viscosity

This subroutine is called up from GRID and its function is to add terms for artificial viscosity to the expressions in the difference schemes (in both integration steps). The coefficients of artificial viscosity, c_{cx} and c_{cy} , are determined by MAIN.

3) CNBC - Boundary Condition at the Entry Section

This subroutine computes the conditions at the entry section, which remain fixed in the course of the iterations and which are only dependent on the flow data Mo , Re_{x_s} , x_s , p_r and T_o . The computation is carried out per the Polhausen method.

4) DATA - Processing of Flow Data and Grid Preparation

This subroutine calls up flow data like Mo , Re_{x_s} , x_s , p_r and p_e/p_o and also the definitions of the computational field dimensions through ratios l_1/r_o , l_2/r_o , $\Delta x/r_o$, $\Delta y/r_o$. From these data the dimensions of the computation grid are calculated, as well as the time interval for integration (based on the criterion for steadiness).

5) DISC - Loading/Unloading of Intermediate Results into/from Assembler

Through designation of $N\psi$ and/or NI for the I/O units this subroutine is employed to write and/or call up the appropriate results from the assembler on the disc.

6) FLOW - Accompanying Calculations from the Results Obtained

In this subroutine the Mach number and the flow function for the whole field, as well as the friction and heat transfer coefficients along the plate, are computed from the results of the computation.

7) GRID - Operation of the Finite Difference Schemes

In this subroutine the two-stage integration for the Brailovskaya difference scheme with second order finite differences is carried out, in which the variables u , v , p , t are calculated. (The subroutine includes a possibility for omitting the section along the shock wave in the case of the non-continuous computation method).

8) INCND - Computation of Initial Conditions

This subroutine computes the initial conditions for all the variables in the entire field and this is done based on considerations that were determined for the choice of initial conditions.

9) OTPT - Printout of Results

/119

Since the printout of the results is a required condition this subroutine produces results for the variables in the computational field x , u , v , p , ρ , t , μ , m , ψ (The friction and heat transfer coefficients are printed by the FLOW subroutine).

10) PP - Pressure Computation

This function computes the pressure from the equation of state.

11) SHOCK - Computation of the External Boundary Condition Next to the Shock Wave

This subroutine computes the boundary conditions on both sides of the shock wave, at the external boundary of the flow, and also permits calculation of the boundary conditions on both sides of the shock wave, along its entire length, by means of the non-continuous method in which the shock wave is removed from the computational field.

12) STAB - Computation of Steadiness Coefficients

In this subroutine the steadiness coefficients for each iteration are computed and they are printed out in tables, according to existing printout conditions (see note).

13) VRBC - Computation of Boundary Conditions (Except for the Shock Wave)

In this subroutine those boundary conditions are computed that require updating for each iteration. They are located: along the plate, in the downstream flow and in the external boundary (except for downstream of the shock wave).

14) YY - Computation of Viscosity

This function computes the viscosity from Sutherland's formula.

Note: Because STAB requires a very large memory and is not absolutely necessary for each computation, it can be dispensed with to save a lot of room and computer time (the method is described in paragraph c).

b. Description of Additional Options

1) The Difference Scheme by MacCormack

The subroutine GRIDM (which exists parallel to GRID) performs the finite difference computation according to MacCormack's method. (there is no possibility for the use of artificial viscosity and, therefore, no way to remove the shock wave from the computational field as is done in GRID).

2) Difference Computation to the Fourth Order of Accuracy

The subroutine GRID1 (which exists parallel to GRID) permits computation of the finite differences in the x-direction below the shock wave to the fourth order of accuracy, in contrast to the other parts of the field where second order accuracy prevails.

3) Use of a Grid with Non-Uniform Meshes in the x-Direction

The computation program can also be used for a grid with non-uniform meshes in the x-direction (which decrease in the direction towards the center) when $\Delta x_{\min} = 1.6\Delta y$ in the center of the grid. For that purpose the following subroutines exist (parallel to the subroutines of the uniform grid):

Subroutine DATAx instead of DATA to process flow data and grid preparation. /120

Subroutine GRIDx instead of GRID to compute finite differences (per Brailovskaya method only).

Subroutine VRBCX instead of VRBC to compute the boundary conditions.

In addition to these subroutines there are two more functions HH and HL, by means of which the location and size of the meshes in the x-direction are determined.

Note: The two functions HH and HL must be included in the program for the use of a uniform grid as well, since there are subroutines common to both types of grids (like CNBC, SHOCK and others) that require the use of those functions.

c. Operation of the Program

1) Control Card

A batch type run of the program includes the following control cards:

```
// JOB ...  
// EXEC ...  
// FORT.SYSIN DD x  
MAIN program cards  
/x  
data cards  
//
```

Parameters of the JOB -card:

Memory: without the use of STAB (250-350) K
with the use of STAB (500-700) K

Time for 200 iterations - without the use of STAB (200-300) sec
with the use of STAB (400-500) sec

Lines of print for 200 iterations including the printing of the initial conditions -

without the use of STAB about 1700 lines
with the use of STAB about 2300 lines

(the ranges for change in the parameters are for the use of various options).

For that reason it is recommended to use the following values with the JOB-card:

without the use of STAB - T60, L02, R350
with the use of STAB - T85, L03, R700

2) Preparation of MAIN for a Run

/121

There are a number of indices in the MAIN program that control the procedure of the run and they must be defined before each run, in accordance with the requirements:

NI - Use of a data assembler as initial condition:

NI = 1 without use of assembler initial conditions are computed with INCND.

NI \neq 1 initial conditions are read from assembler (whose logic number is identical to NI).

NO - Use of data assembler to store output results:

NO = 1 without use of assembler to conserve output

NO \neq 1 results of the final iteration IMAX are loaded into the assembler (whose logic number is identical to NO); the condition NO \neq NI must also exist.

JAV - Use of artificial viscosity:

JAV = 0 without use of artificial viscosity

JAV = 1 with use of artificial viscosity

CCX

- Coefficients of artificial viscosity (generally in the range 0.01 - 0.1)

CCY

MODE - Use of continuous and non-continuous computation of the shock wave path:

MODE = 1 continuous computation (regular computation method)

MODE = 2 non-continuous computation (does not produce good results at this time).

KPRT - Use of uniform and non-uniform grid:

KPRT = 0 uniform grid

KPRT = 1 non-uniform grid

Q - Ratio of adjacent mesh lengths in a non-uniform grid (generally recommended Q = 1.1)

IPRO - Possibility for printout of initial condition:

I_{PRO} = 0 without printout of initial condition

I_{PRO} = 1 with printout of initial condition

I - Number of the first iteration in the run:

I = 0 when the run starts with initial conditions
calculated through INCND

I > 0 when the run starts with previous conditions
called up from the assembler

NC - Approximate boundary of the sonic line:

This index indicates the value of the η -th point in the
y-direction, in which the approximated sonic line exists (for
computations of the non-continuous method)

SSH - Initial value for the pressure ratio on both sides
of the incident wave (this value is to a first approximation equal
to the root of the overall pressure ratio between the downstream
and upstream flow).

Note: For the basic computation method it is required that
KPRT = 0, MODE = 1, JAV = 1. Additional parameters that are
not in use during this stage are introduced as fixed values
into all runs. They are:

SK = 1, J = 0, ISP = 0, INCD = 2, IGRD = 1, NCl = 2

3) Preparation of Additional Data for DATA (or DATAX)

/122

In accordance with the input format the following data
must be inputted:

First card -

EMO - Mach number of the external flow

RE - Reynolds number at the intersection of the continuing
shock wave with the plate

PR - Prandtl number

TPS - Initial value for the overall pressure ratio between
downstream and upstream flow

XSH - Distance, of the point of intersection between the
continuing shock wave and the plate, from the leading
edge

SY - Constant of the Sutherland equation ($SY = 110^{\circ}C$)

ALT - Reference altitude (M'), used actually only to obtain the external temperature (in its dimensional value in $^{\circ}C$), which is required for the viscosity formula. (Generally $ALT = 0$ is used).

Second card -

G - The constant $\gamma = 1.4$

G1 - Ratio between the field length and the boundary layer thickness at entry section

G2 - Ratio between the field width and the boundary layer thickness at entry section

Z1 - Ratio between the grid mesh length and the boundary layer thickness at entry section

Z2 - Ratio between the field width and the boundary layer thickness at entry section

EC - Criterion for convergence (for the moment an exaggerated value of $EC = 1 \times 10^{-20}$ is introduced so that the program should stop before reaching IMAX)

SD - Criterion for divergence (for the moment an exaggerated value of $SD = 1 \times 10^{20}$ is introduced; usually, when there is a tendency for divergence the program will stop at a much earlier stage when negative values for temperatures are obtained, which causes calculation of the root of a negative expression in the viscosity formula, so conditions for termination of the run and printout of the results are inputted into GRID when the temperature has a minus sign).

Third card -

IMAX - The maximum number of required iterations (generally no more than 200, so as to avoid overly long runs; when a larger number of iterations is required it is recommended to divide the run into stages, with the results of each stage loaded into the assembler and serving as initial conditions for the next stage).

KPR - The number of iterations between printouts (recommended is $KPR \leq 100$).

4) General Notes

a) Before the run it should be verified that the ratios $61/Z1$ and $62/Z2$ (whose integral value is the number of grid-points in the x and y directions, respectively) match the size of the defined dimensions in COMMON and in DIMENSION.

b) From experience it is known that the initial value of the pressure ratio between the downstream and the upstream flow, TPS, must be very little smaller (about 2-5%) than the required final value.

c) When the operation of subrouting STAB must be prevented (for reasons of saving space and computer time) a fictitious subroutine called STAB must be introduced together with MAIN, which will be designated:

/123

```
SUBROUTINE STAB
```

```
COMMON/B/
```

```
IDIV = 0
```

```
ICONV = 0
```

```
RETURN
```

```
END
```

This subroutine (which will eliminate the original STAB) will generate the values ICONV, IDIV, which will prevent the needless stopping of the program.

In place of this operation the callup CALL STAB can also be eliminated in MAIN and in its place to define IDIV = 0 and ICONV = 0. As far as the computation is concerned there is nearly no difference between those two alternatives.

d) To run the non-uniform grid (instead of the uniform grid) the following cards in MAIN must be changed:

```
CALL DATAX instead of CALL DATA
```

```
CALL GRID instead of CALL GRID
```

```
CALL VRBCX instead of CALL VRBC
```

e) To use fourth order differences below the shock wave (instead of second order differences) the following card in MAIN must be changed:

CALL GRID¹ instead of CALL GRID

f) To use the MacCormack scheme instead of the Brailovskaya scheme, the following card must be changed in MAIN:

CALL GRIDM instead of CALL GRID

Also, at the end of the subroutine DATA the command DT = DTY must be introduced.

D) List of general FORTRAN symbols

Name of Variable	COMMON	Explanation	Location in the subroutines																					
			MAIN	ARVIS	CNEC	DATA	DATA	DISC	FLOW	GRID(I)	GRID(J)	GRID(K)	GRID(L)	INCND	OPT	PP	SHOCK	STAB	VELOC	VISC	YY	ZZ	HL	
A		Aux. value in subroutine DATA					X																	
AA		" " " " CNBC			X																			
AB1(M,N)		" " " " GRID(M)																						
AB2(M,N)		" " " " "																						
AB3(M,N)		" " " " "																						
AB4(M,N)		" " " " "																						
ABU1		Aux. value in subroutine ARVIS	X																					
ABU2		" " " " "	X																					
ABV1		" " " " "	X																					
ABV2		" " " " "	X																					
ADP		Designated value of DP																						
ADT		" " " " VT																						
ADU		" " " " DU																						
ALT		Level(M') for calc. of ref. temp.				X	X																	
AM		Mach number at external boundary																						
AQ	F																							
ARS1		Designated value of RES1																						
ARS2		" " " " RES2																						
ARS3		" " " " RES3																						
ARS4		" " " " RES4																						
VIS		Name of subrout. for art. viscos.	X							X		X	X											
AO		Dimensional sonic vel. (Ref.)				X	X																	
A1(M,N)		Aux. value in subroutine GRID(M)																						
A2(M,N)		" " " " "																						
A3(M,N)		" " " " "																						
A4(M,N)		" " " " "																						
B		" " " " " DATA																						
BB		" " " " " CNBC			X																			
BB1(M,N)		" " " " " GRID(M)																						
BB2(M,N)		" " " " " "																						
BB3(M,N)		" " " " " "																						
BB4(M,N)		" " " " " "																						
EE		Corner of characteristic																						
E1(M,N)		Aux. value in subroutine GRID(M)																						
E2(M,N)		" " " " " "																						
E3(M,N)		" " " " " "																						
E4(M,N)		" " " " " "																						
CCX	G	Art. viscos. coeff. in x-direction	X	X																				
CCY	G	" " " " " y- "	X	X																				
CK		Aux. value in subroutine DATA				X	X																	
CK1		" " " " " "				X	X																	
CK2		" " " " " "				X	X																	
CNEC		Subrout. for entry cross-seg. data	X	X																				
C1		Aux. value for subroutine INCND																						
C2		" " " " " SHOCK, INCND																						
DATA		Subrout. for use of field & grid	X			X																		
DATA		As above, for nonuniform grid data	X			X																		
DDX		Aux. value in subroutine DATA																						
DELO		(Dimens) width of " at entry				X	X																	
DISC		Subroutine for data incr./decr.						X																
DP(M,N)		Coeff. for pressure change																						

Name of Variable	CO/MO/W	Explanation	Location in the subroutines																				
			MAIN	ARVIS	CNBC	DATA	DATA*	DISC	FLOW	GRID(B)	GRID(H)	GRID(I)	GRID(X)	INCLD	OTPT	PP	SHOCK	STAB	VRBC	VRBCX	YY	YH	YI
MSH1	B	=MSH-1				X	Y							X									
MSH11	B	=MSH+1				X	X							X		X							
MSH111		=MSH+5												X									
MSM		Aux. index in subroutine INCND												X									
MSU		" " " " " "												X									
MS1		=MSM-1												X									
MS2		=MSM+1												X									
MT		REAL value of MS(N)												X									
MT1		Aux. index in subroutine INCND												X									
MT2		" " " " " " " "												X									
MU		Auxiliary index										X								Y	X		
MUO		Reference viscosity (dimensional)				X	X																
MY		Auxiliary value in subroutine				X	X	X															
MZ		" " " " " " " "																					
MZ1		Aux. index in subroutine INCND												X									
MZ11		" " " " " " " "												X									
MZ2		" " " " " " " "												X									
MZ22		" " " " " " " "												X									
M1	B	Half of grid-points in x-direct.				X	X	X														X	X
M11		Aux. index in subroutine INCND												X									
M22		" " " " " " " "												X									
N	B	Current index in y-dir. of grid	X	X	X	X	X	X	X	X	X	X	X	X	X	X	X	X	X	X	X	X	X
NC	B1	Loc. of sonic line in y-direction	X							X	X	X	X			X							
NC1	S	Index not in use	X																				
NE		Aux. index in subroutine CNBC				X																	
NJ	B3	Number of logic units of input coll.	X			X	X	Y					X		X					X	X		
NJ1		Aux. index in subroutine GRID(M)											X										
NK		" " " " " " CNBC				X																	
NL		" " " " " " GRID(M)											Y										
NO	B3	Nr of logic units of output coll.	X					X															
NN	B	Nr. of grid-points in y-direction				X	X	X	X	X	X	X	X	X	X	X	X	X	X	X	X	X	X
NNC		Aux. index in subr. INCND, =NC-1												X									
NNCC		" " " " " " " "												X									
NN1	B	=NN-1				X	X	X	X	X	Y	X	Y	X		X		X	Y				
NH		Auxiliary index											X										
NX		Aux. index in subroutine DATA				X	X																
N1		Half of grid-points in y-direction				X	X																
O		Corner of flow direct. at ext. boundary																		X	X		
OE		" " " " " " " "																					
OTPT		Subroutine for printing results	X					X		X	X	X	X	X	X								
P(M,N)	C	Pressure				X		X		X	X	X	X	X	X	X	X	X	X	X	X	X	X
PA		Pressure upstream of shock wave																	X				
PB(M,N)		Pressure after first integration								X	X	Y	X										
PE		Init. pressure downstr. of shock wave																	X				
PM		REAL value of																	X				
PM1		Aux. value in subroutine INCND																	X				
PN		REAL value of N																	X				
PNN		" " " " " " NN																	X				
PP		Function of pressure computation									X	X	X	X	X	X	X	X	X	X	X	X	X
PR	A	Prandtl number				X					X	X	X	X									
PSH		Aux. value in subroutine INCND																	X				
PS1		" " " " " " " "																	X				
PSI(M,N)	C	Flow function																	X				
PO		Reference pressure (dimensional)																					

Name of Variable	COMMENT	Explanation	Location in the subroutines																				
			MAIN	ARVIS	CANBC	DATA	DATAF	DISC	FLOW	GRID(C)	GRID(F)	GRID(E)	GRID(S)	INCND	OTFT	PP	SHOCK	STGE	VRBC	VRBCX	YY	HH	HI
S31		Aux. expr. for visc. in moment. y equ.						X	X	X													
S32		" " " " " " " "						X	X	X													
S33		" " " " " " " "						X	X	X													
S34		" " " " " " " "						X	X	X													
S4(M,N)		Visc. term in energy equation						X	X	X													
S41		Aux. expr. for visc. in energy equ.						X	X	X													
S42		" " " " " " " "						X	X	X													
S43		" " " " " " " "						X	X	X													
S44		" " " " " " " "						X	X	X													
S45		" " " " " " " "						X	X	X													
S46		" " " " " " " "						X	X	X													
S47		" " " " " " " "						X	X	X													
S48		" " " " " " " "						X	X	X													
S49		" " " " " " " "						X	X	X													
S4A		" " " " " " " "						X	X	X													
T(M,N)	C	Temp.		X			Y	X	Y	X	X	X	X	X		X	X	X	X				
TA		Temp. upstream														X							
TAUW		Friction strength along the plate						X															
TAUEO		Ref. value for friction(not used)			X	X																	
TAUW1		Friction strength along the plate						X															
TB(M,N)		Temp. after the first integration								X													
TE		Init. temp. downstream of shock w.														X							
TPS		Init. press. ratio betw. field ends		X	X								X										
TREF		Ref. time for comp. of time step			X	X																	
TP		Dummy parameter in function PP													X								
T(L)		Temperature as function of ETA		X																			
TW		Plate temp. at entry cross-section		X																			
TO		Dimensional ref. temperature			X	X																	
TO		Ref. temp. at entry cross-section		X																			
T00		" " " " " " " "T00=TO			X	X																	
TO(M,N)		Temperature in iteration I-2																				X	
T1(M,N)		" " " " " " " "I-1																				X	
U(M,N)		Velocity in x-direction		X				X	X	X	X	X	X	X	X	X	X	X	X				
UA		Velocity x upstream of shock wave														X							
UB(M,N)		Velocity x after first integration						X	X	X	X												
UU(L)		Velocity x as function of ETA		X																			
UO(M,N)		Velocity x in iteration I-2																				X	
U1(M,N)		" " " " " " " "I-1																				X	
UE		Init. velocity x downstream of wave														X							
V(M,N)		Velocity in x-direction		X				X	X	X	X	X	X	X	X	X	X	X	X				
VA		Velocity y upstream of shock wave														X							
VB(M,N)		Velocity y after first integration						X	X	X	X												
VE		Init. velocity y downstream of wave														X							
VN1		Aux. value in subroutine INCND											X										
VN2		" " " " " " " "											X										
VRBC		Subroutine for comp. of bound. cond.																				X	
VRBCX		As above, for non-uniform grid																				X	
VT(M,N)		Coeff. of temperature change																				X	
VT1		Aux. value in subroutine INCND											X										
VT2		" " " " " " " "											X										
VTN		Aux. value in subroutine SHOCK														X							
VV1		" " " " " " " "														X							
VV2		" " " " " " " "														X							

1. Ackroyd, J.A.D. - "Shock-induced Laminar Boundary Layers", The Aeronautical J. of the Roy. Aero. Soc. , Vol.74 , Nov.1970 , pp.908-911.
2. Allen, J.S. ; Cheng, S.I. - "Numerical solution of the compressible Navier-Stokes equations for the Laminar near Wake", The Physics of Fluids, Vol.13 , N^o 1 , Jan.1970 , pp.37-52.
3. Anderson, G.F. ; Murthy, V.S. ; Suter, S.P. - "Laminar Boundary Layer Control by combined Blowing and Suction in the presence of surface roughness", J. of Hydronautics , Vol.3 , N^o 3 , July 1969, pp.145-151.
4. Barry, F.W. ; Shapiro, A.H. ; Newmann, E.P. - "Some Experiments on the Interaction of Shock-Waves with Boundary Layers on a flat plate", J. of App. Mech. , Vol.17 , June 1950 , pp.126-131.
5. Baum, E. - "An Interaction model of a Supersonic Laminar Boundary Layer on sharp and rounded backward facing steps", AIAA J. , Vol.6 , N^o 3 , Mars 1968 , pp.440-447.
6. Blankenship, V.D. ; Chung, P.M. - "Compressible Boundary Layer - Inviscid flow Interactions in Entrance region of internal flows", ASME Paper 67-HT-2 , Aug.1967 , 8pp.
7. Blottner, F.G. - "Finite Difference methods of solution of the Boundary Layer equation", AIAA J. , Vol.8 , N^o 2 , Feb.1970 , pp.193-205.
8. Brailovskaya, I.Y. - "A Difference Scheme for Numerical Solution of the Two-Dimensional Nonstationary Navier-Stokes equations for a compressible gas", Sov. Phys. , DOKLADY , Vol.10 , N^o 2 , Aug.1965 , pp.107-110.
9. Brailovskaya, I.Y. ; Kuskava, T.V. ; Chudov, L.A. - "Difference methods of solving the Navier-Stokes equations", Int. Chemical Eng. , Vol.10 , N^o 2 , Apr.1970 , pp.228-236.
10. Bray, K.N.C. ; Gadd, C.E. ; Woodger, M. - "Some calculations by the Crocco-Lees and other methods of interactions between Shock-Waves and Laminar Boundary Layers , including effects of Heat Transfer and Suction", A.R.C. CP N^o 556 , 1961 , 67pp.
11. Brilliant, H.M. ; Adamson, T.C. - "Shock Wave - Boundary Layer Interaction in Laminar Transonic Flow", AIAA J. , Vol.12 , N^o 3 , Mars 1974 , pp.323-329.
12. Byrkin, A.P. - "Exact solution of the Navier-Stokes equations for a Compressible Gas", PMM Vol.33 , N^o 1 , 1969 , pp.152-157.

13. Carter, J.E. - "Numerical solutions of the Navier-Stokes equations for 13: the Supersonic Laminar Flow over a Two-Dimensional Compression Corner", NASA TR-R-385 , July 1972 , 79pp.
14. Chapman, D.R. ; Kuehn, D.M. ; Larson, H.K. - "Investigations on Separated Flows in Supersonic and Subsonic Streams with emphasis on the effect of Transition", NACA Rep. N^o1356 , 1958 , pp.421-460.
15. Charwat, A.F. - "Supersonic Flows with Imbedded Separated Regions", Advances in Heat Transfer , 1970 , pp.1-133.
16. Cheng, S.I. - "Numerical Integration of Navier-Stokes Equations", AIAA J. , Vol.8 , N^o12 , Dec.1970 , pp.2115-2122.
17. Cooke, J.C. ; Brebner, G.G. - "The nature of Separation and its prevention by geometric design in a wholly Subsonic Flow", "Boundary Layer and Flow Control" Edited by G.V. Lachman , Pergamon Press , 1961 , pp.144-185.
18. Courant, R. ; Friedrichs, K.O. ; Lewy, H. - "On the Partial Difference Equation of Mathematical Physics", Mathematische Annalen , N^o 100 , 1928 , pp.32-74.
19. Crocco, L. . Lees, L. - "A mixing theory of the Interaction between Dissipative Flows and nearly Isentropic Streams", J. of Aero. Sci. , Vol.19 , 1952 , pp.649-676.
20. Crocco, L. - "A suggestion for the Numerical Solution of the Navier-Stokes Equations", AIAA J. , Vol.3 , N^o10 , Oct.1965 , pp.1824-1832.
21. Davis, G.V. ; Mallinson, G.D. - "False Diffusion in Numerical Fluid Mechanics", (Unpublished Note) , Jan. 1972 .
22. Dorodnitsyn, A.A. ; Lulka, S.A. ; Meller, N.A. - "Review of the studies on Navier-Stokes Equations at the Computing Center of the Academy of Sciences USSR Moscow", 10th Symposium on advanced problems and methods in Fluid Mechanics , Poland , Warsaw , Proc. Pt. 2 , Sept.1971 , pp.131-133.
23. Dorrance, W.H. - "Viscous Hypersonic Flow", (Book) , McGraw-Hill, New-York , 1962 .
24. Emery, A.F. - "An evaluation of several differencing methods for Inviscid Fluid flow problems", J. of Comp. Phys., Vol.2, 1968, pp.306-331.
25. Erdos, J. ; Pallone, A. - "Shock Boundary Layer Interaction and Flow Separation", Proc. of the 1962 Heat Trans. and Fluid Mech. Inst. , 1962, pp.239

26. Ffügge-Lotz, I ; Er-Young, Y. - "Development of a Finite Difference /133 method for computing a Compressible Laminar Boundary Layer with interactions"; Stanford Univ. , Div. Eng. Mech., TR 127 , May 1960.
27. Forsythe, G.E. ; Wasov, W.R. - "Finite Difference Methods for Partial Differential Equations", (Book) , John Wiley & Sons Inc. , New-York , 1960 .
28. Gadd, G.E. ; Holder, D.W. ; Regan, J.D. - "An Experimental Investigation of the Interaction between Shock-Wave and Boundary Layer", Proc. Roy. Soc. , Vol. A226 , 1954 , pp.227-253.
29. Gai, S.L. - "Effect of Suction on the Upstream Influence in Shock Wave - Boundary Layer Interactions", Zeitschrift für Ang. Math. und Phys. (ZAMP) , Vol.20 , N^o2 , 1969 , pp.265-272.
30. Gai, S.L. - "On the Upstream Influence associated with the critical pressure rise in Shock - Boundary Layer Interactions", Zeitschrift für Flugwissenschaften , Vol.18 , N^o1 , 1970 , pp.8-12.
31. Georgeff, M.P. - "A comparison of Integral Methods for the prediction of Laminar Boundary Layer - Shock Wave Interaction", Imperial College of Sci. and Tech. , London , IC-Aero-72-01 , Jan.1972 , 56pp.
32. Georgeff, M.P. - "Momentum Integral Method for Viscous - Inviscid Interactions with arbitrary wall cooling", AIAA J. , Vol.12 , N^o10 , Oct. 1974 , pp.1393-1400.
33. Gerhart, P.M. - "On prediction of Separated Boundary Layers with pressure distribution specified", AIAA J. , Vol. 12 , N^o9 , Sept. 1974 pp. 1278-1279.
34. Ghia, U. ; Davis, R.T. - "Navier-Stokes Solutions for flow past a class of Two-Dimensional Semi Infinite Bodies", AIAA J. , Vol.12 , N^o12 , Dec.1974 , pp.1659-1665.
35. Glick, H.S. - "Modified Crocco-Lees mixing theory for Hypersonic Separated and Reattaching Flows", Cal. Inst. of Tech. , Hypersonic Res. Rep. Memo. N^o53 , May 1960 , 108 pp.
36. Goodman, T.R. - "A theory of Shock Wave - Boundary Layer Interaction", J. of Aero. Sci. , Vol.21 , N^o10 , 1954 , pp.715
37. Goodrich, W.D. ; Lamb, J.P. ; Bertin, J.J. - "On the Numerical Solution of Two-Dimensional Laminar Compressible Flows with Imbedded Shock-Waves", J. of Basic Eng. , , Dec.1972 , pp.765-770.

38. Goodwin, F.K. ; Nielsen, J.N. ; Lynes, L.L. - "Calculation of Laminar 134
Boundary Layer - Shock Wave Interaction by the method of Integral
Relations", Nielsen Eng. and Res. Inc. , NEAR Rep. TR 2 , July 1967.
39. Gosman, A.D. ; Pun, W.M. ; Runchal, A.K. ; Spalding, D.B. ; Wolfstein, M.
- "Heat and Mass Transfer in Recirculating Flows", (Book) , Academic
Press , London & New-York , 1969 , 338pp.
40. Gottlieb, D. ; Gustafsson, B. - "Navier-Stokes Equations with constant
Total Temperature", NASA CR-132664 , 1975 , 33pp.
41. Hakkinen, R.J. ; Greber, I. ; Trilling, L. ; Abarbanel, S.S. - "The
Interaction of an Oblique Shock Wave with a Laminar Boundary Layer",
NASA Memo. 2-18-59W , 1959 , 49pp.
42. Hanin, M ; Wolfstein, M. ; Landau, U.E. - "Numerical solution of Navier-
Stokes Equations for Interaction of Shock Wave with Laminar Boundary
Layer", ICAS 9th Paper 74-17 , Aug. 1974 , 5pp.
43. Harlow, F.H. ; Amsden, A.A. - "A Numerical Fluid Dynamics calculation
method for all flow speeds", J. of Comp. Phys. , Vol.8, 1971,pp.197-213.
44. Hirt, C.W. - "Heuristic Stability Theory for Finite Difference Equations",
J. of Comp. Phys. , Vol.2 , N^o4 , June 1968 , pp.339-355.
45. Holden, M.S. - "An Analytical study of Separated Flows induced by Shock-
Wave - Boundary Layer Interaction", NASA CR-600 , 1966 , 58pp.
46. Holder, D.W. ; Gadd, G.E. - "The Interaction between Shock Waves and
Boundary Layers and its relation to base pressure in Supersonic Flow",
"Boundary Layer Effects in Aerodynamics" (Symposium) , National Phys.
Lab. , London , Paper 8 , 1955 , 67pp.
47. Horton, H.P. - "Adiabatic Laminar Boundary Layer / Shock Wave Interaction
on flared axisymmetric bodies", AIAA J. , Vol.9 , N^o11 , Nov.1971 ,
pp.2141-2148.
48. Inger, G.R. ; Swann, T.F. - "Vectored Injection into Laminar Boundary
Layer with Heat Transfer", AIAA J. Vol.13 , N^o5 , May 1975,pp.616-622.
49. Isenberg, J. ; Davis, G.V. - "Finite Difference Methods in Heat and
Mass Transfer", Technion- Israel Inst. of Tech. Report , June 1974 .
50. Jaffe, N.A. ; Smith, A.M.O. - "Calculation of Laminar Boundary Layer by
means of a Differential Difference Method", Progress in Aerospace Sci.
Vol.12 , Oxford , 1972 , pp.49-212.
51. Jamet, P. ; Lascaux, P. ; Raviart, P.A. - "A method of numerical
solution of Navier-Stokes equations." Numerische Mathematik,
Vol.16 , 1970 , pp.93-114.

52. Klineberg, J.H. ; Lees, L. - "Theory of Laminar Viscous Inviscid Interactions in Supersonic Flow", AIAA Paper 69-7 , Jan.1969 , 17pp.
53. Korkegi, R.H. - "Survey of Viscous Interactions associated with high Mach Number Flight", AIAA J. , Vol.9 , N^o5 , May 1971 , pp.771-784.
54. Kronzon, I. - "Numerical solution for the Laminar Supersonic Flow over a Two-Dimensional Backward Facing Step", Ph.D. Thesis , (in Hebrew) , Technion - Israel Inst. of Tech. , Haifa , Oct.1974 , 155pp.
55. Lachman, G.V. (Editor) - "Boundary Layer and Flow Control", (Book) , Pergamon Press , New-York , 1961 .
56. Lascaux, ; Raviart, P. "A numerical method of solving Navier-Stokes equations,"
57. Lax, P.D. - "Hyperbolic Difference Equations: A review of the Courant-Friedrichs-Lewy Paper in the light of recent developments," IBM J. of Research and Development, Vol.11 , N^o2 , Mars 1967 , pp.235-238.
58. Lax, P.D. ; Wendroff, B. - "Difference Schemes for Hyperbolic Equations with high order of Accuracy", Comm. on Pure and App. Math. , Vol.13 , N^o3 , Aug.1964 , pp.381-398.
59. Lees, L. ; Reeves, B.L. - "Supersonic Separated and Reattaching Laminar Flows: 1. General Theory and Application to Adiabatic Boundary Layer/ Shock Wave Interaction", AIAA J. , Vol.2 , N^o11, Nov.1964, pp.1907-1920.
60. Lewis, J.E. ; Kobota, T. ; Lees, L. - "Experimental Investigation of Supersonic Laminar, Two-Dimensional Boundary Layer Separation in a Compression Corner with and without Cooling", AIAA J. , Vol.6 , N^o1 , Jan.1968 , pp.7-14.
61. Liepmann, H.W. ; Roshko, A. ; Dhawan, S. - "On Reflection of Shock Waves from Boundary Layers", NACA Rep. 1100 , Aug.1949 , pp.889-917.
62. Lighthill, M.J. - "Reflection at a Laminar Boundary Layer of a Weak Steady Disturbance to a Supersonic Stream, neglecting Viscosity and Heat Conduction", Quart. J. of Mech. and App. Math. , Vol.3 , Pt.3 , 1950 , pp.303-325.
63. Lighthill, M.J. - "On Boundary Layers and Upstream Influence: 2. Supersonic Flows without Separation", Proc. Roy. Soc. , Vol. A217 , 1953 , pp.478-507.
64. Loer, V.S. - "A numerical method for solution of Navier-Stokes equations for the two-dimensional, incompressible, stationary flow along a thin plate," Ingenieur Archiv, Vol. 41, 1971, pp. 28-30.

65. Lubard, S.C. ; Shetz, J.A. - "The Numerical Solution of Boundary Layer problems," 1968, pp.138-150.
66. MacCormack, R.W. - "Effect of Viscosity in Hypervelocity Cratering", AIAA Paper 69-354 , May 1969 , 7 pp.
67. MacCormack, P.W. - "Numerical Solution of the Interaction of a Shock-Wave with a Laminar Boundary Layer", Proc. 2nd Int. Conf. on Num. Methods in Fluid Dyn. , Vol.8 , 1971 , pp.151-163.
68. MacCormack, R.W. ; Warming, R.F. - "Survey of Computational Methods for Three-Dimensional Supersonic Inviscid Flows with Shocks", VKI Lecture Notes , 1973 , 20pp.
69. MacCormack, R.W. ; Baldwin, B.S. - "A Numerical Method for solving the Navier-Stokes Equations with application to Shock-Boundary Layer Interactions", AIAA Paper 75-1 , Jan.1975 , 8pp.
70. Makofski, R.A. - "A Two Parameter Method for Shock Wave - Laminar Boundary Layer Interaction and Flow Separation", 1963 Heat Tran. and Fluid Mech. Inst. , 1963 , pp.112-127.
71. Messiter, A.F. ; Feo, A. ; Melnik, R.E. - "Shock Wave Strength for Separation of a Laminar Boundary Layer at Transonic Speeds", AIAA J. , Vol.9 , N^o6 , June 1971 , pp.1197-1198.
72. Miller, G. - "Mathematical formulation of Viscous - Inviscid Interaction problems in Supersonic Flow", AIAA J. , Vol.11 , N^o7 , July 1973 , pp.938-942.
73. Morduchow, M. - "Analysis and Calculation by Integral Methods of Laminar Compressible Boundary Layer with Heat Transfer and without Pressure Gradient", NACA Rep. 1245 , Apr.1955 , pp.1065-1083.
74. Murphy, J.D. - "A critical Evaluation of Analytic Methods for predicting Laminar Boundary Layer - Shock Wave Interaction", NASA SP 228 , Paper 21 , Oct.1969 , pp.515-539.
75. Needham, ; Stollery, - "Hypersonic Studies of Incipient Separation and Separated Flows", AGARD Conf. Proc. , N^o4 , Pt. 1 , 1966 , pp.89.
76. Nielsen, J.N. ; Lynes, L.L. ; Goodwin, F.K. - "Calculation of Laminar Separation with Free Interaction by the Method of Integral Relations , Parts 1. & 2 " , AFFDL TR 65-107 , Oct.1965 - Jan.1966 .
77. Page, R.H. - "A Theory for Incipient Separation", "Boundary Layer and Flow Control" Edited by G.V. Lachman , Pergamon Press, 1961, pp.563-577.

78. Palumbo, D.J. ; Rubin, E.L. - "Solution of the Two-Dimensional Unsteady /137
Compressible Navier-Stokes Equations using a second order accurate
Numerical Scheme", J. of Comp. Phys. , Vol.9 , 1972 , pp.466-495.
79. Panov, L.A. ; Shvets, A.I. - "Methods of calculating Shock Wave - Boun-
dary Layer Interaction", Gidraeromekhanika ; Teoriia Uprugosti , N°6
1967 , pp.8-16 .
80. Paskonov, V.M. ; Chudov, L.A. - "Difference Methods of computing the
flow in the Boundary Layer", (Survey) , Vychisl. Metody i Programm-
irovanie , N°11 , 1968 .
81. Pearcey, H.H. - "Shock Induced Separation and its prevention by design
and Boundary Layer Control", "Boundary Layer and Flow Control" Edited
by G.V. Lachman , Pergamon Press , New-York , 1961 , pp.1167-1344.
82. Popinski, Z. - "Shock Wave - Boundary Layer Interaction", Lockheed Cal.
Co. Rep. 18307 , 1965 , 12pp.
83. Ray, A.K. - "Critical Viscous Sublayer", 10th Congress of App. Mech. ,
Italy , 1960 , pp.1391-1397 .
84. Reyhner, R.D. ; Flüge-Lotz, I. - "The Interaction of a Shock Wave with
a Laminar Boundary Layer", Int. J. of Non-Linear Mech. , Vol.3 , 1968 ,
pp.173-199 .
85. Richtmyer, R.D. ; Morton, K.W. - "Difference Methods for Initial Value
Problems", (Book) , John Wiley & Sons , New-York , 1967 .
86. Roache, P.J. - "Computational Fluid Dynamics", (Book) , Hermosa Publi-
shers , Albuquerque , 1972 , 434pp.
87. Roache, P.J. - "On Artificial Viscosity", J. of Comp. Phys. , Vol.10 ,
N°2 , Oct.1972 , pp.169-184 .
88. Rose, W.C. - "A Method for analyzing the Interaction of an Oblique
Shock Wave and a Boundary Layer", NASA SP 228 , Paper 20 , 1969 ,
pp.541-567 .
89. Rosenhead, L. (Editor) - "Laminar Boundary Layers ", (Book) , Oxford
Univ. Press , Oxford , 1963 , 687 pp.
90. Rubin, E.L. ; Burstein, S.Z. - "Difference Methods for the Inviscid
and Viscous Equations of a Compressible Gas", J. of Comp. Phys. ,
Vol.2 , 1967 , pp.178-196 .
91. Scala, S.M. ; Gordon, P. - "Solution of the Time Dependant Navier-
Stokes Equations for the flow around a circular cylinder", AIAA
Paper 67-221 , Jan.1967 , 13pp.

92. Schlichting, H. - "Boundary Layer Theory" (Book) , 6th Edition , /138
McGraw-Hill Book Co. Inc. , New-York , 1968 .
93. Shapiro, A.H. - "The Dynamics and Thermodynamics of Compressible Fluid
Flow" (Book) , Ronald Press Co. , New-York , 1953 , 1185 pp.
94. Skoglund, V.J. ; Gay, B.D. - "Improved Numerical Technique and Solution
of a Separated Interaction of an Oblique Shock Wave and a Laminar
Boundary Layer", Univ. of New-Mexico ,ME-41(69)s-068,June 1969,141 pp.
95. Stewartson, K. - "On the motion of a Flat Plate at high speed in a
Viscous Compressible Fluid , Pt. 2: Steady Motion" , J. of Aero. Sci.
May 1955 , pp. 303-309.
96. Stewartson, K. - "The Theory of Laminar Boundary Layers in Compressible
Fluids" (Book) , Oxford Univ. Press , Oxford , 1964 , 191 pp.
97. Stewartson, K. ; Williams, P.G. - "Self Induced Separation", Proc. Roy.
Soc. , Vol. A312 , 1969 , pp. 181-206 .
98. Tani, I. - "Note on the Separation of the Laminar Boundary Layer" ,
(Unpublished) , 1953 , 9 pp.
99. Taylor, T.D. ; Ndefo, E. ; Masson, B.S. - "A study of Numerical
Methods for solving Viscous and Inviscid Flow Problems", J. of Comp.
Phys. , Vol.9 , 1972 , pp. 99-119.
100. Thommen, H.U. - "Numerical Methods of the Integration of the Navier-
Stokes Equations" , ZAMP , Vol.17 ,1966 , pp. 369-384 .
101. Vincenti, V.G. ; Kruger, C.H. - "Introduction to Physical Gas Dynamics",
(Book) , John Wiley & Sons Inc. , New-York , 1965 .
102. Waiter, S.A. ; Leblanc, L.P. - "Solution of the Compressible Boundary
Layer / Laminar, Transition, Turbulent / by an Implicit Finite Diffe-
rence Technique", Astronautica Acta ,Vol.16, Nov.1971, pp.265-276.
103. Welch, J.E. ; Harlow, F.H. ; Shann, J.P. ; Daly, S.J. - "The MAC Method:
a Computing Technique for solving Viscous Incompressible , Transient
Fluid Flow Problems involving Free Surfaces", Los Alamos Sci. Lab. ,
La - 3425 , Nov. 1965 .
104. Werle, M.J. ; Bertke, S.P. - "A Finite Difference Method for Boundary
Layers with Reverse Flow", AIAA J. Vol.10,N^o9,Sept. 1972, pp.1250-1252
105. Wuest, W. - "Theory of Boundary Layer Suction to prevent Separation",
"Boundary Layer and Flow Control" Edited by G.V. Lachman , Pergamon
Press , 1961 , pp. 144-185 .

TABLES OF COMPUTER RUNS

TABLE 1A. CHECK OF COMPUTATION METHOD

Flow conditions for all runs: $p_e/p_o = 1.4$; $Re_{x_s} = 3 \cdot 10^5$;
 $M_o = 2.0$

Run No.	IMAX	ISTB	IGRD	JAV	KPRT	MODE	Notes
001	200	0	1	0	0	1	Reference Run
003	200	0	2	0	0	1	
005	350	0	1	1	0	1	Artificial viscosity only for the first 150 iterations.
006	200	0	1	0	1	1	
007	200	0	1	0	0	2	Component downstream of the shock wave's whole length, computed by average approximation same as above
008	200	0	2	0	0	2	
009	200	0	1	0	1	2	Isolation after 150 iterations
021	400	1	1	0	0	1	
022	400	1	1	0	1	1	
031	400	1	1	0	0	1	Computation is carried out with double accuracy (13 digits instead of 6-7 digits)
041	600	1	1	0	0	1	Computation carried out with fine grid 147x48 (instead of the regular 76x25)
051	400	1	1	0	0	1	computation is carried out by integration

Notation: MODE = 1 continuous computation
 = 2 noncontinuous computation of the shock wave path

 KPRT = 0 uniform grid
 = 1 nonuniform grid in x direction

 JAV = 0 without artificial viscosity
 = 1 with artificial viscosity

 IGRD = 1 the entire field with second order differences
 = 2 part of the field below the shock wave with fourth order differences

 ISTB = 0 without computations of stability
 = 1 with computations of stability

 IMAX - maximum number of iterations for the run

TABLE 1B. CHECK OF INFLUENCE OF ARTIFICIAL VISCOSITY

/140

Run No.	CC_2	CC_4	$P.C. \Delta t$	σ_c / ρ_0	M_0
081	.05	.01	3×10^5	1.4	2
082	.10	.01	3×10^5	1.4	2
083	.10	.05	3×10^5	1.4	2
091	.10	.01	1×10^6	1.4	2
092	.10	.01	5×10^4	1.4	2
093	.10	.01	3×10^5	3.15	4

Note: The first 150 iterations in this series of runs were performed with artificial viscosity, the following 200 without it.

TABLE 2. CHECK OF DEPENDENCE OF RESULTS ON PERIMETERS
 (All runs were performed according to the basic method
 of run 001, up to 200 iterations)

/141

Run No.	P_1	X_s/m	$S_e X_s$	P_2/P_1	M_0	Notes
101	.72	.05	3×10^5	1.2	2.0	These results are used for comparison with previous analytical and experimental results
102 *	.72	.05	3×10^5	1.4	2.0	
103	.72	.05	3×10^5	1.9	2.0	
104	.72	.05	3×10^5	3.15	2.0	
105	.72	.05	3×10^5	3.7	2.0	No solution available for the boundary conditions of the characteristics since a subsonic region is downstream of the shock wave
111	.72	.05	3×10^5	3.15	3.0	
112	.72	.05	3×10^5	3.15	4.0	
113	.72	.05	3×10^5	3.15	4.5	
114	.72	.05	3×10^5	3.15	5.0	The solution is isolated after 150 iterations
121	.72	.05	1×10^4	1.4	2.0	
122	.72	.05	5×10^4	1.4	2.0	
123	.72	.05	1×10^6	1.4	2.0	
124	.72	.05	5×10^6	1.4	2.0	From a practical point of view the flow is already turbulent and the results therefore questionable
131	.72	.03	1.8×10^5	1.4	2.0	
132	.72	.07	4.2×10^5	1.4	2.0	
133	.72	.09	5.4×10^5	1.4	2.0	
141	1.0	.05	3×10^5	1.4	2.0	

*Run 102 is similar to 001.

TABLE 3. INFLUENCE OF BOUNDARY CONDITIONS (THERMAL CONDUCTIVITY AND MASS TRANSFER BY THE PLATE) ON THE FIELD OF FLOW (All runs were performed according to the basic method of run 001, up to 200 iterations). Flow conditions for all runs: $p_e/p_o = 1.4$; $Re_{x_s} = 3 \cdot 10^5$; $M_o = 2.0$.

Run No.	Suction region w.ref. to start				$\frac{y}{\delta}$	$\frac{c_p T_w}{U_o}$	Notes
	End		Beginning				
	Dist.	Grid pt.	Dist.	Grid pt.			
201						0.4	Check of influence of heating or cooling of plate surface on the interaction
202						0.6	
203					0	0.8	
204						1.0	
205						1.2	
106						1.4	
211	6.8	60	3.2	15	-0.03		Check of influence of suction or injection at the plate surface on the interaction
212	6.8	60	3.2	15	-0.02		
213	6.8	60	3.2	15	-0.01	$\frac{(c_p T_w)}{U_o} = 0$	
214	6.8	60	3.2	15	0.01		
215	6.8	60	3.2	15	0.02		
221	6.8	60	2.6	8	-0.03		Check of influence of location for start of suction on the size of the separated region
222	6.8	60	2.8	8	-0.02		
223	6.8	60	2.9	8	-0.01		
224	6.8	60	3.8	22	-0.03		
225	6.8	60	3.8	22	-0.02	$\frac{(c_p T_w)}{U_o} = 0$	
226	6.8	60	3.8	22	-0.01		
227	6.8	60	4.4	30	-0.03		
228	6.8	60	4.4	30	-0.02		
229	6.8	60	4.4	30	-0.01		

TABLE 4. INFLUENCE OF LENGTH AND LOCATION OF SUCTION ZONE ON THE SEPARATION /143

(All runs were performed according to the basic computation method of run 001, up to 200 iterations). Flow conditions for all runs: $Re_{x_s} = 3 \cdot 10^5$; $p_e/p_o = 1.4$; $M_o = 2.0$. (The length of the separated region without suction, under these conditions, is in the range of $35 < m < 45$ grid points on the plate surface.)

Run No.	Suction Region w. ref. to the Start			
	End		Start	
	Distance (cm)	Grid Point	Distance (cm)	Grid Point
251	4.0	25	3.2	15
252	4.8	35	3.2	15
253	5.6	45	3.2	15
254	6.4	55	3.2	15
255	4.8	35	4.0	25
256	5.2	40	4.0	25
257	5.6	45	4.0	25
258	6.0	50	4.0	25
259	4.8	35	4.4	30
260	5.2	40	4.4	30
261	5.6	45	4.4	30
262	6.0	50	4.4	30
263	5.2	40	4.8	35
264	5.6	45	4.8	35
265	6.0	50	4.8	35
266	5.6	45	5.2	40
267	6.0	50	5.2	40

TABLE 5A. INFLUENCE OF SUCTION ON THE SEPARATION UNDER VARIOUS /144
FLOW CONDITIONS

(All runs were performed according to the basic computation method of run 001, for 200 iterations.) A region of suction is present in the range of $15 < m < 60$ grid points on the plate surface for all runs.

Run No.	$\frac{v_w}{U_0}$	x_s ($\frac{m}{c}$)	Re_{x_s}	M_c	P_c/P_0	Notes
301	-0.03	.05	3×10^5	2.0	1.9	Influence of Suction on the Intensity of various Shock Waves
302	-0.02		3×10^5	2.0	1.9	
303	-0.01		3×10^5	2.0	1.9	
304	-0.03		3×10^5	2.0	3.15	
305	-0.02		3×10^5	2.0	3.15	
306	-0.01		3×10^5	2.0	3.15	
311	-0.03	.05	5×10^4	2.0	1.4	Influence of Suction on the various Reynolds Numbers
312	-0.02		5×10^4	2.0	1.4	
313	-0.01		5×10^4	2.0	1.4	
314	-0.03		1×10^6	2.0	1.4	
315	-0.02		1×10^6	2.0	1.4	
316	-0.01		1×10^6	2.0	1.4	
321	-0.03	.05	3×10^5	3.0	3.15	Influence of Suction on the various Mach Numbers
322	-0.02		3×10^5	3.0	3.15	
323	-0.01		3×10^5	3.0	3.15	
324	-0.03		3×10^5	4.0	3.15	
325	-0.02		3×10^5	4.0	3.15	
326	-0.01		3×10^5	4.0	3.15	

TABLE 5A (continued) PARAMETRIC CHECK FOR VARIOUS x_s

Run No.	$\frac{v_w}{U_0}$	x_s (cm)	Re_{y_2}	M_0	P_2/P_0	Notes
331	-0.005	0.03	3×10^5	2.0	1.4	Influence of suction on the various shock wave intensities
332	-0.015		3×10^5	2.0	1.4	
333	-0.005		3×10^5	2.0	1.9	
334	-0.015		3×10^5	2.0	1.9	
335	-0.005		3×10^5	2.0	3.15	
336	-0.015		3×10^5	2.0	3.15	
341	-0.005	0.03	5×10^4	2.0	1.4	Influence of suction on the various Reynolds numbers
342	-0.015		5×10^4	2.0	1.4	
343	-0.005		1×10^6	2.0	1.4	
344	-0.015		1×10^6	2.0	1.4	
351	-0.005	0.03	3×10^5	3.0	3.15	Influence of suction on the various Mach numbers
352	-0.015		3×10^5	3.0	3.15	
353	-0.005		3×10^5	4.0	3.15	
354	-0.015		3×10^5	4.0	3.15	
361	-0.015	0.07	3×10^5	2.0	1.4	Influence of suction on the various shock wave intensities
362	-0.025		3×10^5	2.0	1.4	
363	-0.015		3×10^5	2.0	1.9	
364	-0.025		3×10^5	2.0	1.9	
365	-0.015		3×10^5	2.0	3.15	
366	-0.025		3×10^5	2.0	3.15	
371	-0.015	0.07	5×10^4	2.0	1.4	Influence of suction on the various Reynolds numbers
372	-0.025		5×10^4	2.0	1.4	
373	-0.015		1×10^6	2.0	1.4	
374	-0.025		1×10^6	2.0	1.4	
381	-0.015	0.07	3×10^5	3.0	3.15	Influence of suction on the various Mach numbers
382	-0.025		3×10^5	3.0	3.15	
383	-0.015		3×10^5	4.0	3.15	
384	-0.025		3×10^5	4.0	3.15	

TABLE 5B. CHECK OF VARIOUS COMBINATIONS OF FLOW CONDITIONS DURING SUCTION

(All runs were performed according to the basic computation method of run 001, up to 200 iterations). The suction zone is located for all runs in the range $15 < m < 60$ grid points on the plate surface.

	$\frac{V_{17}}{U_0}$	x_s (cm)	Re_{x_s}	Mo	P_2/P_3
401	-0.010	.05	3×10^5	3.0	1.4
402	-0.005		3×10^5	4.0	1.4
403	-0.015		3×10^5	3.0	1.9
404	-0.010		3×10^5	4.0	1.9
405	-0.005		5×10^4	3.0	1.4
406	.0		5×10^4	4.0	1.4
407	-0.015		5×10^4	2.0	1.9
408	-0.010		5×10^4	3.0	1.9
409	-0.005		5×10^4	4.0	1.9
410	-0.020		5×10^4	2.0	3.15
411	-0.015		5×10^4	3.0	3.15
412	-0.010		5×10^4	4.0	3.15
413	-0.010		1×10^6	3.0	1.4
414	-0.010		1×10^6	4.0	1.4
415	-0.010		1×10^6	2.0	1.9
416	-0.010		1×10^6	3.0	1.9
417	-0.020		1×10^6	4.0	1.9
418	-0.010		1×10^6	2.0	3.15
419	-0.010		1×10^6	3.0	3.15
420	-0.010		1×10^6	4.0	3.15
431	-0.016		3×10^5	2.0	1.4
432	-0.025		3×10^5	2.0	1.9

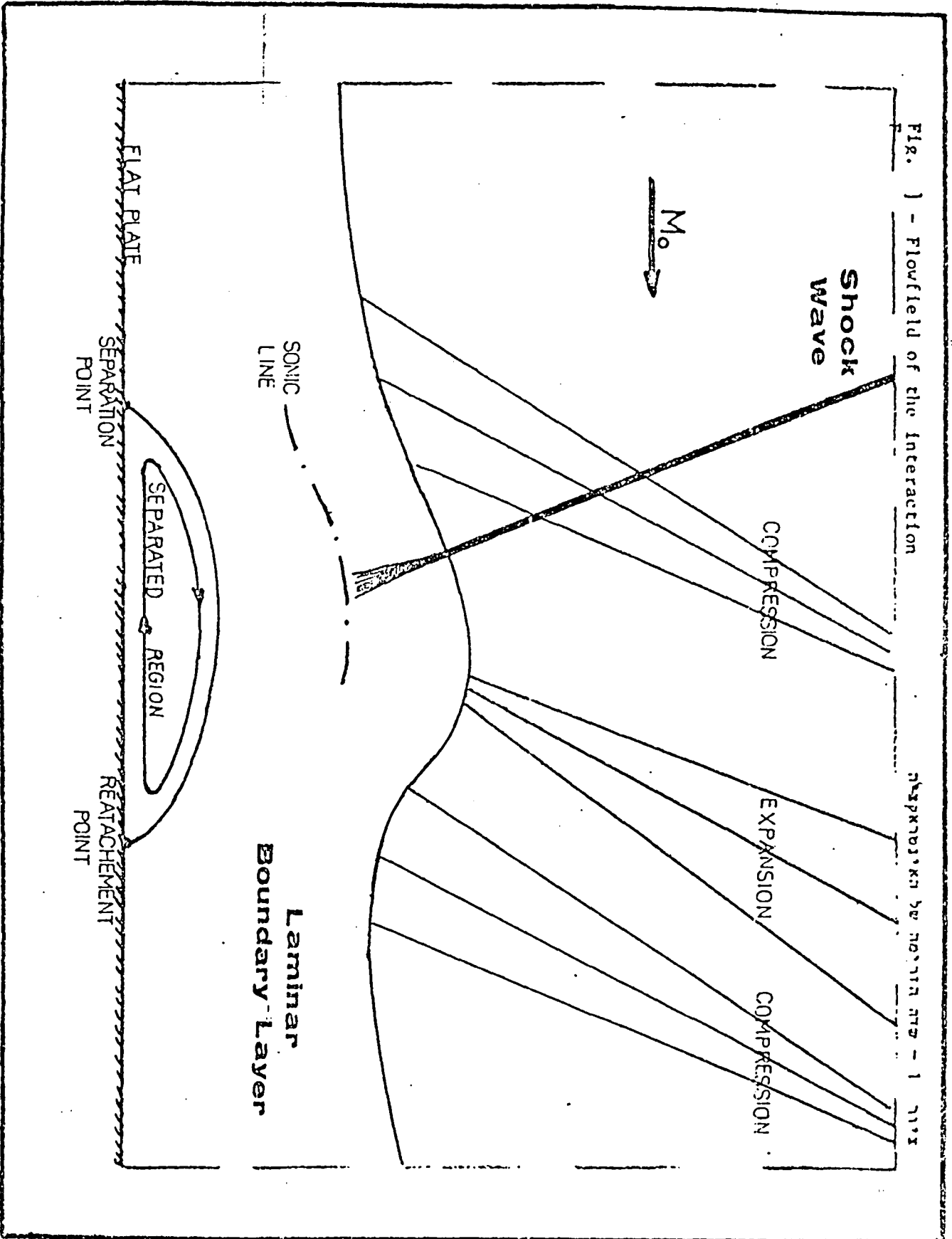
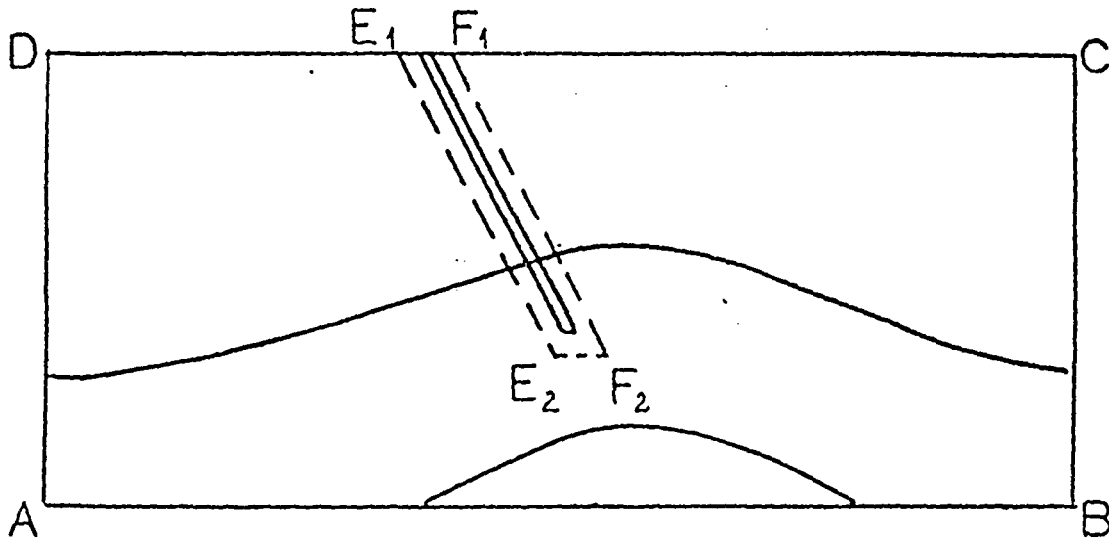


Fig. 2 - Boundary Conditions

ציור 2. - תנאים חגאי הגבול



- | | |
|---|--|
| AD - Upstream section: Pohlhausen Boundary Layer Profile | AD - חתך הכניסה: פרופיל שכבה גבול לפי פולהאוזן |
| AB - Adiabatic Wall: zero velocity components | AB - קיר אדיאבטי: אפס רכיבי מהירות |
| BC - Downstream section: zero downstream gradients | BC - חתך היציאה: אפס גרדיאנטים כיוון הזרימה |
| CD - External flow: extended Characteristics from flowfield | CD - זרימה חיצונית: קרקטריסטיקה משוכות מסדה הזרימה |

The boundaries in the discontinuous method are: הגבולות בשיטה הבלתי-רציפה הם:

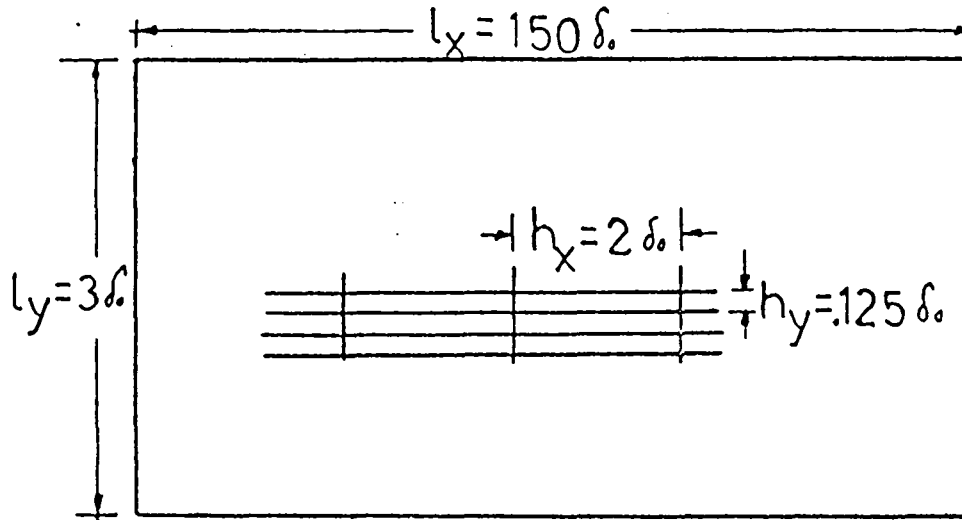
$AD; AB; BC; CF_1; F_1F_2; F_2E_2; E_2E_1; E_1D$

where the additional boundaries: כאשר הגבולות הנוספים הם:

- | | |
|--------------------------------------|------------------------------------|
| E_1E_2 - Shock upstream boundary | E_1E_2 - מעלה גל ההלם החוזר |
| F_1F_2 - Shock downstream boundary | F_1F_2 - מורד גל ההלם החוזר |
| E_2F_2 - Sonic line boundary | E_2F_2 - הקו הקולי (קצה גל ההלם) |

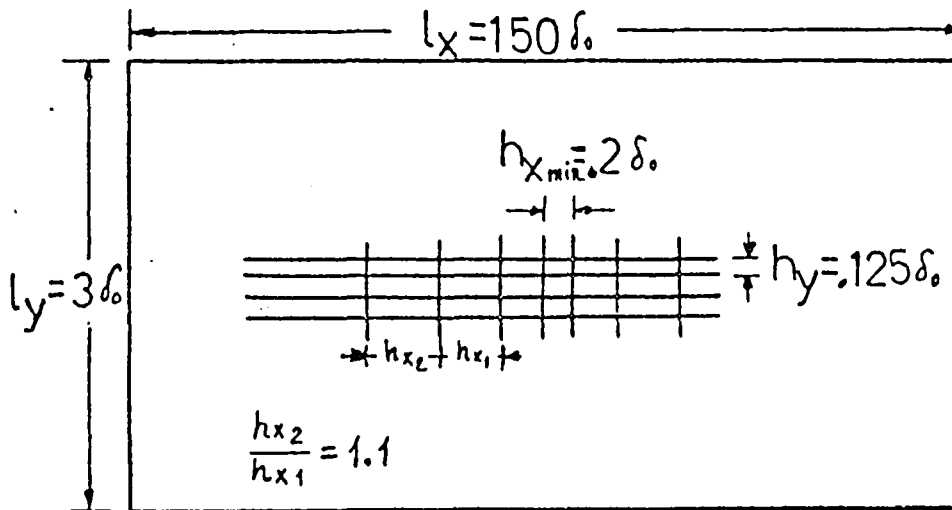
Fig. 3 - Grid description

ציור 3 - תיאור רשתות החישוב



Uniform Grid

רשת אחידה



Variable Grid

רשת משתנה

Fig. 4 - Computation program Flowchart

ציוד 4 - חישוב זרימה על
תוכנית החישוב

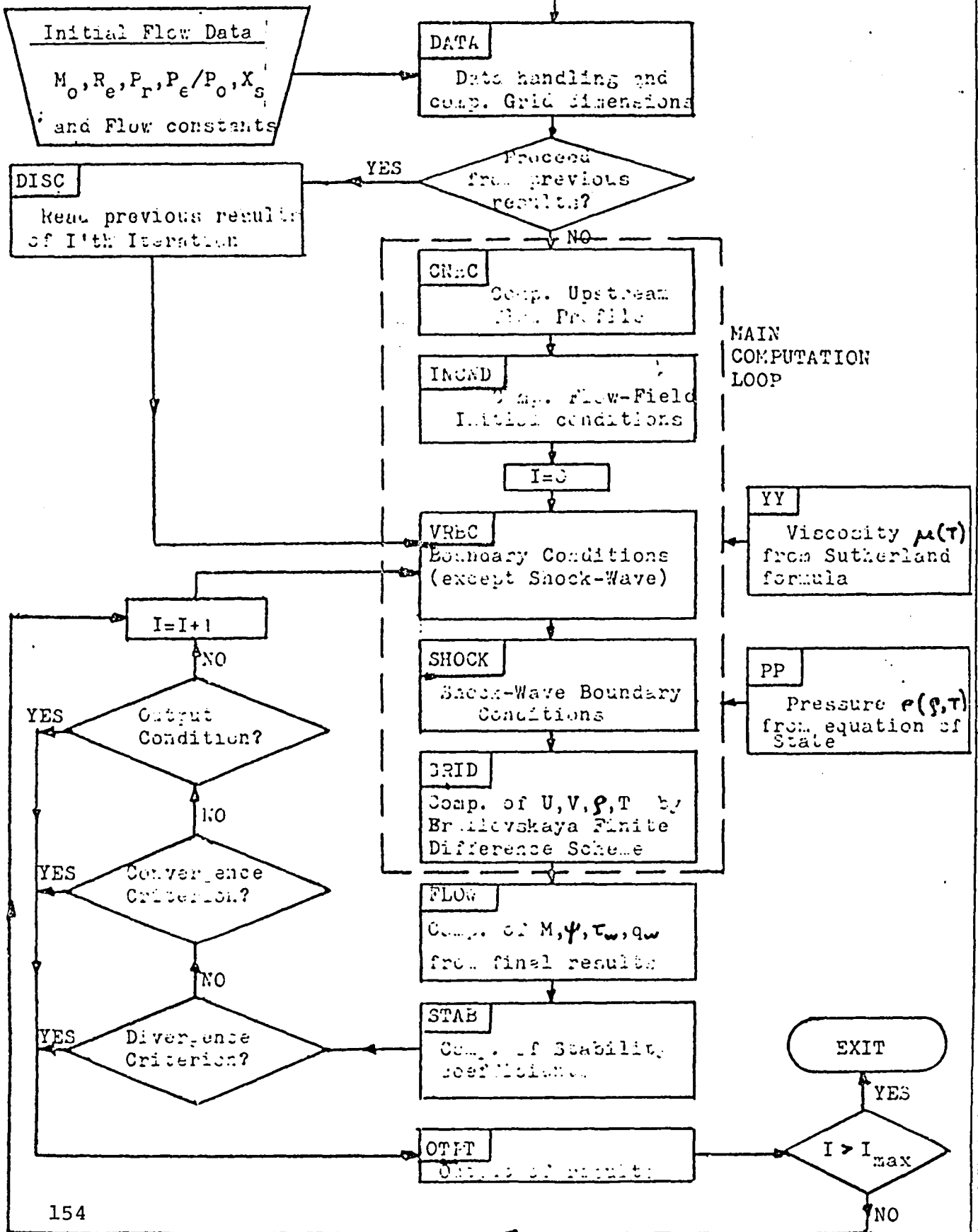


Fig. 5 - Comparison between various computational methods

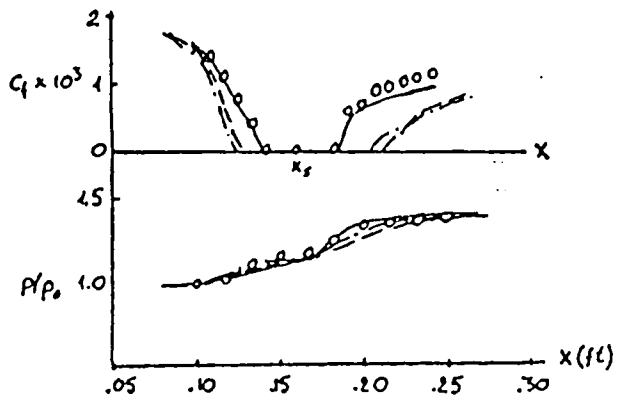
ציור 5 - השוואה חזקתה חישוב קייסות

o o o Hakkinen⁴¹
 x x x Lewis⁶⁰
 Δ Δ Δ Needham⁷⁵

} Experimental results

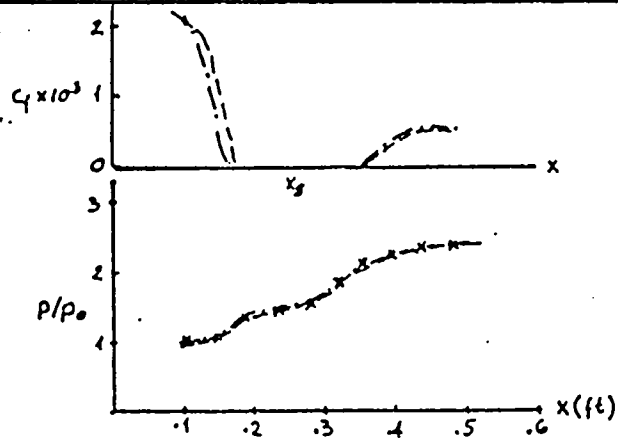
- - - Nielsen⁷⁶
 - - - Reyhner⁸⁴
 — MacCormack⁶⁷

} Computational results



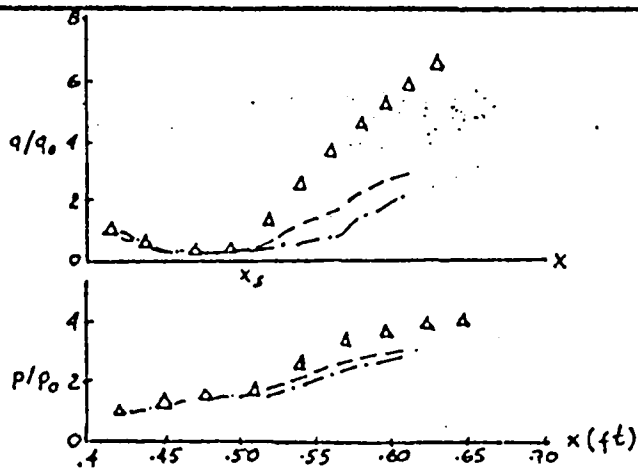
$M_0 = 2$
 $P_0/P_1 = 4.4$
 $Re = 1.78 \times 10^6 \text{ ft}^{-1}$
 $T_w/T_{aw} = 4.0$

(Shock impingement)



$M_0 = 4.0$
 $P_0/P_1 = 2.35$
 $Re = 1.08 \times 10^6 \text{ ft}^{-1}$
 $T_w/T_{aw} = 4.0$

(Compression corner)



$M_0 = 7.4$
 $P_0/P_1 = 3.8$
 $Re = 4.4 \times 10^6 \text{ ft}^{-1}$
 $T_w/T_{aw} = 0.264$

(Compression corner)

Fig. 6a - Comparison of computational options

ציור 6א - השוואה בין
אופציות חישוב
שונות

$M_0 = 2 \quad Re_{x_0} = 3 \times 10^5 \quad \rho_e / \rho_0 = 1.4$

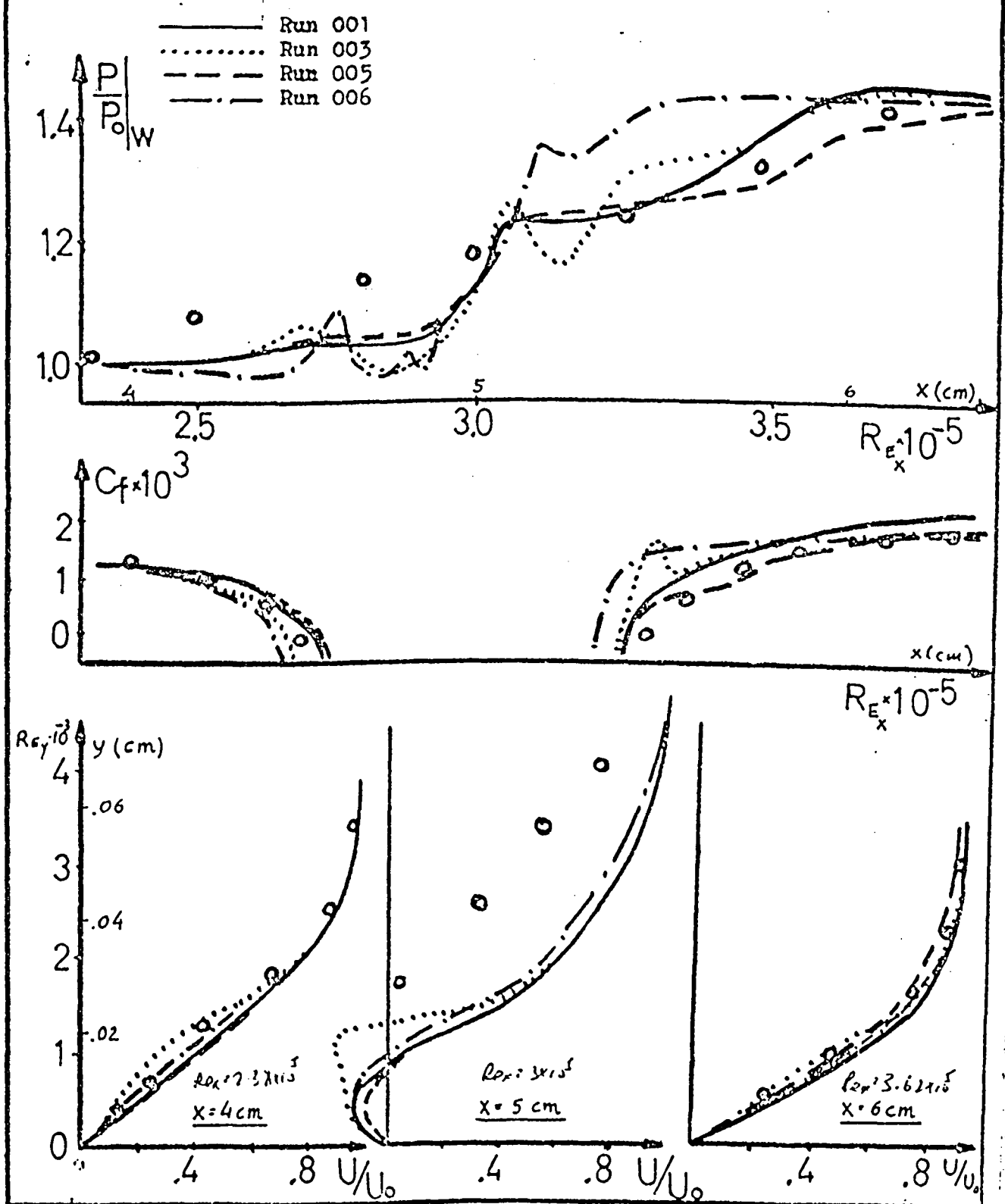


Fig. 6b - Comparison of computational options

ציר 6 - הטוראה כין
אופציות חישוב
עונות

$Mo=2$ $Re_{x_3}=3 \cdot 10^5$ $P_c/P_0=1.4$

Run 001
Run 007
Run 008

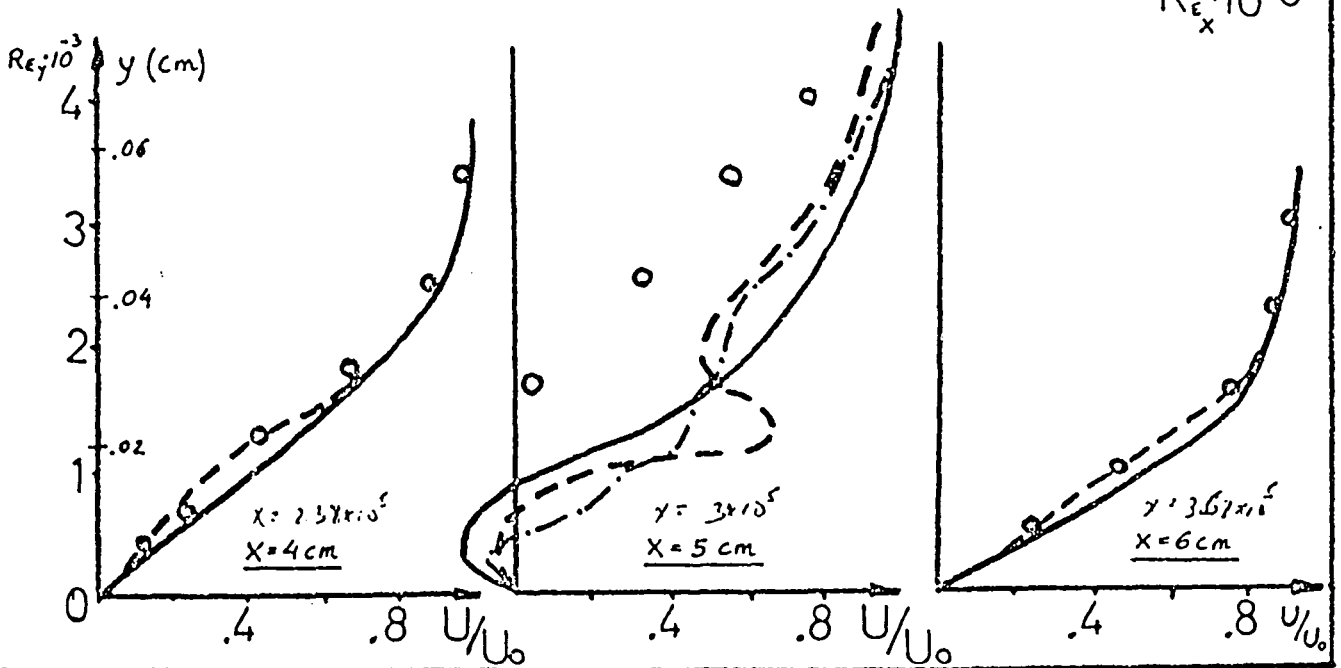
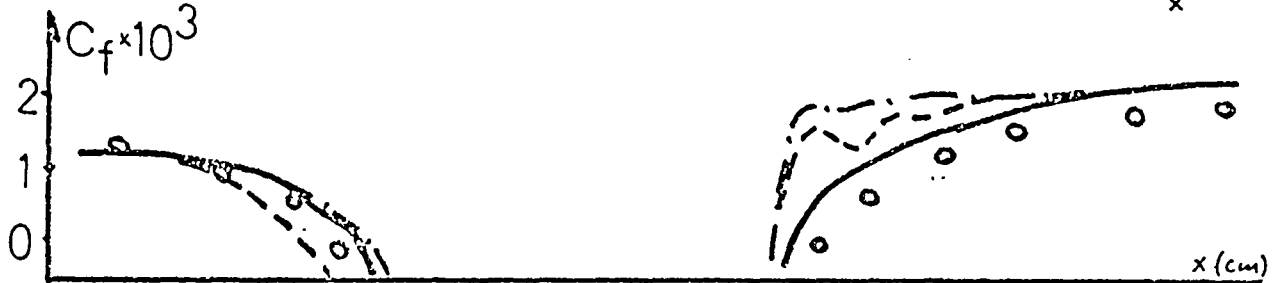
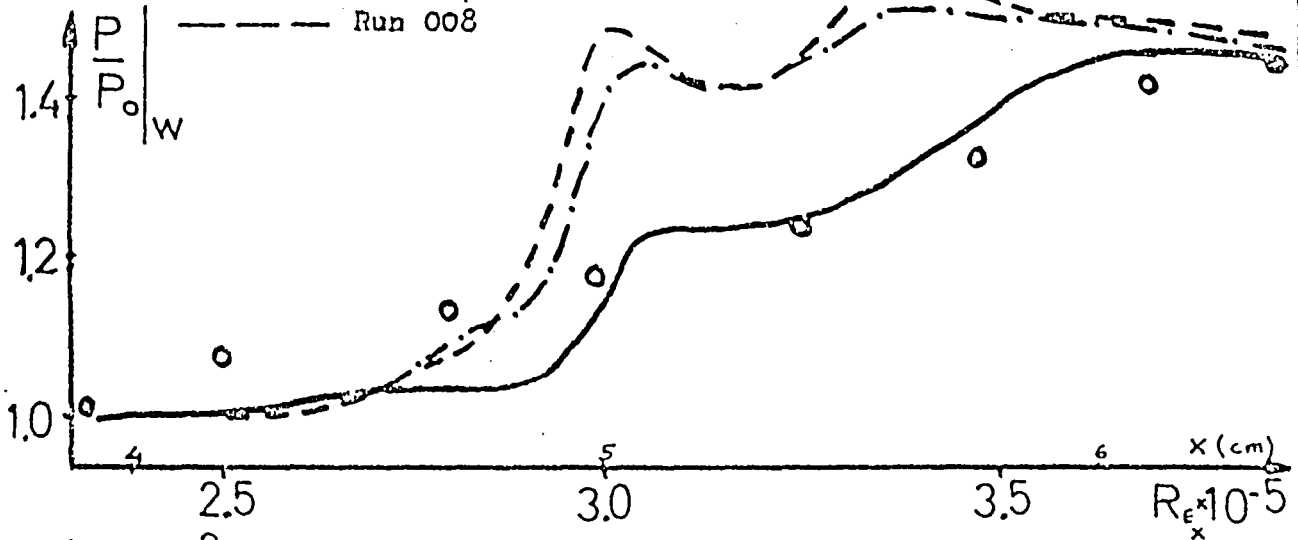


Fig. 7 - Sensitivity of the results to artificial viscosity coefficients

צורה 7 - רגישות התוצאות
למקומי הצמיגות
המלאכותיים

$M_0 = 2.0$

$\frac{P}{P_0} = 1.4$

$Re_{X_s} = 3 \times 10^5$

o o o Hakkinen ⁴¹ (Experiment)

	C_{0x}	C_{0y}
---	.05	.01
—	.10	.01
-.-	.10	.05

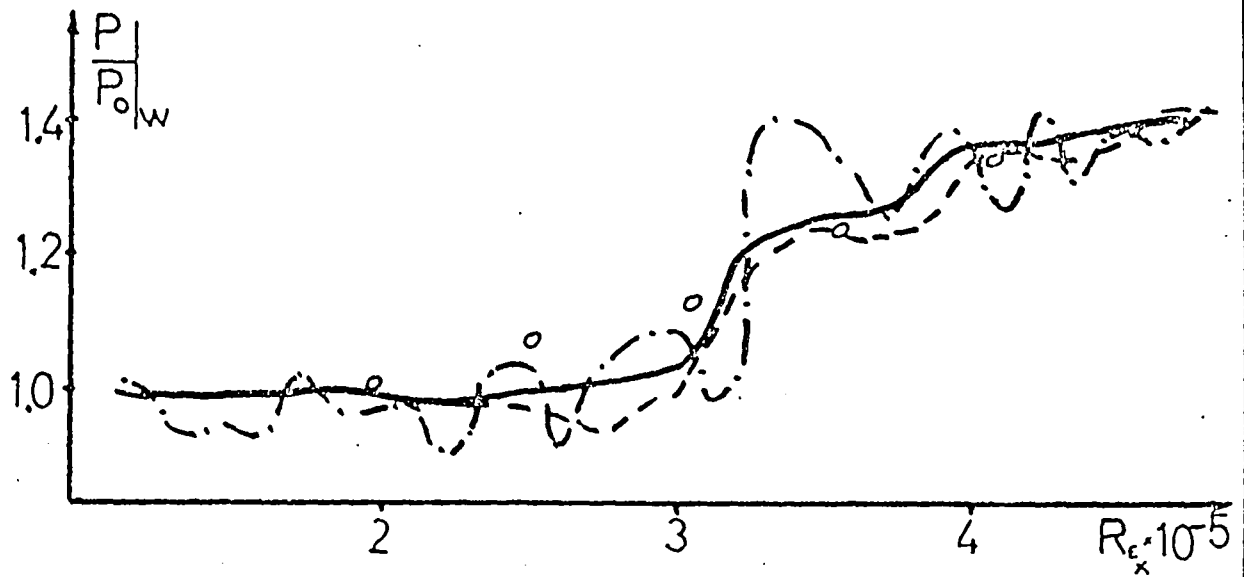


Fig. 7a - Influence of non-optimal Artificial Viscosity coeff.

צירור 7א - השפעה אטיביות סלאכותיה לא אופטימלית

- without Artificial Viscosity
- - - with Artificial Viscosity ($C_{cx}=.10$) ($C_{cy}=.01$)

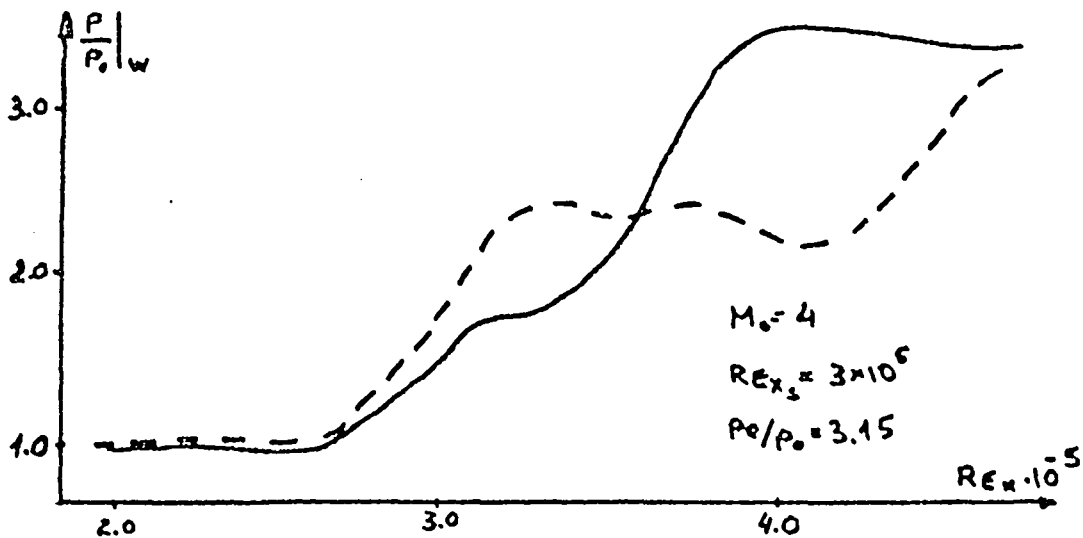
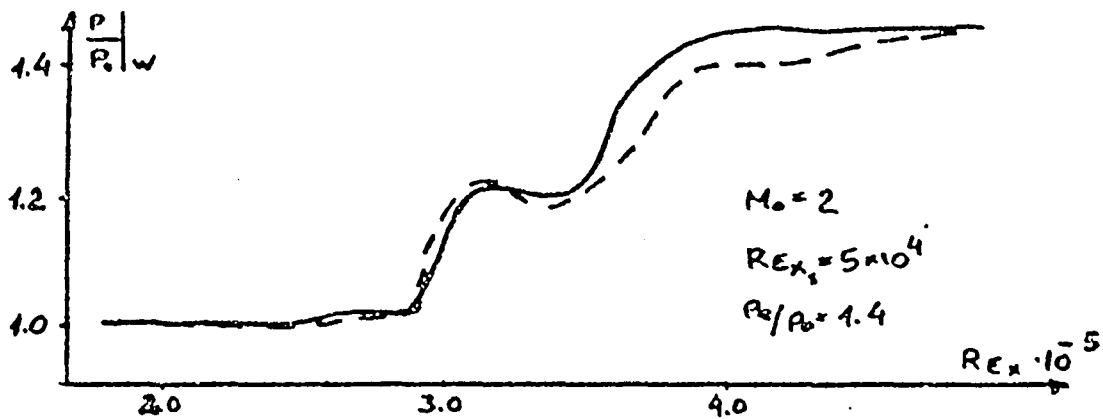
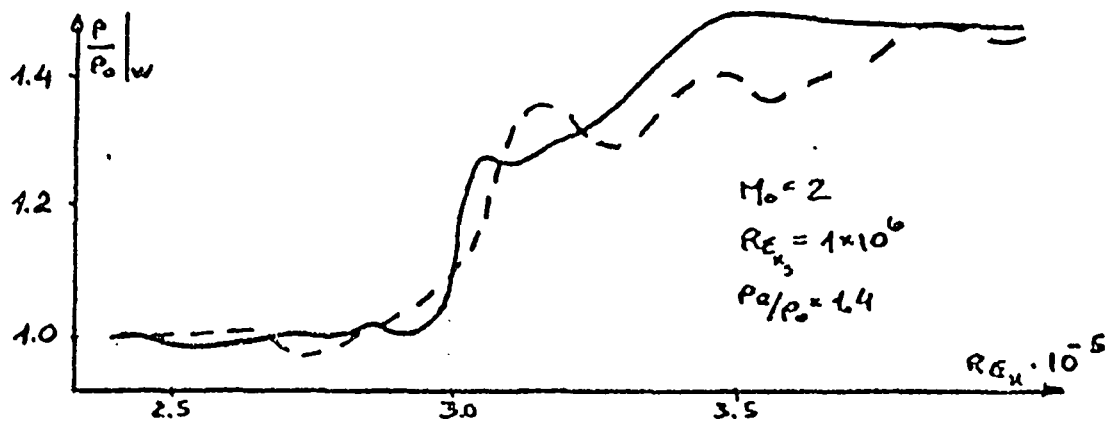


Fig. 8 - Comparison of computation in different grid sizes.

צירוף 8 - השוואת החישוב כרשתות בעלות גודל שונה

$M_0 = 2 \quad Re_{x,5} = 3 \cdot 10^5 \quad \rho_0 / \rho_w = 1.4$

- Grid of 76x25 (Run 001)
- - - Grid of 147x48 (Run 041)
- o o o Hakkinen (Experimental)

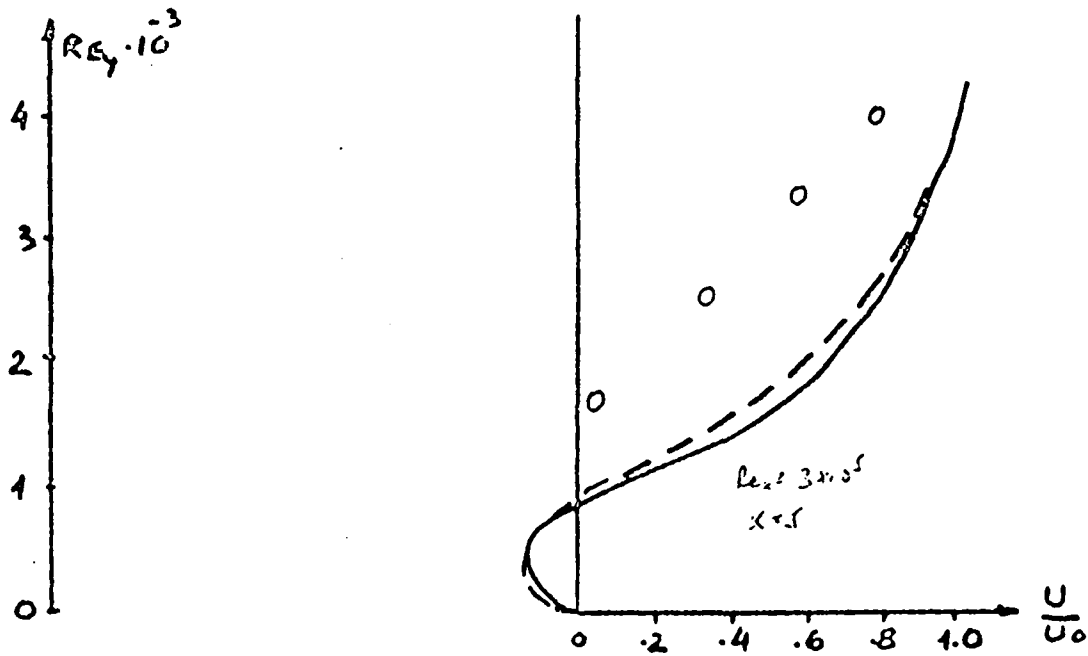
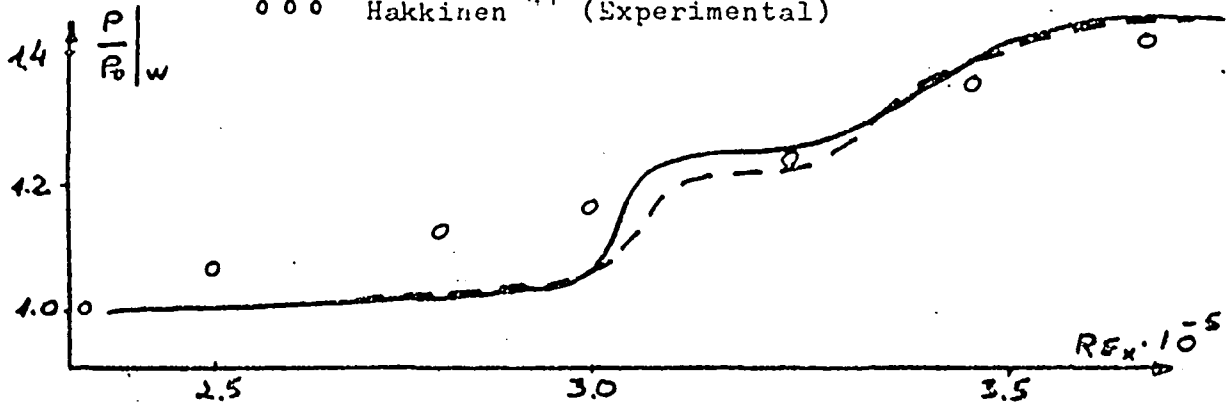


Fig. 9 - Comparison of computation
in different Difference Schemes

ציור 9 - השוואה החישובית בסכמות
בסכמות הפרשים שונות

$M_0 = 2 \quad Re_{x_1} = 3 \times 10^5 \quad \rho_0 / \rho_w = 1.4$

- Brailovskaya Scheme (Run 001)
- - - - MacCormack Scheme (Run 051)
- o o o Hakkinen ⁴¹ (Experimental)

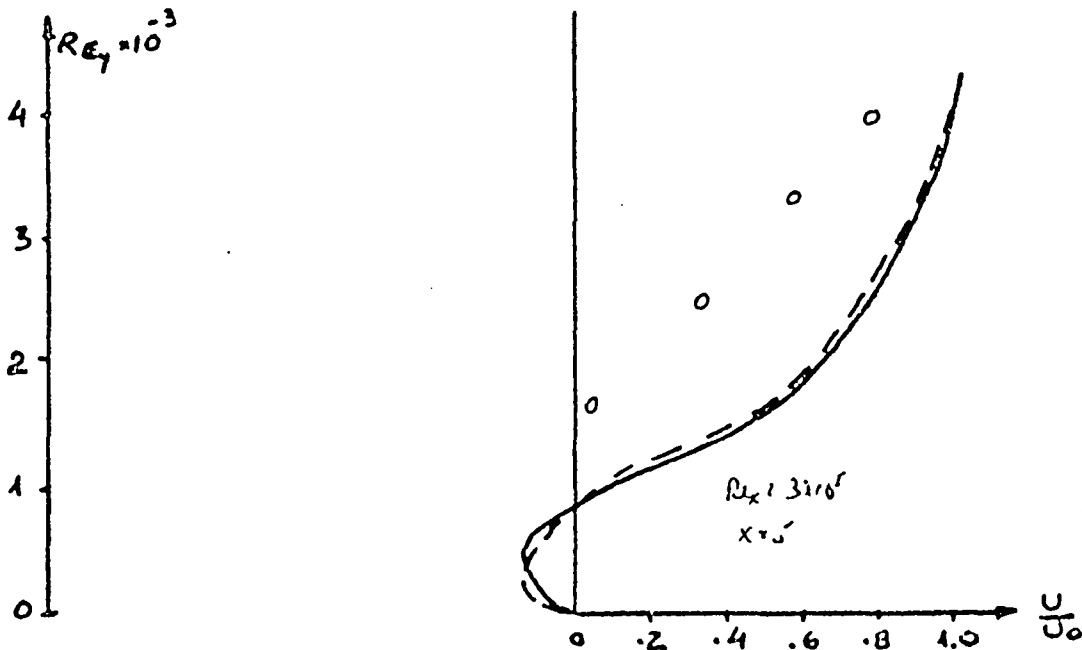
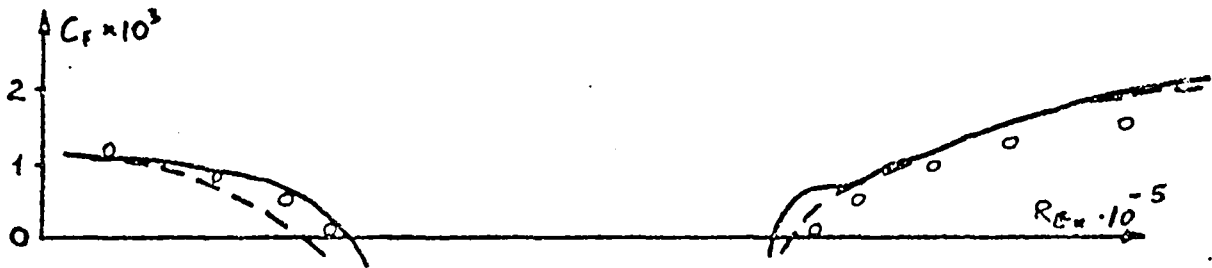
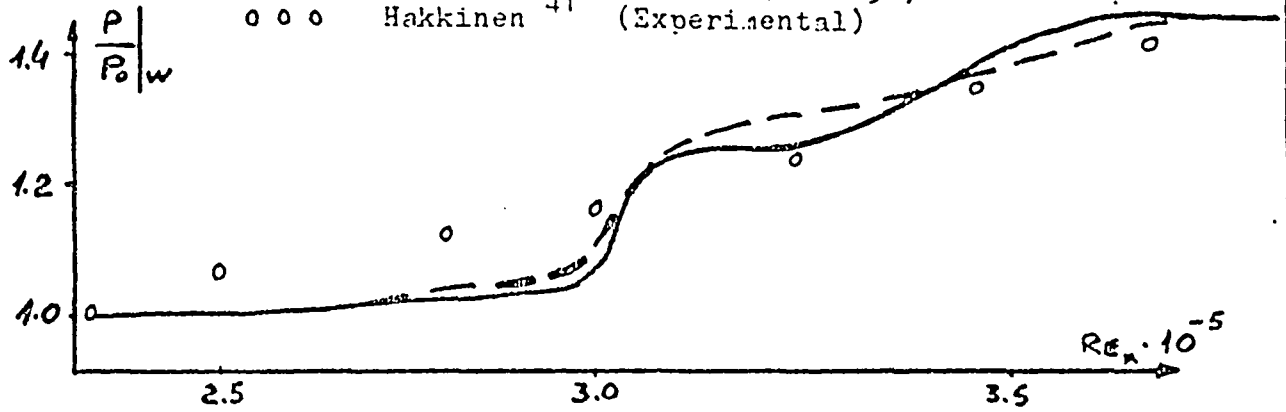


Fig. 10 - Stability coefficients (Run 021) $M_0 = 2$ $Re_x = 3 \times 10^5$ $P_0/P_\infty = 14$

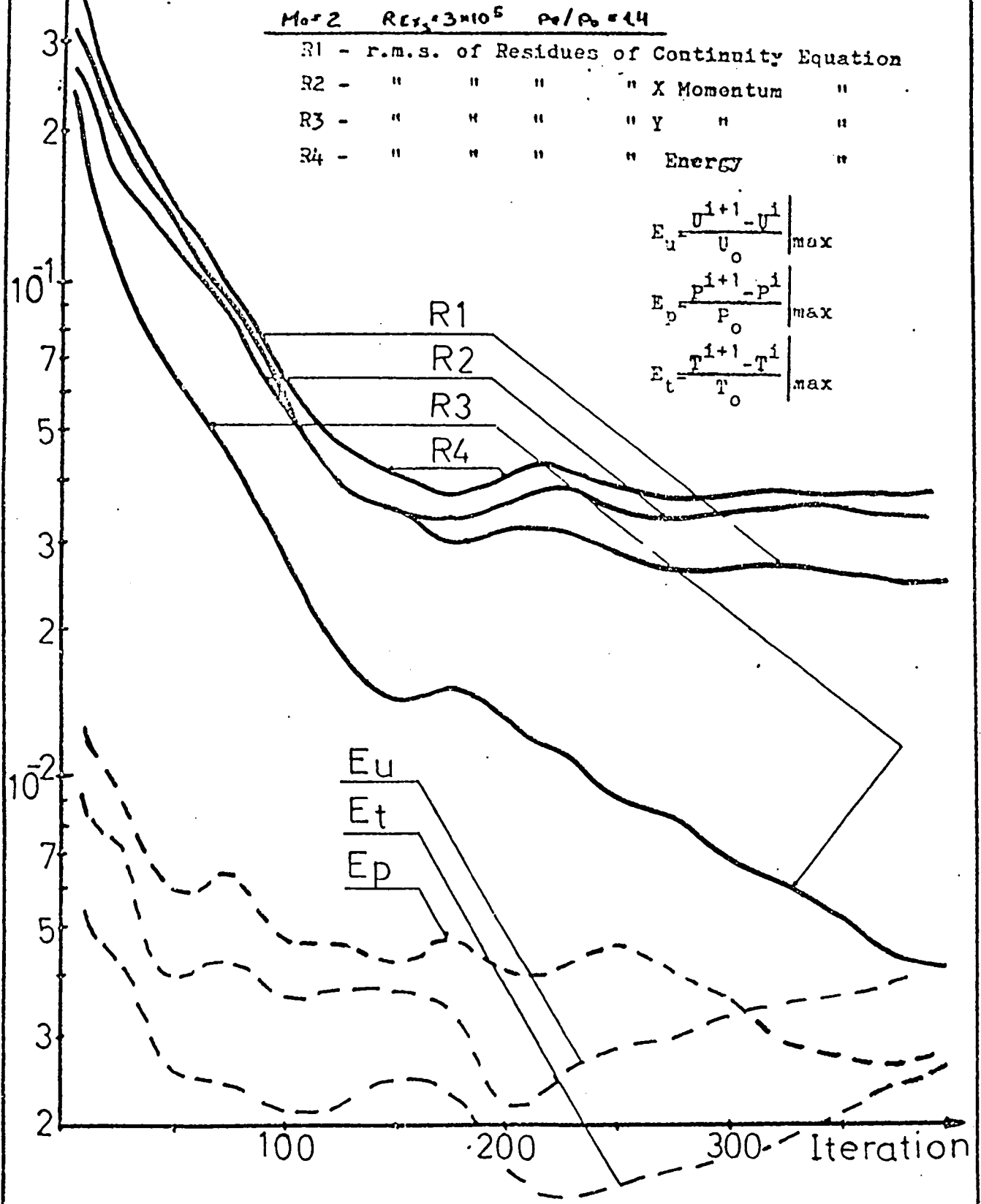
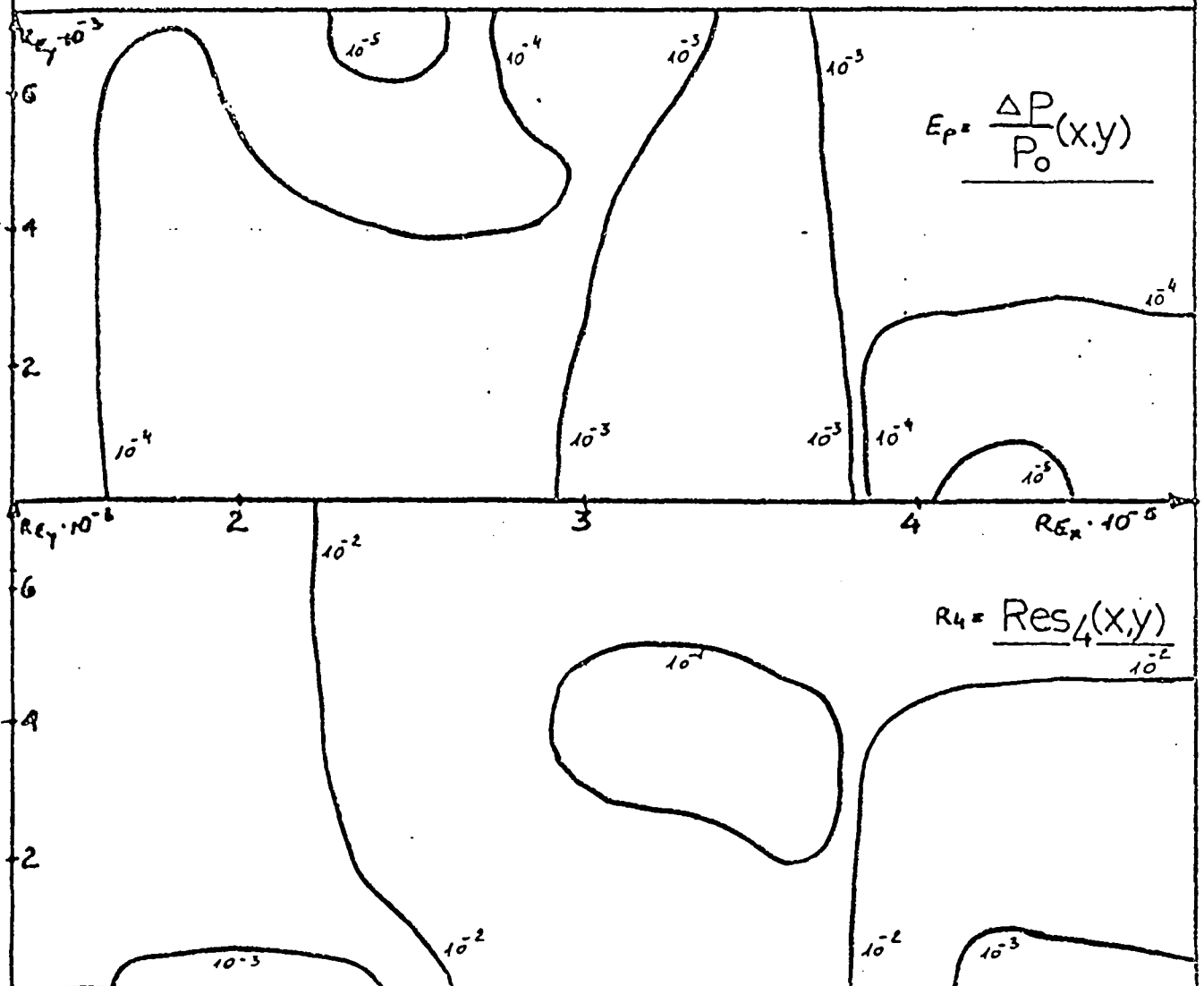


Fig. 11 - Distribution of Stability coefficients R_4 and E_p in the flowfield (Run 021)

ציור 11 - תפוצת מקדמי יציבות R_4 ו- E_p בשדה הזרימה (ריצה 021)



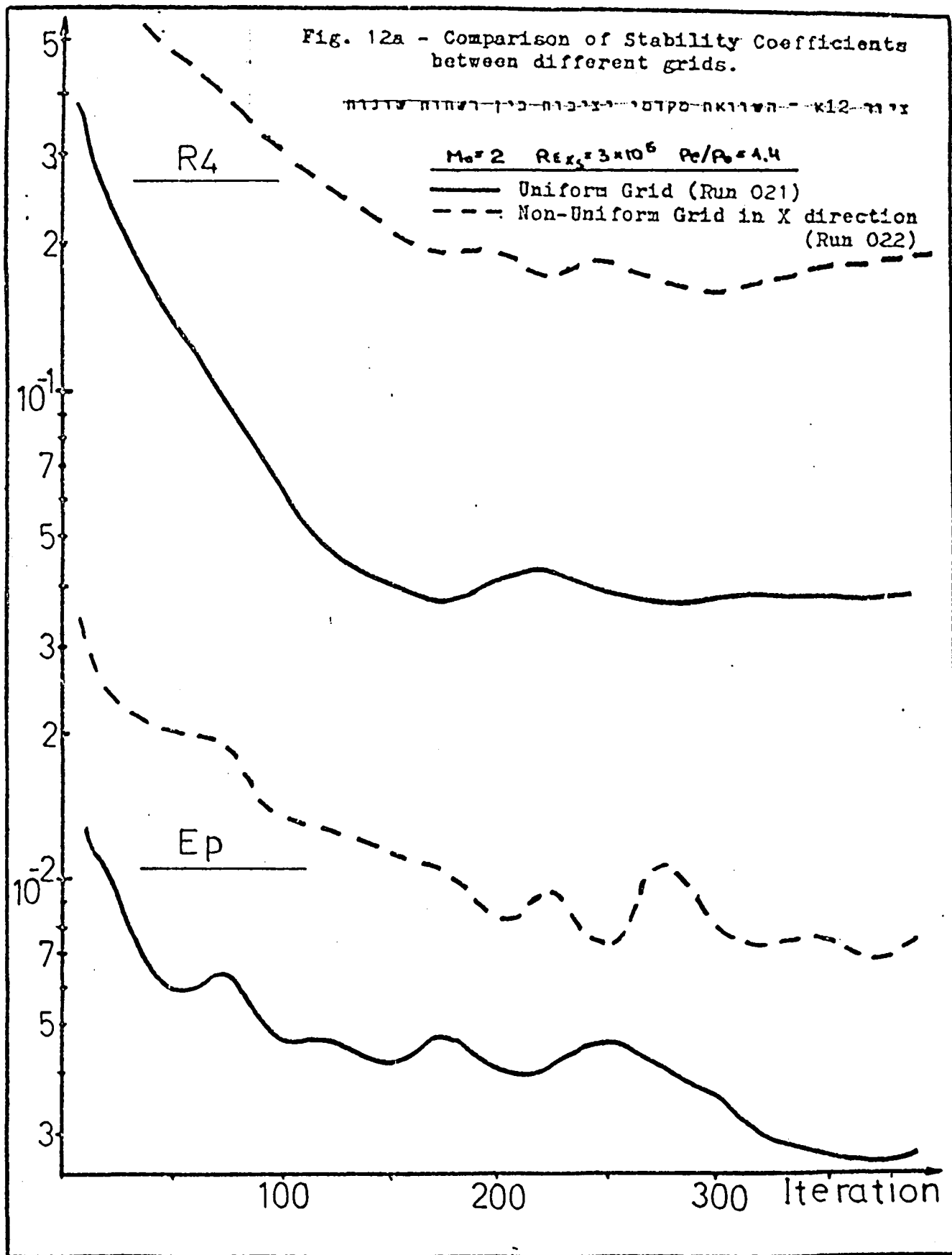


Fig. 13 - Comparison of Stability Coefficients between different Difference Schemes.

ציור 13 - השוואת מקדמי יציבות בין שתי שיטות הפרטים שונות

$M_0=2 \quad Re_{x_1}=3 \cdot 10^5 \quad \rho_0/\rho_\infty=1.4$

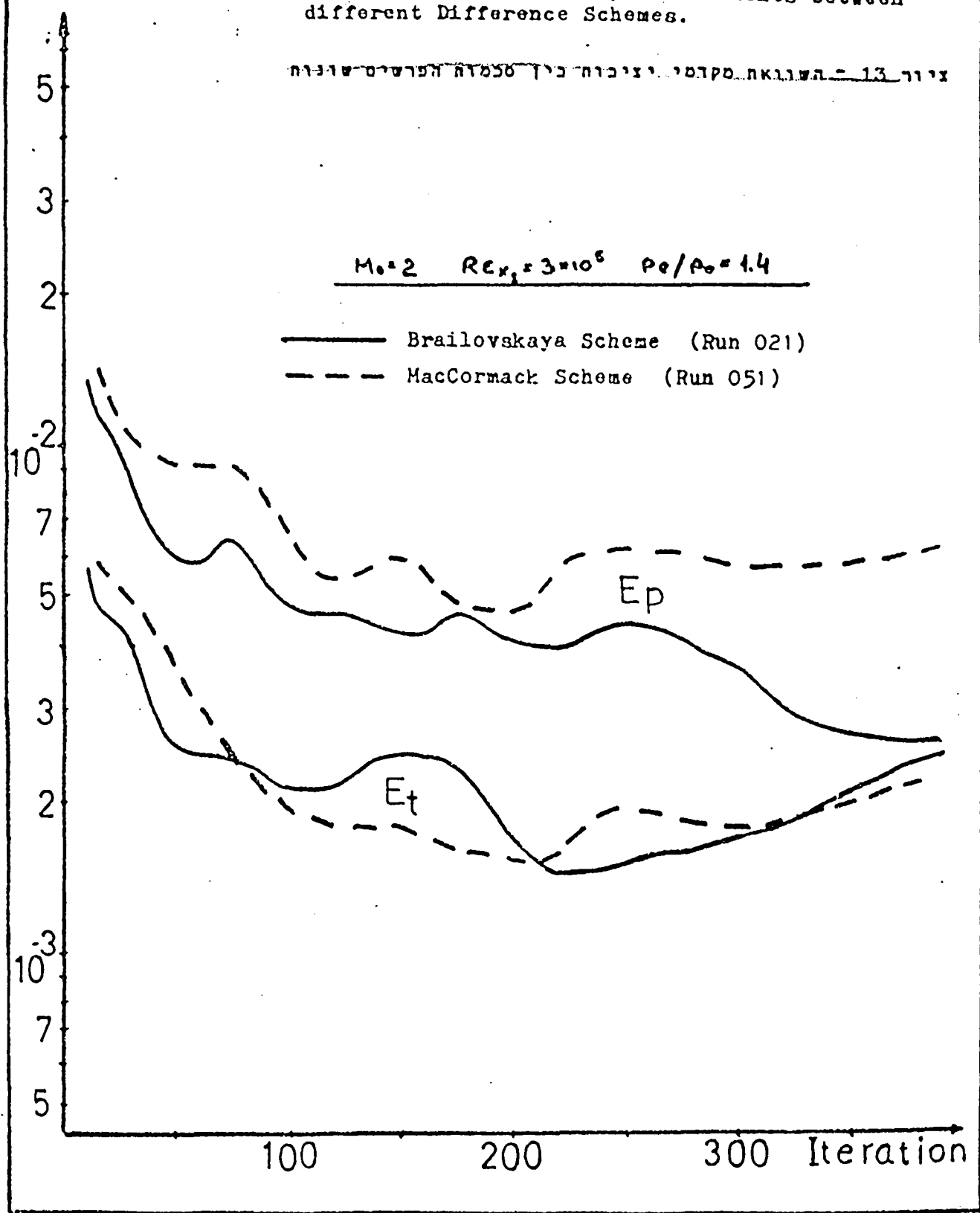


Fig. 15 - Comparison of Run 101 to Experimental and Computational results

ציור 15 - השוואה בין תוצאות ריצת 101 לניסויים וחישובים

$M_0 = 2 \quad Re_x = 3 \times 10^5 \quad \rho_e / \rho_0 = 1.2$

- o o o Hakkinen⁴¹ (Experimental)
- - - MacCormack⁶⁷
- Skoglund, Gay⁹⁴
- Present Study (Run 101)

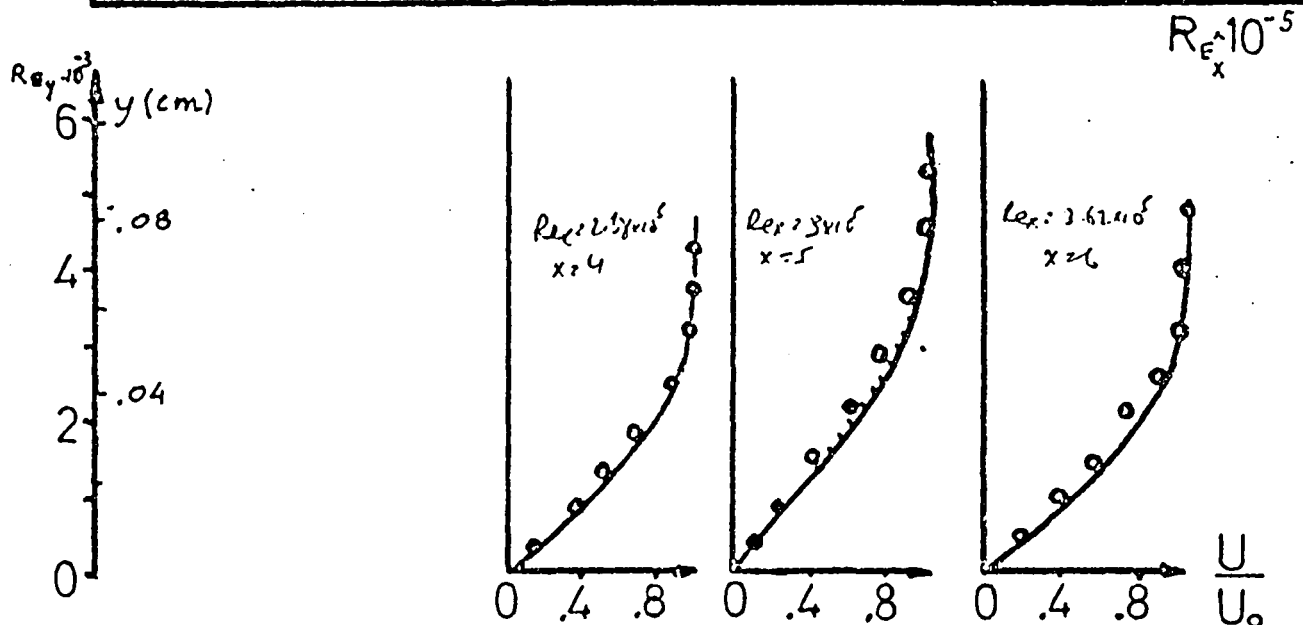
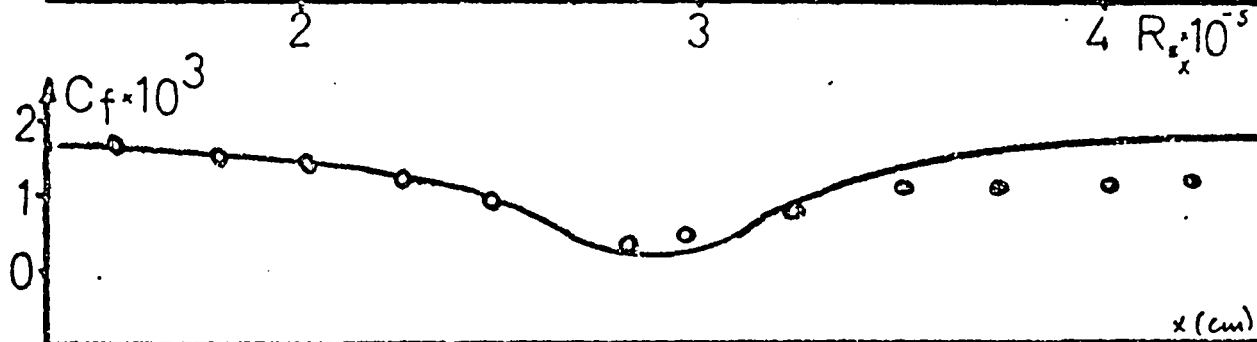
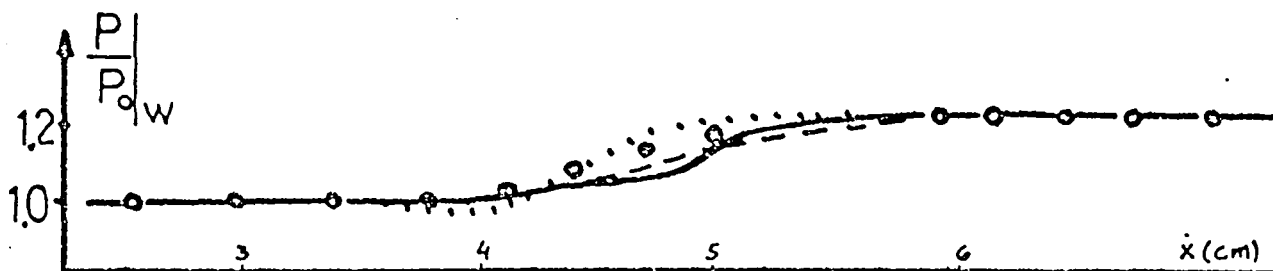


Fig. 16 - Flowfield for Run 101

ציור 16 - תאור דדה הזרימה בריצה 101

$M_0 = 2$ $\rho_0/\rho_\infty = 1.2$ $Re_{x_0} = 3 \times 10^5$

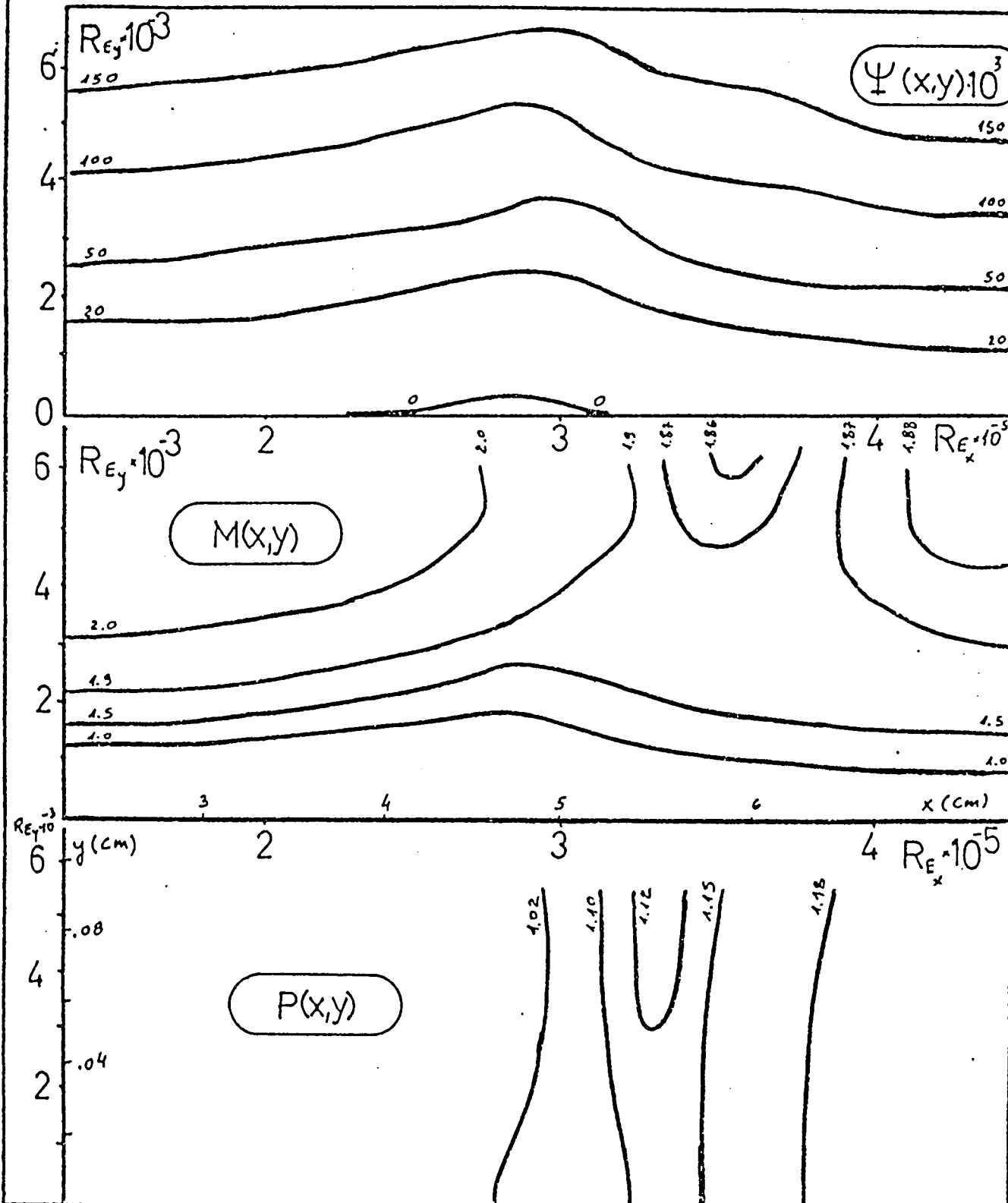


Fig. 17 - Comparison of Run 102 to Experimental and Computational results

ציור 17 - השוואה בין תוצאות 102 לחישובים ניסיוניים וחישוביים

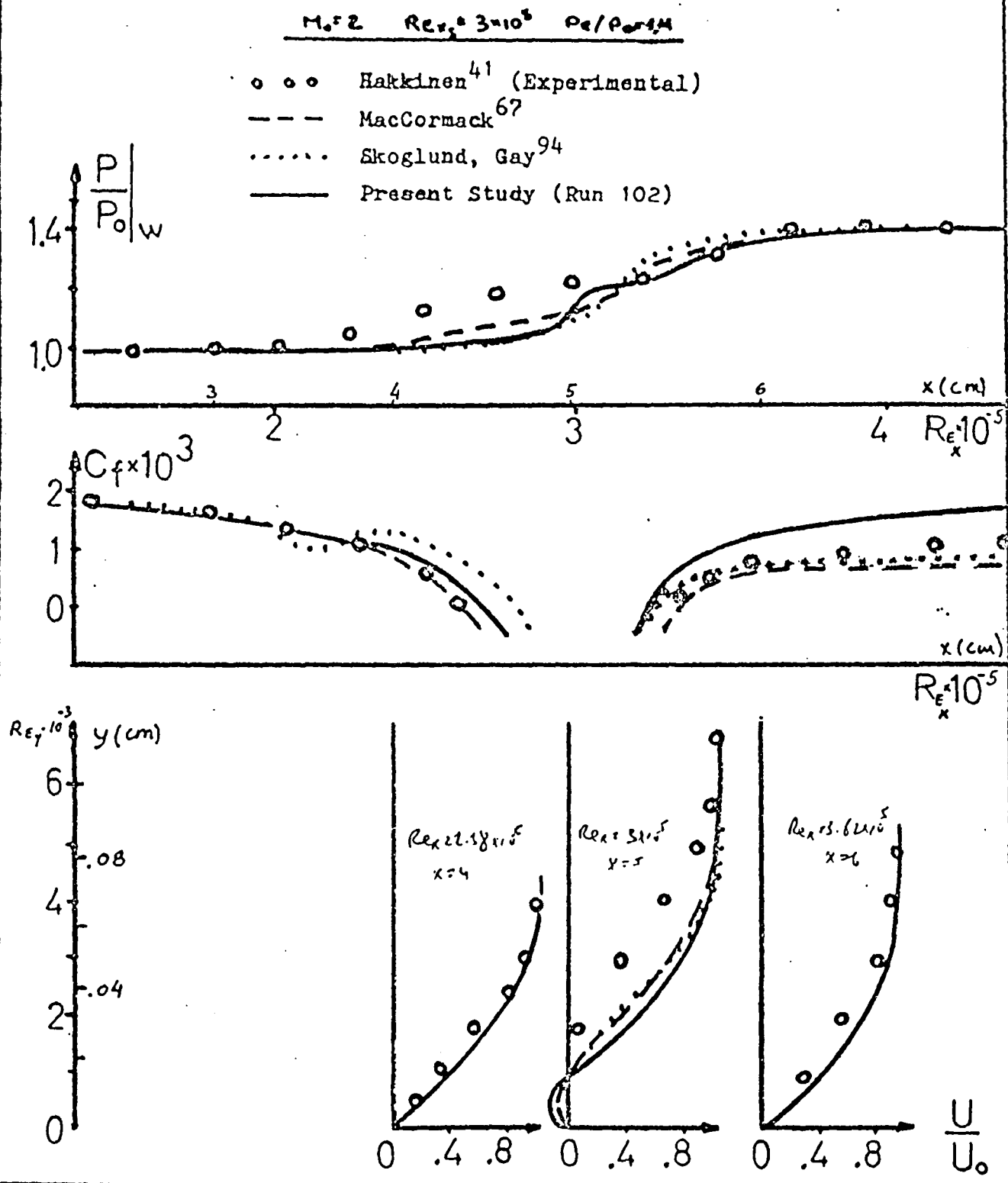


Fig. 18 - Flowfield for Run 102

ציור 18 - תאור שדה הזרימה לריצה 102

$M_0 = 2$ $\rho_0/\rho_\infty = 1.4$ $Re_{x_1} = 3 \times 10^5$

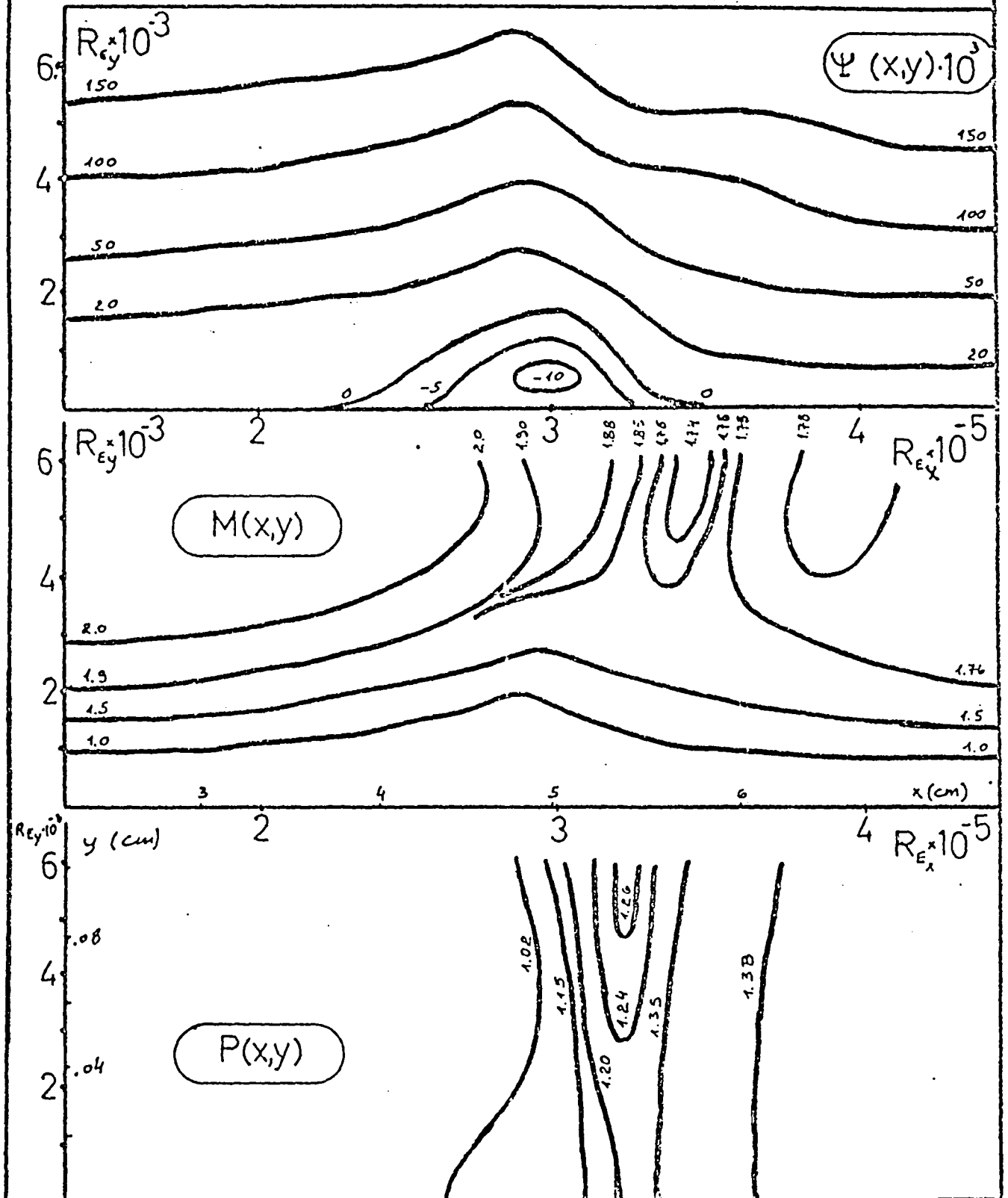


Fig. 19 - Comparison of Run 103 to Experimental results
 ציור 19 - השוואה בין-103 להוצאה ניסיונית והישוכיה

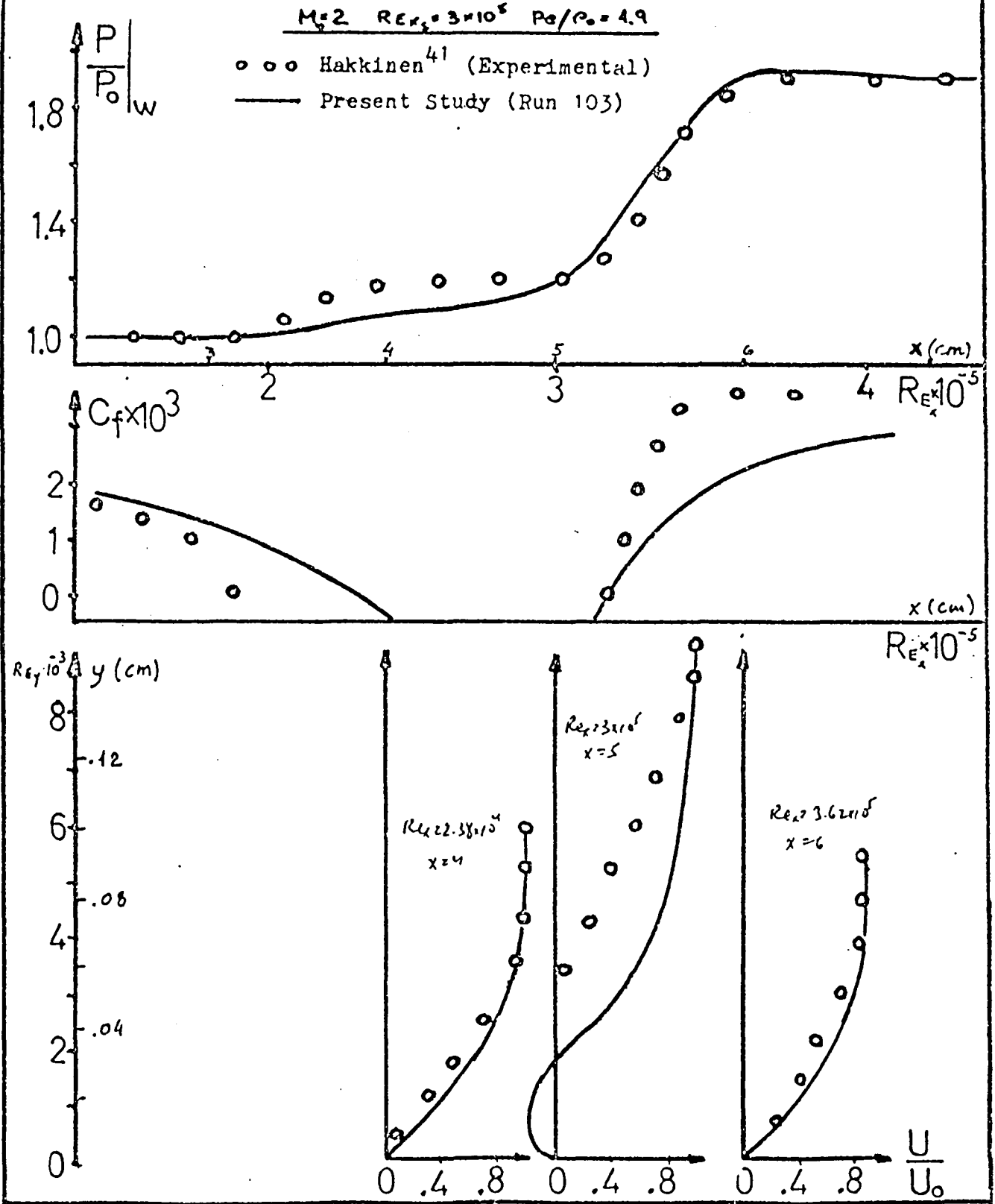
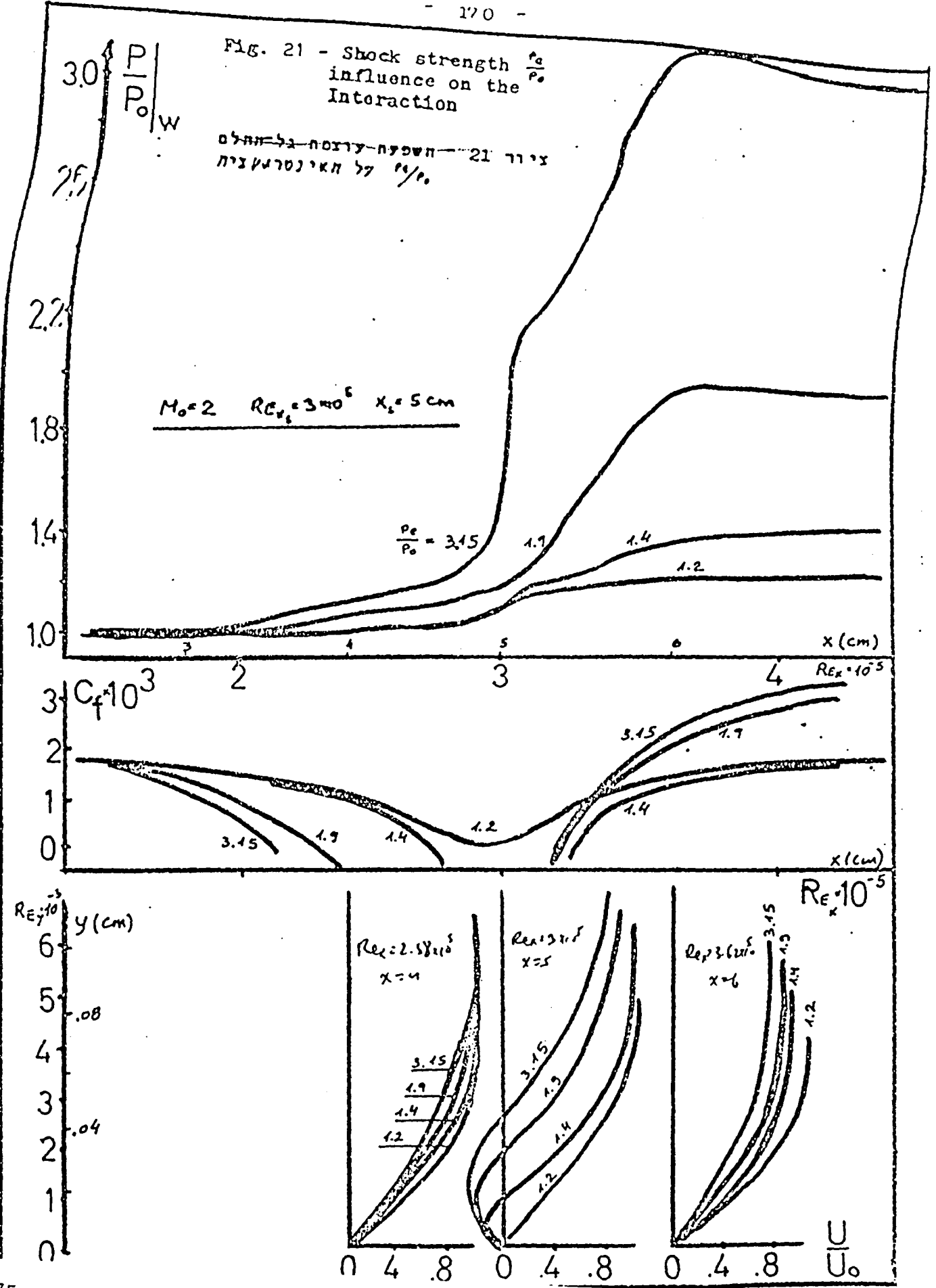
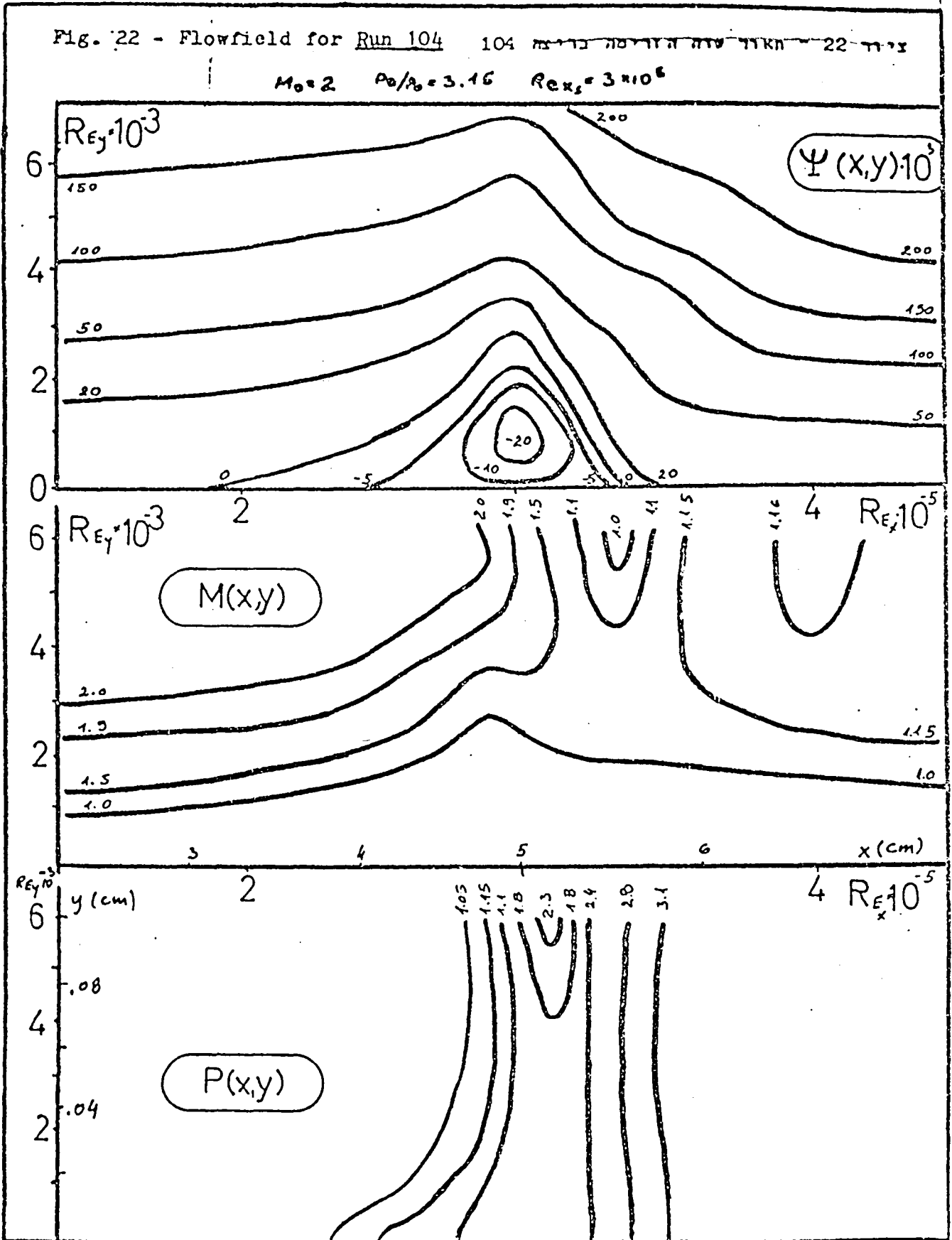
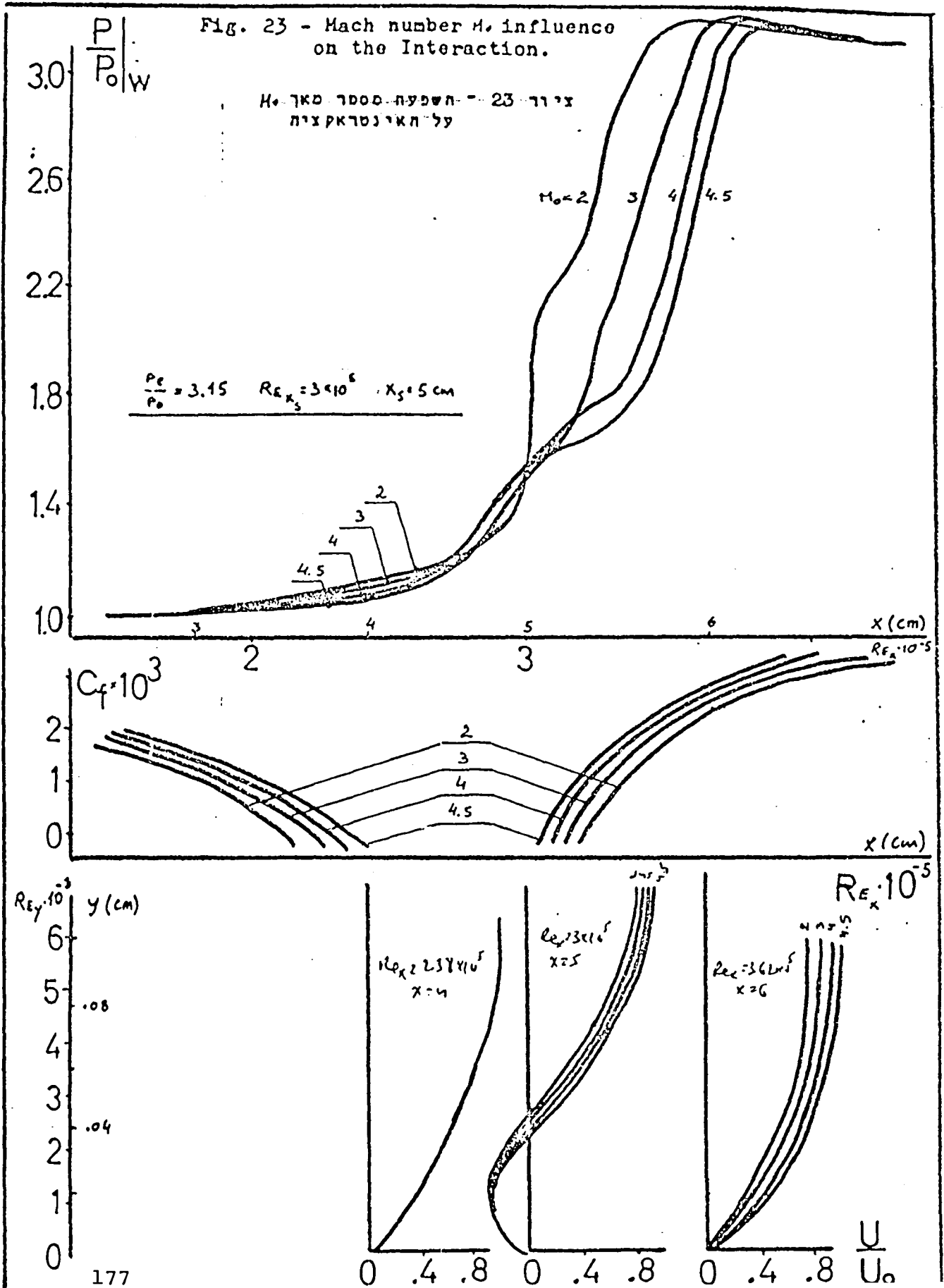


Fig. 21 - Shock strength $\frac{p_2}{p_0}$ influence on the interaction

ציור 21 - השפעת עוצמת גלי הלם על האינטראקציה $\frac{p_2}{p_0}$







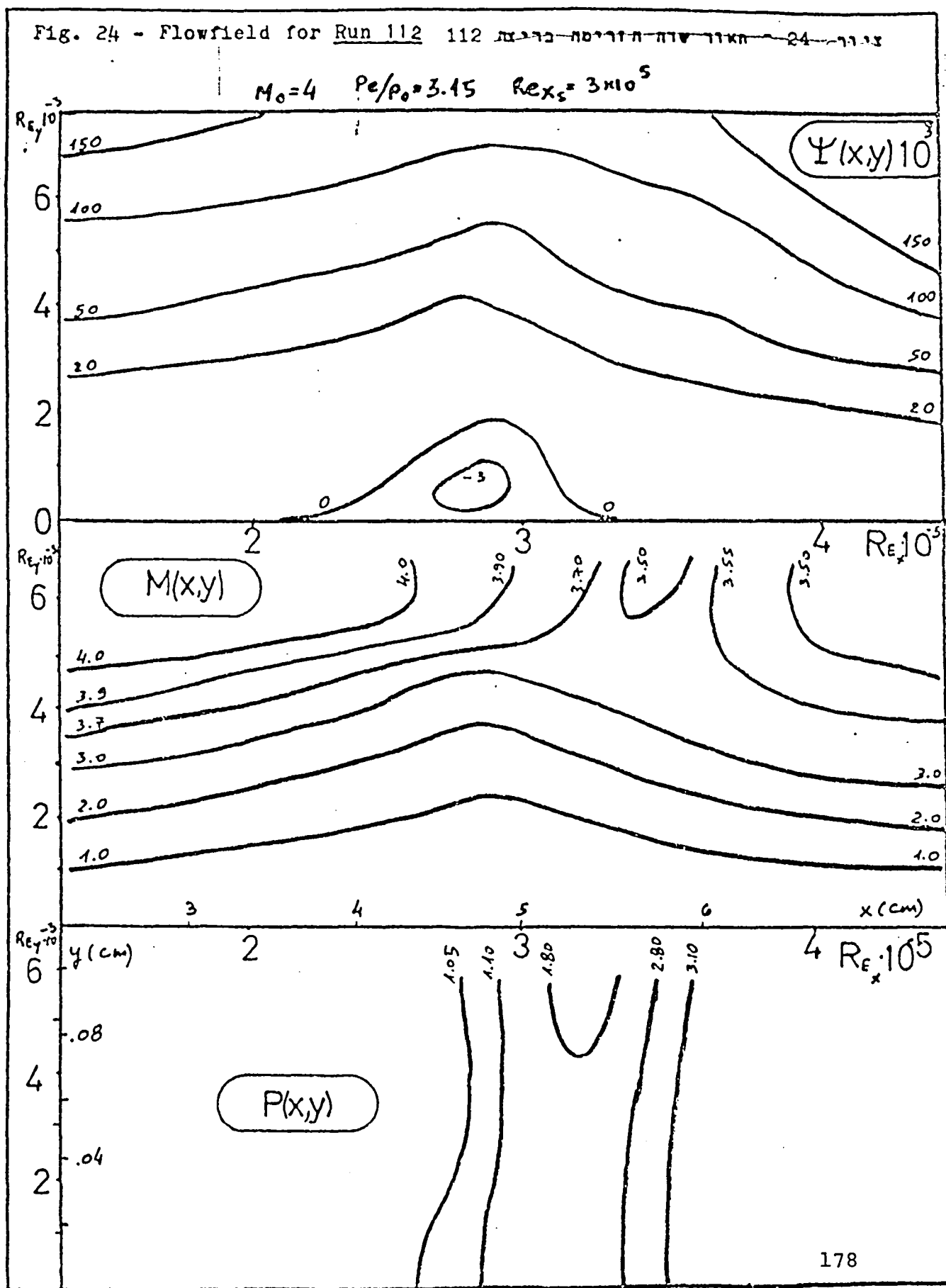


Fig. 25 - Reynolds number Re_{x_3} influence on the Interaction.

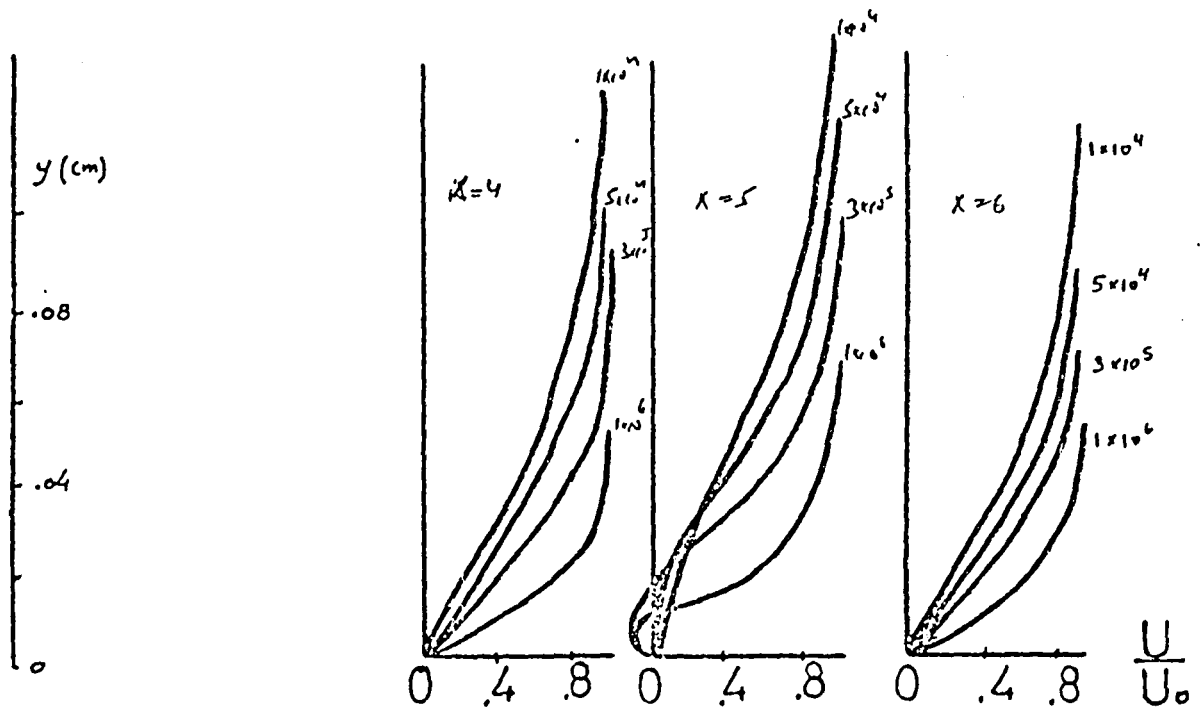
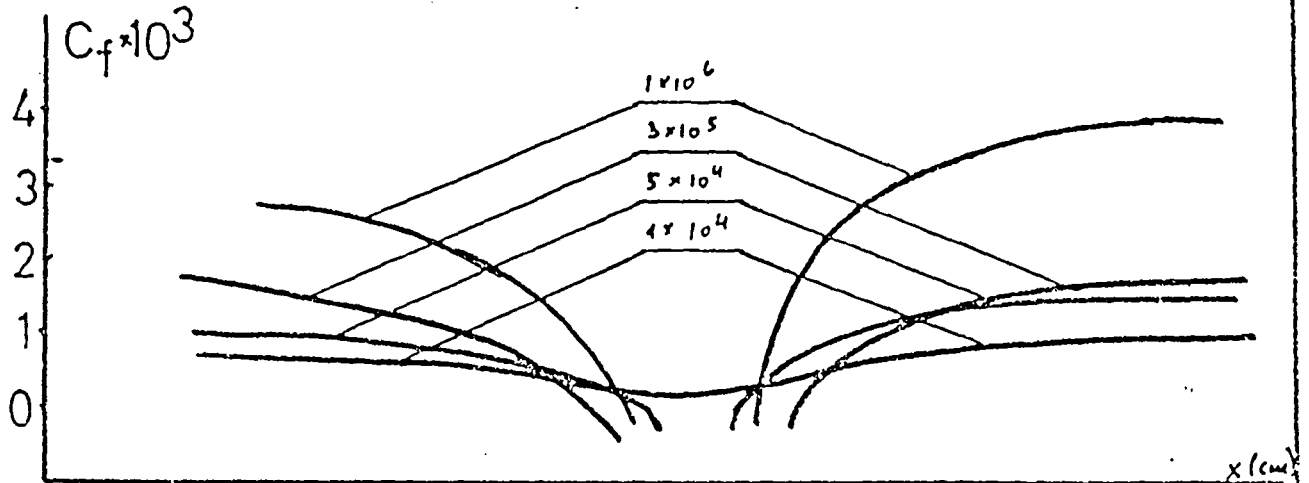
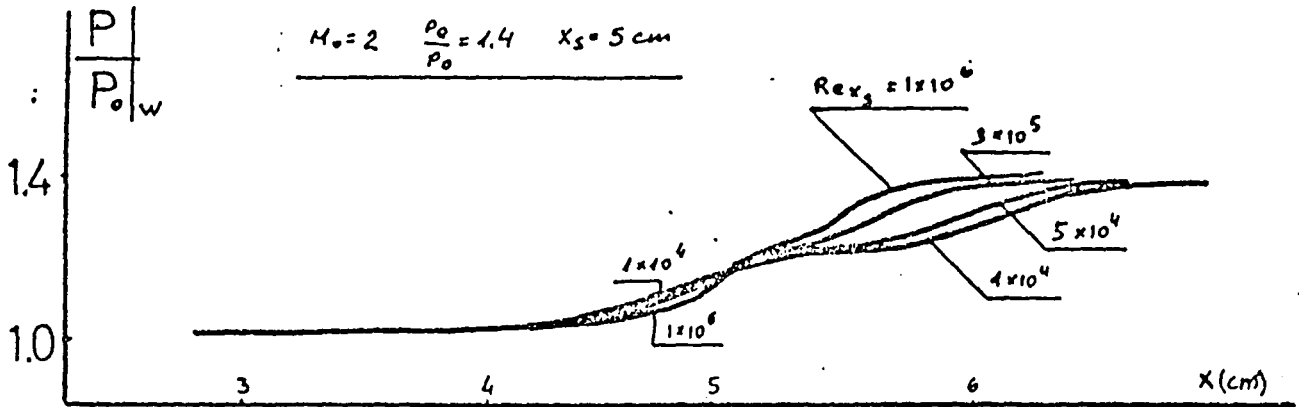


Fig. 26 - Flowfield for Run 121 26 ציור האור שדה הזרימה כנגד 121

$M_0 = 2$ $\rho_e/\rho_0 = 4.4$ $Re_{x_2} = 1 \times 10^4$

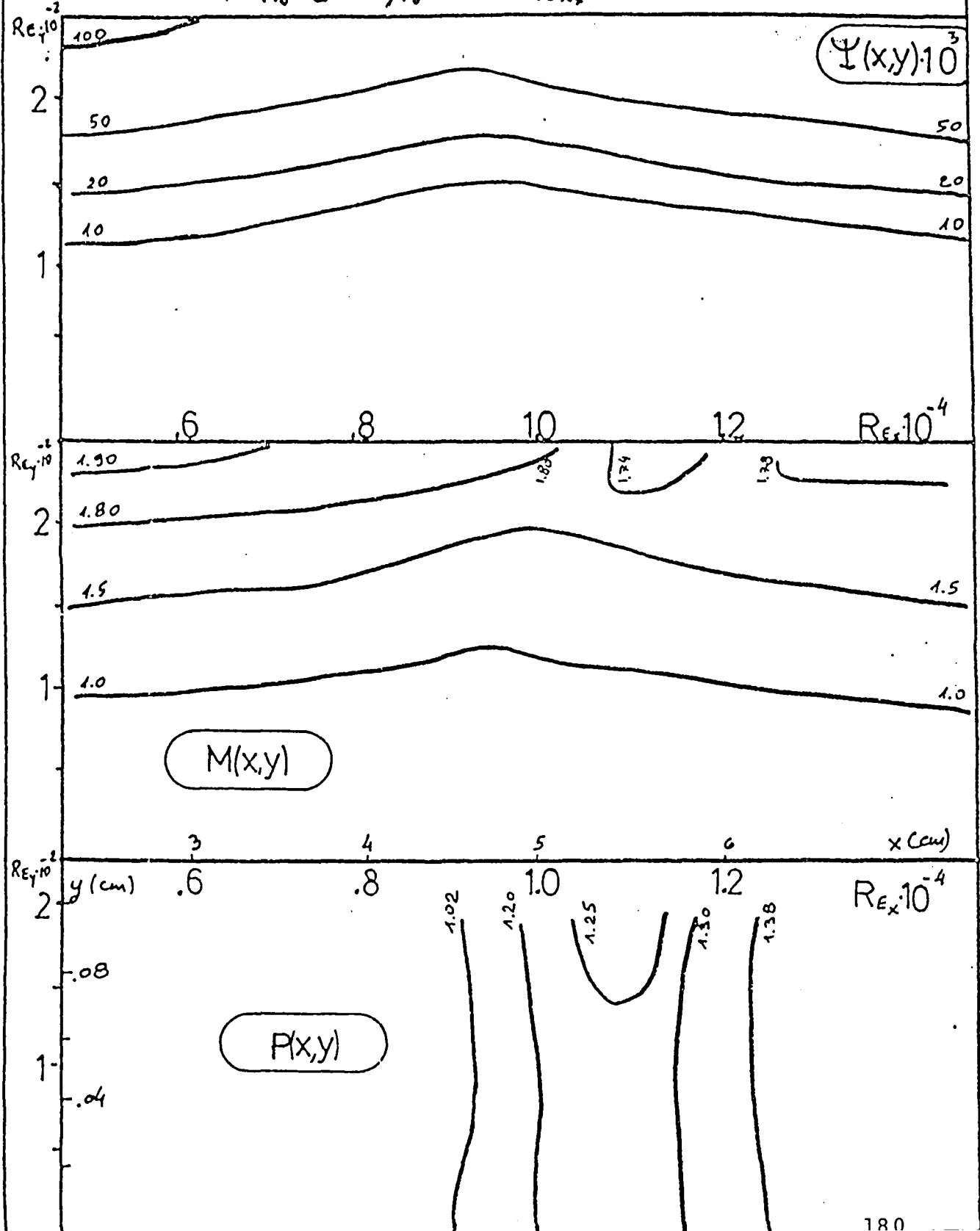


Fig. 27 - Shock impingement location x_s influence on the Interaction.

ציור 27 - השפעת מקום המפגש של המעטפת על תהליך האינטראקציה

$$M_0 = 2 \quad \frac{P_0}{P_\infty} = 1.4 \quad \frac{Re}{x_s} = \frac{3 \times 10^5}{0.05}$$

$$Re_{x_s=3} = 1.8 \times 10^5$$

$$Re_{x_s=5} = 3.0 \times 10^5$$

$$Re_{x_s=7} = 4.8 \times 10^5$$

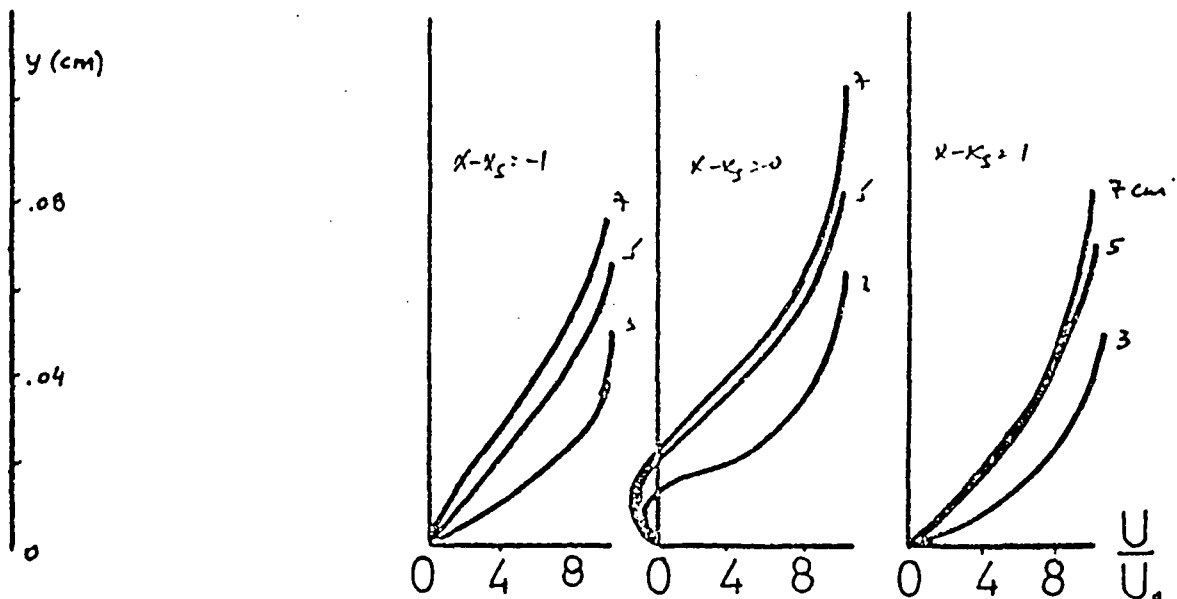
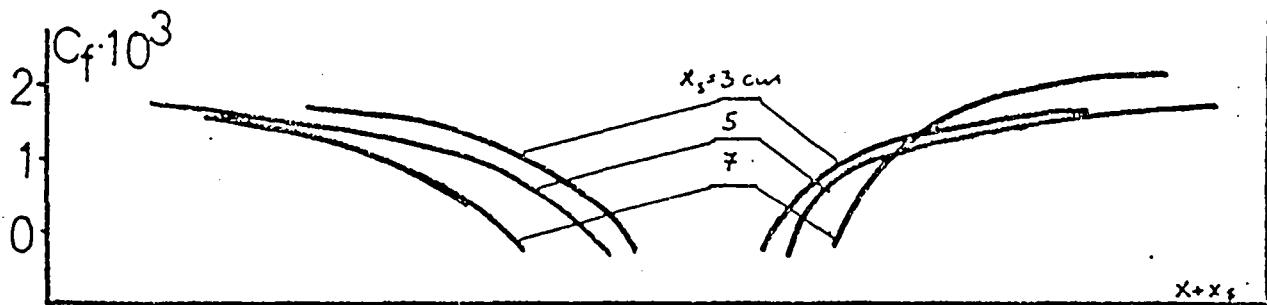
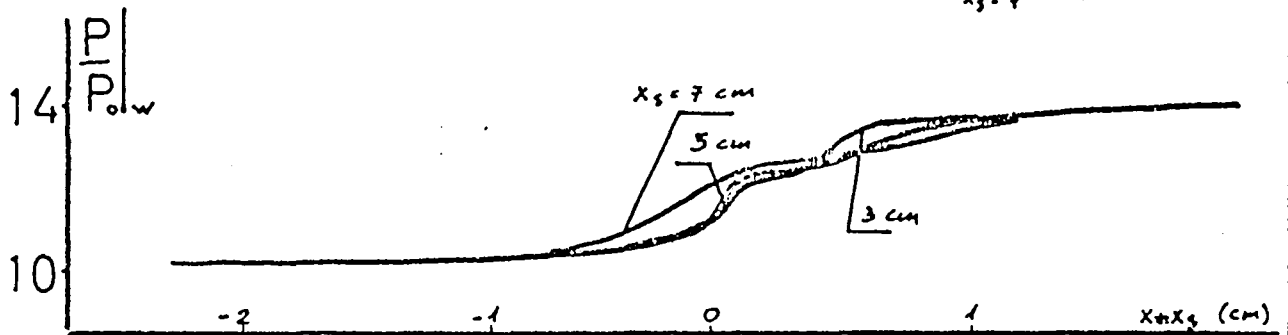


Fig. 28 - Prandtl number ϵ influence on the Interaction.

~~407370-1000 חשמה 28-11-52~~
~~... חשמה 28-11-52~~

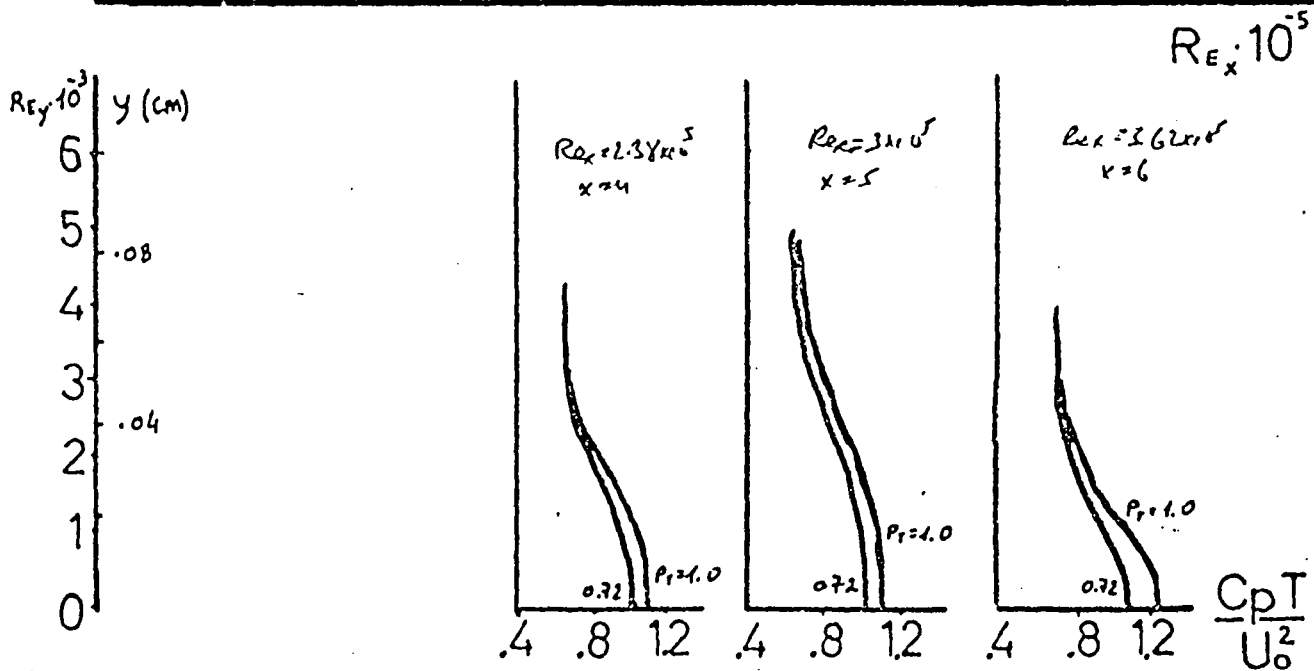
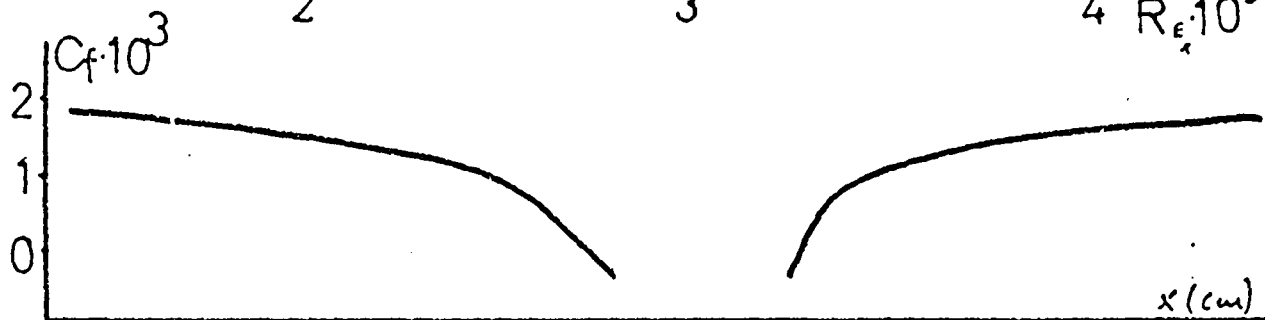
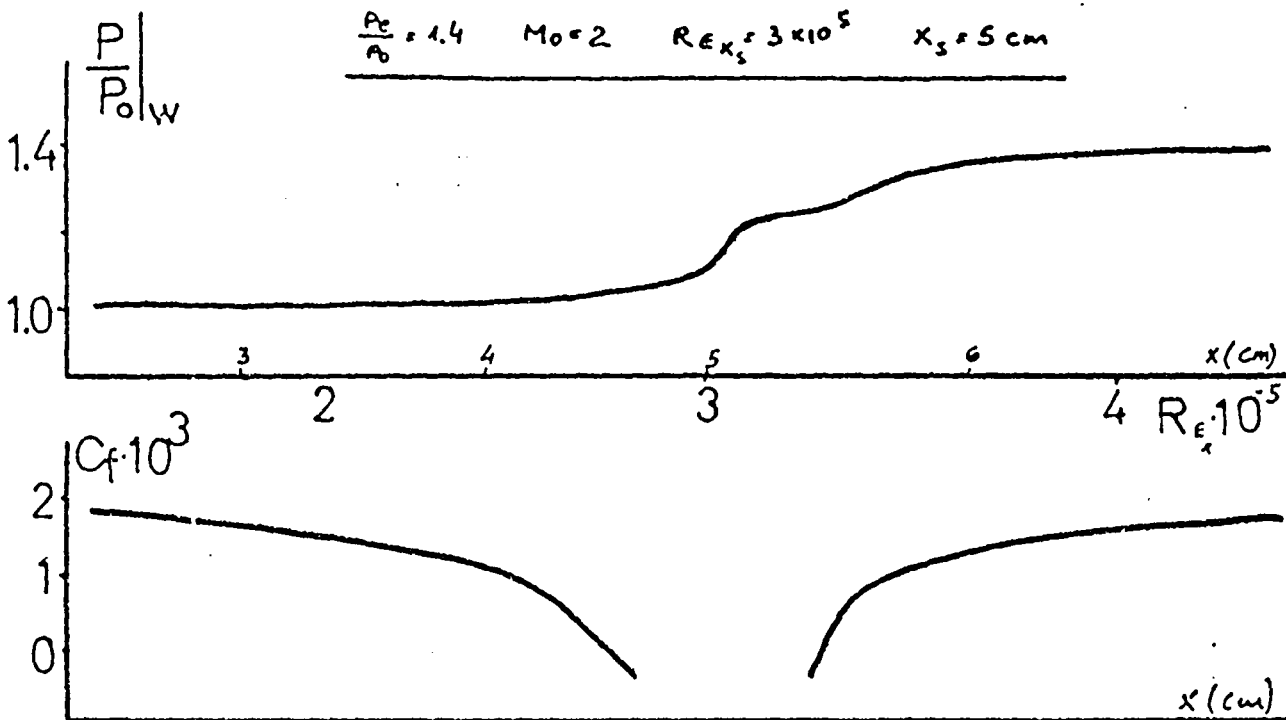


Fig. 29 - Influence of variation of P_0/P_∞ , M_0 , Re_{x_s} on the Boundary Layer shape.

ציור 29 - השפעת שינוי תנאי הזרימה P_0/P_∞ , M_0 , Re_{x_s} על צורת שכבת הגבול.

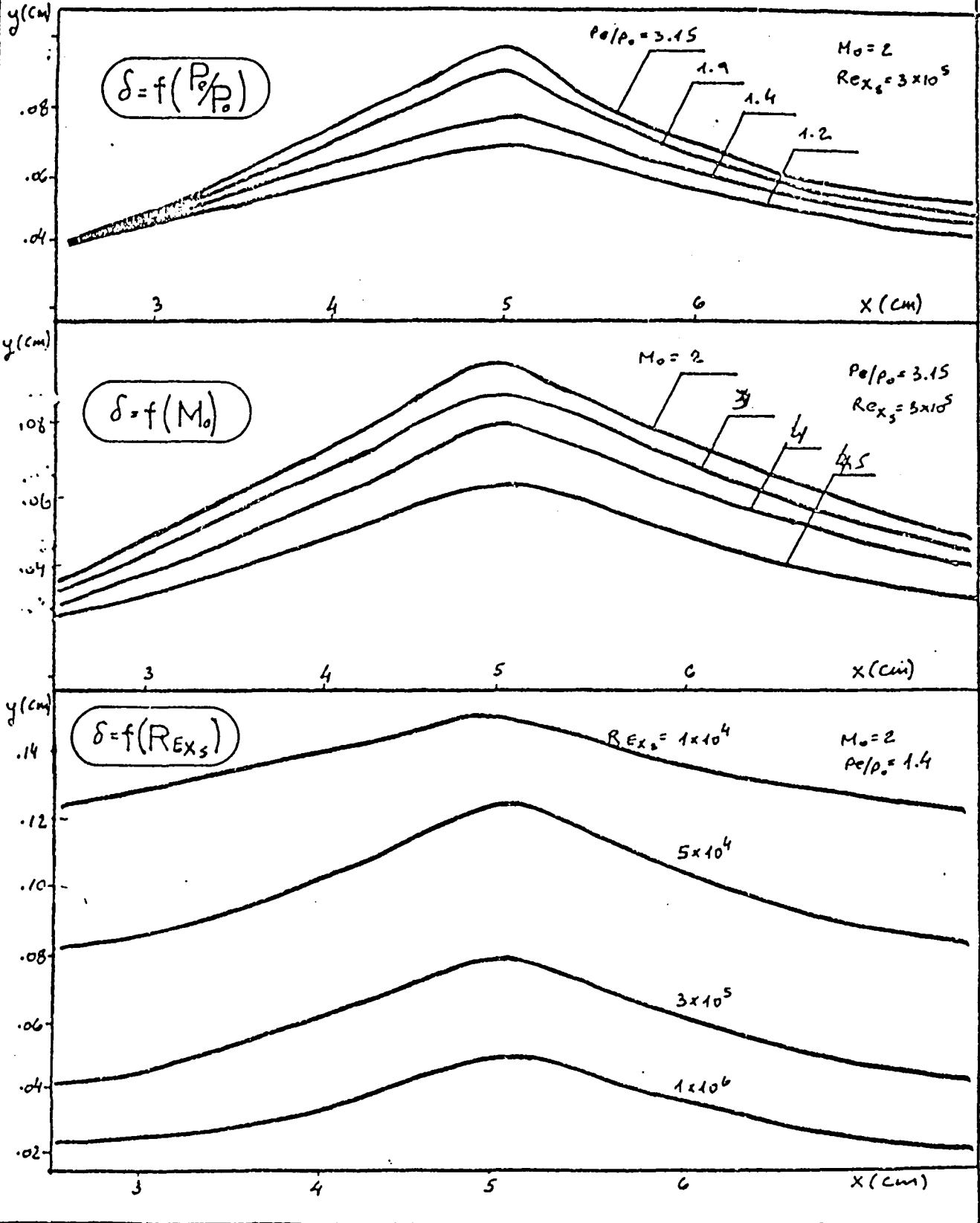


Fig. 30 - Wall Temperature T_w influence on the Interaction.

צינור 30 - השפעת חום-אי-קבוע
הלוח לסמך קבועה T_w
על האינטראקציה

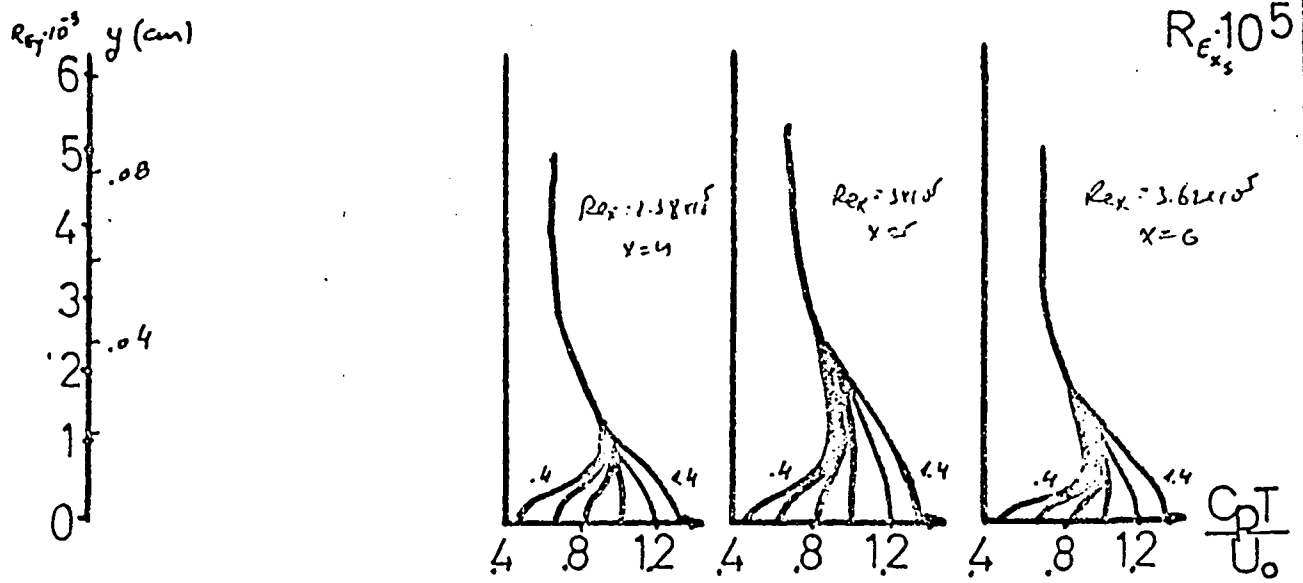
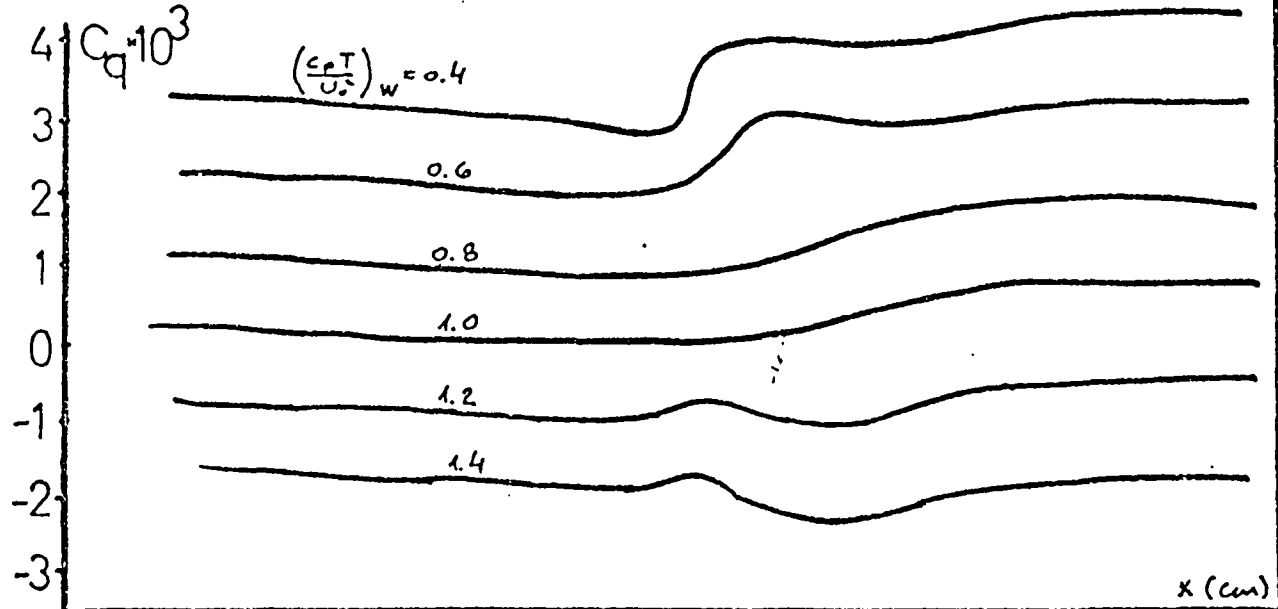
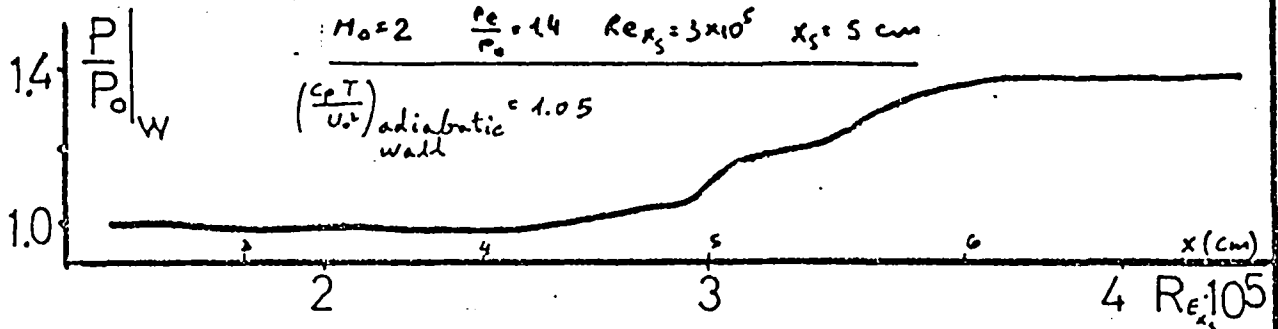


Fig. 31 - Wall Suction/Injection velocity v_w influence on the Interaction.

צירוף 31 - השפעת הניקח או הזדקק ניצבחה במהירות v_w לאורך תלות על האינטראקציה

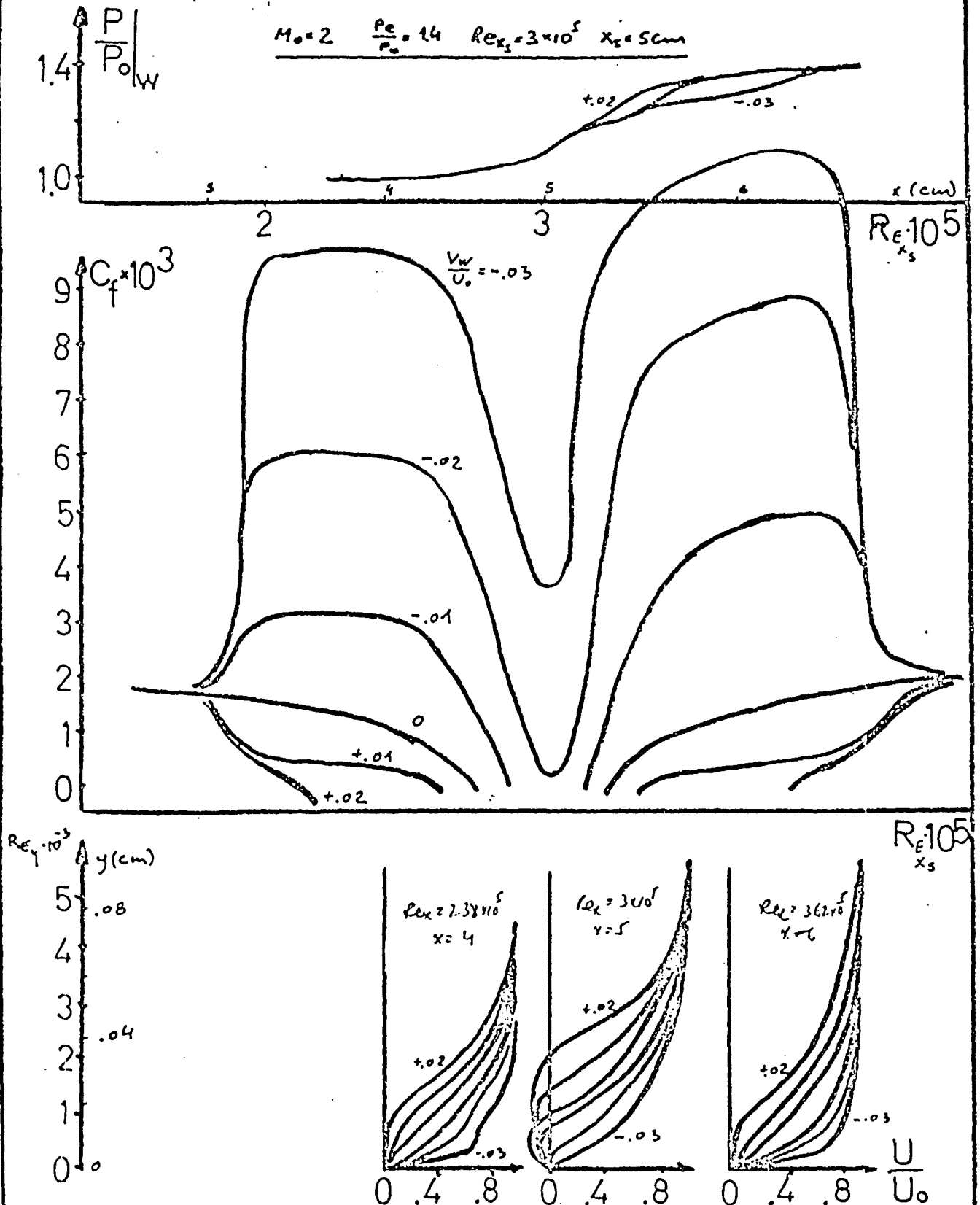


Fig. 32 - Flowfield for Run 212 212 תיבת הניסוי - תוצאות 32-111

$M_0 = 2$ $\rho_0/\rho_\infty = 1.4$ $Re_{x_0} = 3 \times 10^5$ $V_w = -0.02$ (Suction)

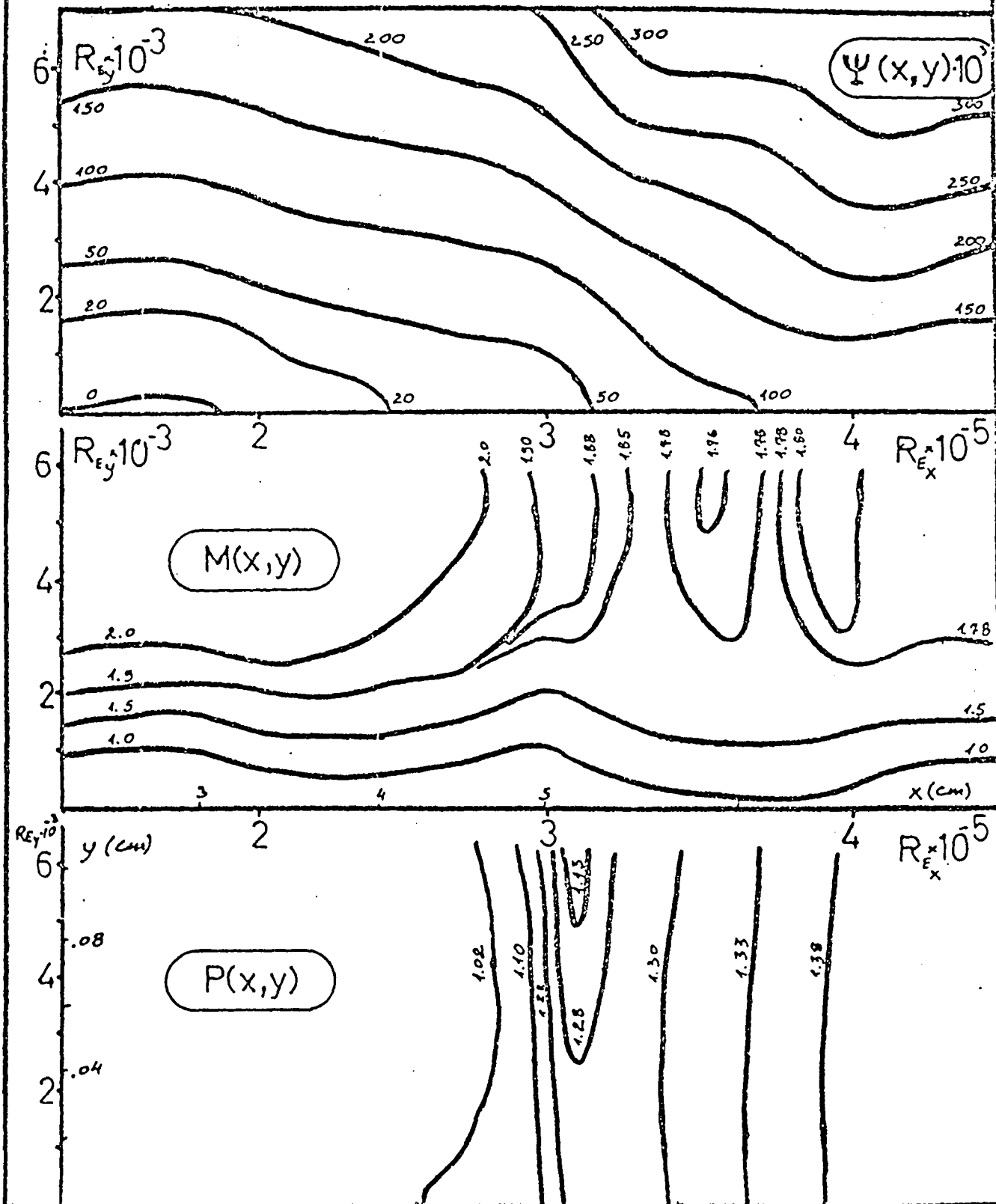
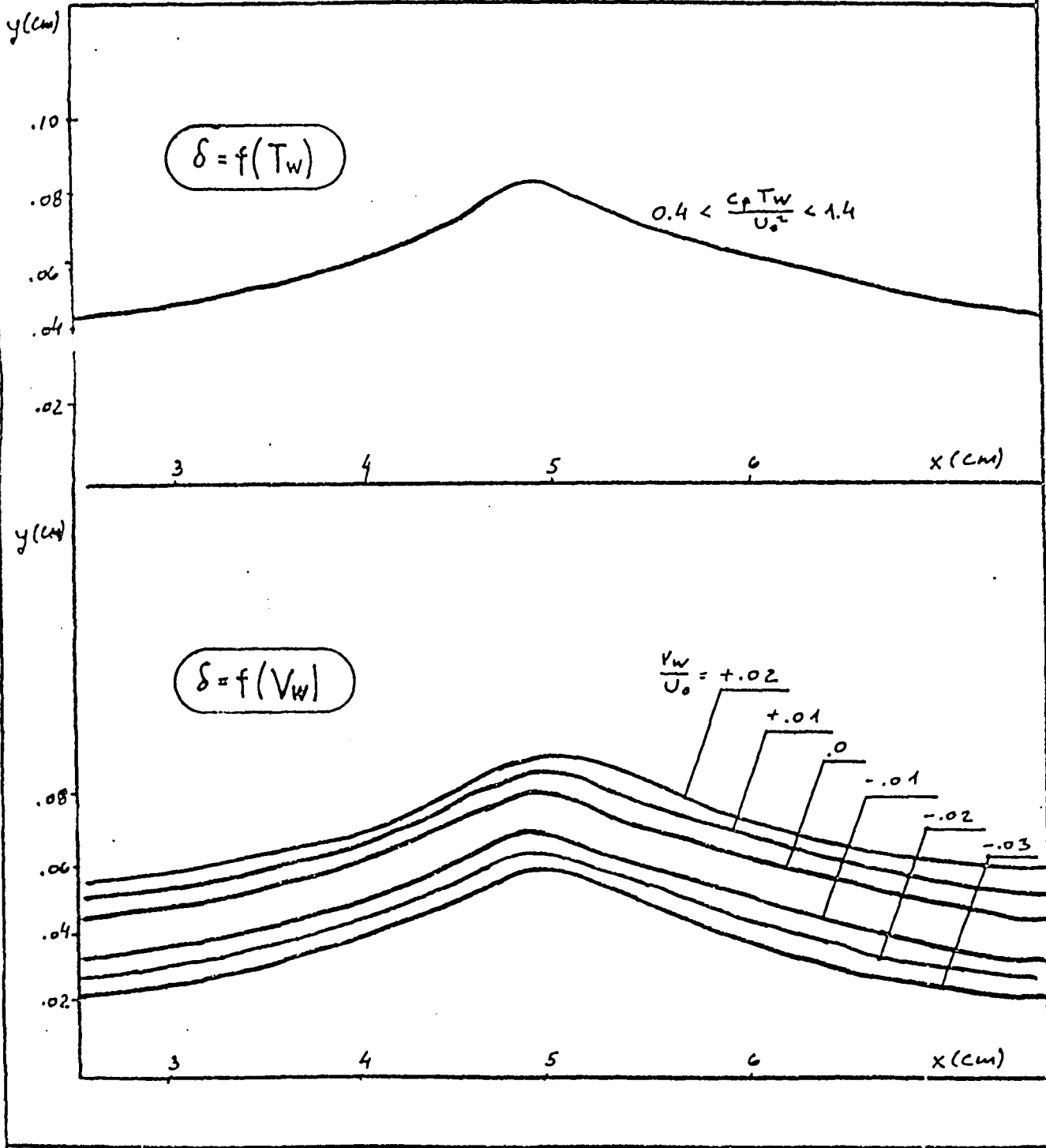


Fig. 33 - Influence of variation of $c_p T_w / U_0^2$; v_w / U_0 on the Boundary Layer shape.

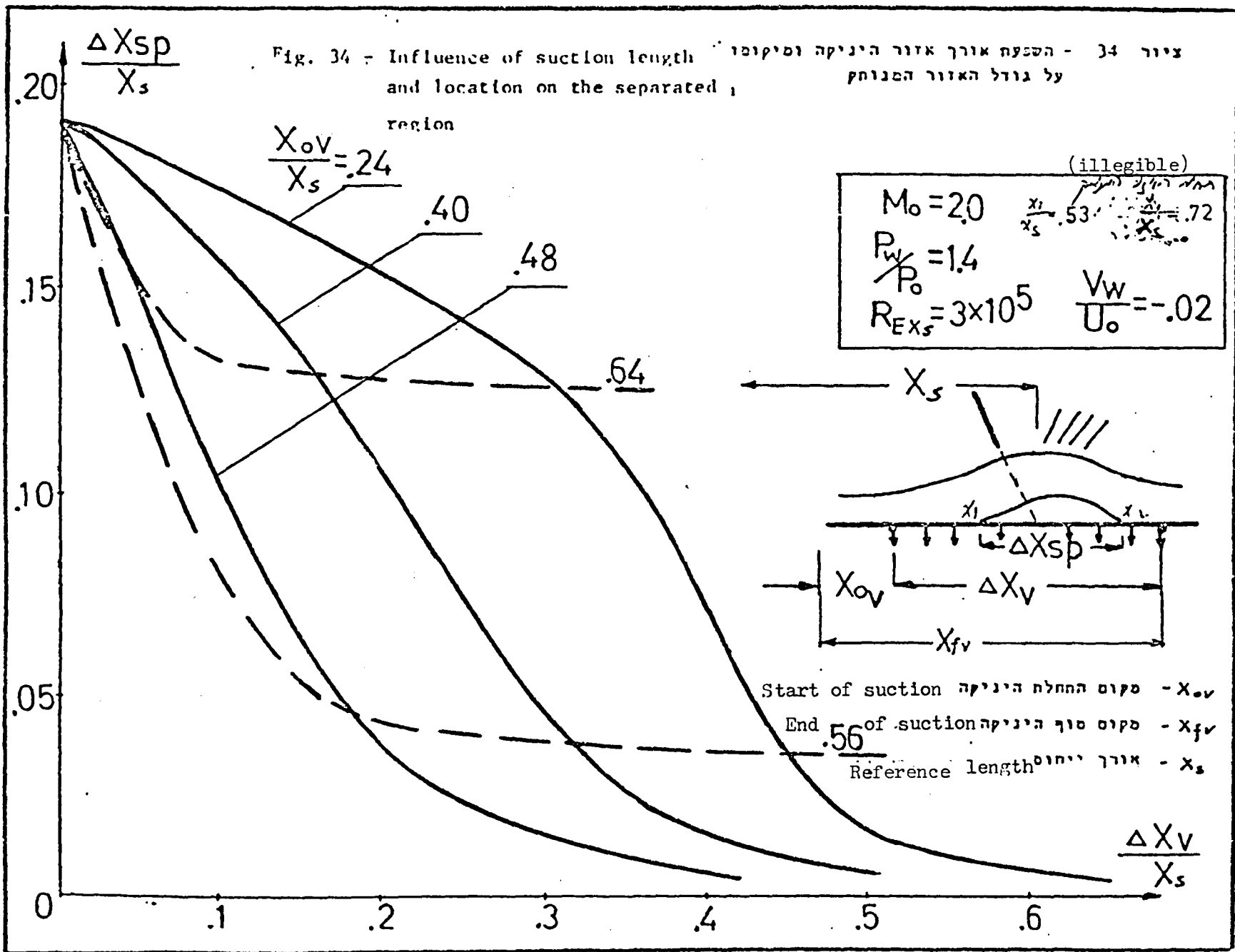
ציור 33 - השפעה של $c_p T_w / U_0^2$; v_w / U_0 על צורת שכבת הגבול.

$M_0 = 2$ $\rho_0 / \rho_w = 1.4$ $Re_{x_5} = 3 \times 10^5$



ציור 34 - השפעה אורך אזור היניקה ומיקומו על גודל האזור המנותק

Fig. 34 - Influence of suction length and location on the separated region



- 183 -

Fig. 34a - Influence of suction length and location on the separated region.

השפעת מיקום החתלה
 ו-אורך הנוקדה
 על גודל האזור המפוזר

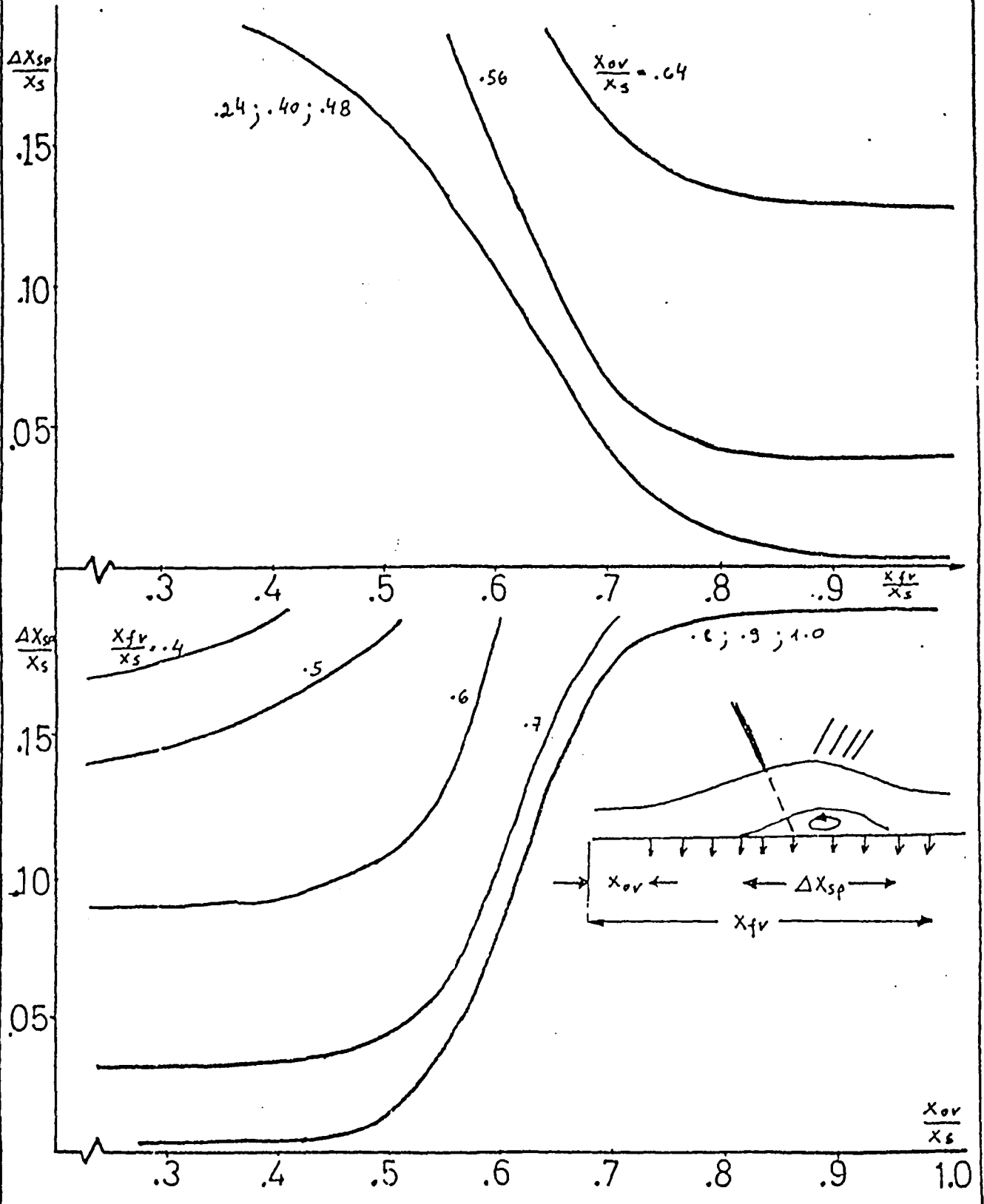


Fig. 35- Dependence of separation length $\frac{\Delta X_{sp}}{X_s}$ on suction velocity $\frac{V_w}{U_0}$ for various pressure ratio

צירוף 35 - תלוי אורך האזור הסניוק במהירות $\frac{V_w}{U_0}$ עבור יחס לחצים שונים

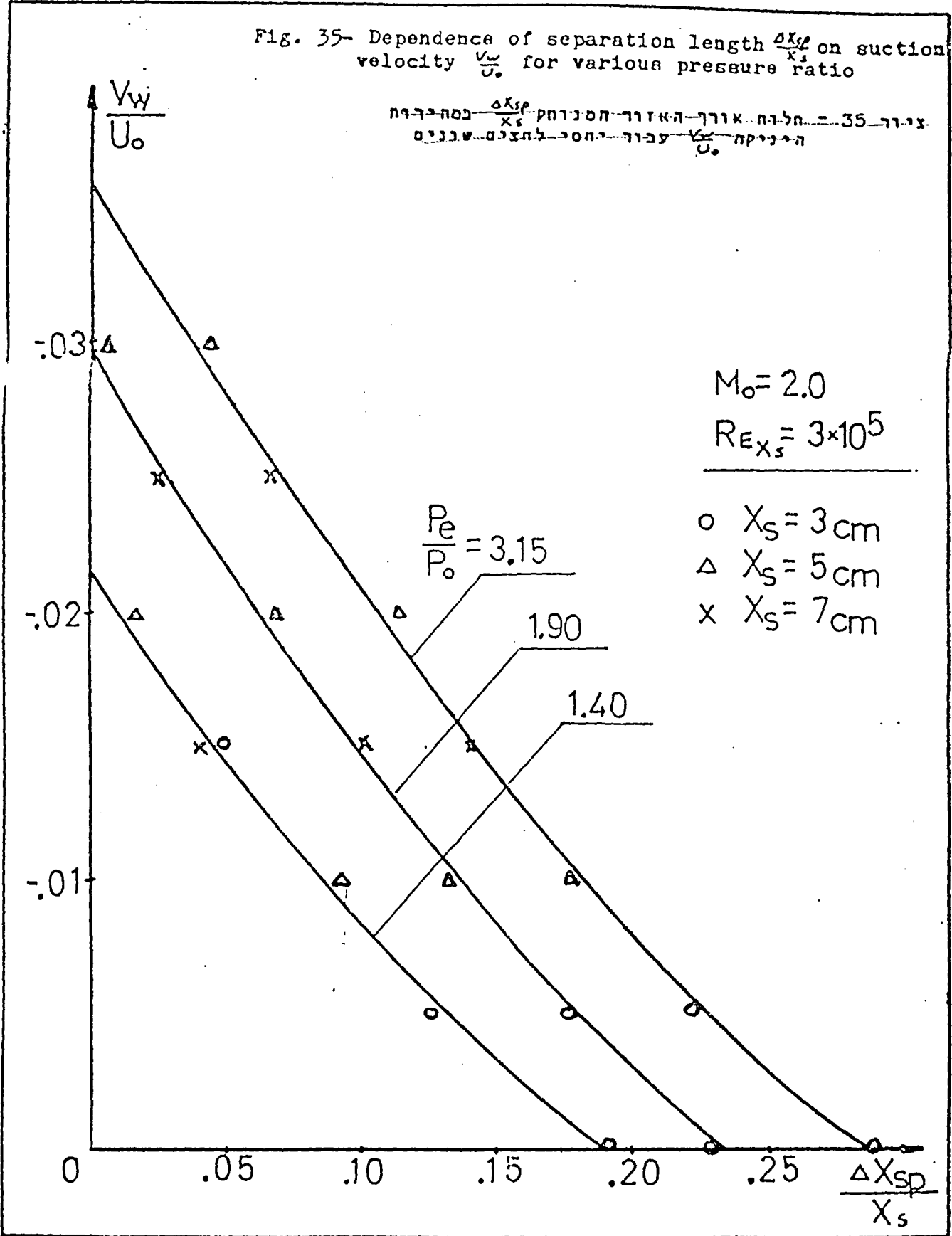


Fig. 36 - Dependence of separation length $\frac{\Delta X_{sp}}{X_s}$ on suction velocity $\frac{V_w}{U_0}$ for various Mach numbers

ציור 36 - תלות אורך האזור המפוזק $\frac{\Delta X_{sp}}{X_s}$ במהירות
הניקת $\frac{V_w}{U_0}$ עבור מספרי מאך שונים

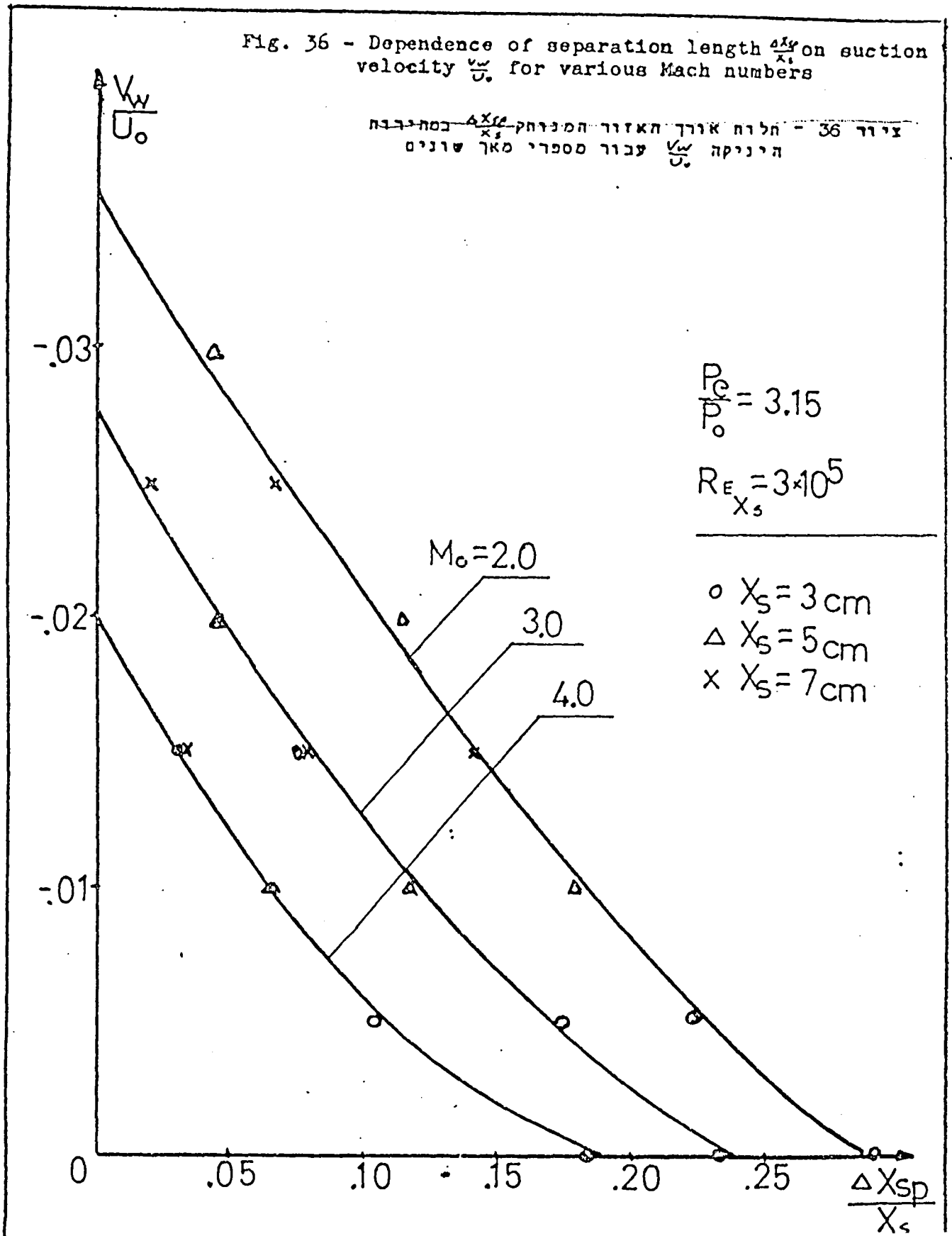


Fig. 37 - Dependence of separation length $\frac{\Delta X_{sp}}{X_s}$ on suction velocity $\frac{V_w}{U_0}$ for various Reynolds numbers

ציור 37 - תלות אורך האזור הסנוח $\frac{\Delta X_{sp}}{X_s}$ במהירות $\frac{V_w}{U_0}$ עבור מספרי ריינולדס שונים

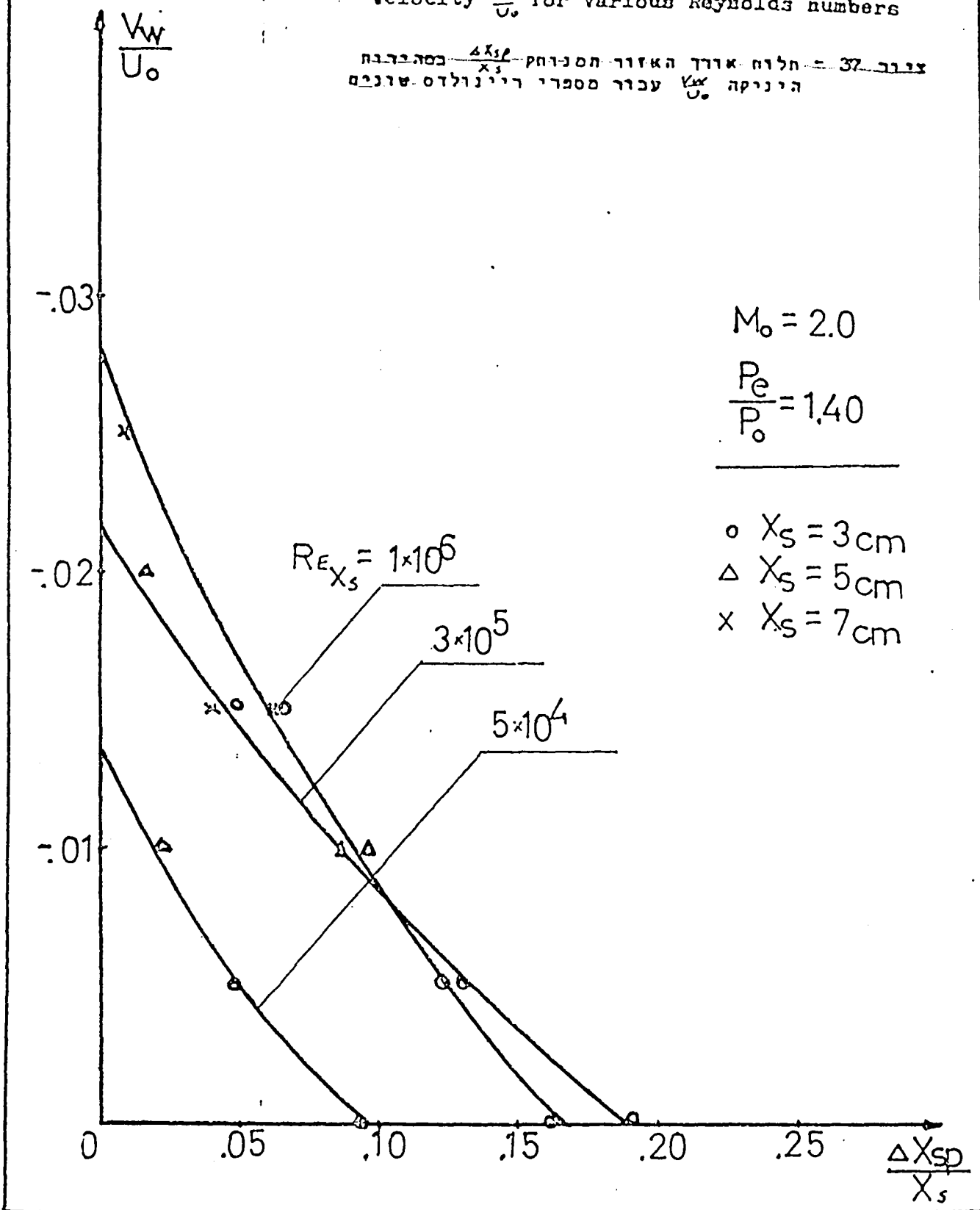


Fig. 38 - Suction velocity $\frac{V_w}{U_o}$ needed to prevent separation in the $\frac{P_e}{P_o}$ vs. M_o plane.

ציור 38 - מהירות הניקת הסדנתה $\frac{V_w}{U_o}$ הנדרשת למניעת הפרדת הזרם במישור $\frac{P_e}{P_o}$ vs. M_o .

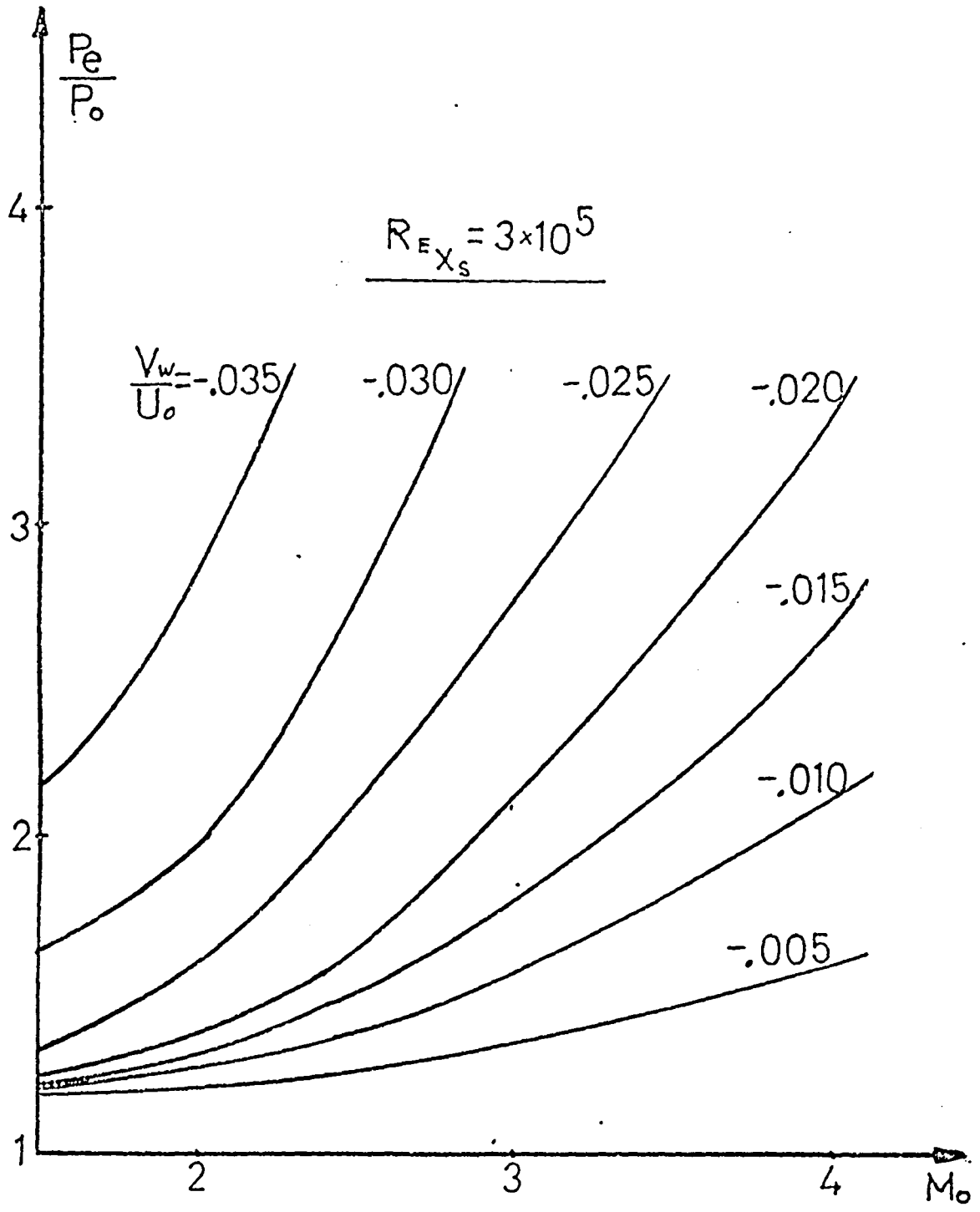


Fig. 39 - Suction velocity $\frac{V_w}{U_o}$ needed to prevent separation in the $\frac{P_e}{P_o}$ vs. Re_{x_s} plane.

צירוף 39 - מהירות הנדיחה $\frac{V_w}{U_o}$ המונעת את הפרדת הזרם
במישור $\frac{P_e}{P_o}$ vs. Re_{x_s}

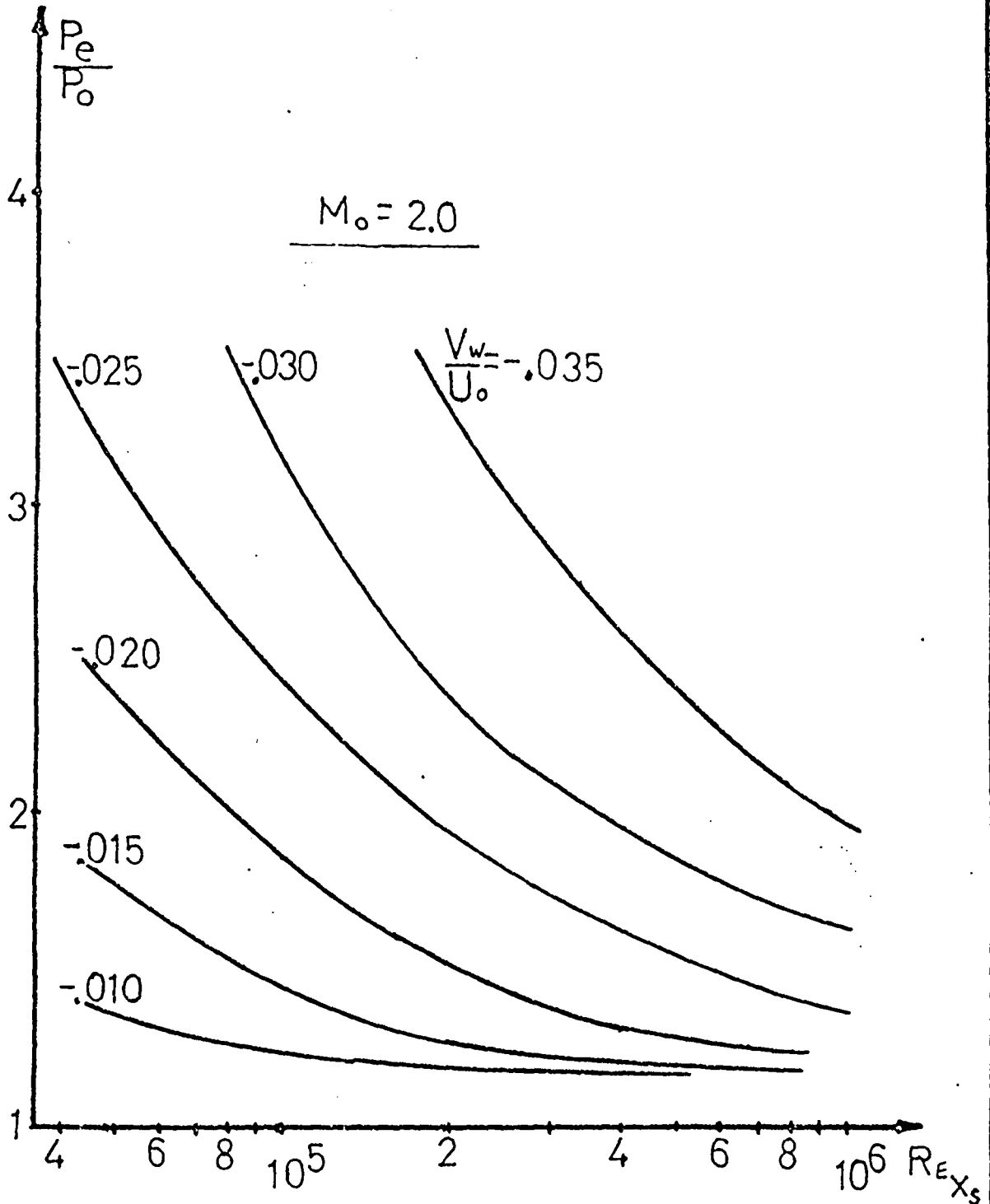
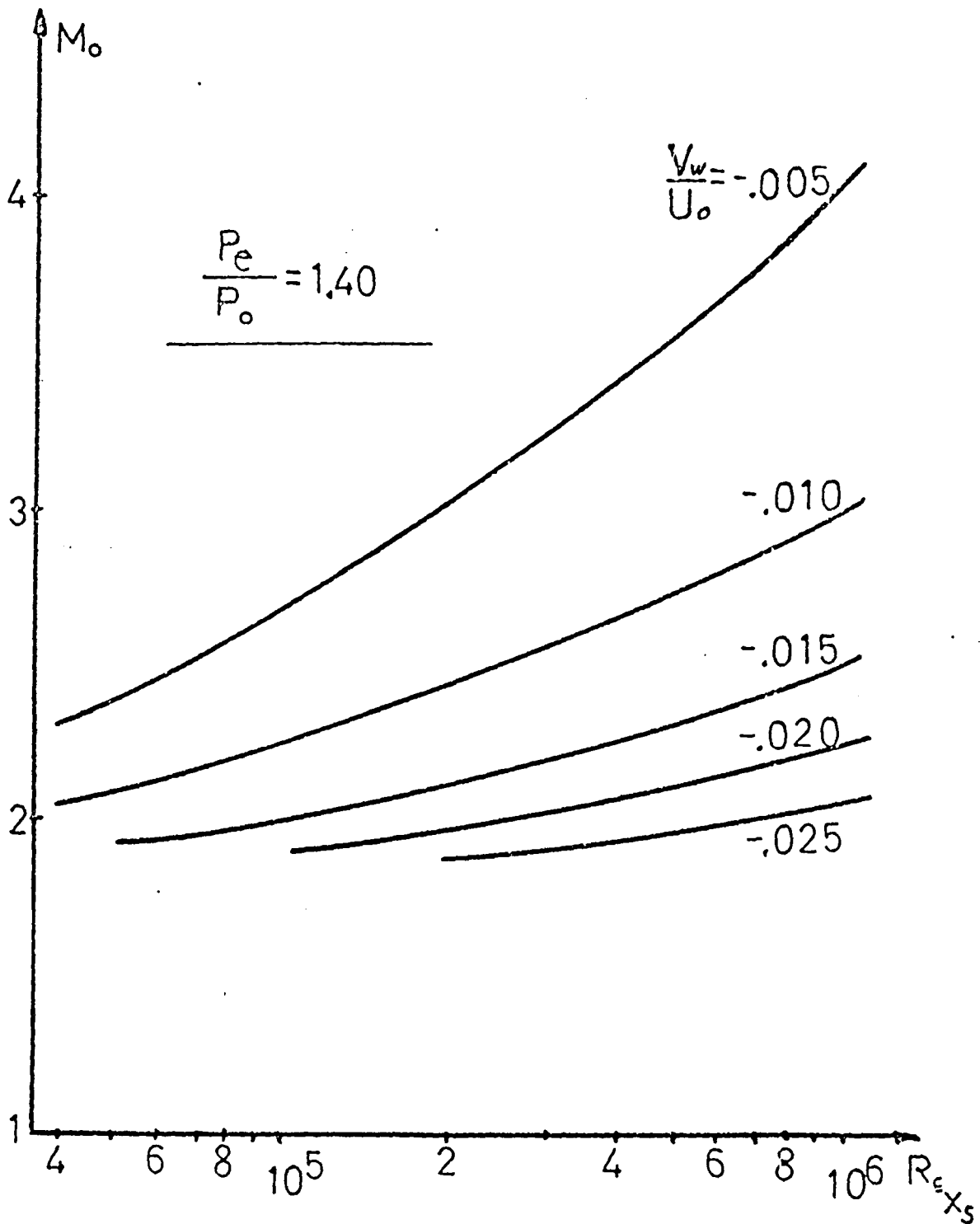


Fig. 40 - Suction velocity $\frac{V_w}{U_o}$ needed to prevent separation in the M_o vs $Re_{x,s}$ plane.

צירוף 40 - מהירות היניקה $\frac{V_w}{U_o}$ המונעת נחוק-בטיסור M_o vs. $Re_{x,s}$



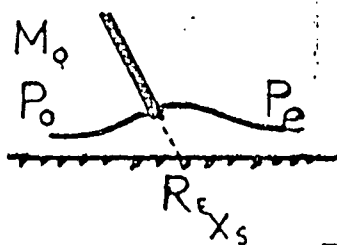


Fig. 41 - Table for the dependence of suction velocity needed to prevent separation on the flow parameters.

צורך 41 - טבלה חלוח מהירות היניקה המונעת
נחוק כפסחנים $M_0 ; R_{e x_s} ; P_e/P_0$

		M_0					
$R_{e x_s}$	P_e/P_0	1.5	2.0	2.5	3.0	3.5	4.0
5×10^4	1.5	-0.015	-0.012	-0.004	0	0	0
	2.0	-0.020	-0.017	-0.011	-0.007	-0.006	-0.004
	2.5	-0.024	-0.021	-0.016	-0.013	-0.012	-0.008
	3.0	-0.028	-0.024	-0.020	-0.018	-0.016	-0.012
	3.5	-0.031	-0.027	-0.023	-0.021	-0.019	-0.016
1×10^5	1.5	-0.020	-0.018	-0.007	-0.003	-0.001	0
	2.0	-0.025	-0.022	-0.016	-0.012	-0.008	-0.006
	2.5	-0.029	-0.026	-0.022	-0.018	-0.015	-0.011
	3.0	-0.032	-0.029	-0.025	-0.022	-0.019	-0.014
	3.5	-0.035	-0.032	-0.028	-0.025	-0.022	-0.018
2×10^5	1.5	-0.027	-0.020	-0.011	-0.000	-0.005	-0.001
	2.0	-0.031	-0.026	-0.019	-0.016	-0.011	-0.008
	2.5	-0.034	-0.030	-0.025	-0.022	-0.017	-0.013
	3.0	-0.038	-0.033	-0.029	-0.026	-0.021	-0.016
	3.5	-0.039	-0.035	-0.031	-0.028	-0.024	-0.020
5×10^5	1.5	-0.029	-0.024	-0.013	-0.008	-0.005	-0.003
	2.0	-0.036	-0.032	-0.022	-0.018	-0.015	-0.010
	2.5	-0.039	-0.036	-0.028	-0.024	-0.019	-0.015
	3.0	-0.041	-0.038	-0.032	-0.028	-0.023	-0.018
	3.5	-0.043	-0.040	-0.035	-0.031	-0.026	-0.022
1×10^6	1.5	-0.032	-0.028	-0.015	-0.010	-0.007	-0.005
	2.0	-0.040	-0.035	-0.025	-0.021	-0.015	-0.012
	2.5	-0.044	-0.041	-0.032	-0.026	-0.021	-0.017
	3.0	-0.046	-0.043	-0.035	-0.030	-0.025	-0.020
	3.5	-0.049	-0.046	-0.038	-0.034	-0.028	-0.024

End of Document